The development of standardized ion mobility and mass spectrometry metabolomics methods for the characterization of plant phenolics

by

Keabetswe Masike

Dissertation presented in fulfilment of the requirements for the degree of **Doctor of Philosophy (PhD)** in the
Faculty of Science
at
Stellenbosch University
Department of Biochemistry

Supervisor: Prof. Marietjie A. Stander
Co-supervisor: Prof. André de Villiers

March 2021

Declaration

By submitting this thesis electronically, I declare that the entirety of the work contained therein is my own, original work, that I am the sole author thereof (save to the extent explicitly otherwise stated), that reproduction and publication thereof by Stellenbosch University will not infringe any third-party rights and that I have not previously in its entirety or in part submitted it for obtaining any qualification.

Date: March 2021

Abstract

Plants and plant-derived products contain a plethora of phenolic compounds, with a broad range of health benefits and useful applications such as in drug design. These phenolic compounds are often amplified by conjugation and rearrangements, thus producing isobaric and isomeric species. The standard analytical method for the identification and characterization of plant phenolics, liquid chromatography (LC) hyphenated to photo diode array (PDA) and/or high-resolution mass spectrometry (HR-MS) detectors, is not able to discriminate isomeric species in complex plant samples. The incorporation of ion mobility spectrometry (IMS) to LC-PDA-HR-MS workflows is being recognized as an additional orthogonal dimension of separation to HR-MS; where ions are separated through a drift region, filled with gas, based on their size, shape, and charge. The attractive component of IMS is the determination of the collisional cross section (CCS/Ω) values, which describes the unique rotationally averaged surface area of the ion, as it interacts and travels through the gas-filled drift region. The CCS as a feature, can be beneficial in the development of an in-house phenolics compound library in analytical laboratories, which can help expedite the characterization of phenolic compounds in varying research fields, such as in plant metabolomics and food science.

The goal of the work reported in this thesis was, therefore, to develop LC-PDA-IM-HR-MS methods capable of structurally characterizing plant phenolics, found in South African indigenous herbal teas and plant species, based on a range of structural descriptors (e.g., t_R, spectroscopic data, mass spectral information (including high resolution and MS/MS data), and CCS value). In the first part of the study, the phenolic profiles of *Protea* pure and hybrid cultivars were characterised by LC-PDA-IM-HR-MS for the first time in detail. Whereby, IMS in conjunction with other structure elucidation techniques, namely tandem MS data, UV-vis spectroscopy, nuclear magnetic resonance (NMR) were used for characterization of 67 metabolites. With the aid of NMR an undescribed hydroxycinnamic acid-polygalatol ester, caffeoyl-*O*-polygalatol (1,5-anhydro-[6-*O*-caffeoyl]-sorbitol(glucitol)) was isolated and characterised for the first time. Furthermore, positional isomers with similar MS/MS profiles were resolved by the IMS-dimension and consequently could be distinguished by their differences in CCS values. The CCS values obtained using two IMS platforms (drift-time ion mobility spectrometry (DTIMS) and travelling wave IMS (TWIMS)) were compared, and it was observed that the CCS values obtained with a TWIMS instrument were underestimated for compounds with CCS values below 200 Å^2. Conversely, good agreement was obtained between both instruments for compounds with higher CCS values. Poor calibration of the TWIMS platform was attributed to the underestimation of the CCS values below 200 Å^2.

In the second part of the study, a detailed comparison of phytochemical profiles of a much larger set of *Protea* species, selections, and cultivars was reported. Using metabolomics tools and the data collected and documented (in the previous study) of phenolic compounds characterised based on their UPLC-PDA-IM-HR-MS profiles, plant metabolites associated with a post-harvesting disorder, leaf blackening, in *Protea* were identified/and annotated. Species, selections, and cultivars susceptible to leaf blackening contained features identified as benzenetriol- and/or hydroquinone-glycoside derivatives. On the other hand, stems not prone to blackening were linked to phenolic compounds with known protective properties against biotic and abiotic stressors. CCS values of the metabolites with protective features against leaf blackening, and those for compounds that instigate the process, were determined. Such observations serve as preliminary insights that can help accelerate plant improvement and aid in the selection of trait-specific markers in plant metabolomics.

In the final portion of the study, using direct injection-IM-MS (DI-IM-MS) and descriptive chemometrics, differences between adulterated herbal teas (rooibos and honeybush) were observed. The diagnostic value of marker compounds in distinguishing the three commercialised honeybush species (*Cyclopia intermedia*, *C. genistoides* and *C. subternata*) for the quality control purpose were observed. To derive CCS values using the TWIMS instrument two calibrants, poly-DL-alanine and poly-L-malic acid, were compared. Poly-DL-alanine is a widely used TWIMS calibrant which results in an underestimation for compounds with CCS values below 200 $Å^2$ (initial study), when compared to poly-L-malic acid an improvement in the underestimation of CCS values below 200 $Å^2$ was observed. DI-IM-MS proved to be a useful tool for quality control purposes, particularly considering the analysis time is 1 minute per sample.

Opsomming

Plante en plantaardige produkte bevat 'n magdom van fenoliese verbindings, met 'n wye verskeidenheid gesondheidsvoordele en ander nuttige toepassings byvoorbeeld die ontwikkeling van geneesmiddels. Hierdie fenoliese verbindings word dikwels verander deur konjugasie en herrangskikkingsreaksies, en sodoende word isobariese spesies en isomere gevorm. Die standaard analitiese metode vir die identifisering en karakterisering van plantfenole, vloeistofchromatografie (LC) wat aan fotodiode-reeks (PDA) en / of hoë-resolusie massa spektrometrie (HR-MS) detektore gekoppel is, kan nie altyd isomere in komplekse plantmonsters onderskei nie. Die integrasie van ioon mobiliteit spektrometrie (IMS) in LC-PDA-HR-MS- werkstrome word erken as 'n aanvullende ortogonale dimensie van skeiding vir HR-MS; waar ione geskei word deur 'n dryfgebied, gevul met gas, gebaseer op hul grootte, vorm en lading. Die voordeel van IMS is die bepaling van die botsingsdeursnee (CCS / Ω) waarde, wat die unieke rotasiegemiddelde oppervlakarea van die ioon beskryf. CCS is voordeling vir die ontwikkeling van 'n biblioteek met fenoliese verbindings in analitiese laboratoriums, wat kan help om die karakterisering van fenoliese verbindings in verskillende navorsingsvelde, soos plantmetabolika en voedselwetenskap, te vergemaklik.

Die doel van die werk wat in hierdie proefskrif oor verslag gedoen word, was dus om LC-PDA-IM-HR-MS-metodes te ontwikkel wat in staat is om die strukture van plantfenoliese stowwe, wat in Suid-Afrikaanse inheemse kruietees en plantspesies voorkom, te karakteriseer gebaseer op 'n reeks strukturele beskrywers (bv. t_R, spektroskopiese data, massa spektrale inligting (insluitend hoë resolusie en MS/MS data) en CCS waarde). In die eerste gedeelte van die studie is die fenoliese profiele van *Protea* suiwer en baster kultivars vir die eerste keer in detail gekarakteriseer deur LC-PDA-IM-HR-MS. Waarvolgens IMS saam met ander struktuur-opklaringsstegnieke, naamlik tandem MS data, UV-vis spektroskopie, kernmagnetiese resonansie (NMR) gebruik is vir die karakterisering van 67 metaboliete. Met behulp van NMR is 'n onbeskrewe hidroksie kaneelsuur-poligalatolester, kaffeoïel-O-polygalatol (1,5-anhidro-[6-O-kaffeoïel]-sobitol(glukitol) geïsoleer en vir die eerste keer gekarakteriseer. Verder is posisionele isomere met soortgelyke MS/MS-profiele geïdentifiseer deur die IMS-dimensie en kan gevolglik onderskei word deur hul verskille in CCS-waardes. Die CCS-waardes wat verkry is met behulp van twee IMS-platforms (dryftyd ioon mobiliteit spektrometrie (DTIMS) en bewegende golf-IMS (TWIMS)) is vergelyk, en daar is waargeneem dat die CCS-waardes wat met 'n TWIMS-instrument verkry is, onderskat is vir verbindings met CCS-waardes onder 200 $Å^2$. Andersins is goeie ooreenkoms tussen beide instrumente verkry vir verbindings met hoër CCS-waardes. Swak kalibrasie van die TWIMS-platform is toegeskryf aan die onderskatting van die CCS-waardes onder 200 $Å^2$.

In die tweede deel van die studie word 'n gedetailleerde vergelyking van fitochemiese profiele van 'n veel groter stel *Protea*-spesies, seleksies en kultivars gerapporteer. Met behulp van metabolomika-tegnieke en die data wat versamel en gedokumenteer is (in die vorige studie) van fenoliese verbindings op grond van hul UPLC-PDA-IM-HR-MS-profiele, die plantmetaboliete wat verband hou met 'n na-oes probleem, blaarverswarting in *Protea,* geïdentifiseer/en geannoteer. Spesies, seleksies en kultivars wat vatbaar is vir blaarverswarting bevat benseentriol- en / of hidrokinoon-glikosiedderivate. Daarteenoor bevat stingels wat nie geneig is tot verswarting nie, weer meer fenoliese verbindings met bekende beskermende eienskappe teen biotiese en abiotiese stresfaktore. CCS-waardes van die metaboliete met beskermende eienskappe teen blaarverswarting, en die waardes vir verbindings wat die proses begin, is bepaal. Sulke waarnemings voeg waarde toe tot bestaande inligting wat kan help om plantverbetering te versnel en te help met die keuse van eienskapspesifieke merkers in plantmetabolomika.

In die laaste gedeelte van die studie, is daar met behulp van direkte inspuiting-IMS (DI-IM-MS) en chemometrie, is verskille waargeneem tussen vervalsde kruietee (rooibos en heuningbos). Merkerverbindings om tussen die drie kommersiële heuningbosspesies (*Cyclopia intermedia*, *C. genistoides* en *C. subternata*) te onderskei is waargeneem. Om CCS-waardes met behulp van die TWIMS-instrument af te lei, is twee kalibrante, poli-DL-alanien en poli-L-appelsuur, vergelyk. Poli-DL-alanien is die algemeen gebruikte TWIMS kalibrant wat lei tot 'n onderskatting van verbindings met CCS waardes onder 200 $Å^2$ (aanvanklike studie), in vergelyking met poly-L-appelsuur, 'n verbetering in die onderskatting van CCS waardes onder 200 $Å^2$. DI-IM-MS blyk 'n nuttige hulpmiddel te wees vir doeleindes van gehaltebeheer, veral aangesien die ontledingstyd 1 minuut per monster is.

Preface

This thesis has been compiled in a form of published and manuscripts under preparation, and presented at an international conference:

Review and Articles published

Masike, K., Stander, M. A. & de Villiers, A. Recent applications of ion mobility spectrometry in natural product research. *Journal of Pharmaceutical and Biomedical Analysis*, 2021; 195:113846. doi.org/10.1016/j.jpba.2020.113846. Presented in Chapter 2 (a portion) and Appendix A (full paper).

Masike, K., de Villiers, A., Hoffman, E.W., Brand, D.J., Causon, T. & Stander, M. A. Detailed Phenolic Characterization of *Protea* Pure and Hybrid Cultivars by Liquid Chromatography-Ion Mobility-High Resolution Mass Spectrometry (LC-IM-HR-MS). *Journal of Agricultural and Food Chemistry*, 2020; 68: 485-502. doi.org/10.1021/acs.jafc.9b06361. Presented in Chapter 3.

Masike, K., de Villiers, A., Hoffman, E.W. & Stander, M. A. Application of Metabolomics Tools to Determine Possible Biomarker Metabolites Linked to Leaf Blackening in *Protea*. *Journal of Agricultural and Food Chemistry*, 2020; 68: 12595-12605. doi.org/10.1021/acs.jafc.0c03607. Presented in Chapter 4.

Articles in preparation

Masike, K., de Villiers, A., de Beer, D., Joubert, E. & Stander, M. A. Application of direct injection-ion mobility mass spectrometry (DI-IM-MS) for the analysis of Honeybush and Rooibos tea samples. Presented in Chapter 5.

Conference output

Masike, K., de Villiers, A. & Stander, M. A. Phytochemical characterization of *Protea* pure and hybrid cultivars with the aid of liquid chromatography-ion mobility mass spectrometry (LC-IMMS) and the application of metabolomics tools in determining possible metabolites linked to leaf blackening. 48th International Symposium on High-Performance Liquid Phase Separations and Related Techniques, University of Milano-Bicocca, Milan, June 2019.

Other publications

Stander, M., Redelinghuys, H., Masike, K., Long, H. & Van Wyk, B. Patterns of Variation and Chemosystematic Significance of Phenolic Compounds in the Genus *Cyclopia* (Fabaceae, Podalyrieae). *Molecules*, 2019; 24: 1-20. doi.org/10.3390/molecules24132352.

Acknowledgements

I would like to thank my academic supervisor Prof. Marietjie A. Stander for your guidance, patience, and allowing me access to the LC-MS instruments. I would also like to thank my co-supervisor; Prof. André J. de Villiers for your guidance, support, and your attention to detail. Without you this thesis would not have come to fruition and I am wholeheartedly thankful.

I would also like to thank Dr. Eleanor W. Hoffman, Prof. Dalene de Beer, Dr. D. Jacobus Brand, and Dr. Tim Causon for their individual contributions to this thesis.

I would like to thank Stellenbosch University, especially the Central Analytical Facility (CAF) for the bursary awarded and to and the National Research Foundation (NRF, grant 118530 to AdV (bursary awarded to KM) and grant 121613 to KM) for financial support.

In addition, gratitude is extended to Mrs Nicole Windell from FynBloem farm to Prof. Marius Huysamer from Berghoff Farm, and the chief horticulturist, Karen Wall, from the Harold Porter National Botanical Garden for their gracious donation of the analysed plants. Furthermore, gratitude is sent to the Agricultural Research Council (ARC) Infruitec-Nietvoorbij for their supply of the herbal teas and analytical samples analysed in this thesis.

A friendly thank you to Mrs. Fransien Kamper, Mr. Malcolm Taylor and Mr. Erick Van Schalkwyk for your input and support in invaluable ways.

To my fellow colleagues Nqobile A. Masondo, Gaalebalwe E. Ntlhokwe, Sithandile Ngxangxa, Magriet Muller, Pieter Venter, and Tlou Mosekiemang, I thank you for all the laughs we shared.

Lastly but not least, to my family; my mother Mrs. Catherine M. Masike your support, tenacity, and words “e ka se ho hlole” will forever be my anchor. To my older brother Mr. Tumisang J. Masike I thank you for your protection and the laughs. To my father Mr. Lucas M. Masike, your words “life was not meant to be easy” will forever be my guide. To my sister-in-law, Mrs. Duduzile M. Masike, I thank you for the little boy and girl whom you brought into this world and who light up my life.

List of abbreviations

Å, angstrom;

ATD, arrival time distibution;

CCS/Ω, collision cross-section;

CID, collision induced dissociation;

cIM-MS, cyclic ion mobility-mass spectrometry;

cIMS, cyclic ion mobility spectrometry;

^{13}C NMR, carbon-13 nuclear magnetic resonance spectroscopy;

Da, Daltons;

DDA, data dependent acquisition;

DI, direct injection;

DIA, data independent acquisition;

DM-MS, differential mobility-mass spectrometry;

DMS, differential mobility spectrometry (DMS);

DMSO, dimethyl sulfoxide;

DMSO-d_6, deuterated DMSO;

$^{DT}CCS_{He}$, drift tube ion mobility derived collision cross in helium;

DTIM-MS, drift tube ion mobility-mass spectrometry;

DTIMS, drift tube ion mobility spectrometry;

E, electric field;

E_c, compensation field;

ESI, electrospray ionisation;

ESI$^-$, electrospray ionisation negative mode;

ESI$^+$, electrospray ionisation positive mode;

FAIM-MS, field asymmetric ion mobility-mass spectrometry;

FAIMS, field asymmetric ion mobility spectrometry;

FWHM, full width at half maximum;

GC, gas chromatography;

GC×GC, comprehensive two-dimensional GC;

HCA, hierarchical cluster analysis;

HMBC, heteronuclear multiple bond correlation;

HSQC, heteronuclear single quantum correlation;

^{1}H NMR, hydrogen-1 (proton) nuclear magnetic resonance spectroscopy;

He, helium;

HPLC, high performance liquid chromatography;

HR-MS, high resolution-mass spectrometry;

IM-MS, ion mobility mass spectrometry;

IMS, ion mobility spectrometry;

K, mobility;

K_0, reduced mobility;

LC, liquid chromatography;

LC×LC, comprehensive two-dimensional LC;

m/z, mass to charge ratio;

mzML, mass to charge ratio markup language

MALDI, matrix assisted laser desorption ionisation;

ms, milliseconds;

MS, mass spectrometry;

MS^E, high energy mass spectrum;

MS/MS, tandem mass spectrometry;

MS^3, 2nd generation product ion spectra;

MS^4, 3rd generation product ion spectra;

MVDA, multivariate data analysis;

N_2, nitrogen;

NMR, nuclear magnetic resonance spectroscopy;

1D NMR, one dimensional nuclear magnetic resonance spectroscopy;

2D NMR, two-dimensional nuclear magnetic resonance spectroscopy;

PASEF, parallel accumulation serial fragmentation;

PCA, principal component analysis;

PDA, photo diode array;

ppm, part per million;

q, quadrupole;

q-TOF, quadrupole-time of flight;

RPLC, reverse phase liquid chromatography;

Rp, resolving power;

RSD%, relative standard deviation %;

S/N, signal to noise ratio;

SLIM-IMS, structures for lossless ion manipulations ion mobility spectrometry;

SLIM-IM-MS, structures for lossless ion manipulations ion mobility-mass spectrometry;

TAP, time-aligned parallel;

t_D, drift time;

TIM-MS, trapped ion mobility-mass spectrometry;

TIMS, trapped ion mobility spectrometry;

TOCSY, total correlation spectroscopy;

TOF, time of flight;

t_R, retention time;

$^{TW}CCS_{N2}$, travelling wave ion mobility derived collision cross in nitrogen;

TWIM-MS, travelling wave ion mobility - mass spectrometry;

TWIMS, travelling wave ion mobility spectrometry;

UHPLC, ultra high-pressure liquid chromatography;

UPLC, ultra-high ultra performance liquid chromatography;

UV, ultra violet;

vis, visible.

Table of Contents

Chapter 1: General Introduction and Objectives

1.1. General Introduction

Plants produce a collection of diverse metabolites which vary in structure and biosynthetic origin. These metabolites can be classified as either primary or secondary metabolites.[1] Primary metabolites are responsible for the growth, development, and reproduction of the plant; whereas secondary metabolites are produced to facilitate interactions between the plant and its environment.[1] The most common secondary metabolites are phenolic compounds, which comprise of flavonoids and non-flavonoid classes. Phenolics contribute favorably to the human diet and the sensory properties of a range of plant-derived commodities, thus their comprehensive identification in food, beverages of plant origin, and medicinal plants has become important, particularly when in search of new biologically active metabolites.

Liquid chromatography (LC) hyphenated to photo diode array (PDA) and/or mass spectrometry (MS) detectors have become the standard analytical method for the identification and characterization of plant phenolics.[2–4] However, the complexity of phenolics poses an undisputed analytical challenge; as these metabolites have underwent chemical modification processes such as isomerisation and conjugation which hamper LC resolution and, in some cases, produce identical/similar MS/MS spectra.[5–10] For instance, biologically active phenolic acids collectively referred to as chlorogenic acids (CGAs), which are esters of quinic acid and hydroxycinnamates (i.e. caffeic acid, *p*-coumaric acid and/or ferulic acid), exist as both positional (regio-) and geometrical isomers within plants.[7,10] Although improved chromatographic separation may be obtained using ultra high-performance LC (UPLC) or multidimensional LC systems, the biggest challenge has been the ability to distinguish isomers using high-resolution MS (HR-MS) and/or tandem MS (MS/MS). Thus, reliable-standardised analytical methods need to be put in place for the characterization of such plant phenolics. Methods capable of rapidly separating and detecting plant phenolics, particularly isomeric and isobaric compounds in complex plant samples.

The post-ionisation coupling of ion mobility spectrometry to MS (IM-MS) has become an attractive instrument for the separation and detection of such structurally similar metabolites.[11–14] During ion mobility analysis, ions drift through a gas (helium or nitrogen) filled chamber using a weak electric field and separated based on the ions size, shape and charge. This allows ions to be separated beyond their mass-to-charge ratio (*m/z*). The recorded drift time/mobility (in milliseconds) is then converted into the collisional cross section (CCS/Ω) value, which describes the physicochemical property of the ion travelling through the drift region.[11,12,15,16]

There are varying ion mobility methods, with the time-dispersive platforms - drift-time ion mobility spectrometry (DTIMS) and travelling wave IMS (TWIMS) - being the most commercially

used IMS platforms in omics and natural product research. Of the two IMS platforms, DTIMS are capable of directly measuring CCS values. Whereas, TWIMS instruments require calibration using molecules with known CCS values under defined conditions to derive experimental CCS values of unknowns.[17,18]

The CCS value obtained is unique for each ion as it reflects interactions between the ion and the neutral buffer gas, and from these interactions chemical structural and three-dimensional conformational information are inferred. Hence, isobaric and isomeric phenolics will interact differently with the buffer gas and provide different CCS values, thus leading to their enhanced separation identification. Coupling IMS to LC-HR-MS (MS/MS) workflows provides complementary information, and will allow species to be characterised based on an range of complementary descriptors (e.g. retention time (t_R) , accurate mass information, tandem MS, drift time and related CCS values) which will help increase molecular information content and specificity in the structural identification of phenolic compounds.[19–30] Thus, decreasing the number of false and positive identifications which are often obtained when analysis is based only on accurate mass and/or t_R.[31]

Such structural information (e.g., t_R, mass spectral information (including high resolution and tandem MS data), spectroscopic data and CCS value) can be beneficial in the development of an in-house phenolics compound library in analytical laboratories, which can help expedite the characterization of phenolic compounds in natural product research and other research involving phenolic compound characterization.

1.2. Aim and objectives

The aim of the study is to design improved liquid chromatography-photodiode array-ion mobility-high resolution mass spectrometry (LC-PDA-IM-HR-MS) methods capable of structurally characterizing plant phenolics, for a wide range of natural products of importance in South Africa, such as indigenous herbal teas and indigenous plant species. The characterization of phenolics based on a range of structural descriptors can be beneficial in varying research fields, such as in plant metabolomics and food science.

To achieve this, the following objectives were formulated:

OBJECTIVE 1: Extraction of phenolic compounds from natural products (*Protea* species and cultivars, and herbal teas (rooibos, and honeybush)).

OBJECTIVE 2: Optimization of robust UPLC-PDA-IM-HR-MS and IMS methodologies capable of separating different classes of plant derived phenolics.

OBJECTIVE 3: Data collection and the documentation of phenolic compounds characterised based on their UPLC-PDA-IM-HR-MS profiles, whereby the incorporation of CCS values to LC-MS workflows will 1) expedite the characterization of phenolic compounds in natural product research, 2) improve metabolite identification confidence in plant metabolomics, 3) assist in the use of phenolic compounds as markers to aid in the differentiation of plant species from the same Genus and 4) assist in the use of phenolic compound markers in food adulteration studies.

1.3. References

(1) Crozier, A.; Jaganath, B. I.; Clifford, N. M. Phenols, Polyphenols and Tannins: An overview. In *Plant Secondary Metabolites: Occurrence, Structure and Role in the Human Diet*; Crozier, A., Clifford, N. M., Ashihara, H., Eds.; Blackwell Publishing Ltd, 2006; pp 1–25. https://doi.org/1-4051-2509-8 Library.

(2) Piovesana, S.; Cavaliere, C.; Cerrato, A.; Montone, C. M.; Laganà, A.; Capriotti, A. L. Developments and pitfalls in the characterization of phenolic compounds in food: From targeted analysis to metabolomics-based approaches. *TrAC - Trends Anal. Chem.* **2020**, *133*. https://doi.org/10.1016/j.trac.2020.116083.

(3) De Villiers, A.; Venter, P.; Pasch, H. Recent advances and trends in the liquid-chromatography-mass spectrometry analysis of flavonoids. *J. Chromatogr. A* **2015**, *1430*, 16–78. https://doi.org/10.1016/j.chroma.2015.11.077.

(4) Xing, J.; Xie, C.; Lou, H. Recent applications of liquid chromatography-mass spectrometry in natural products bioanalysis. *J. Pharm. Biomed. Anal.* **2007**, *44* (2), 368–378. https://doi.org/10.1016/j.jpba.2007.01.010.

(5) Zuardi, A. W.; Crippa, J. A. S.; Hallak, J. E. C.; Moreira, F. A.; Guimarães, F. S. Cannabidiol, a *Cannabis sativa* constituent, as an antipsychotic drug. *Brazilian J. Med. Biol. Res.* **2006**, *39* (4), 421–429. https://doi.org/10.1590/S0100-879X2006000400001.

(6) Tose, L. V.; Santos, N. A.; Rodrigues, R. R. T.; Murgu, M.; Gomes, A. F.; Vasconcelos, G. A.; Souza, P. C. T.; Vaz, B. G.; Romão, W. Isomeric separation of cannabinoids by UPLC combined with ionic mobility mass spectrometry (TWIM-MS)—Part I. *Int. J. Mass Spectrom.* **2017**, *418*, 112–121. https://doi.org/10.1016/j.ijms.2016.10.018.

(7) Clifford, M. N.; Kirkpatrick, J.; Kuhnert, N.; Roozendaal, H.; Salgado, P. R. LC-MS^n analysis of the *cis* isomers of chlorogenic acids. *Food Chem.* **2008**, *106* (1), 379–385. https://doi.org/10.1016/j.foodchem.2007.05.081.

(8) Masike, K.; Mhlongo, M. I.; Mudau, S. P.; Nobela, O.; Ncube, E. N.; Tugizimana, F.; George, M. J.; Madala, N. E. Highlighting mass spectrometric fragmentation differences and similarities between hydroxycinnamoyl-quinic acids and hydroxycinnamoyl-isocitric acids. *Chem. Cent. J.* **2017**, *11* (1), 1–7. https://doi.org/10.1186/s13065-017-0262-8.

(9) Masike, K.; Tugizimana, F.; Ndlovu, N.; Smit, E.; du Preez, L.; Dubery, I.; Madala, E.

Deciphering the influence of column chemistry and mass spectrometry settings for the analyses of geometrical isomers of L-chicoric acid. *J. Chromatogr. B Anal. Technol. Biomed. Life Sci.* **2017**, *1052*, 73–81. https://doi.org/10.1016/j.jchromb.2017.03.023.

(10) Clifford, M. N.; Johnston, K. L.; Knight, S.; Kuhnert, N. Hierarchical scheme for LC-MS^n identification of chlorogenic acids. *J. Agric. Food Chem.* **2003**, *51* (10), 2900–2911. https://doi.org/10.1021/jf026187q.

(11) Wu, Q.; Wang, J.-Y.; Han, D.-Q.; Yao, Z.-P. Recent advances in differentiation of isomers by ion mobility mass spectrometry. *TrAC Trends Anal. Chem.* **2020**, *124*, 115801. https://doi.org/10.1016/j.trac.2019.115801.

(12) Burnum-Johnson, K. E.; Zheng, X.; Dodds, J. N.; Ash, J.; Fourches, D.; Nicora, C. D.; Wendler, J. P.; Metz, T. O.; Waters, K. M.; Jansson, J. K.; Smith, R. D.; Baker, E. S. Ion mobility spectrometry and the Omics: Distinguishing isomers, molecular classes and contaminant ions in complex samples. *TrAC - Trends Anal. Chem.* **2019**, *116*, 292–299. https://doi.org/10.1016/j.trac.2019.04.022.

(13) Kuhnert, N.; Yassin, G. H.; Jaiswal, R.; Matei, M. F.; Grün, C. H. Differentiation of prototropic ions in regioisomeric caffeoyl quinic acids by electrospray ion mobility mass spectrometry. *Rapid Commun. Mass Spectrom.* **2015**, *29* (7), 675–680. https://doi.org/10.1002/rcm.7151.

(14) Gonzales, G. B.; Smagghe, G.; Coelus, S.; Adriaenssens, D.; De Winter, K.; Desmet, T.; Raes, K.; Van Camp, J. Collision Cross Section prediction of deprotonated phenolics in a Travelling-Wave Ion Mobility Spectrometer using molecular descriptors and chemometrics. *Anal. Chim. Acta* **2016**, *924*, 68–76. https://doi.org/10.1016/j.aca.2016.04.020.

(15) Dodds, J. N.; Baker, E. S. Ion Mobility Spectrometry: Fundamental concepts, instrumentation, applications, and the road ahead. *J. Am. Soc. Mass Spectrom.* **2019**, *30* (11), 2185–2195. https://doi.org/10.1007/s13361-019-02288-2.

(16) Paglia, G.; Smith, A. J.; Astarita, G. Ion Mobility Mass Spectrometry in the Omics era: Challenges and opportunities for metabolomics and lipidomics. *Mass Spectrom. Rev.* **2021**, *22* (8), mas.21686. https://doi.org/10.1002/mas.21686.

(17) Hines, K. M.; May, J. C.; McLean, J. A.; Xu, L. Evaluation of collision cross section calibrants for structural analysis of lipids by traveling wave ion mobility-mass spectrometry. *Anal. Chem.* **2016**, *88* (14), 7329–7336. https://doi.org/10.1021/acs.analchem.6b01728.

(18) Hofmann, J.; Struwe, W. B.; Scarff, C. A.; Scrivens, J. H.; Harvey, D. J.; Pagel, K. Estimating collision cross sections of negatively charged n-glycans using traveling wave ion mobility-mass spectrometry. *Anal. Chem.* **2014**, *86* (21), 10789–10795. https://doi.org/10.1021/ac5028353.

(19) Gonzales, G. B.; Raes, K.; Coelus, S.; Struijs, K.; Smagghe, G.; Van Camp, J. Ultra(high)-pressure liquid chromatography-electrospray ionization-time-of-flight-ion mobility-high definition mass spectrometry for the rapid identification and structural characterization of flavonoid glycosides from cauliflower waste. *J. Chromatogr. A* **2014**, *1323*, 39–48. https://doi.org/10.1016/j.chroma.2013.10.077.

(20) Paglia, G.; Williams, J. P.; Menikarachchi, L.; Thompson, J. W.; Tyldesley-Worster, R.; Halldórsson, S.; Rolfsson, O.; Moseley, A.; Grant, D.; Langridge, J.; Palsson, B. O.; Astarita, G. Ion mobility derived collision cross sections to support metabolomics applications. *Anal. Chem.* **2014**, *86* (8), 3985–3993. https://doi.org/10.1021/ac500405x.

(21) Masike, K.; De Villiers, A.; Hoffman, E. W.; Brand, D. J.; Causon, T.; Stander, M. A. Detailed phenolic characterization of *Protea* pure and hybrid cultivars by liquid chromatography-ion mobility-high resolution mass spectrometry (LC-IM-HR-MS). *J. Agric. Food Chem.* **2020**, *68* (2), 485–502. https://doi.org/10.1021/acs.jafc.9b06361.

(22) Schroeder, M.; Meyer, S. W.; Heyman, H. M.; Barsch, A.; Sumner, L. W. Generation of a collision cross section library for multi-dimensional plant metabolomics using UHPLC-Trapped Ion Mobility-MS/MS. *Metabolites* **2020**, *10* (1). https://doi.org/10.3390/metabo10010013.

(23) Pacini, T.; Fu, W.; Gudmundsson, S.; Chiaravalle, A. E.; Brynjolfson, S.; Palsson, B. O.; Astarita, G.; Paglia, G. Multidimensional analytical approach based on UHPLC-UV-Ion Mobility-MS for the screening of natural pigments. *Anal. Chem.* **2015**, *87* (5), 2593–2599. https://doi.org/10.1021/ac504707n.

(24) Zhang, H.; Zheng, D.; Li, H. H.; Wang, H.; Tan, H. S.; Xu, H. X. Diagnostic filtering to screen polycyclic polyprenylated acylphloroglucinols from *Garcinia oblongifolia* by ultra high performance liquid chromatography coupled with ion mobility quadrupole time-of-flight mass spectrometry. *Anal. Chim. Acta* **2016**, *912*, 85–96. https://doi.org/10.1016/j.aca.2016.01.039.

(25) Wang, Y.; Vorsa, N.; Harrington, P. D. B.; Chen, P. Nontargeted metabolomic study on

variation of phenolics in different cranberry cultivars using UPLC-IM-HRMS. *J. Agric. Food Chem.* **2018**, *66* (46), 12206–12216. https://doi.org/10.1021/acs.jafc.8b05029.

(26) Yang, X.; Wei, S.; Liu, B.; Guo, D.; Zheng, B.; Feng, L.; Liu, Y.; Tomás-Barberán, F. A.; Luo, L.; Huang, D. A Novel integrated non-targeted metabolomic analysis reveals significant metabolite variations between different lettuce (*Lactuca sativa*. L) varieties. *Hortic. Res.* **2018**, *5* (1), 1–14. https://doi.org/10.1038/s41438-018-0050-1.

(27) Zang, X.; Monge, M. E.; Gaul, D. A.; Fernández, F. M. Flow injection-traveling-wave ion mobility-mass spectrometry for prostate-cancer metabolomics. *Anal. Chem.* **2018**, *90* (22), 13767–13774. https://doi.org/10.1021/acs.analchem.8b04259.

(28) Causon, T. J.; Ivanova-Petropulos, V.; Petrusheva, D.; Bogeva, E.; Hann, S. Fingerprinting of traditionally produced red wines using liquid chromatography combined with drift tube ion mobility-mass spectrometry. *Anal. Chim. Acta* **2019**, *1052*, 179–189. https://doi.org/10.1016/j.aca.2018.11.040.

(29) Jia, L.; Zuo, T.; Zhang, C.; Li, W.; Wang, H.; Hu, Y.; Wang, X.; Qian, Y.; Yang, W.; Yu, H. Simultaneous profiling and holistic comparison of the metabolomes among the flower buds of *Panax ginseng*, *Panax quinquefolius*, and *Panax notoginseng* by UHPLC/IM-QTOF-HDMS^{E}-based metabolomics analysis. *Molecules* **2019**, *24* (11), 2188. https://doi.org/10.3390/molecules24112188.

(30) Fenclova, M.; Stranska-Zachariasova, M.; Benes, F.; Novakova, A.; Jonatova, P.; Kren, V.; Vitek, L.; Hajslova, J. Liquid chromatography–drift tube ion mobility–mass spectrometry as a new challenging tool for the separation and characterization of silymarin flavonolignans. *Anal. Bioanal. Chem.* **2020**, *412* (4), 819–832. https://doi.org/10.1007/s00216-019-02274-3.

(31) Kaufmann, A.; Butcher, P.; Maden, K.; Walker, S.; Widmer, M. Does the ion mobility resolving power as provided by commercially available ion mobility quadrupole time-of-flight mass spectrometry instruments permit the unambiguous identification of small molecules in complex matrices? *Anal. Chim. Acta* **2020**, *1107*, 113–126. https://doi.org/10.1016/j.aca.2020.02.032.

Declaration with signatures in possession of candidate and supervisor.

Declaration by the candidate:

Chapter 2 contains a portion of the review paper on ion mobility spectrometry in natural product research published in 2021 in *Journal of Biomedical Analysis*, the full paper can be found in Appendix A

Regarding **Chapter 2**, the nature and scope of my contribution were as follows:

Nature of contribution	**Extent of contribution (%)**
Literature search, co-wrote paper	85

The following co-authors have contributed to **Chapter 2**:

Name	**E-mail address**	**Nature of contribution**	**Extent of contribution (%)**
Marietjie A. Stander	lcms@sun.ac.za	Supervisor of the student, literature search, editing	3
André de Villiers	ajdevill@sun.ac.za	Co-supervisor of the student, conceptualised the idea for the topic and content of the paper, contributed to editing, co-wrote paper	12

Signature of candidate: … 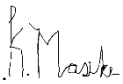 ……

Date: …25 February 2021……

Declaration by co-authors:

The undersigned confirm that:

The declaration above accurately reflects the nature and extent of the contributions of the candidate and the co-authors to **Chapter 2**,
No other authors contributed to **Chapter 2** besides those specified above, and
Potential conflicts of interest have been revealed to all interested parties and that the necessary changes have been made to use the material in Chapter 2 of this thesis.

Signature	**Institutional affiliation**	**Date**
	Stellenbosch University	17 February 2021
	Stellenbosch University	17 February 2021

Chapter 2: Literature Review

2.1. Natural compounds: An overview

Natural products have been used by humanity for centuries, and since the first isolation of morphine more than 200 years ago, isolated natural products have been a consistent source of new drug molecules.[1] The relative success of natural products in drug discovery stems from their versatile chemical structures and physiological targets, allowing them to be effective for a range of potential clinical uses.[2]

Often sparking confusion, the terms natural products and secondary metabolites are used interchangeably.[3–5] Secondary metabolites refer to chemical compounds that are not directly linked to the development, normal growth and the reproduction of the organism but are produced as a response to the organism's interaction with the environment.[3] Based on their biosynthetic origin, plant secondary metabolites include phenolics (flavonoid and non-flavonoids), alkaloids and terpenoids (such as saponins, steviol glycosides, etc.).[6,7] Whereas microbial secondary metabolites are classified as peptides, polyketides, alkaloids, lipids, and terpenes.[8–10] Some secondary metabolites such as terpenoid derivatives, carotenoids[11] and saponins,[12,13] are found both in terrestrial and marine sources. For the purpose of this work, we will be discussing plant secondary metabolites, specifically phenolic compounds.

2.2. Phenolic compounds

Phenolic compounds are biosynthesised from the shikimate-phenylpropanoid-flavonoid pathways.[14] These structurally diverse chemical compounds, range from single aromatic compounds to multi-ringed compounds, and are classified based on the number and arrangement of their carbon atoms (Table 2.1).[7] Phenolic compounds are revered for their purported biological activities, ranging from anti-inflammatory[15] to anti-cancer[16] properties. As stated above, phenolic compounds can be grouped into two classes: flavonoids and non-flavonoids and can exist as aglycones or conjugated to sugar derivatives.

2.2.1. Non-flavonoids

Non-flavonoids can further be divided into two main groups of dietary significance, whereby a benzene ring is attached to a carboxyl group to produce phenolic acids (C_6–C_1), or hydroxycinnamic acids (C_6–C_3)[7,14] (Table 2.1).

Table 2.1: Generic structures of phenolic and polyphenolic compounds (hydroxyl groups not shown). Reprinted with permission from Crozier *et al*. [7]

Number of carbons	Carbon skeleton	Classification	Example	Basic structure
7	C_6-C_1	Phenolic acids	Gallic acid	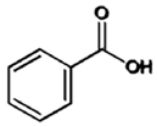
8	C_6-C_2	Acetophenones	Gallacetophenone	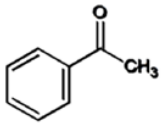
8	C_6-C_2	Phenylacetic acid	*p*-Hydroxyphenyl-acetic acid	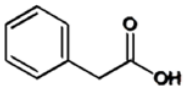
9	C_6-C_3	Hydroxycinnamic acid	*p*-Coumaric acid	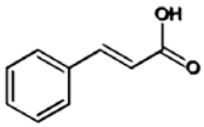
9	C_6-C_3	Coumarins	Esculetin	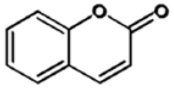
10	C_6-C_4	Naphthoquinones	Juglone	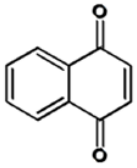
13	C_6-C_1-C_6	Xanthones	Mangiferin	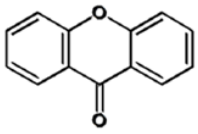
14	C_6-C_2-C_6	Stilbenes	Resveratrol	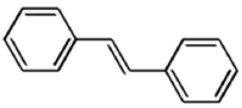
15	C_6-C_3-C_6	Flavonoids	Naringenin	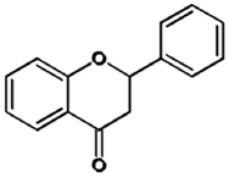

2.2.1.1. Phenolic acids

Phenolic acids are also referred to as benzoic acids or hydroxybenzoates and produced through the shikimate pathway.[7,16] The most widely distributed of phenolic acids being gallic,

protocatechuic, vanillic, and syringic acids.[16] Gallic acid is the most prominent phenolic acid due to its role in the biosynthetic production of hydrolysable tannins (grouped into gallotannins and ellagitannins).[7] The industrial applications of hydrolysable tannins in leather making and their contribution to the sensory properties (i.e. astringency) of tea and wine, highlight the importance of tannins.[7]

2.2.1.2. Hydroxycinnamic acids

Hydroxycinnamic acids are synthesised from the phenylpropanoid pathway, resulting in a range of hydroxycinnamates; *p*-coumaric acid, caffeic acid and ferulic acid.[7] These hydroxycinnamic acids form conjugates with organic acids (Figure 2.1) such as 1) tartaric acid resulting in derivatives such as caftaric acid[17] and dicaffeoyltartaric acid (L-chicoric acid),[18] 2) isocitric acid producing derivatives such as caffeoylisocitric acid[19] and, 3) quinic acid forming a class of compounds collectively referred to as chlorogenic acids[17] (e.g. caffeoylquinic acid, and dicaffeoylquinic acid). Furthermore, hydroxycinnamic acids can form conjugates with amino acids (producing caffeoylated amino acids such as clovamide)[20] and esters with sugar derivatives.

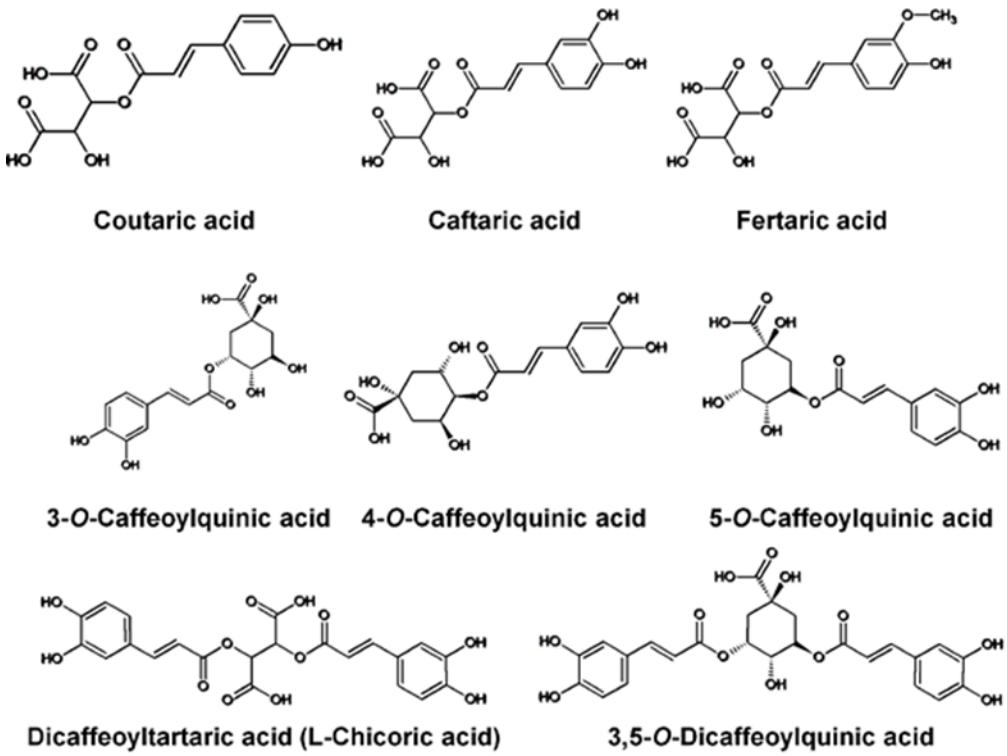

Figure 2.1: Structural representation of hydroxycinnamate (HCA) conjugates. Reprinted with permission from Crozier *et al*.[7]

2.2.2. Flavonoids

Flavonoids are the most ubiquitous compounds in the plant kingdom with varying structures, consisting of fifteen carbons distributed between two aromatic rings (A- and B-ring; Figure 2.2) which are connected by a three-carbon cyclic bridge (C-ring), C_6-C_3-C_6.[21] Flavonoids can be divided into a variety of classes such as flavonols (e.g. quercetin), flavones (e.g. luteolin), flavan-3-ols (e.g. catechin), anthocyanidins (e.g. cyanidins), flavanones (e.g. hesperetin), and isoflavones (e.g. biochanin A) (Figure 2.2).[7,21]

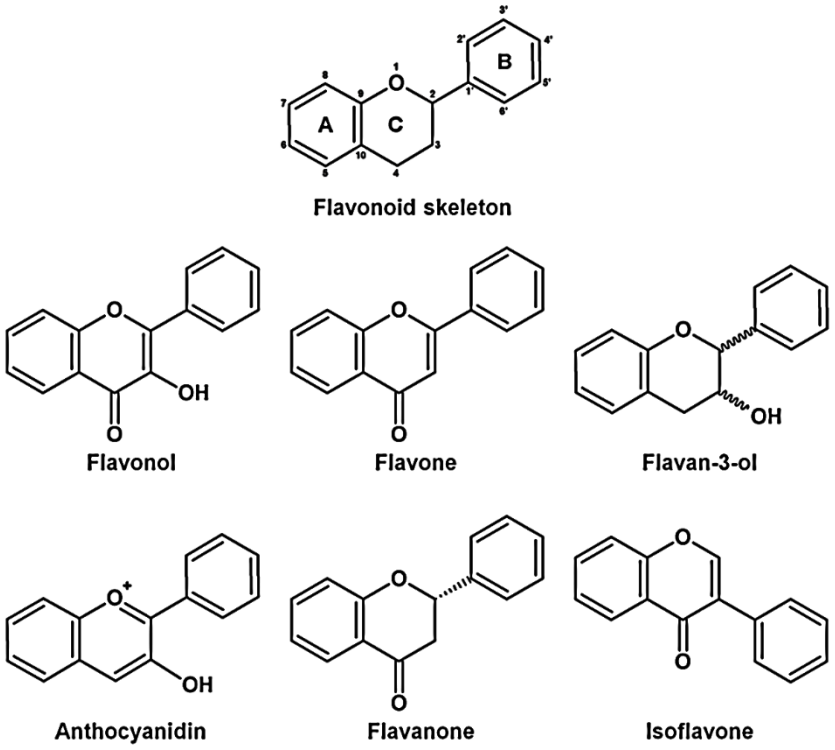

Figure 2.2: Generic structures of the flavonoids.

2.3. Analyses of plant secondary metabolites

Due to their vital role in the discovery of drug candidates,[22] the identification of plant secondary metabolites in what are often highly complex matrices is of paramount importance in the search for new biologically active compounds. In this endeavour, advanced analytical methods based on high resolution liquid- or gas chromatographic separation and/or mass spectrometric (LC- or GC and/or MS) detection are playing an increasingly important role, especially in screening analyses prior to isolation and structural elucidation by nuclear magnetic resonance (NMR).[23] Modern GC on high-efficiency capillary columns offer excellent performance for complex samples, with

noteworthy developments in sample preparation, comprehensive two-dimensional GC (GC×GC)[24] and detectors.[25,26] On the other hand, significant recent developments in HPLC, including the use of ultra-high pressures,[27] core-shell particles[28] and comprehensive two-dimensional LC (LC×LC)[29] have revolutionised the field and have played an important role in improving the performance of the technique for complex samples.

In the field of natural product analysis, however, advances in MS have arguably overshadowed those in chromatographic separations. Nowadays, exceptionally powerful high resolution and multi-stage MS instruments capable of a range of acquisition modes for different analysis goals are commercially available, and indeed are essential tools in any natural product laboratory.[23,30] Considering that the majority of natural products are non-volatile, state-of-the-art LC-MS has played an important role in the improvement of screening analyses of natural products.[31–35]

The availability of high resolution (HR) MS data allows determination of analyte molecular formulae, whereas tandem MS (MS/MS) instruments deliver fragmentation information essential for tentative identification purposes, the latter often acquired in data dependent acquisition (DDA) mode for complex unknown samples. Moreover, data-independent acquisition (DIA) strategies can be used to acquire both low- and high collision energy data (MS^E) in a single chromatographic run[36,37] at the expense of selectivity. These technologies greatly facilitate the tentative assignment of compounds in complex natural product extracts.

Nevertheless, chromatographic methods hyphenated to MS also show some limitations for natural product analysis. The complexity of biological matrices means that chromatographic resolution of all compounds is virtually impossible to attain, an important consideration especially in LC-MS, where mass spectra of natural products are often very similar for a given compound class and considering the susceptibility of electrospray ionisation (ESI) to matrix effects. Further analysis challenges include isomerisation encountered in biological samples.[38,39] For instance, hydroxycinnamic acids, such as caffeic acid, are understood to be synthesised in the *trans*-configuration by the phenylpropanoid pathway[40] however, these compounds readily convert to the *cis*-form when exposed to UV-light, thus the *trans*- and *cis*-geometry both exist in the chromatographic space.[40,41] In some cases, the *trans*-form results in three *cis*-isomers upon UV-irradiation, further complicating the chromatographic space.[41–43] Relying on the elution order has also been suggested,[41,44] however, notably the elution order is influenced by the column matrix.[44] Geometrical isomers of plant secondary metabolites were previously understood to exist in low/undetectable quantities and were thus considered to be biologically insignificant.[40] Some studies have noted, however, a prominence of these isomers in plant tissues that have been

exposed to the sun's UV rays,[45] possibly due to environmental changes. A natural occurrence of these geometrical isomers has also been highlighted.[46] This has prompted inquiry into the biological importance of *cis*-isomers, with significant bioactivity being attributed to the *cis*-forms.[43,47,48] The identification of these geometrical compounds using MS has proven to be challenging as these metabolites produce similar/identical tandem MS spectra. For instance, the isomeric constituents of *Cannabis sativa* (cannabis) are noted to produce the same MS/MS spectra but contrasting psychological effects.[38,39]

HR-MS instruments can mostly resolve isobaric compounds, but cannot differentiate isomers in most cases, necessitating long chromatographic runs to aid in their separation. This has driven efforts aimed at developing analytical methods capable of rapidly separating and detecting isomeric secondary metabolites.[42,49]

It is partially in the context of these limitations that the integration of ion mobility spectrometry (IMS) with MS has become such an appealing technology for the separation and detection of such structurally similar compounds.[50–52] IMS can be thought of as a form of gas-phase electrophoresis, whereby ions are separated based on their mobilities through a region filled with a buffer gas (typically either helium or nitrogen) under the influence of an electric field. The mobility of the ion is based on their physical properties (charge, size, and shape), with ions of lower masses (*m/z*) and/or more compact structures characterised by faster mobilities than larger and/or bulkier ions. For this reason, the application of IMS in complex biological samples allows the qualitative separation of biomolecules of different classes (Figure 2.3), with compact structures such as oligonucleotides having shorter drift times and stretched out compounds like lipids eluting from the drift cell later. Resulting in the increased application of IM-MS and LC-IM-MS in different biological fields.[53–67] Where the post-ionisation coupling of IMS to MS along with front-end separation techniques (like LC), allows species to be characterised based on an array of complementary descriptors (e.g. retention time, accurate mass information, tandem MS, and drift time) which helps increase molecular information content and specificity in structural identification.[56,57,65–74] A further benefit of IMS is that an ion's mobility can be converted to its collision cross section (CCS), a measure of an ion's average surface area. As different ions interact differently with the buffer gas, the incorporation of the IMS dimension to LC-HR-MS workflows provides additional structural information, which can help expedite the characterization of unknown isomeric compounds, particularly in untargeted workflows, such is the case in the omics era.[73,75–77]

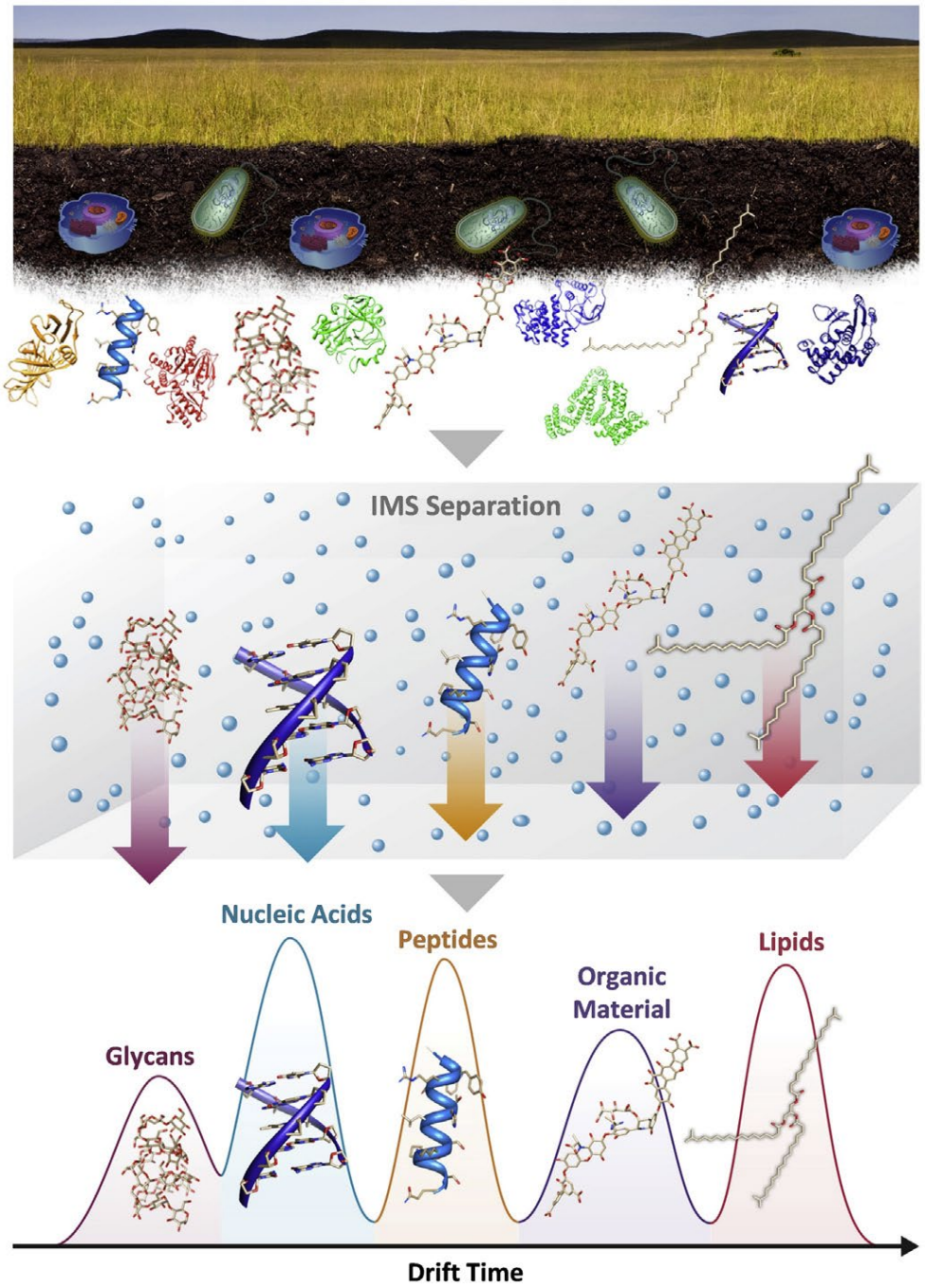

Figure 2.3: The application of IMS in complex biological samples allows the qualitative separation of biomolecules of different classes. Ions are separated based on their physical properties, oligonucleotides will transverse the IMS drift cell faster due to their compact nature, while lipids are slowest due to their rigid linear backbone. Reprinted with permission from Burnum-Johnson *et al*.[50]

2.3.1. Ion mobility spectrometry (IMS) techniques and instrumentation

The origins of IMS can be traced back to X-ray experiments in the late 19th century.[78] The technique, referred to as plasma chromatography[79,80] and ion chromatography[81] in early literature,

only found extensive analytical application since the 1970s following instrumental developments, including the hyphenation of IMS to MS from the early 1960s.[82] A major application area of IMS was (and remains) in security analyses, such as for the detection of chemical warfare agents, explosives, and drugs.[83,84] IMS was explored in biological research in the mid-1980s,[85] but it was only from the 1990s, when significant advances in both IMS and MS instrumentation coincided to drastically improve performance, that a resurgence in IMS applications occurred, mostly focusing on the analysis of biomolecules such as peptides and proteins.[86–89] The next decade saw the genesis of home-built IM-MS instruments,[90,91] a process continuing in recent years,[61,92–100] followed by the commercial availability of a travelling wave IM-MS instrument in 2006,[101] a drift tube IM-MS instrument in 2014,[78] a trapped IM-MS instrument in 2016[102] and in 2019 a cyclic IMS instrument.[103]

2.3.1.1. IMS platforms

According to the classification introduced by May and McLean, IM-MS instruments can be grouped based on their operational principles into time-dispersive, space-dispersive or ion confinement with selective release systems (Figure 2.4).[78] Time-dispersive techniques generate an arrival time spectrum reflecting the flow of ions past a specific location in the instrument. Drift tube IMS (DTIMS) and travelling wave IMS (TWIMS) devices are common time-dispersive platforms, where ions are directed through a stationary buffer gas. These techniques primarily differ in the applied electric field, which is a weak constant field in the case of DTIMS[79] and an oscillating electric field in the case of TWIMS.[92] Time-dispersive instruments allow all ions to be analysed simultaneously, and have found widespread application in untargeted omics approaches[75,76,78,104,105] as well as for targeted analyses in food and natural product research[39,66,73,106–110]. In ion confinement and selective release methods, such as trapped ion mobility spectrometry (TIMS), ions are trapped in position against a flow of buffer gas using an electric field, and released according to their mobilities as the electric field is incrementally decreased.[111,112] In space-dispersive platforms such as field asymmetric IMS (FAIMS; also known as differential mobility spectrometry (DMS) or differential IMS (DIMS)) and the differential mobility analyser (DMA), an electric field and carrier gas flow are used to direct ions of different mobilities along different drift paths, resulting in their separation in space.[83,111]

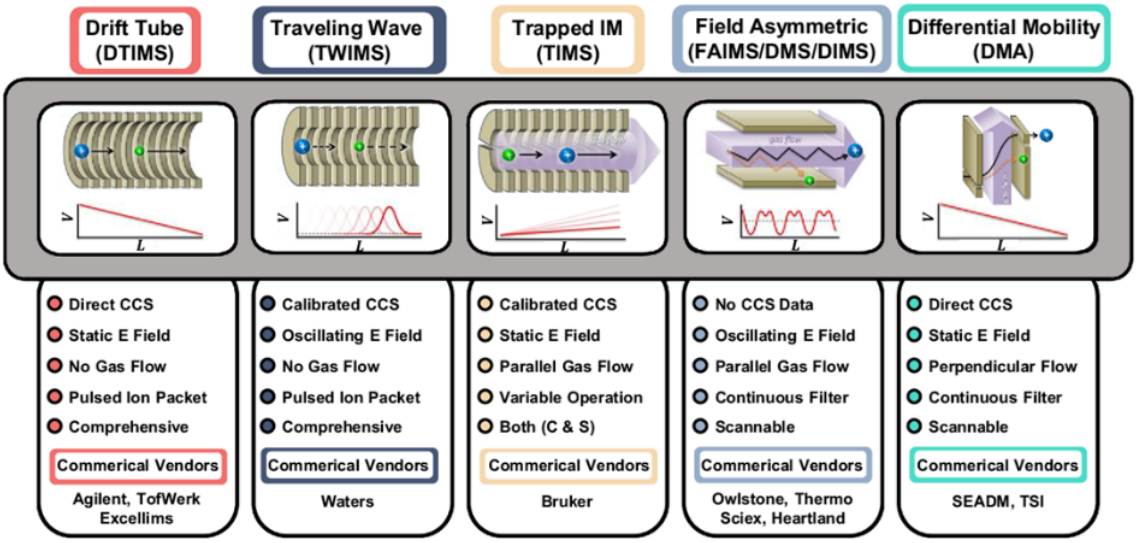

Figure 2.4: The five most common IMS platforms, which separate ions either in a time-dispersive (DTIMS and TWIMS), space-dispersive (FAIMS and DMA) or ion confinement with selective release (TIMS) manner. Reprinted with permission from Dodds and Baker.[111]

2.3.1.2. IM-MS instrumentation configurations

Commercial instrumentation from different manufacturers, ranging from portable devices to MS imaging instruments and systems incorporated in high-end mass spectrometers,[111,113] are available nowadays. A simplified generic schematic of an IMS-MS instrument is shown in Figure 2.5A. Most ionisation sources, as well as ambient ionisation techniques, can be used in combination with IMS, with the most common being ESI and matrix-assisted laser desorption/ionisation (MALDI). Similarly, most mass analysers have been combined with IMS, although time-of-flight based mass spectrometers (TOF) and quadrupole-TOF, (q-TOF) are mostly employed due to their fast duty cycles.[114] For tandem MS systems incorporating IMS, three configurations are possible, depending on the relative positions of the collision and IMS cells, i.e. where collision induced dissociation (CID) is performed.[84,115] Firstly, fragmentation can precede IMS separation if the collision cell is located before the IMS drift region (pre-mobility fragmentation), where mobility measurements are acquired for produced fragment ions (and unfragmented precursor ions). Secondly, in post-mobility fragmentation, fragmentation occurs after IMS separation and fragment ions have arrival times that align with their parent ions. This mode of operation is common in DTIM-MS instruments due to manufacturer's design.[114] Lastly, a combination of both modes of operation, termed time-aligned-parallel (TAP) fragmentation, is possible using commercial TWIM-MS instruments.[32,116] Here fragmentation occurs both before (in the trap ion guide) and after (in the transfer ion guide) the IMS separation (i.e. CID-IMS-CID) to produce 'MS^3' data[117] (Figure 2.5B). First generation fragment ions are separated by IMS, while

second generation ions share their arrival times. Incorporation of in-source fragmentation may be used to produce 'MS^4' spectra to discriminate between co-eluting isobaric compounds.[57]

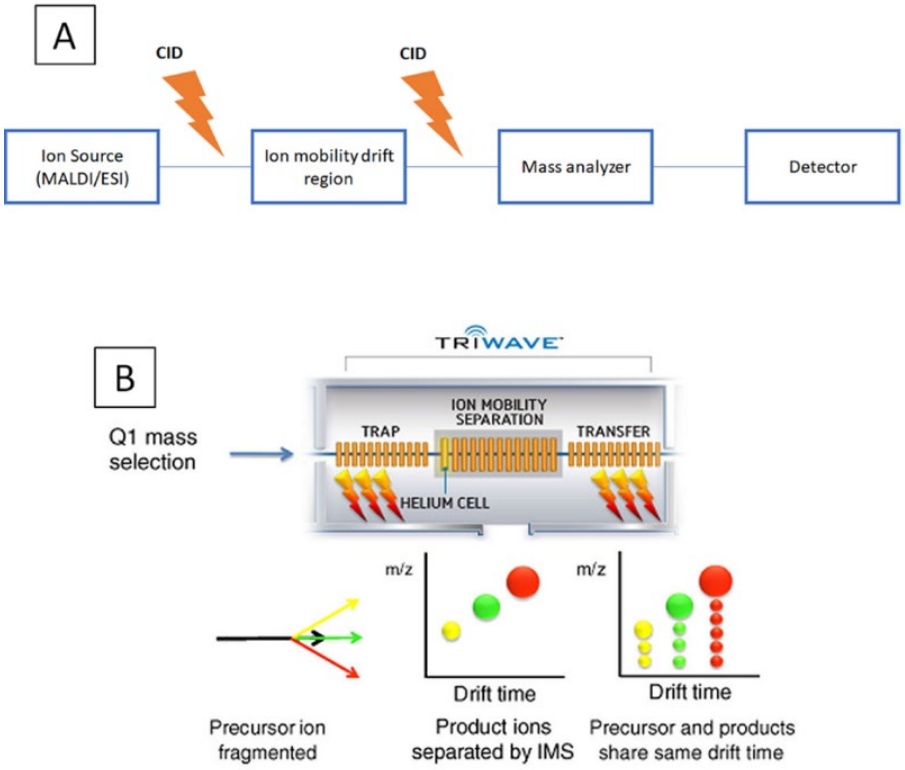

Figure 2.5: A simplified schematic of an IMS-MS instrumental configuration **A**). Depending on manufacturer design, fragmentation can occur before or after IMS separation. On a commercial TWIMS instrument, fragmentation can occur before and/or after IMS separation; the time-aligned-parallel (TAP) procedure is illustrated where fragmentation occurs in both trap and transfer ion guides **B**). **B**) is reprinted with permission from Sun *et al*.[117]

For data independent acquisition (DIA) methods such as 'MS^E', where low and high collision energy data are alternately measured without pre-selecting particular parent ions, IMS offers the clear benefit that co-eluting precursor ions can be separated by IMS prior to their fragmentation, thereby greatly increasing the performance of the method.[116] Alternative data acquisition strategies have been developed for different IMS instruments, parallel accumulation–serial fragmentation (PASEF) for TIMS being a notable example, where the quadrupole is rapidly scanned to allow large numbers of MS/MS experiments.[118]

2.3.1.3. IMS separation performance

The separation performance of IMS, is typically evaluated by means of the resolving power (R_p). However, comparing R_p values between different instruments is complicated by the fact that

separation principles differ between platforms.[78,119] For example, for DTIMS instruments a time-based definition of R_p, ($t/\Delta t$), is used,[120] whereas for TWIMS devices, although the time-based definition has been used, a definition of R_p in terms of the ions collision cross section is preferred ($CCS/\Delta CCS$).[119,121] In TIMS, R_p is defined in terms of mobility ($K/\Delta K$),[122,123] and for the filtering devices, FAIMS/DMS/DIMS, a definition for R_p in terms of the compensation field ($E_c/\Delta E_c$) is used.[124,125] DMA platforms can be used to measure K,[111] such that R_p can be defined in terms of the CCS-based definition.[119,126]

Due to the differences in separation mechanisms between IMS platforms, Dodds and colleagues suggested using a CCS-based definition of R_p to enable the cross-platform comparison of instruments (with the exception of FAIMS/DMS/DIMS, since CCS values cannot be determined using this platform).[119] According to this definition, R_p values for commercial DTIMS devices are ~60,[119,127] for TWIMS instruments ~40-50, and for TIMS systems between ~170-180 and as high as ~400.[128] For this reason, TIMS devices are considered ultra- high resolution instruments.[83]

The above rough comparison highlights that the most used commercial IMS instruments (DTIMS and TWIMS) are characterised by relatively low resolving power (40-60), which is typically sufficient to resolve ions differing in CCS values by ~1.5-3%, but not for the resolution of most stereoisomers (ΔCCS <1%) and enantiomers (ΔCCS ~0.1%).[119,127] Recent instrumental advances in TIMS[122,128] and TWIMS-based technologies, such as cyclic ion mobility (cIM)[103] and structures for lossless ion manipulations (SLIM)[98,129,130], as well as high pressure DTIMS instruments[61,90,96,131] and cyclic DTIMS[93,132] show promising improvement in IMS performance (R_p > 300, and up to 1000) for such demanding separations.

2.3.1.4. CCS values and their determination

The primary measured variable in IMS is an ion's mobility, K, which reflects the interactions between the ion and buffer gas molecules under conditions prevalent in the IMS cell. Measured mobilities are normalised to standard temperature and pressure conditions (STP 273.15 K and 760 Torr), providing the reduced mobility, K_0, for comparison purposes. An ion's reduced mobility can be converted to the collision cross section (CCS or Ω) via the Mason-Schamp equation.[80,133]

$$CCS = \frac{3}{16}\sqrt{\frac{2\pi}{\mu k_B T}}\frac{ze}{N_0 K_0} \qquad (1)$$

Where μ is the reduced mass of the ion-neutral collision complex ($=m_i m_g/(m_i+m_g)$, with m_i and m_g the mass of the ion and the buffer gas, respectively), k_B is Boltzmann's constant, T is the temperature of the gas in Kelvin, z is the ion's charge, e the elementary charge, N_0 is the number density of the drift gas at STP, and K_0 is the reduced mobility.

The CCS value, in units of square Ångström (Å^2), describes the number of collisions the molecular species' 3-dimensional structure encounters with the neutral buffer gas – a momentum transfer cross section[111,134] - which provides information about the ion's conformation. The CCS value therefore provides a potentially important descriptor of the ion, which is characteristic under defined conditions. It is for this reason that CCS values are increasingly being used as an additional identification criterion in compound assignment; it is therefore relevant to discuss briefly how CCS values can be determined in a reliable manner.

An important condition for the use of the Mason-Schamp equation is that measurements be performed under low-field conditions. A consequence of this is that FAIMS cannot be used to determine CCS values. If this condition is met, and provided a constant field is used, equation 1 can be used to derive CCS values from measured mobilities. This scenario applies to DTIMS instruments, where one of two methods may be used: single-field (calibrant-dependent)[135,136] and stepped-field (calibrant-independent)[120,136] approaches. The stepped-field method is considered the gold standard, as CCS values can be calculated directly from the drift time (derived from the measured arrival time) according to the Mason-Schamp equation[120,136], provided all other parameters in equation 1 are known to a high degree of accuracy. This method uses multiple measurements at different field strengths to derive the drift time used to calculate K. The stepped field method is not compatible with chromatographic separation due to its long cycle times. In contrast, the single-field approach uses a single drift voltage to measure arrival times[135,136], and CCS values of unknowns are derived from regression analysis of arrival times vs. CCS values measured for calibrants with known, standardized CCS values under identical conditions as used for the unknown(s). Agilent's ESI-L Low Concentration Tune Mix, which contains betaine, trifluoracetic acid ammonium salt, and a series of fluorinated phosphazenes and triazines, is commonly used as calibrant during DTIMS analyses. Stow *et al*. showed in a recent inter-laboratory study that CCS values obtained using the stepped field method are exceptionally reproducible.[136] Comparison of the two methods showed an average error of 0.54% attributed to the single-field measured CCS values, compared to a 0.34% for the stepped-field values.[136]

TWIMS uses low but variable fields, and as such requires calibration to derive experimental CCS values. Similar to the single-field DTIMS method, CCS values of unknowns are obtained

from calibration using molecules with known CCS values under defined conditions.[62,137] The most used calibrant is poly-DL-alanine, for which CCS reference values were measured by DTIMS. Clearly, the accuracy of CCS values derived using such calibration procedures depends on the suitability of the calibrant. Calibration errors have been noted when using calibrants structurally and chemically unrelated to the target molecules, as when peptide calibrants were used to determine CCS values of lipid[62] and small drug-like compounds.[138] Poly-DL-alanine (n=3 to n=14) covers the mass range 231 to 1012 Da (CCS values of 150-308 $Å^2$ in ESI^- and 151-306 $Å^2$ in ESI^+ with nitrogen as drift gas),[59,67,139] and small compounds outside this mass range are subject to higher CCS errors.[138] Such issues can be circumvented by the judicious selection of suitable calibrants, such as a mixture of poly-DL-alanine and drug-like molecules used by Hines *et al*.[138] It is worth noting that calibration strategies using negative ion mode have received relatively little attention, even though many plant secondary metabolites for instance are acidic in nature and are preferentially ionised in negative mode. Dextran has been used as a calibrant to measure CCS values of oligosaccharides in negative ionisation mode,[137] and poly-L-malic acid (n=1 to n=8, mass range 134 to 946 Da) as calibrant for the analysis of negatively-charged analytes under 1 kilodalton (kDa).[140]

Although CCS measurements using TIMS is in theory possible from first principles, in practice calibration procedures are often used as outlined in[112,122,141]. Schroeder *et al*. used the Agilent Tune Mix as calibrant to generate a CCS library for 146 plant secondary metabolites.[69] DMA can be used to measure *K* directly, although DTIMS is more commonly used as a reference method for CCS determination since DMA is primarily applied for very large molecules. In practice, calibration approaches are also used to derive CCS in DMA.[142]

Inconsistencies in how IMS data was reported, especially in earlier work, prompted Gabelica and co-workers to describe a comprehensive set of recommendations for IMS measurements.[134] These authors called for the standardization of the manner in which CCS values are measured and reported on particular platforms,[67,136] and highlighted considerations for comparing CCS data obtained on different platforms.[134] A notable consideration is that the drift gas composition should always be specified, as calibrant CCS values obtained using nitrogen (N_2) are often larger compared to those obtained using helium (He).[139,143] The nomenclature $^{TW}CCS_{N2}$ or $^{DT}CCS_{He}$ was suggested, where the superscript denotes the IMS technique and the subscript specifies the buffer gas composition used to derive the CCS value;[144,145] this nomenclature is also used in the present work.

2.3.1.4.1. The utility of CCS values in compound annotation

CCS values can be used to study gas-phase phenomena, and as such are useful in physical chemistry[146,147] and in the study of biological molecules' conformations.[148] From an analytical chemistry perspective, though, the main application of CCS values is as a complementary descriptor to chromatographic, spectroscopic and MS data for the identification of compounds. Databases such as HMDB[149] and METLIN[150] often suggest multiple potential metabolite hits based on HR-MS data, thus using CCS values to aid with identity confirmation is of analytical interest. One of the attractive features of CCS values in this context is their precision. For example, in inter-laboratory studies Paglia *et al*. found $^{TW}CCS_{N2}$ values to be more reproducible (97% of compounds within 2% RSD) than retention times (80% within 2% RSD) for 125 common metabolites,[67] while the stepped-field method using DTIMS demonstrated a 0.29% RSD for CCS measurements.[136]

Experimental CCS searchable databases have been created for lipids,[59,151,152] peptides,[55,94] N-glycans,[137] toxins,[153] pesticides,[154] drug-like compounds,[138,154] metabolites[58,67] and various biomolecules.[120,155] Furthermore, prediction of CCS values using computation methods is a fast-growing field.[156–161]

While it is essential to consider the requirements of accuracy in reported CCS values as discussed above, the availability of reliable CCS databases clearly shows promise for the incorporation of IMS into hyphenated chromatography-MS workflows for the identification of unknown compounds (Figure 2.6). In this endeavour, a distinction between "known-unknowns" (i.e., an analyte for which MS and CCS data determined for the standard are available online) and "unknown-unknowns" (representing analytes without a database hit, no *m/z* or CCS value) can be made. In the case of "unknown-unknowns", mass-mobility trendlines (CCS values vs *m/z*) can be used to assign the chemical class of the analyte.[58,138,155] Furthermore, one study showed that the addition of CCS filters as an identification criterion to a < 5 ppm (parts per million) mass window also decreased the number of false positive results,[162] thus increasing identification reliability.

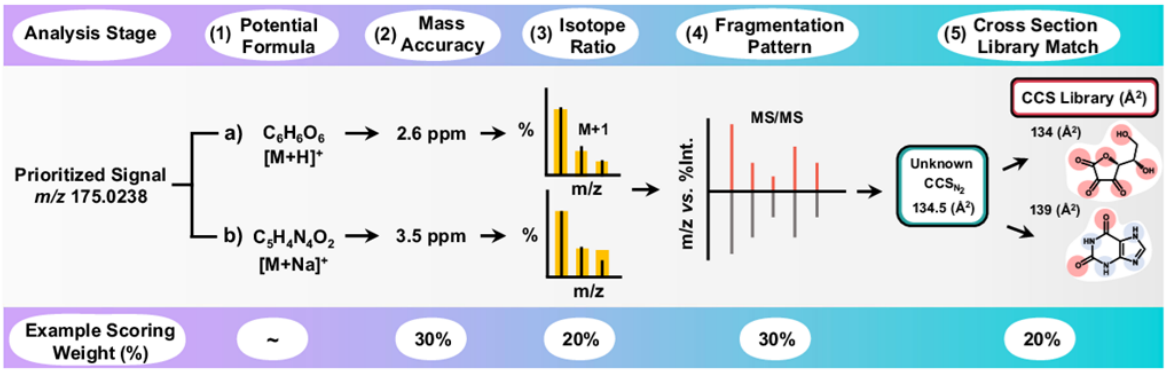

Figure 2.6: Example of a workflow used in the identification of a "known-unknown" analyte using both *m/z* and CCS data to increase confidence in annotation. Reprinted with permission from Dodds and Baker.[111]

2.3.1.5. IMS data analysis and chemometrics

Incorporating IMS into chromatography-MS workflows increases data dimensionality (Figure 2.7): in principle, a hyphenated chromatography-IM-MS methods produces three-dimensional data, whereas comprehensive two-dimensional chromatographic (LC×LC) analysis adds a further dimension.[106,163,164] IMS also greatly increases datafile size, such that data storage and analyses of large datasets, as is common in the omics fields, are of concern.[165]

While a range of commercial software packages are available for the analysis of IMS data (Figure 2.7A), these are mostly instrument specific. However, 2D IM-MS data (Figure 2.7B) can also be exported and processed (peak alignment and picking) using different pre-processing and pattern recognition techniques,[165] and online tools such as XCMS[166,167] can be used for alignment to yield a data matrix containing mobility/drift time, *m/z* data and peak intensity. Depending on the goal of the analyses, unsupervised (principal component analysis (PCA), hierarchical cluster analysis (HCA), etc.) or supervised (partial least squares discriminant analysis (PLS-DA) etc.) pattern recognition techniques can be used for data interpretation. Higher dimensional IMS data is compatible with open source packages, as demonstrated by the incorporation of LC-IMS-CID-MS data into Skyline [168] and *ORIGAMI* [169] for data analysis purposes, and freely available software for visualisation and interpretation of comprehensive two-dimensional LC×LC×IM-MS data (Figure 2.7D).[106] Indeed, chemometric methods are increasingly being used for the analysis of IMS data, in natural product analysis.[106,170–190]

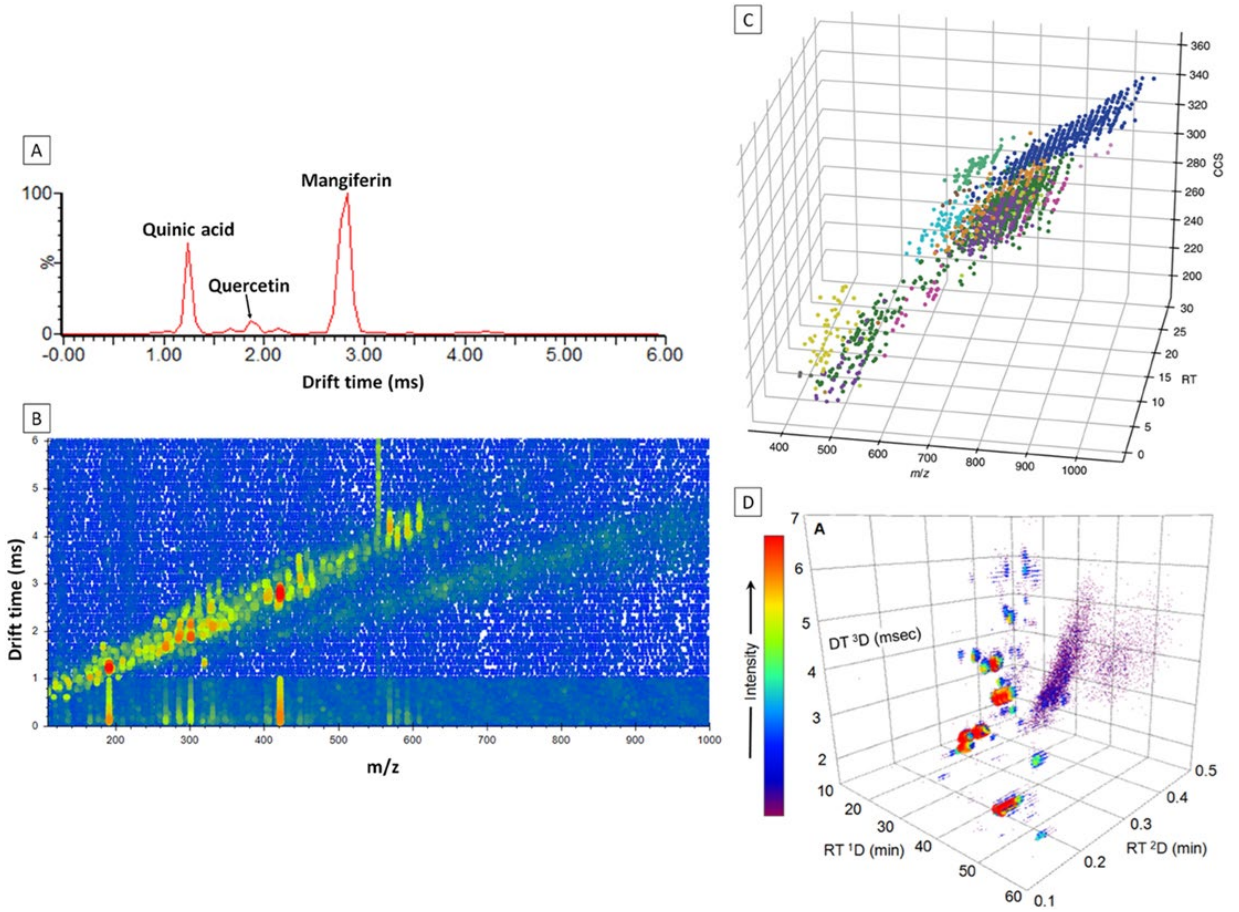

Figure 2.7: Illustration of the data dimensionality in IMS hyphenation. Ion mobility spectrum of *Cyclopia genistoides* (honeybush tea) phytochemicals (1-D data) **A**), corresponding mass-mobility trendlines of *C. genistoides* phytochemicals (2-D data) **B**) (both are unpublished data from our group), LC-IMS-MS separation of lipids (3-D data) **C**) (reprinted with permission from Vasilopoulou *et al*.[191]) and three-dimensional representation of comprehensive two-dimensional LC (LC×LC)×IMS-MS **D**) separation of grape seed phenolics (MS dimension not represented) from Venter *et al*.[106]

Summary

The identification of plant secondary metabolites (specifically phenolic compounds), in what are often highly complex matrices, is of paramount importance in the search for new biologically active compounds. IMS shows promise as an additional tool to enhance the performance of current analytical methods used to identify viable candidates, particularly structurally similar secondary metabolites. The technique extracts complementary structural information to LC-MS workflows. Thus, allowing species to be characterised based on an array of complementary descriptors (e.g., retention time, mass spectral information (including high resolution and tandem MS data), spectroscopic data and CCS value), which increases molecular information content and specificity in structural identification. Such structural information can then be used to develop

an in-house phenolic compound library. As different ions interact differently with the buffer gas, the incorporation of CCS values to LC-HR-MS workflows provides additional structural information, which can help in different studies such as to: 1) expedite the characterization of phenolic compounds in natural product research, 2) improve metabolite identification confidence in plant metabolomics, 3) use phenolic compound as markers to aid in the differentiation of plant species and 4) use phenolic compound markers in food adulteration studies.

2.4. References

(1) Newman, D. J.; Cragg, G. M. Natural Products as Sources of New Drugs over the Nearly Four Decades from 01/1981 to 09/2019. *J. Nat. Prod.* **2020**, *83* (3), 770–803. https://doi.org/10.1021/acs.jnatprod.9b01285.

(2) Newman, D. J.; Cragg, G. M. Natural Products as Sources of New Drugs from 1981 to 2014. *J. Nat. Prod.* **2016**, *79* (3), 629–661. https://doi.org/10.1021/acs.jnatprod.5b01055.

(3) Daniel, M. Secondary Metabolites. *Med. Plants* **2006**, 5–8. https://doi.org/10.1201/b11003-3.

(4) Dias, D. A.; Urban, S.; Roessner, U. A Historical overview of natural products in drug discovery. *Metabolites* **2012**, *2* (2), 303–336. https://doi.org/10.3390/metabo2020303.

(5) Johnson, A. R.; Carlson, E. E. Collision-induced dissociation mass spectrometry: A powerful tool for natural product structure elucidation. *Anal. Chem.* **2015**, *87* (21), 10668–10678. https://doi.org/10.1021/acs.analchem.5b01543.

(6) Bourgaud, F.; Gravot, A.; Milesi, S.; Gontier, E. Production of plant secondary metabolites: A historical perspective. *Plant Sci.* **2001**, *161* (5), 839–851. https://doi.org/10.1016/S0168-9452(01)00490-3.

(7) Crozier, A.; Jaganath, B. I.; Clifford, N. M. Phenols, polyphenols and tannins: An overview. In *Plant Secondary Metabolites: Occurrence, Structure and Role in the Human Diet*; Crozier, A., Clifford, N. M., Ashihara, H., Eds.; Blackwell Publishing Ltd, 2006; pp 1–25. https://doi.org/1-4051-2509-8 Library.

(8) Dittmann, E.; Gugger, M.; Sivonen, K.; Fewer, D. P. Natural product biosynthetic diversity and comparative genomics of the cyanobacteria. *Trends Microbiol.* **2015**, *23* (10), 642–652. https://doi.org/10.1016/j.tim.2015.07.008.

(9) Hasan, S.; Ansari, M.; Ahmad, A.; Mishra, M. Major bioactive metabolites from marine fungi: A review. *Bioinformation* **2015**, *11* (4), 176–181. https://doi.org/10.6026/97320630011176.

(10) Keller, N. P.; Turner, G.; Bennett, J. W. Fungal secondary metabolism - from biochemistry to genomics. *Nat. Rev. Microbiol.* **2005**, *3* (12), 937–947. https://doi.org/10.1038/nrmicro1286.

(11) Walter, M. H.; Strack, D. Carotenoids and their cleavage products: biosynthesis and

functions. *Nat. Prod. Rep.* **2011**, *28* (4), 663–692. https://doi.org/10.1039/c0np00036a.

(12) Sparg, S. G.; Light, M. E.; Van Staden, J. Biological activities and distribution of plant saponins. *J. Ethnopharmacol.* **2004**, *94* (2–3), 219–243. https://doi.org/10.1016/j.jep.2004.05.016.

(13) Bahrami, Y.; Zhang, W.; Franco, C. M. M. Distribution of saponins in the sea cucumber *Holothuria lessoni*; the body wall versus the viscera, and their biological activities. *Mar. Drugs* **2018**, *16* (11). https://doi.org/10.3390/md16110423.

(14) Sytar Oksana. Plant phenolic compounds for food, pharmaceutical and cosmetics production. *J. Med. Plants Res.* **2012**, *6* (13), 2526–2539. https://doi.org/10.5897/JMPR11.1695.

(15) Ambriz-Pérez, D. L.; Leyva-López, N.; Gutierrez-Grijalva, E. P.; Heredia, J. B. Phenolic compounds: natural alternative in inflammation treatment. A review. *Cogent Food Agric.* **2016**, *2* (1). https://doi.org/10.1080/23311932.2015.1131412.

(16) Carocho, M.; Ferreira, I. The role of phenolic compounds in the fight against cancer – A review. *Anticancer. Agents Med. Chem.* **2013**, *13* (8), 1236–1258. https://doi.org/10.2174/18715206113139990301.

(17) Clifford, M. N. Chlorogenic acids and other cinnamates - Nature, occurrence, dietary burden, absorption and metabolism. *J. Sci. Food Agric.* **2000**, *80* (7), 1033–1043. https://doi.org/10.1002/(SICI)1097-0010(20000515)80:7<1033::AID-JSFA595>3.0.CO;2-T.

(18) Lee, J.; Scagel, C. F. Chicoric acid: chemistry, distribution, and production. *Front. Chem.* **2013**, *1* (December), 1–17. https://doi.org/10.3389/fchem.2013.00040.

(19) Masike, K.; Mhlongo, M. I.; Mudau, S. P.; Nobela, O.; Ncube, E. N.; Tugizimana, F.; George, M. J.; Madala, N. E. Highlighting mass spectrometric fragmentation differences and similarities between hydroxycinnamoyl-quinic acids and hydroxycinnamoyl-isocitric acids. *Chem. Cent. J.* **2017**, *11* (1), 29. https://doi.org/10.1186/s13065-017-0262-8.

(20) Masike, K.; Khoza, B. S.; Steenkamp, P. A.; Smit, E.; Dubery, I. A.; Madala, N. E. A Metabolomics-guided exploration of the phytochemical constituents of *Vernonia fastigiata* with the aid of pressurized hot water extraction and liquid chromatography-mass spectrometry. *Molecules* **2017**, *22* (8). https://doi.org/10.3390/molecules22081200.

(21) Kumar, S.; Pandey, A. K. Chemistry and biological activities of flavonoids: An overview. *Sci. World J.* **2013**, *2013* (4), 1–16. https://doi.org/10.1155/2013/162750.

(22) Butler, M. S.; Robertson, A. A. B.; Cooper, M. A. Natural product and natural product derived drugs in clinical trials. *Nat. Prod. Rep.* **2014**, *31* (11), 1612–1661. https://doi.org/10.1039/c4np00064a.

(23) Wolfender, J. L.; Marti, G.; Thomas, A.; Bertrand, S. Current approaches and challenges for the metabolite profiling of complex natural extracts. *J. Chromatogr. A* **2015**, *1382*, 136–164. https://doi.org/10.1016/j.chroma.2014.10.091.

(24) Amaral, M. S. S.; Nolvachai, Y.; Marriott, P. J. Comprehensive two-dimensional gas chromatography advances in technology and applications: Biennial update. *Anal. Chem.* **2020**, *92* (1), 85–104. https://doi.org/10.1021/acs.analchem.9b05412.

(25) Peterson, A. C.; Mcalister, G. C.; Quarmby, S. T.; Griep-raming, J.; Coon, J. J. Development and characterization of a gc-enabled qlt-orbitrap for high-resolution and high-mass accuracy GC/MS. **2010**, *82* (20), 8618–8628.

(26) Schug, K. A.; Sawicki, I.; Carlton, D. D.; Fan, H.; McNair, H. M.; Nimmo, J. P.; Kroll, P.; Smuts, J.; Walsh, P.; Harrison, D. Vacuum ultraviolet detector for gas chromatography. *Anal. Chem.* **2014**, *86* (16), 8329–8335. https://doi.org/10.1021/ac5018343.

(27) Broeckhoven, K.; Desmet, G. Advances and challenges in extremely high-pressure liquid chromatography in current and future analytical scale column formats. *Anal. Chem.* **2020**, *92* (1), 554–560. https://doi.org/10.1021/acs.analchem.9b04278.

(28) Hayes, R.; Ahmed, A.; Edge, T.; Zhang, H. Core-shell particles: Preparation, fundamentals and applications in high performance liquid chromatography. *J. Chromatogr. A* **2014**, *1357*, 36–52. https://doi.org/10.1016/j.chroma.2014.05.010.

(29) Pirok, B. W. J.; Stoll, D. R.; Schoenmakers, P. J. Recent developments in two-dimensional liquid chromatography: Fundamental improvements for practical applications. *Anal. Chem.* **2019**, *91* (1), 240–263. https://doi.org/10.1021/acs.analchem.8b04841.

(30) Ganzera, M.; Sturm, S. Recent advances on HPLC/MS in medicinal plant analysis—An update covering 2011–2016. *J. Pharm. Biomed. Anal.* **2018**, *147*, 211–233. https://doi.org/10.1016/j.jpba.2017.07.038.

(31) De Villiers, A.; Venter, P.; Pasch, H. Recent advances and trends in the liquid-

chromatography-mass spectrometry analysis of flavonoids. *J. Chromatogr. A* **2015**, *1430*, 16–78. https://doi.org/10.1016/j.chroma.2015.11.077.

(32) Holčapek, M.; Jirásko, R.; Lísa, M. Recent developments in liquid chromatography-mass spectrometry and related techniques. *J. Chromatogr. A* **2012**, *1259*, 3–15. https://doi.org/10.1016/j.chroma.2012.08.072.

(33) Wu, H.; Guo, J.; Chen, S.; Liu, X.; Zhou, Y.; Zhang, X.; Xu, X. Recent developments in qualitative and quantitative analysis of phytochemical constituents and their metabolites using liquid chromatography-mass spectrometry. *J. Pharm. Biomed. Anal.* **2013**, *72* (151), 267–291. https://doi.org/10.1016/j.jpba.2012.09.004.

(34) Xing, J.; Xie, C.; Lou, H. Recent applications of liquid chromatography-mass spectrometry in natural products bioanalysis. *J. Pharm. Biomed. Anal.* **2007**, *44* (2), 368–378. https://doi.org/10.1016/j.jpba.2007.01.010.

(35) Xu, W.; Luo, G.; Yu, F.; Jia, Q.; Zheng, Y.; Bi, X.; Lei, J. Characterization of anthocyanins in the hybrid progenies derived from *Iris dichotoma* and *I. domestica* by HPLC-DAD-ESI/MS analysis. *Phytochemistry* **2018**, *150*, 60–74. https://doi.org/10.1016/j.phytochem.2018.03.003.

(36) Doerr, A. DIA mass spectrometry. *Nat. Methods* **2015**, *12* (1), 35. https://doi.org/10.1038/nmeth.3234.

(37) Plumb, R. S.; Johnson, K. A.; Rainville, P.; Smith, B. W.; Wilson, I. D.; Castro-Perez, J. M.; Nicholson, J. K. UPLC/MS^{E}; a new approach for generating molecular fragment information for biomarker structure elucidation. *Rapid Commun. Mass Spectrom.* **2006**, *20* (13), 1989–1994. https://doi.org/10.1002/rcm.2550.

(38) Zuardi, A. W.; Crippa, J. A. S.; Hallak, J. E. C.; Moreira, F. A.; Guimarães, F. S. Cannabidiol, a *Cannabis sativa* constituent, as an antipsychotic drug. *Brazilian J. Med. Biol. Res.* **2006**, *39* (4), 421–429. https://doi.org/10.1590/S0100-879X2006000400001.

(39) Tose, L. V.; Santos, N. A.; Rodrigues, R. R. T.; Murgu, M.; Gomes, A. F.; Vasconcelos, G. A.; Souza, P. C. T.; Vaz, B. G.; Romão, W. Isomeric separation of cannabinoids by UPLC combined with ionic mobility mass spectrometry (TWIM-MS)—Part I. *Int. J. Mass Spectrom.* **2017**, *418*, 112–121. https://doi.org/10.1016/j.ijms.2016.10.018.

(40) Salum, M. L.; Erra-Balsells, R. High Purity *cis*-cinnamic acid preparation for studying

physiological role of *trans*-cinnamic and *cis*-cinnamic acids in higher plants. *Environ. Control Biol.* **2013**, *51* (1), 1–10. https://doi.org/10.2525/ecb.51.1.

(41) Clifford, M. N.; Kirkpatrick, J.; Kuhnert, N.; Roozendaal, H.; Salgado, P. R. LC-MS^n analysis of the *cis* isomers of chlorogenic acids. *Food Chem.* **2008**, *106* (1), 379–385. https://doi.org/10.1016/j.foodchem.2007.05.081.

(42) Makola, M. M.; Steenkamp, P. A.; Dubery, I. A.; Kabanda, M. M.; Madala, N. E. Preferential alkali metal adduct formation by *cis* geometrical isomers of dicaffeoylquinic acids allows for efficient discrimination from their *trans* isomers during ultra-high-performance liquid chromatography/quadrupole time-of-flight mass spectrometry. *Rapid Commun. Mass Spectrom.* **2016**, *30* (8), 1011–1018. https://doi.org/10.1002/rcm.7526.

(43) Masike, K.; Tugizimana, F.; Ndlovu, N.; Smit, E.; du Preez, L.; Dubery, I.; Madala, E. Deciphering the influence of column chemistry and mass spectrometry settings for the analyses of geometrical isomers of L-chicoric acid. *J. Chromatogr. B Anal. Technol. Biomed. Life Sci.* **2017**, *1052*, 73–81. https://doi.org/10.1016/j.jchromb.2017.03.023.

(44) Masike, K.; Dubery, I.; Steenkamp, P.; Smit, E.; Madala, E. Revising reverse-phase chromatographic behavior for efficient differentiation of both positional and geometrical isomers of dicaffeoylquinic acids. *J. Anal. Methods Chem.* **2018**, *2018*. https://doi.org/10.1155/2018/8694579.

(45) Karaköse, H.; Jaiswal, R.; Deshpande, S.; Kuhnert, N. Investigation of the photochemical changes of chlorogenic acids induced by ultraviolet light in model systems and in agricultural practice with *Stevia rebaudiana* cultivation as an example. *J. Agric. Food Chem.* **2015**, *63* (13), 3338–3347. https://doi.org/10.1021/acs.jafc.5b00838.

(46) Mhlongo, M. I.; Piater, L. A.; Steenkamp, P. A.; Madala, N. E.; Dubery, I. A. Metabolomic fingerprinting of primed tobacco cells provide the first evidence for the biological origin of *cis*-chlorogenic acid. *Biotechnol. Lett.* **2015**, *37* (1), 205–209. https://doi.org/10.1007/s10529-014-1645-8.

(47) Makola, M. M.; Dubery, I. A.; Koorsen, G.; Steenkamp, P. A.; Kabanda, M. M.; Du Preez, L. L.; Madala, N. E. The effect of geometrical isomerism of 3,5-dicaffeoylquinic acid on its binding affinity to hiv-integrase enzyme: A molecular docking study. *Evidence-based Complement. Altern. Med.* **2016**, *2016* (Ccd), 1–10. https://doi.org/10.1155/2016/4138263.

(48) Chen, Y. L.; Huang, S. T.; Sun, F. M.; Chiang, Y. L.; Chiang, C. J.; Tsai, C. M.; Weng, C.

J. Transformation of cinnamic acid from *trans*- to *cis*-form raises a notable bactericidal and synergistic activity against multiple-drug resistant *Mycobacterium tuberculosis*. *Eur. J. Pharm. Sci.* **2011**, *43* (3), 188–194. https://doi.org/10.1016/j.ejps.2011.04.012.

(49) Masike, K.; Madala, N. Synchronized survey scan approach allows for efficient discrimination of isomeric and isobaric compounds during LC-MS/MS analyses. *J. Anal. Methods Chem.* **2018**, *2018*, 1–9. https://doi.org/10.1155/2018/2046709.

(50) Burnum-Johnson, K. E.; Zheng, X.; Dodds, J. N.; Ash, J.; Fourches, D.; Nicora, C. D.; Wendler, J. P.; Metz, T. O.; Waters, K. M.; Jansson, J. K.; Smith, R. D.; Baker, E. S. Ion mobility spectrometry and the Omics: Distinguishing isomers, molecular classes and contaminant ions in complex samples. *TrAC - Trends Anal. Chem.* **2019**, *116*, 292–299. https://doi.org/10.1016/j.trac.2019.04.022.

(51) Levy, A. J.; Oranzi, N. R.; Ahmadireskety, A.; Kemperman, R. H. J.; Wei, M. S.; Yost, R. A. Recent progress in metabolomics using ion mobility-mass spectrometry. *TrAC - Trends Anal. Chem.* **2019**, *116*, 274–281. https://doi.org/10.1016/j.trac.2019.05.001.

(52) Wu, Q.; Wang, J.-Y.; Han, D.-Q.; Yao, Z.-P. Recent advances in differentiation of isomers by ion mobility mass spectrometry. *TrAC Trends Anal. Chem.* **2020**, *124*, 115801. https://doi.org/10.1016/j.trac.2019.115801.

(53) Baker, E. S.; Burnum-Johnson, K. E.; Ibrahim, Y. M.; Orton, D. J.; Monroe, M. E.; Kelly, R. T.; Moore, R. J.; Zhang, X.; Théberge, R.; Costello, C. E.; Smith, R. D. Enhancing bottom-up and top-down proteomic measurements with ion mobility separations. *Proteomics* **2015**, *15* (16), 2766–2776. https://doi.org/10.1002/pmic.201500048.

(54) Dwivedi, P.; Schultz, A. J.; Hill, H. H. Metabolic profiling of human blood by high-resolution ion mobility mass spectrometry (IM-MS). *Int. J. Mass Spectrom.* **2010**, *298* (1–3), 78–90. https://doi.org/10.1016/j.ijms.2010.02.007.

(55) Valentine, S. J.; Plasencia, M. D.; Liu, X.; Krishnan, M.; Naylor, S.; Udseth, H. R.; Smith, R. D.; Clemmer, D. E. Toward plasma proteome profiling with ion mobility-mass spectrometry. *J. Proteome Res.* **2006**, *5* (11), 2977–2984. https://doi.org/10.1021/pr060232i.

(56) Zang, X.; Monge, M. E.; Gaul, D. A.; Fernández, F. M. Flow injection-traveling-wave ion mobility-mass spectrometry for prostate-cancer metabolomics. *Anal. Chem.* **2018**, *90* (22), 13767–13774. https://doi.org/10.1021/acs.analchem.8b04259.

(57) Zhang, H.; Zheng, D.; Li, H. H.; Wang, H.; Tan, H. S.; Xu, H. X. Diagnostic filtering to screen polycyclic polyprenylated acylphloroglucinols from *Garcinia oblongifolia* by ultrahigh performance liquid chromatography coupled with ion mobility quadrupole time-of-flight mass spectrometry. *Anal. Chim. Acta* **2016**, *912*, 85–96. https://doi.org/10.1016/j.aca.2016.01.039.

(58) Zheng, X.; Aly, N. A.; Zhou, Y.; Dupuis, K. T.; Bilbao, A.; Paurus, V. L.; Orton, D. J.; Wilson, R.; Payne, S. H.; Smith, R. D.; Baker, E. S. A Structural examination and collision cross section database for over 500 metabolites and xenobiotics using drift tube ion mobility spectrometry. *Chem. Sci.* **2017**, *8* (11), 7724–7736. https://doi.org/10.1039/c7sc03464d.

(59) Paglia, G.; Angel, P.; Williams, J. P.; Richardson, K.; Olivos, H. J.; Thompson, J. W.; Menikarachchi, L.; Lai, S.; Walsh, C.; Moseley, A.; Plumb, R. S.; Grant, D. F.; Palsson, B. O.; Langridge, J.; Geromanos, S.; Astarita, G. Ion mobility-derived collision cross section as an additional measure for lipid fingerprinting and identification. *Anal. Chem.* **2015**, *87* (2), 1137–1144. https://doi.org/10.1021/ac503715v.

(60) Fenn, L. S.; Kliman, M.; Mahsut, A.; Zhao, S. R.; McLean, J. A. Characterizing ion mobility-mass spectrometry conformation space for the analysis of complex biological samples. *Anal. Bioanal. Chem.* **2009**, *394* (1), 235–244. https://doi.org/10.1007/s00216-009-2666-3.

(61) Groessl, M.; Graf, S.; Knochenmuss, R. High resolution ion mobility-mass spectrometry for separation and identification of isomeric lipids. *Analyst* **2015**, *140* (20), 6904–6911. https://doi.org/10.1039/c5an00838g.

(62) Hines, K. M.; May, J. C.; McLean, J. A.; Xu, L. Evaluation of collision cross section calibrants for structural analysis of lipids by traveling wave ion mobility-mass spectrometry. *Anal. Chem.* **2016**, *88* (14), 7329–7336. https://doi.org/10.1021/acs.analchem.6b01728.

(63) Hinneburg, H.; Hofmann, J.; Struwe, W. B.; Thader, A.; Altmann, F.; Varón Silva, D.; Seeberger, P. H.; Pagel, K.; Kolarich, D. Distinguishing N-acetylneuraminic acid linkage isomers on glycopeptides by ion mobility-mass spectrometry. *Chem. Commun.* **2016**, *52* (23), 4381–4384. https://doi.org/10.1039/c6cc01114d.

(64) Hofmann, J.; Hahm, H. S.; Seeberger, P. H.; Pagel, K. Identification of carbohydrate anomers using ion mobility-mass spectrometry. *Nature* **2015**, *526* (7572), 241–244. https://doi.org/10.1038/nature15388.

(65) Masike, K.; De Villiers, A.; Hoffman, E. W.; Brand, D. J.; Causon, T.; Stander, M. A. Detailed

phenolic characterization of *Protea* pure and hybrid cultivars by liquid chromatography-ion mobility-high resolution mass spectrometry (LC-IM-HR-MS). *J. Agric. Food Chem.* **2020**, *68* (2), 485–502. https://doi.org/10.1021/acs.jafc.9b06361.

(66) Pacini, T.; Fu, W.; Gudmundsson, S.; Chiaravalle, A. E.; Brynjolfson, S.; Palsson, B. O.; Astarita, G.; Paglia, G. Multidimensional analytical approach based on UHPLC-UV-Ion mobility-ms for the screening of natural pigments. *Anal. Chem.* **2015**, *87* (5), 2593–2599. https://doi.org/10.1021/ac504707n.

(67) Paglia, G.; Williams, J. P.; Menikarachchi, L.; Thompson, J. W.; Tyldesley-Worster, R.; Halldórsson, S.; Rolfsson, O.; Moseley, A.; Grant, D.; Langridge, J.; Palsson, B. O.; Astarita, G. Ion mobility derived collision cross sections to support metabolomics applications. *Anal. Chem.* **2014**, *86* (8), 3985–3993. https://doi.org/10.1021/ac500405x.

(68) Fenclova, M.; Stranska-Zachariasova, M.; Benes, F.; Novakova, A.; Jonatova, P.; Kren, V.; Vitek, L.; Hajslova, J. Liquid chromatography–drift tube ion mobility–mass spectrometry as a new challenging tool for the separation and characterization of silymarin flavonolignans. *Anal. Bioanal. Chem.* **2020**, *412* (4), 819–832. https://doi.org/10.1007/s00216-019-02274-3.

(69) Schroeder, M.; Meyer, S. W.; Heyman, H. M.; Barsch, A.; Sumner, L. W. Generation of a collision cross section library for multi-dimensional plant metabolomics using UHPLC-trapped ion mobility-MS/MS. *Metabolites* **2020**, *10* (1). https://doi.org/10.3390/metabo10010013.

(70) Gonzales, G. B.; Raes, K.; Coelus, S.; Struijs, K.; Smagghe, G.; Van Camp, J. Ultra(High)-pressure liquid chromatography-electrospray ionization-time-of-flight-ion mobility-high definition mass spectrometry for the rapid identification and structural characterization of flavonoid glycosides from cauliflower waste. *J. Chromatogr. A* **2014**, *1323*, 39–48. https://doi.org/10.1016/j.chroma.2013.10.077.

(71) Wang, Y.; Vorsa, N.; Harrington, P. D. B.; Chen, P. Nontargeted metabolomic study on variation of phenolics in different cranberry cultivars using UPLC-IM-HRMS. *J. Agric. Food Chem.* **2018**, *66* (46), 12206–12216. https://doi.org/10.1021/acs.jafc.8b05029.

(72) Yang, X.; Wei, S.; Liu, B.; Guo, D.; Zheng, B.; Feng, L.; Liu, Y.; Tomás-Barberán, F. A.; Luo, L.; Huang, D. A novel integrated non-targeted metabolomic analysis reveals significant metabolite variations between different lettuce (*Lactuca sativa*. L) varieties.

Hortic. Res. **2018**, *5* (1), 1–14. https://doi.org/10.1038/s41438-018-0050-1.

(73) Causon, T. J.; Ivanova-Petropulos, V.; Petrusheva, D.; Bogeva, E.; Hann, S. Fingerprinting of traditionally produced red wines using liquid chromatography combined with drift tube ion mobility-mass spectrometry. *Anal. Chim. Acta* **2019**, *1052*, 179–189. https://doi.org/10.1016/j.aca.2018.11.040.

(74) Jia, L.; Zuo, T.; Zhang, C.; Li, W.; Wang, H.; Hu, Y.; Wang, X.; Qian, Y.; Yang, W.; Yu, H. Simultaneous profiling and holistic comparison of the metabolomes among the flower buds of *Panax ginseng*, *Panax quinquefolius*, and *Panax notoginseng* by UHPLC/IM-QTOF-HDMS^{E}-based metabolomics analysis. *Molecules* **2019**, *24* (11), 2188. https://doi.org/10.3390/molecules24112188.

(75) May, J. C.; Goodwin, C. R.; McLean, J. A. Ion mobility-mass spectrometry strategies for untargeted systems, synthetic, and chemical biology. *Curr. Opin. Biotechnol.* **2015**, *31*, 117–121. https://doi.org/10.1016/j.copbio.2014.10.012.

(76) Luo, M.-D.; Zhou, Z.-W.; Zhu, Z.-J. The application of ion mobility-mass spectrometry in untargeted metabolomics: From separation to identification. *J. Anal. Test.* **2020**, *4* (3), 163–174. https://doi.org/10.1007/s41664-020-00133-0.

(77) Paglia, G.; Smith, A. J.; Astarita, G. Ion mobility mass spectrometry in the omics era: Challenges and opportunities for metabolomics and lipidomics. *Mass Spectrom. Rev.* **2021**, *22* (8), mas.21686. https://doi.org/10.1002/mas.21686.

(78) May, J. C.; McLean, J. A. Ion mobility-mass spectrometry: Time-dispersive instrumentation. *Anal. Chem.* **2015**, *87* (3), 1422–1436. https://doi.org/10.1021/ac504720m.

(79) Cohen, M. J.; Karasek, F. W. Plasma chromatography^{tm}-A new dimension for gas chromatography and mass spectrometry. *J. Chromatogr. Sci.* **1970**, *8* (6), 330–337. https://doi.org/10.1093/chromsci/8.6.330.

(80) Revercomb, H. E.; Mason, E. A. Theory of plasma chromatography/gaseous electrophoresis: A review. *Anal. Chem.* **1975**, *47* (7), 970–983. https://doi.org/10.1021/ac60357a043.

(81) Von Helden, G.; Hsu, M. T.; Gotts, N.; Bowers, M. T. Carbon cluster cations with up to 84 atoms: Structures, formation mechanism, and reactivity. *J. Phys. Chem.* **1993**, *97* (31), 8182–8192. https://doi.org/10.1021/j100133a011.

(82) Barnes, W. S.; Martin, D. W.; McDaniel, E. W. Mass spectrographic identification of the ion observed in hydrogen mobility experiments. *Phys. Rev. Lett.* **1961**, *6* (3), 110–111. https://doi.org/10.1103/PhysRevLett.6.110.

(83) Kirk, A. T.; Bohnhorst, A.; Raddatz, C.-R.; Allers, M.; Zimmermann, S. Ultra-high-resolution ion mobility spectrometry—current instrumentation, limitations, and future developments. *Anal. Bioanal. Chem.* **2019**, *411* (24), 6229–6246. https://doi.org/10.1007/s00216-019-01807-0.

(84) Stow, S. M.; Lareau, N. M.; Hines, K. M.; Mcnees, C. R.; Goodwin, C. R.; Bachmann, B. O.; Mclean, J. A. Structural separations for natural product characterization by ion mobility-mass spectrometry: Fundamental theory to emerging applications. *Nat. Prod. Anal. Instrumentation, Methods, Appl.* **2014**, *9781118466*, 397–431. https://doi.org/10.1002/9781118876015.ch11.

(85) Gieniec, J.; Mack, L. L.; Nakamae, K.; Gupta, C.; Kumar, V.; Dole, M. Electrospray mass spectroscopy of macromolecules: Application of an ion-drift spectrometer. *Biol. Mass Spectrom.* **1984**, *11* (6), 259–268. https://doi.org/10.1002/bms.1200110602.

(86) Clemmer, D. E.; Hudgins, R. R.; Jarrold, M. F. Naked protein conformations: Cytochrome *c* in the gas phase. *J. Am. Chem. Soc.* **1995**, *117* (40), 10141–10142. https://doi.org/10.1021/ja00145a037.

(87) Von Helden, G.; Wyttenbach, T.; Bowers, M. T. Conformation of macromolecules in the gas phase: Use of matrix-assisted laser desorption methods in ion chromatography. *Science* **1995**, *267* (5203), 1483–1485. https://doi.org/10.1126/science.267.5203.1483.

(88) Wyttenbach, T.; von Helden, G.; Bowers, M. T. Gas-phase conformation of biological molecules: Bradykinin. *J. Am. Chem. Soc.* **1996**, *118* (35), 8355–8364. https://doi.org/10.1021/ja9535928.

(89) Shelimov, K. B.; Clemmer, D. E.; Hudgins, R. R.; Jarrold, M. F. Protein structure in vacuo: Gas-phase conformations of bpti and cytochrome *c*. *J. Am. Chem. Soc.* **1997**, *119* (9), 2240–2248. https://doi.org/10.1021/ja9619059.

(90) Wu, C.; Siems, W. F.; Asbury, G. R.; Hill, H. H. Electrospray ionization high-resolution ion mobility spectrometry-mass spectrometry. *Anal. Chem.* **1998**, *70* (23), 4929–4938. https://doi.org/10.1021/ac980414z.

(91) Wyttenbach, T.; Kemper, P. R.; Bowers, M. T. Design of a new electrospray ion mobility mass spectrometer. *Int. J. Mass Spectrom.* **2001**, *212* (1–3), 13–23. https://doi.org/10.1016/S1387-3806(01)00517-6.

(92) Giles, K.; Pringle, S. D.; Worthington, K. R.; Little, D.; Wildgoose, J. L.; Bateman, R. H. Applications of a travelling wave-based radio-frequency-only stacked ring ion guide. *Rapid Commun. Mass Spectrom.* **2004**, *18* (20), 2401–2414. https://doi.org/10.1002/rcm.1641.

(93) Merenbloom, S. I.; Glaskin, R. S.; Henson, Z. B.; Clemmer, D. E. High-resolution ion cyclotron mobility spectrometry. *Anal. Chem.* **2009**, *81* (4), 1482–1487. https://doi.org/10.1021/ac801880a.

(94) Bush, M. F.; Hall, Z.; Giles, K.; Hoyes, J.; Robinson, C. V.; Ruotolo, B. T. Collision cross sections of proteins and their complexes: A calibration framework and database for gas-phase structural biology. *Anal. Chem.* **2010**, *82* (22), 9557–9565. https://doi.org/10.1021/ac1022953.

(95) Zucker, S. M.; Lee, S.; Webber, N.; Valentine, S. J.; Reilly, J. P.; Clemmer, D. E. An ion mobility/ion trap/photo dissociation instrument for characterization of ion structure. *J. Am. Soc. Mass Spectrom.* **2011**, *22* (9), 1477–1485. https://doi.org/10.1007/s13361-011-0179-8.

(96) Zhang, X.; Knochenmuss, R.; Siems, W. F.; Liu, W.; Graf, S.; Hill, H. H. Evaluation of hadamard transform atmospheric pressure ion mobility time-of-flight mass spectrometry for complex mixture analysis. *Anal. Chem.* **2014**, *86* (3), 1661–1670. https://doi.org/10.1021/ac403435p.

(97) Ibrahim, Y. M.; Baker, E. S.; Danielson, W. F.; Norheim, R. V.; Prior, D. C.; Anderson, G. A.; Belov, M. E.; Smith, R. D. Development of a new ion mobility (quadrupole) time-of-flight mass spectrometer. *Int. J. Mass Spectrom.* **2015**, *377* (1), 655–662. https://doi.org/10.1016/j.ijms.2014.07.034.

(98) Deng, L.; Ibrahim, Y. M.; Hamid, A. M.; Garimella, S. V. B.; Webb, I. K.; Zheng, X.; Prost, S. A.; Sandoval, J. A.; Norheim, R. V.; Anderson, G. A.; Tolmachev, A. V.; Baker, E. S.; Smith, R. D. Ultra-high resolution ion mobility separations utilizing traveling waves in a 13 m serpentine path length structures for lossless ion manipulations module. *Anal. Chem.* **2016**, *88* (18), 8957–8964. https://doi.org/10.1021/acs.analchem.6b01915.

(99) Hamid, A. M.; Garimella, S. V. B.; Ibrahim, Y. M.; Deng, L.; Zheng, X.; Webb, I. K.;

Anderson, G. A.; Prost, S. A.; Norheim, R. V.; Tolmachev, A. V.; Baker, E. S.; Smith, R. D. Achieving high resolution ion mobility separations using traveling waves in compact multiturn structures for lossless ion manipulations. *Anal. Chem.* **2016**, *88* (18), 8949–8956. https://doi.org/10.1021/acs.analchem.6b01914.

(100) Ujma, J.; Giles, K.; Morris, M.; Barran, P. E. New high resolution ion mobility mass spectrometer capable of measurements of collision cross sections from 150 to 520 K. *Anal. Chem.* **2016**, *88* (19), 9469–9478. https://doi.org/10.1021/acs.analchem.6b01812.

(101) Pringle, S. D.; Giles, K.; Wildgoose, J. L.; Williams, J. P.; Slade, S. E.; Thalassinos, K.; Bateman, R. H.; Bowers, M. T.; Scrivens, J. H. An investigation of the mobility separation of some peptide and protein ions using a new hybrid quadrupole/travelling wave IMS/Oa-ToF instrument. *Int. J. Mass Spectrom.* **2007**, *261* (1), 1–12. https://doi.org/10.1016/j.ijms.2006.07.021.

(102) Fernandez-Lima, F. A.; Kaplan, D. A.; Park, M. A. Note: Integration of trapped ion mobility spectrometry with mass spectrometry. *Rev. Sci. Instrum.* **2011**, *82* (12), 1–5. https://doi.org/10.1063/1.3665933.

(103) Giles, K.; Ujma, J.; Wildgoose, J.; Pringle, S.; Richardson, K.; Langridge, D.; Green, M. A. Cyclic ion mobility-mass spectrometry system. *Anal. Chem.* **2019**, *91* (13), 8564–8573. https://doi.org/10.1021/acs.analchem.9b01838.

(104) Basit, A.; Pontis, S.; Piomelli, D.; Armirotti, A. Ion mobility mass spectrometry enhances low-abundance species detection in untargeted lipidomics. *Metabolomics* **2016**, *12* (3), 1–10. https://doi.org/10.1007/s11306-016-0971-3.

(105) Mairinger, T.; Causon, T. J.; Hann, S. The potential of ion mobility–mass spectrometry for non-targeted metabolomics. *Current Opinion in Chemical Biology*. Elsevier Ltd 2018, pp 9–15. https://doi.org/10.1016/j.cbpa.2017.10.015.

(106) Venter, P.; Muller, M.; Vestner, J.; Stander, M. A.; Tredoux, A. G. J.; Pasch, H.; De Villiers, A. Comprehensive three-dimensional LC × LC × ion mobility spectrometry separation combined with high-resolution MS for the analysis of complex samples. *Anal. Chem.* **2018**, *90* (19), 11643–11650. https://doi.org/10.1021/acs.analchem.8b03234.

(107) Esquenazi, E.; Daly, M.; Bahrainwala, T.; Gerwick, W. H.; Dorrestein, P. C. Ion mobility mass spectrometry enables the efficient detection and identification of halogenated natural products from cyanobacteria with minimal sample preparation. *Bioorganic Med. Chem.*

2011, *19* (22), 6639–6644. https://doi.org/10.1016/j.bmc.2011.06.081.

(108) Bauer, A.; Luetjohann, J.; Hanschen, F. S.; Schreiner, M.; Kuballa, J.; Jantzen, E.; Rohn, S. Identification and characterization of pesticide metabolites in *Brassica* species by liquid chromatography travelling wave ion mobility quadrupole time-of-flight mass spectrometry (UPLC-TWIMS-QTOF-MS). *Food Chem.* **2018**, *244* (September 2017), 292–303. https://doi.org/10.1016/j.foodchem.2017.09.131.

(109) Decroo, C.; Colson, E.; Lemaur, V.; Caulier, G.; De Winter, J.; Cabrera-Barjas, G.; Cornil, J.; Flammang, P.; Gerbaux, P. Ion mobility mass spectrometry of saponin ions. *Rapid Commun. Mass Spectrom.* **2019**, *33* (S2), 22–33. https://doi.org/10.1002/rcm.8193.

(110) McCullagh, M.; Douce, D.; Van Hoeck, E.; Goscinny, S. Exploring the complexity of steviol glycosides analysis using ion mobility mass spectrometry. *Anal. Chem.* **2018**, *90* (7), 4585–4595. https://doi.org/10.1021/acs.analchem.7b05002.

(111) Dodds, J. N.; Baker, E. S. Ion mobility spectrometry: Fundamental concepts, instrumentation, applications, and the road ahead. *J. Am. Soc. Mass Spectrom.* **2019**, *30* (11), 2185–2195. https://doi.org/10.1007/s13361-019-02288-2.

(112) Ridgeway, M. E.; Lubeck, M.; Jordens, J.; Mann, M.; Park, M. A. Trapped ion mobility spectrometry: A short review. *Int. J. Mass Spectrom.* **2018**, *425*, 22–35. https://doi.org/10.1016/j.ijms.2018.01.006.

(113) Cumeras, R.; Figueras, E.; Davis, C. E.; Baumbach, J. I.; Gràcia, I. Review on ion mobility spectrometry. Part 2: Hyphenated methods and effects of experimental parameters. *Analyst* **2015**, *140* (5), 1391–1410. https://doi.org/10.1039/c4an01101e.

(114) D'Atri, V.; Causon, T.; Hernandez-Alba, O.; Mutabazi, A.; Veuthey, J. L.; Cianferani, S.; Guillarme, D. Adding a new separation dimension to MS and LC–MS: What is the utility of ion mobility spectrometry? *J. Sep. Sci.* **2018**, *41* (1), 20–67. https://doi.org/10.1002/jssc.201700919.

(115) Hines, K. M.; Enders, J. R.; McLean, J. A. Multidimensional separations by ion mobility-mass spectrometry. In *Encyclopedia of Analytical Chemistry*; John Wiley & Sons, Ltd: Chichester, UK, 2012. https://doi.org/10.1002/9780470027318.a9313.

(116) Astarita, G.; Paglia, G.; Yu, K. Ion-mobility mass spectrometry in metabolomics and lipidomics. *LC-GC North Am.* **2015**, *33* (9), 702–709.

(117) Sun, J.; Baker, A.; Chen, P. Profiling the indole alkaloids in yohimbe bark with ultraperformance liquid chromatography coupled with ion mobility quadrupole time-of-flight mass spectrometry. *Rapid Commun. Mass Spectrom.* **2011**, *25* (18), 2591–2602. https://doi.org/10.1002/rcm.5158.

(118) Meier, F.; Beck, S.; Grassl, N.; Lubeck, M.; Park, M. A.; Raether, O.; Mann, M. Parallel accumulation-serial fragmentation (PASEF): Multiplying sequencing speed and sensitivity by synchronized scans in a trapped ion mobility device. *J. Proteome Res.* **2015**, *14* (12), 5378–5387. https://doi.org/10.1021/acs.jproteome.5b00932.

(119) Dodds, J. N.; May, J. C.; McLean, J. A. Correlating resolving power, resolution, and collision cross section: Unifying cross-platform assessment of separation efficiency in ion mobility spectrometry. *Anal. Chem.* **2017**, *89* (22), 12176–12184. https://doi.org/10.1021/acs.analchem.7b02827.

(120) May, J. C.; Goodwin, C. R.; Lareau, N. M.; Leaptrot, K. L.; Morris, C. B.; Kurulugama, R. T.; Mordehai, A.; Klein, C.; Barry, W.; Darland, E.; Overney, G.; Imatani, K.; Stafford, G. C.; Fjeldsted, J. C.; McLean, J. A. Conformational ordering of biomolecules in the gas phase: Nitrogen collision cross sections measured on a prototype high resolution drift tube ion mobility-mass spectrometer. *Anal. Chem.* **2014**, *86* (4), 2107–2116. https://doi.org/10.1021/ac4038448.

(121) Giles, K.; Williams, J. P.; Campuzano, I. Enhancements in travelling wave ion mobility resolution. *Rapid Commun. Mass Spectrom.* **2011**, *25* (11), 1559–1566. https://doi.org/10.1002/rcm.5013.

(122) Silveira, J. A.; Ridgeway, M. E.; Park, M. A. High resolution trapped ion mobility spectrometery of peptides. *Anal. Chem.* **2014**, *86* (12), 5624–5627. https://doi.org/10.1021/ac501261h.

(123) Michelmann, K.; Silveira, J. A.; Ridgeway, M. E.; Park, M. A. Fundamentals of trapped ion mobility spectrometry. *J. Am. Soc. Mass Spectrom.* **2015**, *26* (1), 14–24. https://doi.org/10.1007/s13361-014-0999-4.

(124) Shvartsburg, A. A.; Prior, D. C.; Tang, K.; Smith, R. D. High-resolution differential ion mobility separations using planar analyzers at elevated dispersion fields. *Anal. Chem.* **2010**, *82* (18), 7649–7655. https://doi.org/10.1021/ac101413k.

(125) Shvartsburg, A. A.; Seim, T. A.; Danielson, W. F.; Norheim, R.; Moore, R. J.; Anderson, G.

A.; Smith, R. D. High-definition differential ion mobility spectrometry with resolving power up to 500. *J. Am. Soc. Mass Spectrom.* **2013**, *24* (1), 109–114. https://doi.org/10.1007/s13361-012-0517-5.

(126) Amo-González, M.; Pérez, S. Planar differential mobility analyzer with a resolving power of 110. *Anal. Chem.* **2018**, *90* (11), 6735–6741. https://doi.org/10.1021/acs.analchem.8b00579.

(127) Dodds, J. N.; May, J. C.; McLean, J. A. Investigation of the complete suite of the leucine and isoleucine isomers: toward prediction of ion mobility separation capabilities. *Anal. Chem.* **2017**, *89* (1), 952–959. https://doi.org/10.1021/acs.analchem.6b04171.

(128) Adams, K. J.; Montero, D.; Aga, D.; Fernandez-Lima, F. Isomer separation of polybrominated diphenyl ether metabolites using NanoESI-TIMS-MS. *Int. J. Ion Mobil. Spectrom.* **2016**, *19* (2–3), 69–76. https://doi.org/10.1007/s12127-016-0198-z.

(129) Deng, L.; Webb, I. K.; Garimella, S. V. B.; Hamid, A. M.; Zheng, X.; Norheim, R. V.; Prost, S. A.; Anderson, G. A.; Sandoval, J. A.; Baker, E. S.; Ibrahim, Y. M.; Smith, R. D. Serpentine ultralong path with extended routing (SUPER) high resolution traveling wave ion mobility-ms using structures for lossless ion manipulations. *Anal. Chem.* **2017**, *89* (8), 4628–4634. https://doi.org/10.1021/acs.analchem.7b00185.

(130) Tolmachev, A. V.; Webb, I. K.; Ibrahim, Y. M.; Garimella, S. V. B.; Zhang, X.; Anderson, G. A.; Smith, R. D. Characterization of ion dynamics in structures for lossless ion manipulations. *Anal. Chem.* **2014**, *86* (18), 9162–9168. https://doi.org/10.1021/ac502054p.

(131) Kirk, A. T.; Raddatz, C. R.; Zimmermann, S. Separation of isotopologues in Ultra-High-resolution ion mobility spectrometry. *Anal. Chem.* **2017**, *89* (3), 1509–1515. https://doi.org/10.1021/acs.analchem.6b03300.

(132) Glaskin, R. S.; Ewing, M. A.; Clemmer, D. E. Ion trapping for ion mobility spectrometry measurements in a cyclical drift tube. *Anal. Chem.* **2013**, *85* (15), 7003–7008. https://doi.org/10.1021/ac4015066.

(133) Mason, E. A.; Schamp, H. W. Mobility of gaseous Ions in weak electric fields. *Ann. Phys. (N. Y).* **1958**, *4* (3), 233–270. https://doi.org/10.1016/0003-4916(58)90049-6.

(134) Gabelica, V.; Shvartsburg, A. A.; Afonso, C.; Barran, P.; Benesch, J. L. P.; Bleiholder, C.; Bowers, M. T.; Bilbao, A.; Bush, M. F.; Campbell, J. L.; Campuzano, I. D. G.; Causon, T.;

Clowers, B. H.; Creaser, C. S.; De Pauw, E.; Far, J.; Fernandez-Lima, F.; Fjeldsted, J. C.; Giles, K.; Groessl, M.; Hogan, C. J.; Hann, S.; Kim, H. I.; Kurulugama, R. T.; May, J. C.; McLean, J. A.; Pagel, K.; Richardson, K.; Ridgeway, M. E.; Rosu, F.; Sobott, F.; Thalassinos, K.; Valentine, S. J.; Wyttenbach, T. Recommendations for reporting ion mobility mass spectrometry measurements. *Mass Spectrom. Rev.* **2019**, *38* (3), 291–320. https://doi.org/10.1002/mas.21585.

(135) Kurulugama, R. T.; Darland, E.; Kuhlmann, F.; Stafford, G.; Fjeldsted, J. Evaluation of drift gas selection in complex sample analyses using a high performance drift tube ion mobility-qtof mass spectrometer. *Analyst* **2015**, *140* (20), 6834–6844. https://doi.org/10.1039/c5an00991j.

(136) Stow, S. M.; Causon, T. J.; Zheng, X.; Kurulugama, R. T.; Mairinger, T.; May, J. C.; Rennie, E. E.; Baker, E. S.; Smith, R. D.; McLean, J. A.; Hann, S.; Fjeldsted, J. C. An interlaboratory evaluation of drift tube ion mobility-mass spectrometry collision cross section measurements. *Anal. Chem.* **2017**, *89* (17), 9048–9055. https://doi.org/10.1021/acs.analchem.7b01729.

(137) Hofmann, J.; Struwe, W. B.; Scarff, C. A.; Scrivens, J. H.; Harvey, D. J.; Pagel, K. Estimating collision cross sections of negatively charged n- glycans using traveling wave ion mobility-mass spectrometry. *Anal. Chem.* **2014**, *86* (21), 10789–10795. https://doi.org/10.1021/ac5028353.

(138) Hines, K. M.; Ross, D. H.; Davidson, K. L.; Bush, M. F.; Xu, L. Large-scale structural characterization of drug and drug-like compounds by high-throughput ion mobility-mass spectrometry. *Anal. Chem.* **2017**, *89* (17), 9023–9030. https://doi.org/10.1021/acs.analchem.7b01709.

(139) Bush, M. F.; Campuzano, I. D. G.; Robinson, C. V. Ion mobility mass spectrometry of peptide ions: Effects of drift gas and calibration strategies. *Anal. Chem.* **2012**, *84* (16), 7124–7130. https://doi.org/10.1021/ac3014498.

(140) Forsythe, J. G.; Petrov, A. S.; Walker, C. A.; Allen, S. J.; Pellissier, J. S.; Bush, M. F.; Hud, N. V.; Fernández, F. M. Collision cross section calibrants for negative ion mode traveling wave ion mobility-mass spectrometry. *Analyst* **2015**, *140* (20), 6853–6861. https://doi.org/10.1039/c5an00946d.

(141) Hernandez, D. R.; DeBord, J. D.; Ridgeway, M. E.; Kaplan, D. A.; Park, M. A.; Fernandez-

Lima, F. Ion dynamics in a trapped ion mobility spectrometer. *Analyst* **2014**, *139* (8), 1913–1921. https://doi.org/10.1039/c3an02174b.

(142) Ouyang, H.; Larriba-Andaluz, C.; Oberreit, D. R.; Hogan, C. J. The collision cross sections of iodide salt cluster ions in air via differential mobility analysis-mass spectrometry. *J. Am. Soc. Mass Spectrom.* **2013**, *24* (12), 1833–1847. https://doi.org/10.1007/s13361-013-0724-8.

(143) B. Morris, C.; C. May, J.; L. Leaptrot, K.; A. McLean, J. Evaluating separation selectivity and collision cross section measurement reproducibility in helium, nitrogen, argon, and carbon dioxide drift gases for drift tube ion mobility–mass spectrometry. *J. Am. Soc. Mass Spectrom.* **2019**, *30* (6), 1059–1068. https://doi.org/10.1021/jasms.8b06014.

(144) Pacholarz, K. J.; Barran, P. E. Distinguishing loss of structure from subunit dissociation for protein complexes with variable temperature ion mobility mass spectrometry. *Anal. Chem.* **2015**, *87* (12), 6271–6279. https://doi.org/10.1021/acs.analchem.5b01063.

(145) May, J. C.; Morris, C. B.; McLean, J. A. Ion mobility collision cross section compendium. *Anal. Chem.* **2017**, *89* (2), 1032–1044. https://doi.org/10.1021/acs.analchem.6b04905.

(146) Warnke, S.; Seo, J.; Boschmans, J.; Sobott, F.; Scrivens, J. H.; Bleiholder, C.; Bowers, M. T.; Gewinner, S.; Schöllkopf, W.; Pagel, K.; Von Helden, G. Protomers of benzocaine: Solvent and permittivity dependence. *J. Am. Chem. Soc.* **2015**, *137* (12), 4236–4242. https://doi.org/10.1021/jacs.5b01338.

(147) Xia, H.; Attygalle, A. B. Effect of electrospray ionization source conditions on the tautomer distribution of deprotonated *p*-hydroxybenzoic acid in the gas phase. *Anal. Chem.* **2016**, *88* (11), 6035–6043. https://doi.org/10.1021/acs.analchem.6b01230.

(148) Lanucara, F.; Holman, S. W.; Gray, C. J.; Eyers, C. E. The power of ion mobility-mass spectrometry for structural characterization and the study of conformational dynamics. *Nat. Chem.* **2014**, *6* (4), 281–294. https://doi.org/10.1038/nchem.1889.

(149) Wishart, D. S.; Tzur, D.; Knox, C.; Eisner, R.; Guo, A. C.; Young, N.; Cheng, D.; Jewell, K.; Arndt, D.; Sawhney, S.; Fung, C.; Nikolai, L.; Lewis, M.; Coutouly, M. A.; Forsythe, I.; Tang, P.; Shrivastava, S.; Jeroncic, K.; Stothard, P.; Amegbey, G.; Block, D.; Hau, D. D.; Wagner, J.; Miniaci, J.; Clements, M.; Gebremedhin, M.; Guo, N.; Zhang, Y.; Duggan, G. E.; MacInnis, G. D.; Weljie, A. M.; Dowlatabadi, R.; Bamforth, F.; Clive, D.; Greiner, R.; Li, L.; Marrie, T.; Sykes, B. D.; Vogel, H. J.; Querengesser, L. HMDB: The Human Metabolome

Database. *Nucleic Acids Res.* **2007**, *35* (SUPPL. 1), 521–526. https://doi.org/10.1093/nar/gkl923.

(150) Smith, C. A.; O'Maille, G.; Want, E. J.; Qin, C.; Trauger, S. A.; Brandon, T. R.; Custodio, D. E.; Abagyan, R.; Siuzdak, G. METLIN: A metabolite mass spectral database. *Ther. Drug Monit.* **2005**, *27* (6), 747–751. https://doi.org/10.1097/01.ftd.0000179845.53213.39.

(151) Kyle, J. E.; Aly, N.; Zheng, X.; Burnum-Johnson, K. E.; Smith, R. D.; Baker, E. S. Evaluating lipid mediator structural complexity using ion mobility spectrometry combined with mass spectrometry. *Bioanalysis* **2018**, *10* (5), 279–289. https://doi.org/10.4155/bio-2017-0245.

(152) Leaptrot, K. L.; May, J. C.; Dodds, J. N.; McLean, J. A. Ion mobility conformational lipid atlas for high confidence lipidomics. *Nat. Commun.* **2019**, *10* (1). https://doi.org/10.1038/s41467-019-08897-5.

(153) Righetti, L.; Bergmann, A.; Galaverna, G.; Rolfsson, O.; Paglia, G.; Dall'Asta, C. Ion mobility-derived collision cross section database: Application to mycotoxin analysis. *Anal. Chim. Acta* **2018**, *1014*, 50–57. https://doi.org/10.1016/j.aca.2018.01.047.

(154) Stephan, S.; Hippler, J.; Köhler, T.; Deeb, A. A.; Schmidt, T. C.; Schmitz, O. J. Contaminant screening of wastewater with HPLC-IM-QTOF-MS and LC+LC-IM-QTOF-MS using a ccs database. *Anal. Bioanal. Chem.* **2016**, *408* (24), 6545–6555. https://doi.org/10.1007/s00216-016-9820-5.

(155) Picache, J. A.; Rose, B. S.; Balinski, A.; Leaptrot, K. L.; Sherrod, S. D.; May, J. C.; McLean, J. A. Collision cross section compendium to annotate and predict multi-omic compound identities. *Chem. Sci.* **2019**, *10* (4), 983–993. https://doi.org/10.1039/c8sc04396e.

(156) Zhou, Z.; Shen, X.; Tu, J.; Zhu, Z. J. Large-scale prediction of collision cross-section values for metabolites in ion mobility-mass spectrometry. *Anal. Chem.* **2016**, *88* (22), 11084–11091. https://doi.org/10.1021/acs.analchem.6b03091.

(157) Zhou, Z.; Tu, J.; Xiong, X.; Shen, X.; Zhu, Z. J. LipidCCS: Prediction of collision cross-section values for lipids with high precision to support ion mobility-mass spectrometry-based lipidomics. *Anal. Chem.* **2017**, *89* (17), 9559–9566. https://doi.org/10.1021/acs.analchem.7b02625.

(158) Plante, P. L.; Francovic-Fontaine, É.; May, J. C.; McLean, J. A.; Baker, E. S.; Laviolette, F.; Marchand, M.; Corbeil, J. Predicting ion mobility collision cross-sections using a deep

neural network: DeepCCS. *Anal. Chem.* **2019**, *91* (8), 5191–5199. https://doi.org/10.1021/acs.analchem.8b05821.

(159) Bijlsma, L.; Bade, R.; Celma, A.; Mullin, L.; Cleland, G.; Stead, S.; Hernandez, F.; Sancho, J. V. Prediction of collision cross-section values for small molecules: Application to pesticide residue analysis. *Anal. Chem.* **2017**, *89* (12), 6583–6589. https://doi.org/10.1021/acs.analchem.7b00741.

(160) Colby, S. M.; Thomas, D. G.; Nunez, J. R.; Baxter, D. J.; Glaesemann, K. R.; Brown, J. M.; Pirrung, M. A.; Govind, N.; Teeguarden, J. G.; Metz, T. O.; Renslow, R. S. ISiCLE: A quantum chemistry pipeline for establishing *in silico* collision cross section libraries. *Anal. Chem.* **2019**, *91* (7), 4346–4356. https://doi.org/10.1021/acs.analchem.8b04567.

(161) Colby, S. M.; Nuñez, J. R.; Hodas, N. O.; Corley, C. D.; Renslow, R. R. Deep learning to generate *in silico* chemical property libraries and candidate molecules for small molecule identification in complex samples. *Anal. Chem.* **2020**, *92* (2), 1720–1729. https://doi.org/10.1021/acs.analchem.9b02348.

(162) Kaufmann, A.; Butcher, P.; Maden, K.; Walker, S.; Widmer, M. Does the ion mobility resolving power as provided by commercially available ion mobility quadrupole time-of-flight mass spectrometry instruments permit the unambiguous identification of small molecules in complex matrices? *Anal. Chim. Acta* **2020**, *1107*, 113–126. https://doi.org/10.1016/j.aca.2020.02.032.

(163) Donato, P.; Giuffrida, D.; Oteri, M.; Inferrera, V.; Dugo, P.; Mondello, L. Supercritical fluid chromatography × ultra-high pressure liquid chromatography for red chilli pepper fingerprinting by photodiode array, quadrupole-time-of-flight and ion mobility mass spectrometry (SFC × RP-UHPLC-PDA-Q-ToF MS-IMS). *Food Anal. Methods* **2018**, *11* (12), 3331–3341. https://doi.org/10.1007/s12161-018-1307-x.

(164) Lipok, C.; Hippler, J.; Schmitz, O. J. A Four dimensional separation method based on continuous heart-cutting gas chromatography with ion mobility and high resolution mass spectrometry. *J. Chromatogr. A* **2018**, *1536*, 50–57. https://doi.org/10.1016/j.chroma.2017.07.013.

(165) Szymańska, E.; Davies, A. N.; Buydens, L. M. C. Chemometrics for ion mobility spectrometry data: Recent advances and future prospects. *Analyst* **2016**, *141* (20), 5689–5708. https://doi.org/10.1039/c6an01008c.

(166) Smith, C. A.; Want, E. J.; O'Maille, G.; Abagyan, R.; Siuzdak, G. XCMS: Processing mass spectrometry data for metabolite profiling using nonlinear peak alignment, matching, and identification. *Anal. Chem.* **2006**, *78* (3), 779–787. https://doi.org/10.1021/ac051437y.

(167) Martínez-Lozano, P.; Criado, E.; Vidal, G.; Cristoni, S.; Franzoso, F.; Piatti, M.; Brambilla, P. Differential mobility analysis-mass spectrometry coupled to XCMS algorithm as a novel analytical platform for metabolic profiling. *Metabolomics* **2013**, *9* (SUPPL.1), 30–43. https://doi.org/10.1007/s11306-011-0319-y.

(168) MacLean, B. X.; Pratt, B. S.; Egertson, J. D.; MacCoss, M. J.; Smith, R. D.; Baker, E. S. Using skyline to analyze data-containing liquid chromatography, ion mobility spectrometry, and mass spectrometry dimensions. *J. Am. Soc. Mass Spectrom.* **2018**, *29* (11), 2182–2188. https://doi.org/10.1007/s13361-018-2028-5.

(169) Migas, L. G.; France, A. P.; Bellina, B.; Barran, P. E. ORIGAMI: A software suite for activated ion mobility mass spectrometry (AIM-MS) applied to multimeric protein assemblies. *Int. J. Mass Spectrom.* **2018**, *427*, 20–28. https://doi.org/10.1016/j.ijms.2017.08.014.

(170) Gallegos, J.; Garrido-Delgado, R.; Arce, L.; Medina, L. M. Volatile metabolites of goat cheeses determined by ion mobility spectrometry. Potential applications in quality control. *Food Anal. Methods* **2015**, *8* (7), 1699–1709. https://doi.org/10.1007/s12161-014-0050-1.

(171) Hu, X.; Wang, R.; Guo, J.; Ge, K.; Li, G.; Fu, F.; Ding, S.; Shan, Y. Changes in the volatile components of candied kumquats in different processing methodologies with headspace-gas chromatography-ion mobility spectrometry. *Molecules* **2019**, *24* (17). https://doi.org/10.3390/molecules24173053.

(172) Li, M.; Yang, R.; Zhang, H.; Wang, S.; Chen, D.; Lin, S. Development of a flavor fingerprint by HS-GC–IMS with PCA for volatile compounds of *Tricholoma matsutake* Singer. *Food Chem.* **2019**, *290* (1), 32–39. https://doi.org/10.1016/j.foodchem.2019.03.124.

(173) Schwolow, S.; Gerhardt, N.; Rohn, S.; Weller, P. Data fusion of GC-IMS data and FT-MIR spectra for the authentication of olive oils and honeys—Is it worth to go the extra mile? *Anal. Bioanal. Chem.* **2019**, *411* (23), 6005–6019. https://doi.org/10.1007/s00216-019-01978-w.

(174) Yang, L.; Liu, J.; Wang, X.; Wang, R.; Ren, F.; Zhang, Q.; Shan, Y.; Ding, S. Characterization of volatile component changes in jujube fruits during cold storage by using

headspace-gas chromatography-ion mobility spectrometry. *Molecules* **2019**, *24* (21), 1–21. https://doi.org/10.3390/molecules24213904.

(175) Wang, X.; Yang, S.; He, J.; Chen, L.; Zhang, J.; Jin, Y.; Zhou, J.; Zhang, Y. A green triple-locked strategy based on volatile-compound imaging, chemometrics, and markers to discriminate winter honey and *Sapium* honey using headspace gas chromatography-ion mobility spectrometry. *Food Res. Int.* **2019**, *119* (January), 960–967. https://doi.org/10.1016/j.foodres.2019.01.004.

(176) Wang, X.; Rogers, K. M.; Li, Y.; Yang, S.; Chen, L.; Zhou, J. Untargeted and targeted discrimination of honey collected by *Apis cerana* and *Apis mellifera* based on volatiles using HS-GC-IMS and HS-SPME-GC–MS. *J. Agric. Food Chem.* **2019**, *67* (43), 12144–12152. https://doi.org/10.1021/acs.jafc.9b04438.

(177) Bocos-Bintintan, V.; Thomas, C. L. P.; Ratiu, I. A. Sensors' array of aspiration ion mobility spectrometer as a tool for bacteria discrimination. *Talanta* **2020**, *206* (August 2019), 1–14. https://doi.org/10.1016/j.talanta.2019.120233.

(178) Erler, A.; Riebe, D.; Beitz, T.; Löhmannsröben, H.-G.; Grothusheitkamp, D.; Kunz, T.; Methner, F.-J. Characterization of volatile metabolites formed by molds on barley by mass and ion mobility spectrometry. *J. Mass Spectrom.* **2020**, *55* (5), 1–10. https://doi.org/10.1002/jms.4501.

(179) Ge, S.; Chen, Y.; Ding, S.; Zhou, H.; Jiang, L.; Yi, Y.; Deng, F.; Wang, R. Changes in volatile flavor compounds of peppers during hot air drying process based on headspace-gas chromatography-ion mobility spectrometry (HS-GC-IMS). *J. Sci. Food Agric.* **2020**, *100* (7), 3087–3098. https://doi.org/10.1002/jsfa.10341.

(180) Lv, W.; Lin, T.; Ren, Z.; Jiang, Y.; Zhang, J.; Bi, F.; Gu, L.; Hou, H.; He, J. Rapid discrimination of *Citrus reticulata* 'Chachi' by headspace-gas chromatography-ion mobility spectrometry fingerprints combined with principal component analysis. *Food Res. Int.* **2020**, *131* (July 2019), 108985. https://doi.org/10.1016/j.foodres.2020.108985.

(181) McCartney, M. M.; Spitulski, S. L.; Pasamontes, A.; Peirano, D. J.; Schirle, M. J.; Cumeras, R.; Simmons, J. D.; Ware, J. L.; Brown, J. F.; Poh, A. J. Y.; Dike, S. C.; Foster, E. K.; Godfrey, K. E.; Davis, C. E. Coupling a branch enclosure with differential mobility spectrometry to isolate and measure plant volatiles in contained greenhouse settings. *Talanta* **2016**, *146*, 148–154. https://doi.org/10.1016/j.talanta.2015.08.039.

(182) Piñero, M. Y.; Amo-González, M.; Ballesteros, R. D.; Pérez, L. R.; de la Mora, G. F.; Arce, L. Chemical fingerprinting of olive oils by electrospray ionization-differential mobility analysis-mass spectrometry: A new alternative to food authenticity testing. *J. Am. Soc. Mass Spectrom.* **2020**, *31* (3), 527–537. https://doi.org/10.1021/jasms.9b00006.

(183) Zhang, X.; Dai, Z.; Fan, X.; Liu, M.; Ma, J.; Shang, W.; Liu, J.; Strappe, P.; Blanchard, C.; Zhou, Z. A study on volatile metabolites screening by HS-SPME-GC-MS and HS-GC-IMS for discrimination and characterization of white and yellowed rice. *Cereal Chem.* **2020**, *97* (2), 496–504. https://doi.org/10.1002/cche.10264.

(184) Gerhardt, N.; Birkenmeier, M.; Sanders, D.; Rohn, S.; Weller, P. Resolution-optimized headspace gas chromatography-ion mobility spectrometry (HS-GC-IMS) for non-targeted olive oil profiling. *Anal. Bioanal. Chem.* **2017**, *409* (16), 3933–3942. https://doi.org/10.1007/s00216-017-0338-2.

(185) Ratiu, I. A.; Bocos-Bintintan, V.; Patrut, A.; Moll, V. H.; Turner, M.; Thomas, C. L. P. Discrimination of bacteria by rapid sensing their metabolic volatiles using an aspiration-type ion mobility spectrometer (a-IMS) and gas chromatography-mass spectrometry GC-MS. *Anal. Chim. Acta* **2017**, *982*, 209–217. https://doi.org/10.1016/j.aca.2017.06.031.

(186) Wang, Y.; Chen, P. Comparison of ion mobility fuzzy chromatography mass spectrometric (ImFCMS) fingerprinting and fcms fingerprinting for differentiation of American cranberry cultivars. *J. Anal. Test.* **2018**, *2* (3), 223–234. https://doi.org/10.1007/s41664-018-0059-3.

(187) Yang, X.; Feng, L.; Zhao, L.; Liu, X.; Hassani, D.; Huang, D. Effect of glycine nitrogen on lettuce growth under soilless culture: A metabolomics approach to identify the main changes occurred in plant primary and secondary metabolism. *J. Sci. Food Agric.* **2018**, *98* (2), 467–477. https://doi.org/10.1002/jsfa.8482.

(188) Arroyo-Manzanares, N.; García-Nicolás, M.; Castell, A.; Campillo, N.; Viñas, P.; López-García, I.; Hernández-Córdoba, M. Untargeted headspace gas chromatography–ion mobility spectrometry analysis for detection of adulterated honey. *Talanta* **2019**, *205* (July), 120123. https://doi.org/10.1016/j.talanta.2019.120123.

(189) Contreras, M. del M.; Jurado-Campos, N.; Arce, L.; Arroyo-Manzanares, N. A robustness study of calibration models for olive oil classification: Targeted and non-targeted fingerprint approaches based on GC-IMS. *Food Chem.* **2019**, *288* (October 2018), 315–324. https://doi.org/10.1016/j.foodchem.2019.02.104.

(190) Gerhardt, N.; Schwolow, S.; Rohn, S.; Pérez-cacho, P. R. Quality assessment of olive oils based on temperature-ramped HS-GC-IMS and sensory evaluation: Comparison of different processing approaches by LDA, kNN, and SVM. *Food Chem.* **2019**, *278* (July 2018), 720–728. https://doi.org/10.1016/j.foodchem.2018.11.095.

(191) Vasilopoulou, C. G.; Sulek, K.; Brunner, A. D.; Meitei, N. S.; Schweiger-Hufnagel, U.; Meyer, S. W.; Barsch, A.; Mann, M.; Meier, F. Trapped ion mobility spectrometry and PASEF enable in-depth lipidomics from minimal sample amounts. *Nat. Commun.* **2020**, *11* (1), 1–11. https://doi.org/10.1038/s41467-019-14044-x.

Declaration with signatures in possession of candidate and supervisor.

Declaration by the candidate:

Regarding **Chapter 3**, the nature and scope of my contribution were as follows:

Nature of contribution	**Extent of contribution (%)**
Performed the experiments, data analysis, co-wrote paper	73

The following co-authors have contributed to **Chapter 3**:

Name	**E-mail address**	**Nature of contribution**	**Extent of contribution (%)**
Marietjie A. Stander	lcms@sun.ac.za	Supervisor of the student, co-conceptualised the idea, contributed to method development and editing	5
André de Villiers	ajdevill@sun.ac.za	Co-supervisor of the student, co-conceptualised the idea, contributed to editing	5
Eleanor W. Hoffman	ewh@sun.ac.za	Hortology/Botany advice, co-conceptualised the idea and contributed to the editing.	3
D. Jacobus Brand	djbrand@sun.ac.za	NMR analysis and interpretation	2
Tim Causon	tim.causon@boku.ac.at	UHPLC-low field drift tube IM-HR-MS analyses	2

Signature of candidate: …… 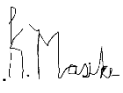 ……

Date: …25 February 2021……

Declaration by co-authors:

The undersigned confirm that:

The declaration above accurately reflects the nature and extent of the contributions of the candidate and the co-authors to **Chapter 3**,
No other authors contributed to **Chapter 3** besides those specified above, and
Potential conflicts of interest have been revealed to all interested parties and that the necessary changes have been made to use the material in Chapter 3 of this thesis.

Signature	**Institutional affiliation**	**Date**
	Stellenbosch University	17 February 2021
	Stellenbosch University	17 February 2021

Chapter 3: Detailed Phenolic Characterisation of *Protea* Pure and Hybrid Cultivars by Liquid Chromatography−Ion Mobility−High Resolution Mass Spectrometry (LC-IM-HR-MS)

Abstract

In this study we report a detailed investigation of the polyphenol composition of *Protea* pure (*P. cynaroides* and *P. neriifolia*) and hybrid cultivars (Black beauty and Limelight). Aqueous methanol extracts of leaf and bract tissues were analysed by ultra-high performance liquid chromatography hyphenated to photodiode array and ion mobility-high resolution mass spectrometric (UPLC-PDA-IM-HR-MS) detection. A total of 67 metabolites were characterised based on their relative reversed phase (RP) retention, UV-Vis spectra, low and high collision energy HR-MS data and collisional cross section (CCS) values. These metabolites included 41 phenolic acid esters and 25 flavonoid derivatives, including 5 anthocyanins. In addition, an undescribed hydroxycinnamic acid-polygalatol ester, caffeoyl-*O*-polygalatol (1,5-anhydro-[6-*O*-caffeoyl]- sorbitol(glucitol)) was isolated and characterised by 1D and 2D NMR for the first time. This compound and its isomer are shown to be potential chemo-taxonomic markers.

3.1. Introduction

Proteaceae is an angiosperm family endemic to Mediterranean-type regions of the Southern hemisphere, including South Africa and Australia. The Proteaceae family is made up of approximately 80 genera and more than 1700 species.[1] *Protea* species are located in fire-prone, semi-acrid environments and pollinated by sugarbirds, sunbirds and rodents.[2] Pure species and hybrid cultivars have become popular ornamental plants due to their vibrant inflorescence, with more than 3 million exported from South Africa in 2017, for example.[3] Historically, *Protea* plant tissue (leaves, stems and flowers) has been used for a range of applications, including in leather tanning, production of wagon wheels (*P. nitida*), and as cough syrup (using the nectar extracted from *P. repens* flowerheads).[4] Studies such as population genetic studies, revealed that different ecological ranges (Eastern vs Western Cape) result in distinct genetic clusters in the same species, e.g. *P. repens*[5] or white *P. mundii*[6] species. In both studies, adaptive and non-adaptive processes are thought to contribute to geographical isolation and potentially lead to evolutionary species. Transcriptomics has also been used to understand adaptive diversification in *P. repens*.[7] Studies dedicated to the phytochemical composition of *Protea* are limited; a few phenolic compounds[4,8,9] and polyol sugars[10] have been identified as leaf constituents. Most of these studies focused on selected compounds characterised by nuclear magnetic resonance (NMR) following their preparative isolation. Phenolic compounds in other Proteaceae members were also reported by Deans *et al*.,[11,12] where they found for example quercetin glycosides and naphthoquinones in *Lomatia* species.[12] No metabolomics studies on *Proteas* have been reported to date. This study forms part of a bigger study to better understand the post-harvesting browning process seen in *Protea* plants by studying the phenolic composition, which has commercial implications. However, to the best of our knowledge, the phytochemical origin of the striking inflorescence of *Proteas* is yet to be explained, and much of the phenolic composition of *Proteas* remains unknown.

High performance liquid chromatography (HPLC), and more recently ultra-high performance LC (UPLC), combined to diode array and especially high resolution-mass spectrometric (HR-MS) detectors, are the methods of choice in natural product research.[13–21] This may be accredited to sensitivity and resolving power of these methods, which enable detection and (tentative) assignment of up to hundreds of metabolites in a single analysis. Advances in tandem MS technology such as the data-independent acquisition strategies allow both the precursor and product ion data to be collected in a single chromatographic run,[22,23] eliminating the requirement of multiple injections. Nevertheless, the complexity of plant samples, which often contain isomeric and/or isobaric metabolites,[24–28] poses a severe analytical challenge.

The integration of ion mobility spectrometry (IMS) into (LC-) MS workflows has become an appealing analytical method for the differentiation of and improved identification of structurally similar metabolites.[29–33] IMS separates ions in the gas phase according to their charge, size and shape (collision cross section, CCS). CCS values are characteristic for each ion and describe the physicochemical properties of the ion as it traverses the IM cell under the influence of a potential difference and interacts with the neutral gas, usually N_2. IMS provides structural and ionic information that may facilitate metabolite identification, as well as the option to clean up MS data by filtering according to drift time. Isomeric compounds have been distinguished based on differences in their CCS values,[31,33] and IMS has been shown to separate prototropic ions of regioisomers.[34,35] For these reasons, it is not surprising that IMS has in recent years increasingly found application in metabolomic,[29] lipidomic[30] and proteomic[36] studies. Coupled to (U)HPLC-MS, IMS provides an additional parameter for compound identification in terms of arrival (drift) time and related CCS values, thereby increasing identification confidence in natural product research.

In this study, we report the detailed phenolic characterization of *Protea* plants; 2 pure species *P. cynaroides* and *P. neriifolia*, 2 hybrid cultivars Black beauty (Sheila (*P. magnifica* x *P. burchelli*) cross) and Limelight (*P. neriifolia* x *P. burchelli*); by exploiting the benefits offered by UPLC-PDA-IM-HR-MS for metabolite identification. These cultivars were selected based on the degree of variation in their LC-MS profiles.

3.2. Materials and methods

3.2.1. Materials

Authentic standards of vanillic acid, caffeic acid, (+)-catechin, (-)-epicatechin, rutin, 5-caffeoylquinic acid and isoquercetin were purchased from Sigma-Aldrich (MO, USA). Analytical-grade acetonitrile and methanol were obtained from Romil (Cambridge, UK). Formic acid was obtained from Merck (MO, USA).

3.2.2. Samples

Four *Protea* plants, comprising two hybrid cultivars, black beauty (Sheila (*P. magnifica* x *P. burchelli*) cross) and limelight (*P. neriifolia* x *P. burchelli*), and two pure species (*P. neriifolia* and *P. cynaroides*) were collected from the commercial farm “FynBloem” (34°09′01″S 19°54′52″E) and from the Harold Porter National Botanical Garden (34°21′06″S 18°55′37″E), respectively. Standard cultivation practices for irrigation and nutrition were followed at Fynbloem, as is recommended for Cape Flora production on nutrient poor soils, under Mediterranean climatic

conditions,[37] whereas inflorescences collected from the Harold Porter National Botanical Garden were obtained from a wild population. After hydration for a one-hour period in tap water at harvest, inflorescences were stored as dry stems at 4°C as stipulated by the South African Perishable Products Export Control Board (PPECB),[38] until extractions were performed.

3.2.3. Methods

3.2.3.1. Sample preparation

For each authentic standard, a 0.500 mg/mL solution was prepared in 50% (*v/v*) methanol in water containing 2% formic acid. The resulting solutions were placed in glass vials for analysis (injected as either mixtures or individual samples).

3.2.3.2. Metabolite extraction

For extraction, 1.00 g of fresh plant tissue (leaves or bracts) was crushed in a mortar and pestle and mixed with 15 mL of methanol/water/formic acid (50:48:2). Samples were prepared in triplicate for each plant tissue per *Protea* species or cultivar. After two hours, samples were subjected to sonication in an ultrasonic bath (0.5 Hz, Integral Systems, RSA) for one hour at room temperature. Post-sonication, samples were centrifuged (Hermle Z 160 M, LaborTechnik, Germany) at 15 994 x*g* for one hour to remove the cell debris. The resulting supernatants were placed in glass vials for analysis.

3.2.3.3. UPLC-PDA-IM-HR-MS analyses

Extracts were analysed on an Acquity UPLC instrument coupled to a Synapt G2 quadrupole time-of-flight (q-TOF) mass spectrometer (Waters Corporation, Manchester, UK) equipped with an Acquity HSS T3 C_{18} column (2.1 mm × 150 mm, 1.8 µm, Waters) using an injection volume of 2 µL. The mobile phases consisted of 0.1% formic acid in MilliQ water (solvent A) (analytical quality water was prepared by filtering using reverse osmosis water through a MilliQ system) and 0.1% formic acid in acetonitrile (solvent B), at a flow rate of 0.25 mL/min. The initial conditions were 0% B, maintained for 1 min, followed by a linear increase to 28% B at 22 min and 60% B at 30 min. A steep gradient was applied to 100% B at 31 min, kept for 1 min before returning to the initial conditions in 1 min; the column was re-equilibrated for 4 min at 0% B (total run time 37 min). The column temperature was maintained at 60°C. Detection was performed using photodiode array (PDA) and MS detectors. The Acquity PDA detector's (Waters) scanning range was from 230 to 650 nm, with a 1.2 nm bandwidth and a sampling rate of 20 Hz. Electrospray ionisation was performed in both negative (ESI^-, for phenolic acids and the majority of flavonoids) and positive ion modes (ESI^+, mainly for the anthocyanins).

For the analysis of anthocyanins, an Acquity BEH C_{18} column (2.1 mm × 100 mm, 1.7 µm particle size, Waters) was used with an injection volume of 3 µL and column temperature of 50°C. Highly acidic mobile phases were used,[39,40] consisting of MilliQ water containing 7.5% formic acid (solvent A) and acetonitrile containing 7.5% formic acid (solvent B). A flow rate of 0.20 mL/min was used. The initial conditions were 1% B, maintained for 0.50 min, followed by linear increases to 22% B at 20 min and 100% B at 20.10 min, kept for 1.40 min before returning the initial conditions in 10 sec; the column was re-equilibrated for 3.4 min at 1% B (total run time 25 min). Anthocyanins were monitored at a wavelength range of 500-550 nm, and by ESI^+-MS.

For MS detection, both ESI^- and ESI^+ were used, using optimised settings presented elsewhere.[41,42] Briefly, the cone voltage was set at 15 V, N_2 was used as desolvation gas at a temperature of 275˚C and a flow rate of 650 L/h. Sodium formate was used for the calibration of the instrument and leucine enkaphalin was used as the lock mass (*m/z* = 554.2615 or 556.2771 reference masses) to achieve high mass resolution. Data were acquired for a mass range of 150-1500 Da in resolution-mode at a rate of 0.2 scans per second. In MS^E mode, data were acquired using two channels: at low collision energy (6 V, mass range 150-1500 Da), and with a collision energy ramped from 20 to 60 V (for mass range 40-1500 Da).

Travelling-wave IMS (TWIMS) was performed using the following settings: extraction cone 4 V, helium cell gas flow 180 mL/min, IM buffer gas (N_2) flow 110 mL/min, IM wave velocity 650 m/s and IM wave height 40 V. Polyalanine (PolyA) was used as calibrant to determine $^{TW}CCS_{N2}$ values from the measured arrival time distributions in both ESI^+ and ESI^- modes and was prepared in H_2O/MeOH (50:50, *v:v*) at a concentration of 277 mg/mL. Calibration was performed using singly charged PolyA oligomers (n = 3 to 14) covering a mass range 231 to 1012 Da and CCS values ranging from 150 to 308 $Å^2$ in ESI^- and from 151 to 306 $Å^2$ in ESI^+. For data acquisition and processing, MassLynx™ 4.1 and Driftscope 2.9 software (Waters) were utilised.

3.2.3.4. UPLC-low field drift tube IM-HR-MS analyses

Separation was performed using an Acquity HSS T3 C_{18} column (2.1 mm × 150 mm, 1.8 µm, Waters) at 40°C. The binary mobile phase comprised (A) 0.1% (*v/v*) formic acid in water, and (B) acetonitrile. Using a flow rate of 0.25 mL/min, an initial composition of 100% A was held for 1 min, followed by a gradient from 0-28% B in 1-22 min, then increasing to 40% from 22-30 min, and finally to 100% B from 30-31 min. After a 1 min wash, the condition was returned to 0% B at 33 min and held for 4 min (total run time of 37 min). Detection was performed using an Agilent 6560 IM-q-TOF MS instrument (Agilent Technologies, Waldbronn, Germany). Nitrogen was used as drying gas at 350°C, a sheath gas temperature of 225 °C and a sheath gas flow rate of 12 L/min.

The nebulizer gas pressure was 30 psi, the MS capillary voltage was -3500 V, the nozzle voltage -500 V and the fragmentor was set to -275 V. Following tuning in the 2 GHz extended dynamic range mode with a mass range of 50-1700 *m/z*, mass calibration was undertaken immediately prior to measurements using the supplied tune mixture of the manufacturer.

The IMS trapping funnel was operated with an accumulation time of 20 000 µs and released packages of ions every 50 ms with a trap release time of 150 µs. The drift tube was operated with an absolute entrance voltage of -1574 V and an exit voltage of -224 V with a drift tube pressure of 3.95 Torr at precise temperature between 26 and 28 °C using high purity N_2 as the collision gas. The acquisition settings were adjusted to yield 30 ion mobility transients per frame corresponding to 0.5 ion mobility frames per second. A single-field calibration approach was employed using ^{DT}CCS values and methodology established in a recent study.[43]

3.2.3.5. Metabolite annotation

For compound annotation and identification, MS^E fragmentation patterns, standards, surrogate standards,[44] and online databases such as Dictionary of Natural Products,[45] KNApSAck,[46] METLIN[47] and ChemSpider[48] were used. The level of identification used for the annotated compounds is indicated as set out by the COSMOS Metabolomics Standards Initiative. Experimental $^{TW}CCS_{N2}$ values (Å^2) were compared to available literature,[32,49] and for selected compounds to $^{DT}CCS_{N2}$ values determined on a drift tube instrument.

*3.2.3.6. Preparative isolation of **25***

The HPLC system used was a Waters 1525 equipped with a Gemini C_{18} column (10.0 mm x 250 mm, 10 µm, Phenomenex) and controlled by a Waters Empower Pro software. The injection volume was 200 µL. A binary solvent mixture was used consisting of MilliQ water containing 0.1% formic acid (solvent A) and acetonitrile containing 0.1% formic acid (solvent B). At a flow rate of 3 mL/min, the initial conditions were 20% B, maintained for 1 min, followed by a linear increase to 100% B at 28 min, maintained for 1 min, followed by a change to the initial conditions (20% B) after 1 min and column re-equilibration for 5 min (total run time 35min). Detection was performed using a dual absorbance detector (Waters 2487) set at 254 and 325 nm, with a sampling rate of 1 Hz. Compound **25**, eluting at 9.83 min, was collected; the purity of the obtained fraction was confirmed by UPLC-PDA analysis. Compound **25** was concentrated by evaporation under vacuum and the residue dried under vacuum over P_2O_5 to give 1.4 mg of a light brown powder.

3.2.3.7. *Nuclear Magnetic Resonance (NMR) spectroscopy*

An Agilent 600 MHz Inova NMR spectrometer fitted with an inverse-detection 5 mm dual channel probe and a pulsed field gradient coil was used to conduct the NMR analyses. The standard Agilent VnmrJ 4.2 1D and 2D pulse sequences were customised for the concentration and resolution requirements of the sample. All the NMR data discussed in this report were derived from ^{1}H, ^{13}C, TOCSY, gHSQCAD, gHMBCAD NMR experiments, run at 25˚C in DMSO-d_6. All spectra were processed using the licensed Mestrenova 12.0.4 software package.

3.3. Results and discussion

Fresh tissue rather than dried leaves and bracts were used in this study, as some *Protea* leaves and stems are known to blacken upon damage or cutting.[50–53] This precautionary measure minimised the risk of metabolite decomposition. The phenolic composition of the 4 *Protea* plants, two pure species (*P. cynaroides* and *P. neriifolia*) and two hybrid cultivars (Black beauty and Limelight) (Figure 3.1), were analysed by UPLC-PDA-IM-HR-MS.

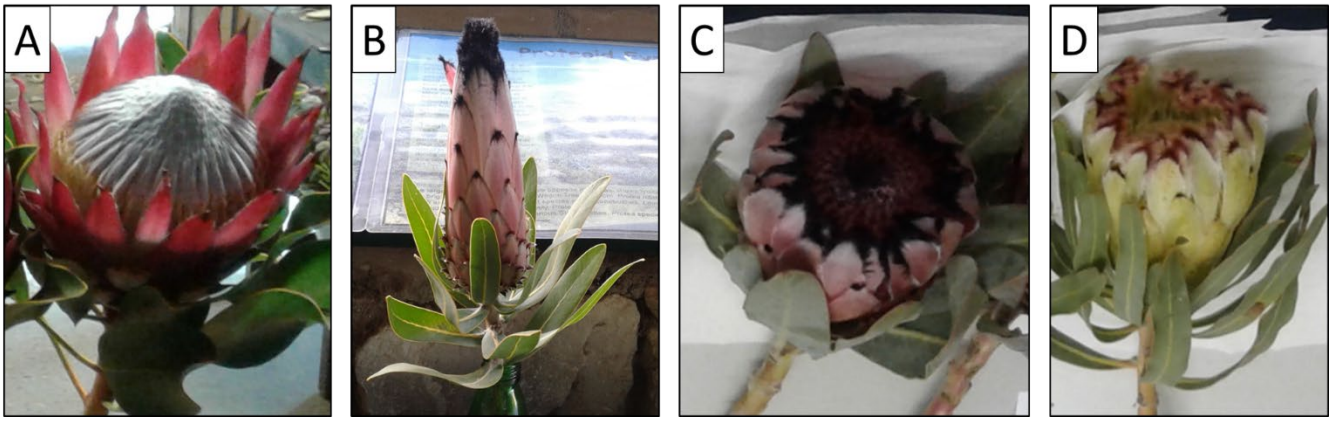

Figure 3.1: The four *Protea* plants studied: two pure species (**A**) *P. cynaroides* (King Protea), (**B**) *P. neriifolia,* and the two hybrid cultivars (**C**) Black beauty (Sheila (*P. magnifica* x *P. burchelli*) cross), **D**) Limelight (*P. neriifolia* x *P. burchelli*).

Figure 3.2 illustrates the differences between the LC-MS chromatograms obtained for aqueous methanol extracts of the leaves of the 4 *Protea* plants studied. Compounds were annotated or identified based on molecular formulae obtained from HR-MS data, MS^E fragmentation patterns (**3, 13, 16, 20, 21, 23, 24, 26-28, 30-32, 34, 40, 41, 44, 47-50, 53, 63-67**) and comparison with literature data for standards (**10, 14, 15, 17, 18, 22, 29, 42, 45, 52, 55-62**), compounds previously unambiguously identified in *Protea* species (**4-9, 12, 33, 35-39**) and databases such as the Dictionary of Natural Products,[45] KNApSAck,[46] METLIN[47] and ChemSpider[48]. Selected

compounds were also unambiguously identified based on comparison with standards (**11, 19, 43, 46, 51, 54**), surrogate standards (**1, 2**) or by preparative isolation and NMR characterization (**25**). Furthermore, CCS values obtained on a travelling wave IM instrument using N_2 as the drift gas ($^{TW}CCS_{N2}$) were compared to literature values where available as an additional means of identification. The accuracy of the experimentally determined $^{TW}CCS_{N2}$ values were confirmed by comparison with the CCS values determined on a low-field drift tube instrument ($^{DT}CCS_{N2}$) for selected compounds (Supplementary; Table S3.1). The metabolites identified in this manner are listed in Table 3.1 (phenol and phenolic acid derivatives) and Table 3.2 (flavonoid derivatives). Structures of the family of phenol, phenolic acids and hydroxycinnamic acids studied are shown in Supplementary; Figure S3.1. Structures of the family of flavan-3-ols, anthocyanidins, flavonols and flavones identified are shown in Supplementary; Figure S3.2. In addition, the distribution of these metabolites across the studied plant species and cultivars are shown in Supplementary; Figure S3.3. In the following sections, the assignment of each of the (tentatively or putatively) identified compounds is discussed according to chemical class.

3.3.1. Phenolic acid derivatives

3.3.1.1. Phenol and hydroxybenzoic acid derivatives

Unless otherwise stated, all compounds in this class showed UV spectra typical of benzoic acid derivatives, with UV absorbance maxima at ≈ 280 nm. Compounds **1** (retention time (t_R) 4.14 min) and **4** (t_R 6.26 min) showed molecular ions at *m/z* 287.0771 ($[M-H]^-$, $C_{12}H_{16}O_8$). $^{TW}CCS_{N2}$ values were calculated as 157.3 and 154.1 $Å^2$ for the respective ions. The MS^E spectra for both peaks revealed an intense product ion at *m/z* 125.0243 ($C_6H_6O_3$), resulting from the neutral loss of a 162 Da fragment, which is characteristic of a neutral loss of a hexose sugar. Perold and Carlton identified the main leaf metabolite in *Protea neriifolia* as neriifolin, which, following acid hydrolysis, released the aglycone benzene-1,2,4-triol (hydroxyquinol; molar mass 126 g/mol).[9] Furthermore, MS/MS analysis of benzene-1,3,5-triol (phloroglucinol)-*O*-hexoside (phlorin) also showed the ion *m/z* 125.0243 as the product ion of *m/z* 287.0771.[54] Phlorin is used as an orange peel marker to determine juice quality in the fruit juice industry.[55] Thus, to distinguish between the two isomeric peaks **1** and **4**, phlorin was extracted from the albedo layer of orange peels and used as a surrogate standard.[44] This allowed the putative identification of the minor peak (**1**) as phlorin, while the more abundant peak (**4**) was tentatively identified as hydroxyquinol-*O*-glycoside.[4,9]

Two peaks with molecular ions at *m/z* 271.0794 ($C_{12}H_{16}O_7$) eluted at t_R's of 5.71 and 5.89 min, respectively. Their high collision energy spectra showed fragment ions at *m/z* 109.0430 ($C_6H_6O_2$) and 108.0193, resulting from the neutral loss of a hexose moiety. The aglycone (*m/z* 109.0430)

and the radical aglycone moiety (*m/z* 108.0193) are consistent with a hydroquinone (benzene-1,4-diol; $C_6H_6O_2$) product ion. Thus, these two peaks were annotated as arbutin (hydroquinone-*O*-hexoside) isomers.[17] Garcia-Jimenez *et al*. noted two hydroquinone glycosides: β-arbutin (found naturally in the plant kingdom) and α-arbutin (which is enzymatically formed from either hydroquinone or β-arbutin).[56] β-Arbutin has been reported in pears,[57,58] and was therefore extracted from a fresh pear fruit and used as a surrogate standard in this study. Compound **2** in the *Protea* samples was accordingly putatively identified as β-arbutin, whereas **3** was tentatively identified as α-arbutin as per the elution order noted by Garcia-Jimenez *et al*.[56] The $^{TW}CCS_{N2}$ values for both arbutin isoforms were identical (156.1 Å^2).

Three compounds (**5**, **6** and **7**) with identical molecular formulae (*m/z* 301.0915, $C_{13}H_{18}O_8$), were detected at t_R's 7.11, 7.23 and 7.43 min, respectively, with $^{TW}CCS_{N2}$ values of 159.2, 161.1 and 162.9 Å^2, respectively. MS^E spectra for these compounds showed fragment ions at *m/z* 139.0376 ($C_7H_8O_3$; bp) and 121.0267, with the abundant ion at *m/z* 139.0376 resulting from the neutral loss of a hexose moiety and the ion at *m/z* 121.0267 representing the dehydrated (-18 Da) moiety of the product ion at *m/z* 139.0376. The abundant ion at *m/z* 139.0376 was tentatively annotated as protocatechuic (3,4-dihydrobenzyl) alcohol, as this metabolite has previously been identified in *Protea* species.[4,59] Thus, **5**, **6** and **7** were tentatively identified as protocatechuic alcohol-hexoside isomers, which likely differ in their position of glycosylation, explaining the slight differences in their $^{TW}CCS_{N2}$ values.

Compounds **8**, **9** and **12** at t_R 8.32, 8.43 and 9.39 min, respectively, showed precursor ions at *m/z* 315.0803 ($C_{13}H_{16}O_9$) and a UV maxima at ≈ 315 nm. Their MS^E spectra showed fragments at *m/z* 153.0198, 152.0099, 109.0268 and 108.0194, where: 1) the fragment at *m/z* 153.0198 ($C_7H_6O_4$) resulted from the neutral loss of a hexose moiety and was annotated as a dihydroxybenzoic acid derivative; 2) the product ion at *m/z* 152.0099 represents the corresponding radical aglycone ion; 3) the ion at *m/z* 109.0268 resulted from the decarboxylation (- 44 Da) of the dihydroxybenzoic acid moiety (*m/z* 153.0198), and 4) the product ion at *m/z* 108.0194 resulted from the decarboxylation of the radical aglycone ion. These fragment ions are characteristic of the dihydroxybenzoic acid glycoside, protocatechuic acid (3,4-dihydroxybenzoic acid)-*O*-hexoside and its aglycone.[13] In a study by Perold *et al*., protocatechuic acid was identified as a leaf constituent of *Protea lacticolor*.[59] Compounds **8**, **9** and **12** were therefore annotated as protocatechuic acid-*O*-hexoside isomers. Compound **8** showed the largest $^{TW}CCS_{N2}$ value (164.4 Å^2), whereas **9** and **12** had identical $^{TW}CCS_{N2}$ values of 160.7 Å^2.

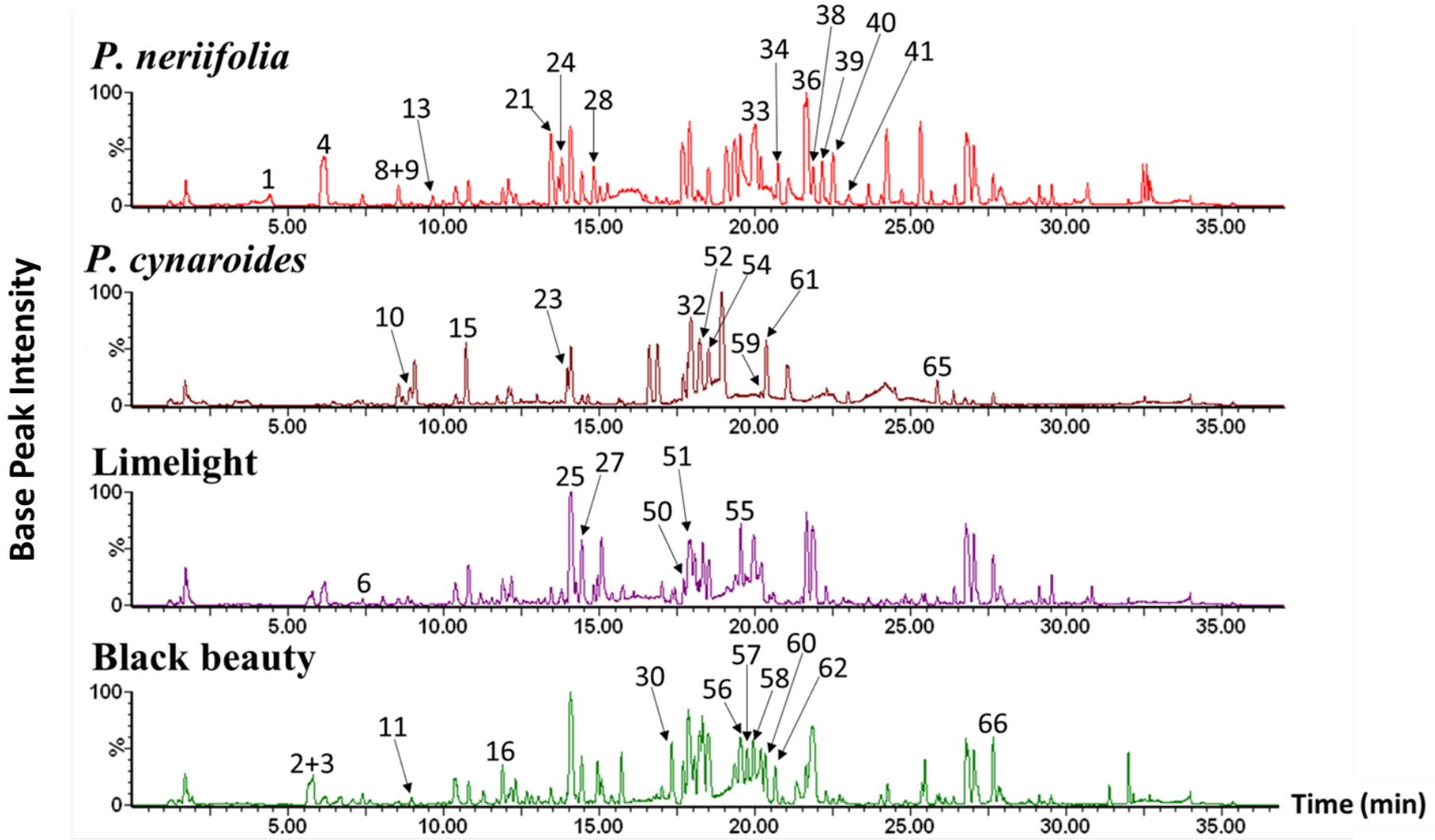

Figure 3.2: Stacked UPLC-HR-MS base peak ion (BPI) chromatograms illustrating the different chromatographic profiles between extracts obtained from leaf tissues of *P. neriifolia*, *P. cynaroides* (King Protea), Limelight (*P. neriifolia* x *P. burchelli*) and Black beauty (Sheila (*P. magnifica* x *P. burchelli*) cross). Compound numbers correspond to Tables 3.1 and 3.2.

Table 3.1: Summary of the phenolic and phenolic acid derivatives (tentatively) identified in the studied *Protea* plants: *P. cynaroides* (King Protea), *P. neriifolia*, Black beauty (Sheila (*P. magnifica* x *P. burchelli*) cross) and Limelight (*P. neriifolia* x *P. burchelli*) by UPLC-PDA-IM-HR-MS. bp = base peak.

Number	Compound	Adduct	t_R (min)	*m/z*	Mass Error (ppm)	Fragments	Chemical Formula	UV-Vis max (nm)	$^{TW}CCS_{N2}$ (Å^2)	Level of Identification	Reference(s)
Phenolic acids											
1	Phlorin (benzene-1,3,5-triol)-*O*-hexoside)[*a]	$[M-H]^-$	4.14	287.0771	-3.5	287-> 125.0243 (bp)	$C_{12}H_{16}O_8$	284	157.3	1	Surrogate standard
2	β-Arbutin (hydroquinone-*O*-hexoside) isomer[*a,c,d]	$[M-H]^-$	5.71	271.0794	-0.7	271-> 109.0430; 108.0193 (bp)	$C_{12}H_{16}O_7$	282	156.1	1	Surrogate standard
3	α-Arbutin (hydroquinone-*O*-hexoside) isomer[*]	$[M-H]^-$	5.89	271.0800	-2.2	271-> 109.0430; 108.0193 (bp)	$C_{12}H_{16}O_7$	283	158.3	2	[17,56]
4	Hydroxyquinol (benzene-1,2,4-triol)-*O*-hexoside[*a,c,d]	$[M-H]^-$	6.26	287.0754	-0.3	287-> 125.0222 (bp)	$C_{12}H_{16}O_8$	282	154.1	2	[4,9]
5	Protocatechuic alcohol (3,4-dihydroxybenzyl alcohol)-*O*-hexoside isomer 1[*#a,b,c,d]	$[M-H]^-$	7.11	301.0915	4.0	301-> 139.0376 (bp); 121.0267	$C_{13}H_{18}O_8$	280	159.2	3	[4,59]
6	Protocatechuic alcohol-*O*-hexoside isomer 2[*#a,b]	$[M-H]^-$	7.23	301.0904	-1.3	301-> 139.0380 (bp); 121.0280	$C_{13}H_{18}O_8$	280	161.0	3	[4,59]
7	Protocatechuic alcohol-*O*-hexoside isomer 3[*a,c,d]	$[M-H]^-$	7.43	301.0925	4.3	301-> 139.0368 (bp); 121.0260	$C_{13}H_{18}O_8$	280	162.9	3	[4,59]
8	Protocatechuic acid (3,4-dihydroxybenzoic acid)-*O*-hexoside isomer 1[*a,b,c,d]	$[M-H]^-$	8.32	315.0803	1.3	315 -> 153.0198 (bp); 109.0298; 108.0194	$C_{13}H_{16}O_9$	315	164.4	3	[13,59]
9	Protocatechuic acid-*O*-hexoside isomer 2[*b,c,d]	$[M-H]^-$	8.43	315.0702	1.9	315 -> 153.0165; 152.0099; 109.0268; 108.0194 (bp)	$C_{13}H_{16}O_9$	315	160.7	3	[13,59]
10	Protocatechuic acid[*b]	$[M-H]^-$	8.81	153.0203	4.6	153 -> 152.0066; 109.0301 (bp); 108.0206	$C_7H_6O_4$	259, 293	107.5	2	[13,59]
11	Vanillic acid (4-hydroxy-3-methoxybenzoic acid)-*O*-hexoside[*a,c,d]	$[M-H]^-$	8.98	329.0862	-1.2	329 -> 167.0331 (bp); 152.0108; 123.0422; 108.0188	$C_{14}H_{18}O_9$	253, 290	177.7	2	[13,49,59]
12	Protocatechuic acid-*O*-hexoside isomer 3[*b]	$[M-H]^-$	9.39	315.0702	-2.9	315 -> 153.0165; 152.0099; 109.0268; 108.0194 (bp)	$C_{13}H_{16}O_9$	315	160.7	3	[13,59]
13	Hydroxyquinol-*O*-hexoside-*O*-acetyl[*a]	$[M-H]^-$	9.53	329.0872	-1.5	329 -> 287.0754; 125.0222 (bp)	$C_{14}H_{18}O_9$	282	169.4	3	[9]
14	3-Caffeoyl-*O*-quinic acid[*#c,d]	$[M-H]^-$	10.01	353.0873	-2.0	353-> 191.0548 (bp); 179.0353; 135.0442	$C_{16}H_{18}O_9$	328	165.4	2	[60,61]
15	*p*-Hydroxybenzoic acid-*O*-deoxy-hexose isomer 1[*#b]	$[M-H]^-$	10.60	283.0808 (bp)	0.0	283-> 137.0228; 93.0324	$C_{13}H_{16}O_7$	258	157.4	3	[13,59]

16	3-*p*-Coumaroyl-*O*-quinic acid*#a,c,d	[M-H]-	11.69	337.0898	0.9	337 -> 191.0573; 163.0396 (bp); 119.0487	$C_{16}H_{18}O_8$	310	175.9 and 160.3	2	61
17	Feruloyl-*O*-hexoside isomer 1*b	[M-H]-	11.96	355.1039	3.5	355 -> 193.0493 (bp); 134.0368	$C_{16}H_{20}O_9$	292	194.3	3	13
18	*p*-Hydroxybenzoic acid-*O*-deoxy-hexose isomer 2*c,d	[M-H]-	12.48	283.0800	2.8	283->137.0203 (bp); 93.0324	$C_{13}H_{16}O_7$	260	161.1	3	13,59
19	5-Caffeoyl-*O*-quinic acid#c,d	[M-H]-	12.54	353.0862	-2.8	353 -> 191.0542 (bp)	$C_{16}H_{18}O_9$	325	177.2	1	Standard
20	3-Feruloyl-*O*-quinic acid*a,c,d	[M-H]-	12.83	367.1043	-4.1	367-> 193.0498 (bp); 191.0502; 134.0365	$C_{17}H_{20}O_9$	325	176.0	2	61
21	Protocatechuic acid-*O*-hexoside-*O*-hydroxyquinol isomer 1*a,d	[M-H]-	13.34	423.0989 (bp)	0.0	423-> 153.0184; 125.0225; 109.0301	$C_{19}H_{20}O_{11}$	258	184.1	3	MS^E
22	Feruloyl-*O*-hexoside isomer 2*b	[M-H]-	13.51	355.1041	-2.5	355 -> 193.0509 (bp); 134.0368	$C_{16}H_{20}O_9$	293	168.9	3	13
23	Protocatechuic acid-*O*-hexoside-*O*-hydroxyquinol isomer 2*a	[M-H]-	13.66	423.0989 (bp)	-2.8	423-> 153.0184; 125.0225; 109.0301	$C_{19}H_{20}O_{11}$	258	194.6	3	MS^E
24	*p*-Hydroxybenzoic acid derivative*a,b,c	[M-H]-	13.89	423.0923	-1.4	423-> 281.0659 (bp); 137.0235; 93.0323	$C_{19}H_{20}O_{11}$	266	187.0	3	MS^E
25	Caffeoyl-*O*-polygalatol (1,5-anhydro-[6-*O*-caffeoyl]-sorbitol(glucitol))*#a,b,c,d	[M-H]- [M+H]+	14.05	325.0934 327.1064	0.6	325-> 179.0350; 161.0247 (bp); 135.0451; 133.0299 327-> 163.0385 (bp)	$C_{15}H_{18}O_8$	325	176.1 and 158.7	1	NMR
26	Protocatechuic acid-*O*-hexoside-*O*-protocatechuic alcohol isomer 1*a,d	[M-H]-	14.25	437.1074	-3.0	437-> 301.0927; 153.0193; 139.0394 (bp); 109.0286	$C_{20}H_{22}O_{11}$	263	191.5	3	47
27	Caffeoyl-*O*-polygalatol isomer*a,c,d	[M-H]- [M+H]+	14.42	325.0911 327.1064	-1.2	325-> 179.0372; 161.0239 (bp); 135.0442; 133.0302 327-> 163.0385 (bp)	$C_{15}H_{18}O_8$	315	176.1 and 158.7	3	MS^E
28	Protocatechuic acid-*O*-hexoside-*O*-hydroxyquinol isomer 3*a,c,d	[M-H]-	14.64	423.0923	-0.9	423-> 153.0196; 125.0241; 109.0287	$C_{19}H_{20}O_{11}$	263	184.1	3	MS^E
29	5-*p*-Coumaroyl-*O*-quinic acid#	[M-H]-	14.76	337.0918	2.7	337 -> 191.0545 (bp)	$C_{16}H_{18}O_8$	312	180.8 and 162.1	2	61
30	*p*-Hydroxybenzyl-*O*-arbutin isomer 1*c,d	[M-H]-	17.16	391.1029 bp	-0.5	391-> 281.0673; 137.0223; 109.0282; 93.0330	$C_{19}H_{20}O_9$	280	176.5	3	MS^E
31	*p*-Hydroxybenzyl-*O*-arbutin isomer 2*c	[M-H]-	17.58	391.1030 (bp)	4.1	391-> 281.0669; 137.0239; 109.0297; 93.0348	$C_{19}H_{20}O_9$	280	176.5	3	MS^E
32	Protocatechuic acid-*O*-hexoside-*O*-protocatechuic alcohol isomer 2*#b	[M-H]-	17.68	437.1083	-2.3	437-> 153.0195 (bp); 109.0295	$C_{20}H_{22}O_{11}$	263	182.4	3	47

33	Neriifolin (benzyl-*O*-hexoside-*O*-hydroxyquinol) isomer 1[*a,c,d]	$[M-H]^-$	19.63	391.1036	2.3	391-> 287.0748; 125.0242 (bp)	$C_{19}H_{20}O_9$	287	184.6	3	[9]
34	Hydroxyquinol-*O*-hexoside derivative isomer 1[*a,c,d]	$[M-H]^-$	20.37	405.1214	-2.5	405-> 287.0725; 125.0228 (bp)	$C_{20}H_{22}O_9$	281	187.3	3	MS[E]
35	Lacticolorin/Pilorubrosin (benzyl-*O*-hexoside-*O*-protocatechuic alcohol) isomer 1[*a,b,c,d]	$[M-H]^-$	21.17	405.1182	-3.0	405-> 139.0372 (bp); 121.0273	$C_{20}H_{22}O_9$	281	191.9	3	[59,62]
36	Neriifolin isomer 2[*a,c,d]	$[M-H]^-$	21.29	391.1034	2.3	391-> 287.0752; 125.0229 (bp); 121.0267	$C_{19}H_{20}O_9$	281	186.0	3	[9]
37	Lacticolorin/Pilorubrosin isomer 2[*a,b,c,d]	$[M-H]^-$	21.49	405.1181	0.7	405-> 139.0389 (bp); 121.0282	$C_{20}H_{22}O_9$	281	193.4	3	[59,62]
38	Eximin (6-*O*-benzyl-*O*-arbutin)[*#a,c,d]	$[M-H]^-$	21.51	375.1069	1.6	375-> 121.0277; 109.0262; 108.0198 (bp)	$C_{19}H_{20}O_8$	282	183.3	2	[4,63]
39	Neriifolin isomer 3[*a,c]	$[M-H]^-$	21.75	391.1024	2.8	391-> 287.0752; 125.0229 (bp); 121.0267	$C_{19}H_{20}O_9$	281	187.5	3	[9]
40	Hydroxyquinol-*O*-hexoside derivative isomer 2[*#a,c,d]	$[M-H]^-$	22.05	405.1192	1.5	405-> 287.0778; 125.0241 (bp)	$C_{20}H_{22}O_9$	280	187.3	3	MS[E]
41	Hydroxyquinol-*O*-hexoside derivative isomer 3[*a]	$[M-H]^-$	22.54	405.1193	1.7	405-> 287.0748; 125.0239 (bp)	$C_{20}H_{22}O_9$	280	188.9	3	MS[E]

[*] detected in leaf tissue; [#] detected in bract tissue; [a-d] specify compounds detected in [a] *P. neriifolia*, [b] *P. cynaroides* (King Protea), [c] black beauty and [d] limelight.

Table 3.2: Summary of the flavonoids (tentatively) identified in the studied *Protea* plants: *P. cynaroides* (King Protea), *P. neriifolia*, Black beauty (Sheila (*P. magnifica* x *P. burchelli*) cross) and Limelight (*P. neriifolia* x *P. burchelli*) by UPLC-PDA-IM-HR-MS.

Number	Compound	Adduct	t_R (min)	*m/z*	Mass Error (ppm)	Fragments	Chemical Formula	UV-Vis max (nm)	$^{TW}CCS_{N2}$ (Å^2)	Level of Identification	Reference(s)
Flavonoids											
42	B-type procyanidin[*#a,c,d]	$[M-H]^-$ $[M+H]^+$	11.25	577.1327 579.1501	0.5	577-> 425.0819; 407.0695; 289.0684; 245.0798; 125.0219 (bp) 579-> 409.0894; 287.0554; 127.0390 (bp)	$C_{30}H_{26}O_{12}$	278	220.1	3	[16,64]
43	(+)-Catechin[*#a,c,d]	$[M-H]^-$	12.17	289.0714 (bp)	0.0	289-> 245.0808; 221.0799; 203.0719; 179.0359; 151.0397; 137.0238; 125.0243; 109.0298; 97.0279; 83.0157	$C_{15}H_{14}O_6$	279	150.1	1	Standard
44	Delphinidin-*O*-hexoside[#a,c]	$[M]^+$	12.86	465.1032	-2.4	465-> 303.0502 (bp); 257.0441; 229.0491; 201.0548	$C_{21}H_{21}O_{12}$	279, 525	204.7	2	[14,65]

45	B-type procyanidin*#c	[M-H]- [M+H]+	13.37	577.1327 579.1501	0.2	577-> 425.0808; 407.0695; 289.0684; 245.0731; 125.0219 (bp) 579-> 409.0894; 287.0554; 127.0390 (bp)	$C_{30}H_{26}O_{12}$	279	220.1	3	16,64
46	(-)-Epicatechin*#c	[M-H]-	14.21	289.0717 (bp)	0.0	289-> 245.0819; 221.0809; 203.0708; 179.0359; 151.0397; 137.0196; 125.0247; 109.0296; 97.0291; 83.0136	$C_{15}H_{14}O_6$	279	150.1	1	Standard
47	Cyanidin-*O*-hexoside#a,b,c	[M]+	14.91	449.1084	-2.0	449-> 287.0555 (bp); 241.0489	$C_{21}H_{21}O_{11}$	279, 520	201.3	2	14,49,65
48	Petunidin-*O*-hexoside#a,c	[M]+	16.42	479.1181	-0.6	479-> 317.0654 (bp); 302. 0422; 274.0473; 245.0444; 217.0493; 203.0341	$C_{22}H_{23}O_{12}$	279, 525	207.8	2	14,65
49	Peonidin-*O*-hexoside#a,c	[M]+	17.64	463.1230	-1.5	463-> 301.0703 (bp); 286.0462; 258.0525; 230.0562; 201.0553	$C_{22}H_{23}O_{11}$	525	204.7	2	14,65
50	Quercetin-*O*-hexoside-*O*-deoxy-hexose*a,b,c,d	[M-H]-	17.66	609.1456 (bp)	-0.8	609 -> 301.0328; 300.0266; 271.0239; 255.0288; 243.0347; 178.9954; 151.0012	$C_{27}H_{30}O_{16}$	255, 352	232.2	2	49
51	Rutin (quercetin-3-*O*-rutinoside (α-L-rhamnopyranosyl-(1→6)-β-D-glucopyranose))*a,b,c,d	[M-H]-	17.86	609.1456 (bp)	0.0	609 -> 301.0330; 300.0276; 271.0228; 255.0283; 243.0334; 178.9966; 151.0018	$C_{27}H_{30}O_{16}$	257, 352	231.0	1	Standard, 49
52	Quercetin-*O*-galactoside*#a,b,c,d	[M-H]-	18.16	463.0877	-0.2	463-> 301.0332; 300.0267 (bp); 271.0237; 255.0282; 243.0278; 178.9978; 151.0029	$C_{21}H_{20}O_{12}$	254, 351	198.5	2	19,66
53	Malvidin-*O*-hexoside#a,c	[M]+	18.37	493.1345	-0.8	493-> 331.0814 (bp); 315.0495; 287.0544; 270.0522; 242.0571	$C_{23}H_{25}O_{12}$	281, 527	212.8	2	14,65
54	Isoquercetin (quercetin-3-*O*-glucoside)*#a,b,c,d	[M-H]-	18.42	463.0878 (bp)	1.9	463-> 301.0337; 300.0267; 271.0244; 255.0288; 243.0287; 178.9993; 151.0019	$C_{21}H_{20}O_{12}$	255, 351	198.5	1	Standard; 19,66
55	Kaempferol-*O*- hexoside-*O*-deoxy-hexose*a,d	[M-H]-	19.45	593.1531 (bp)	0.5	593-> 285.0406; 284.0318; 255.0291; 159.0294	$C_{27}H_{30}O_{15}$	266, 346	228.7	3	14,67
56	Quercetin-*O*-pentoside*#c	[M-H]-	19.46	433.0760	1.2	433-> 301.0324; 300.0267 (bp); 271.0247; 255.0280; 243.0258; 151.0037	$C_{20}H_{18}O_{11}$	256, 351	193.0	3	19
57	Isorhamnetin-*O*-hexoside-*O*-deoxy-hexose isomer 1*c,d	[M-H]-	19.63	623.1597 (bp)	-0.2	623-> 315.0490; 314.0417; 300.0262; 299.0190;	$C_{28}H_{32}O_{16}$	253, 349	234.5	3	18

						271.0233; 255.0296; 243.0296					
58	Isorhamnetin-*O*-hexoside-*O*-deoxy-hexose isomer 2[*a,b,c,d]	$[M-H]^-$	19.87	623.1601 (bp)	-0.8	623 -> 315.0489; 314.0411; 300.0244; 271.0234; 255.0280; 243.0292	$C_{28}H_{32}O_{16}$	253, 351	235.7	3	[18]
59	Kaempferol-3-*O*-glucoside[*a,c,d]	$[M-H]^-$	20.20	447.0920 (bp)	1.3	447-> 285.0374; 284.0322; 255.0288; 159.0299	$C_{21}H_{20}O_{11}$	265, 340	197.3	2	[14]
60	Isorhamnetin-*O*-galactoside[*d]	$[M-H]^-$	20.32	477.1033 (bp)	0.0	477 -> 315.0476; 314.0410; 271.0226; 243.0280; 159.0273	$C_{22}H_{22}O_{12}$	268, 345	205.3	3	[18]
61	Quercetin-*O*-deoxy-hexose[*b]	$[M-H]^-$	20.37	447.0919	-2.2	447 -> 301.0323; 300.0263 (bp); 271.0235; 255.0302; 243.0288; 178.9968; 151.0019	$C_{21}H_{20}O_{11}$	253, 347	192.8	3	[19]
62	Isorhamnetin-*O*-glucoside[*#a,d]	$[M-H]^-$	20.67	477.1033 (bp)	-0.6	477 -> 315.0471; 314.0437; 271.0262; 243.0284	$C_{22}H_{22}O_{12}$	268, 341	205.3	3	[18]
63	Isorhamnetin-*O*-pentoside[*c]	$[M-H]^-$	21.76	447.0927 (bp)	0.0	447 -> 315.0463; 314.0437; 271.0255; 243.0294	$C_{21}H_{20}O_{11}$	268, 347	198.7	3	MS^E
64	Kaempferol-*O*-deoxy-hexose[*b]	$[M-H]^-$	22.37	431.0978	1.9	431 -> 285.0393 (bp); 284.0378; 255.0313	$C_{21}H_{20}O_{10}$	263, 340	193.0	3	[15]
65	Isorhamnetin[*b]	$[M-H]^-$	26.17	315.0503	0.3	315 -> 300.0265 (bp); 271.0240; 255.0296; 243.0306; 153.0183	$C_{16}H_{12}O_7$	268, 350	162.6	2	[47]
66	Diosmetin[*a,b,c,d]	$[M-H]^-$	29.40	299.0557 (bp)	0.7	299 -> 284.0308; 255.0290; 227.0343; 209.1178	$C_{16}H_{12}O_6$	265, 347	161.1	2	[47]
Unknown											
67	205_9.87[*a,b,c,d]	$[M-H]^-$	9.87	205.0713	-0.5	205-> 143.0709; 129.0553; 115.0760 (bp)	$C_8H_{14}O_6$	279	126.4	4	MS^E

[*] detected in leaf tissue; [#] detected in bract tissue; [a-d] specify compounds detected in [a] *P. neriifolia*, [b] *P. cynaroides* (King Protea), [c] black beauty and [d] limelight.

A precursor ion (**10**) at *m/z* 153.0203 ($C_7H_6O_4$) was observed to elute at t_R 8.81 min with two UV maxima at ≈ 259 and 293 nm and a $^{TW}CCS_{N2}$ value of 107.5 Å^2. The fragments observed at *m/z* 152.0066, 109.0301 (bp) and 108.0206 are characteristic of protocatechuic acid (as discussed above),[13] as this compound was tentatively identified.

Two isomeric compounds, **11** and **13**, were detected at *m/z* 329.0862 ($C_{14}H_{18}O_9$) at t_R's 8.98 and 9.53 min; **11** showed two UV maxima at ≈ 253 and 290 nm, and **13** a UV maximum at ≈ 282 nm. The high collision energy spectrum for **11** showed fragment ions at *m/z* 167.0331 (bp), 152.0108, 123.0422 and 108.0188, where: 1) *m/z* 167.0331 ($C_8H_8O_4$) was assigned to vanillic acid, which resulted from the neutral loss of a hexose moiety, 2) *m/z* 152.0108 results from the neutral loss of a methyl group (-15 Da) from vanillic acid, 3) the decarboxylation of vanillic acid produces the fragment ion at *m/z* 123.0422, and 4) subsequent decarboxylation of the 152.0108 fragment produces the product ion at *m/z* 108.0188. Based on these observations, **11** was tentatively identified as vanillic acid-*O*-hexoside. Vanillic acid has been identified as a leaf constituent of *Protea lacticolor*.[59] A vanillic acid standard (t_R 13.28 min) was analysed under the same conditions and showed the same fragments at *m/z* 167.0331, 152.0108, 123.0422 and 108.0188 (although vanillic acid itself was not detected in any of the extracts). The $^{TW}CCS_{N2}$ value of 177.7 Å^2 calculated for **11** is larger than that of 171.0 Å^2 reported by Yang *et al*. for vanillic acid-*O*-glucoside.[49] Compound **13** produced fragment ions at *m/z* 287.0754 and 125.0222 (bp). The ion at *m/z* 287.0754 likely results from the neutral loss of an acetyl moiety (-42 Da), and the ion at *m/z* 125.0222 from the subsequent neutral loss of a hexose moiety. This fragmentation behavior is similar to that discussed earlier for phlorin (**1**) and hydroxyquinol-*O*-glucoside (**4**). Hydroxyquinol-*O*-glucoside (**4**) was observed to be abundant in the *Protea* species studied; **13** was therefore tentatively annotated as hydroxyquinol-*O*-glucoside-*O*-acetyl.

Two isomeric peaks (**15** and **18**) eluting at t_R's 10.60 and 12.48 min were observed to have the *m/z* 283.0808 ($C_{13}H_{16}O_7$), with the UV maxima at ≈ 260 nm and $^{TW}CCS_{N2}$ values of 157.4 and 161.1 Å^2, respectively. MS^E spectra showed product ions at *m/z* 137.0228 and 93.0324, resulting from the neutral loss of 146 Da from the precursor ion and from the decarboxylation of the *m/z* 137.0228 fragment ion, respectively. The 146 Da neutral loss is characteristic of a deoxy-hexose ($C_6H_{12}O_5$) sugar moiety. Perold *et al*. identified *p*-hydroxybenzoic acid as a leaf constituent of *Protea lacticolor*.[59] Accordingly, the ion at *m/z* 137.0228 ($C_7H_6O_3$) was tentatively assigned to *p*-hydroxybenzoic acid,[13] and **15** and **18** were tentatively annotated as *p*-hydroxybenzoic acid-*O*-deoxy-hexose isomers.

Four peaks (**21**, **23**, **24** and **28**) eluting at t_R's 13.34, 13.66, 13.89 and 14.64 min showed a molecular ion at *m/z* 423.0989 ($C_{19}H_{20}O_{11}$) with UV maxima at ≈ 260 nm. For **21**, **23** and **28**, the MS^E spectra showed fragments at *m/z* 153.0184, 125.0225 and 109.0301. The ion at *m/z* 153.0184 ($C_7H_6O_4$) was assigned as protocatechuic acid (as discussed earlier for compounds **8**, **9**, **10** and **12**), while the ion at *m/z* 125.0225 ($C_6H_6O_3$) is characteristic of hydroxyquinol (as discussed above for compound **4**), and the ion at *m/z* 109.0301 results from decarboxylation of the protocatechuic acid fragment ion at *m/z* 153.0184. Thus, these peaks were annotated as protocatechuic acid-*O*-hexoside-*O*-hydroxyquinol isomers with similar $^{TW}CCS_{N2}$ values (184.1, 187.0 and 184.1 Å^2, respectively). Compound **24** revealed fragment ions at *m/z* 281.0659 (bp), 137.0235 and 93.0323 and a $^{TW}CCS_{N2}$ value of 194.6 Å^2. Fragment ions at *m/z* 137.0235 and 93.0323 are characteristic of *p*-hydroxybenzoic acid ($C_7H_6O_3$), as discussed above and noted by Fang *et al*.,[13] which indicates a hexose attached to both *p*-hydroxybenzoic acid and a tetra-hydroxylated benzene derivative as a likely structure.

Two related compounds (**26** and **32**) eluting at 14.25 and 17.68 min with molecular ions at *m/z* 437.1074 ($C_{20}H_{22}O_{11}$) and UV maxima ≈ 263 were also detected. $^{TW}CCS_{N2}$ values were calculated as 191.4 and 182.3 Å^2, respectively. Product ions observed were at *m/z* 153.0193, 139.0394 and 109.0286, representing 1) protocatechuic acid (*m/z* 153.0193), 2) protocatechuic alcohol (*m/z* 139.0394), and 3) the decarboxylated protocatechuic acid fragment (*m/z* 109.0286). From these fragment ions, the two isomeric peaks were tentatively annotated as protocatechuic acid-*O*-hexoside-*O*-protocatechuic alcohol isomers.[47]

30, **31**, **33**, **36** and **39** are isomers showing identical molecular ions at *m/z* 391.1030 ($C_{19}H_{20}O_9$). The former, **30** and **31**, showed UV maxima at ≈ 280 nm and $^{TW}CCS_{N2}$ values of 176.5 Å^2, and their MS^E spectra showed fragments at *m/z* 281.0673, 137.0223, 109.0282 and 93.0330, where fragments at *m/z* 137.0223 and 93.0330 are characteristic of *p*-hydroxybenzoic acid and *m/z* 109.0282 suggests the presence of hydroquinone. These compounds were therefore tentatively annotated as *p*-hydroxybenzyl-*O*-arbutin isomers. Compounds **33**, **36** and **39** showed a UV maxima ≈ 280 nm and fragment ions at *m/z* 287.0748, 125.0242 (bp) and 121.0267, where the ions at *m/z* 287.0748 and 125.0242 are characteristic of hydroxyquinol-*O*-glycoside (compound **4**) and the ion at *m/z* 121.0267 ($C_7H_6O_2$) is annotated as benzoic acid. Perold and Carlton identified the phenolic glycoside ester of hydroxyquinol and benzoic acid, named neriifolin, in *P. neriifolia* leaves by NMR.[9] Thus, **33**, **36** and **39** were assigned as neriifolin isomers.

Five isomeric peaks detected at *m/z* 405.1214 (**34**, **35**, **37**, **40** and **41**) showed the molecular formula $C_{20}H_{22}O_9$. Compounds **34**, **40** and **41** showed fragment ions at *m/z* 287.0725 and

125.0242 characteristic of hydroxyquinol-*O*-hexoside. These three peaks (t_R's 20.37, 22.05 and 22.54 min, respectively) were tentatively annotated as isomers of an unknown hydroxyquinol-*O*-glycoside derivative ($^{TW}CCS_{N2}$ values of 187.3, 187.3 and 188.9 Å^2, respectively). Compounds **35** and **37** eluted at t_R's 21.17 and 21.49 min, with calculated $^{TW}CCS_{N2}$ values of 191.9 and 193.4 Å^2, respectively. These two peaks showed fragments at *m/z* 139.0372 and 121.0273, which represent protocatechuic alcohol and benzoic acid, respectively. Perold *et al*. identified metabolites lacticolorin in the leaves of *P. lacticolor*[59] and pilorubrosin in the beard (tufts) of *P. rubropilosa*;[62] these two metabolites are phenolic glycoside esters of benzoic acid (*m/z* 121.0273) and protocatechuic alcohol (*m/z* 139.0372). The glycosidic core differentiates these compounds, with lacticolorin containing glucose and pilorubrosin containing (+)-allose. **35** and **37** were therefore annotated as lacticolorin or pilorubrosin, although the individual peaks could not be assigned based on the RP-LC retention.

Compound **38** eluted at t_R's 21.51 min with a precursor ion at *m/z* 375.1069 ($C_{19}H_{20}O_8$) and a $^{TW}CCS_{N2}$ value of 183.3 Å^2. The product ions observed were at *m/z* 121.0277, 109.0262 and 108.0198 (bp), with the latter two ions characteristic of hydroquinone, while the ion at *m/z* 121.0277 ($C_7H_6O_2$) was tentatively annotated as belonging to benzoic acid. A phenolic glycoside ester of hydroquinone and benzoic acid, called eximin, was previously identified in *P. eximia* leaves.[4,63] Compound **38** was therefore tentatively assigned as eximin.

3.3.1.2. Hydroxycinnamic acid derivatives

Compounds **14** and **19** with t_R's at 10.01 and 12.54 min, respectively, showed isomeric precursor ions at *m/z* 353.0873 ($C_{16}H_{18}O_9$). These isomers displayed UV spectra characteristic of hydroxycinnamic acids, with maxima at ≈ 328 and 325 nm, respectively; calculated $^{TW}CCS_{N2}$ values were 165.4 and 177.2 Å^2. For **14**, the MS^E spectra revealed ions at *m/z* 191.0548, 179.0353 and 135.0442, which are characteristic of the chlorogenic acid, 3-caffeoyl-*O*-quinic acid. The intense fragment ion at *m/z* 191.0548 corresponds to a quinic acid fragment resulting from the neutral loss of the caffeoyl moiety (-162 Da), whereas the *m/z* 179.0353 ion represents caffeic acid following the neutral loss of a quinic acid moiety (-174 Da), and the ion at *m/z* 135.0442 resulted from the decarboxylation of the caffeic acid moiety.[60] The abundance of the ion at *m/z* 191.0548 (bp) compared to *m/z* 179.0353 (50% relative abundance) is characteristic of 3-caffeoylquinic acid, as this compound was identified.[61] Compound **19** showed an intense, lone quinic acid product ion at *m/z* 191.0548, consistent with the fragmentation behavior of 5-caffeoyl-*O*-quinic acid, as was confirmed by injection of a reference standard. Furthermore, the $^{TW}CCS_{N2}$

value for **19** correlated well with that reported for a 5-caffeoyl-*O*-quinic acid standard analysed by Yang *et al*.[49]

Compounds **16** and **29**, eluting at t_R's 11.69 and 14.76 min, both displayed UV maxima of ≈ 310 nm and molecular formulae of $C_{16}H_{18}O_8$ (*m/z* 337.0898). Compound **16** showed fragments at *m/z* 191.0573, 163.0396 (bp) and 119.0487. The quinic acid fragment at *m/z* 191.0573 results from the neutral loss of a *p*-coumaroyl moiety (-146 Da), while the ion at *m/z* 163.0396 corresponds to a *p*-coumaric acid fragment following neutral loss of quinic acid and the ion at *m/z* 119.0487 results from the decarboxylation *p*-coumaric acid. The relative abundance of the *p*-coumaroyl fragment in the high collision energy spectrum of **16** allowed the putative identification of this peak as the chlorogenic acid, 3-*p*-coumaroyl-*O*-quinic acid.[61] In contrast, **29** showed a lone intense fragment at *m/z* 191.0573 (quinic acid) characteristic of 5-*p*-coumaroyl-*O*-quinic acid.[61] Both compounds showed two distinct IM signals with different arrival times, Supplementary; Figure S3.4. The $^{TW}CCS_{N2}$ measurements yielded 175.9 and 160.3 Å^2 for **16** and 180.8 and 162.1 Å^2 for **29**. As noted by Kuhnert *et al*. for caffeoylquinic acids, the two arrival time signals for each compound likely correspond to prototropic isomers where ionisation occurs at either the phenolate of *p*-coumaric acid or the carboxylate of quinic acid.[34]

Compounds **17** and **22** showed molecular ions at *m/z* 355.1039 ($C_{16}H_{20}O_9$) and UV maxima at ≈ 293 nm. Their MS^E spectra showed fragment ions at *m/z* 193.0493 ($C_{10}H_{10}O_4$, resulting from the neutral loss of a hexoside moiety) and *m/z* 134.0368. These fragments are characteristic of the hydroxycinnamic acid, ferulic acid,[13] with the ion at *m/z* 134.0368 resulting from the decarboxylation of the demethylated feruloyl moiety (178 Da). Thus, these metabolites were annotated as feruloyl-*O*-hexoside isomers. The major difference observed in $^{TW}CCS_{N2}$ values for these compounds suggests that they are geometrical isomers, in which case the later eluting peak, **22,** would be the *cis* isomer (168.9 Å^2), and earlier eluting peak, **17,** the *trans* isomer (194.3 Å^2).

Compound **20** eluted at 12.83 min and was characterised by a molecular ion at *m/z* 367.1043 ($C_{17}H_{20}O_9$), a UV maximum of ≈ 325 nm and a $^{TW}CCS_{N2}$ values of 176.0 Å^2. Product ions were detected at *m/z* 193.0498 (bp), 191.0502 and 134.0365. The ion at *m/z* 193.0498 ($C_{10}H_{10}O_4$) is characteristic of ferulic acid following the loss of a quinic acid moiety, whereas the ion at *m/z* 191.0502 represents quinic acid following the neutral loss of the ferulic acid moiety (-176 Da) and decarboxylation of the demethylated feruloyl moiety (178 Da) results in the ion at *m/z* 134.0365. The relative abundance of the fragment ion at *m/z* 193.0498, as well as the absence of an ion at *m/z* 173, allowed assignment of this compound ion as 3-feruloyl-*O*-quinic acid.[61]

The isomeric compounds **25** and **27**, eluting at 14.05 and 14.42 min, respectively, both showed molecular ions at *m/z* 325.0934 ($C_{15}H_{18}O_8$) and UV maxima at ≈ 325 nm (Figure 3.3). Fragment ions were observed at *m/z* 179.0350, 161.0247 (bp), 135.0451 and 133.0299 (Figure 3.3D). The ions at *m/z* 179.0350 and 135.0451 are diagnostic for caffeic acid,[68] although the highly abundant *m/z* 161.0247 ($C_9H_6O_3$) and *m/z* 133.0299 ions are not. Both isomers showed two distinct IM arrival time distributions (Figure 3.3C), corresponding to calculated $^{TW}CCS_{N2}$ values of 176.1 and 158.7 Å^2, respectively, suggesting the presence of tautomeric anions (i.e., the equivalent of prototropic isomers[34] for deprotonated species in negative ionisation) for both **25** and **27**. This is supported by the fact that the same behavior was observed on the drift tube IMS instrument ($^{DT}CCS_{N2}$ values of 181.6 and 165.5 Å^2, respectively).

Compound **25** was the most abundant metabolite detected in the other 33 *Protea* samples studied (results to be reported elsewhere Chapter 4), pointing to its potential use as a chemo-taxonomic marker. Since this compound could not be identified based on the available data, it was isolated by preparative HPLC (section 3.2.3.6) and its structure elucidated by NMR (section 3.2.3.7).

Isolated, dried **25**, reconstituted in DMSO-d_6 yielded a ^{1}H NMR spectrum displaying aromatic protons (*δ* 6-8 ppm) that are coupled through a classic ABX spin system as H-2 (*δ* 7.05, d, *J* = 2.0 Hz), H-6 (*δ* 7.02, dd, *J* = 8.0, 2.0 Hz) and H-5 (*δ* 6.76, d, *J* = 8.0 Hz); a characteristic tri-substituted benzene ring. This region also had two distinctive single-proton doublets, H-7 (*δ* 7.46, d, *J* = 15.9 Hz) and H-8 (*δ* 6.28, d, *J* = 15.9 Hz), displaying the unique vicinal ^3J = 15.9 Hz coupling constant of a *trans* orientated double bond. The classical carbohydrate region between 3-5 ppm integrated for another eight protons reminiscent of a sugar or open oxygenated chain moiety. These protons, as assigned by 1D and 2D NMR experiments, are summarised in Table 3.3. The ^{13}C NMR spectra displayed 15 distinct carbon signals in line with the proposed molecular formula of $C_{15}H_{18}O_8$. One carbonyl carbon resonated at *δ* 166.5 ppm, and six aromatic and two double bond carbons between 113-149 ppm. Another six aliphatic upfield carbon signals between 64-79 ppm reminiscent of a hexose sugar or an open ring/chain moiety. The remaining five protons comprise two aromatic and three aliphatic OH-groups resonating at *δ* 9.59, 9.11, 5.14, 4.99 and 4.95 ppm, all which were in line with the observed molecular weight of 326 g/mol (*m/z* 325.0911, $[M-H]^-$) and the predicted molecular formula of $C_{15}H_{18}O_8$.

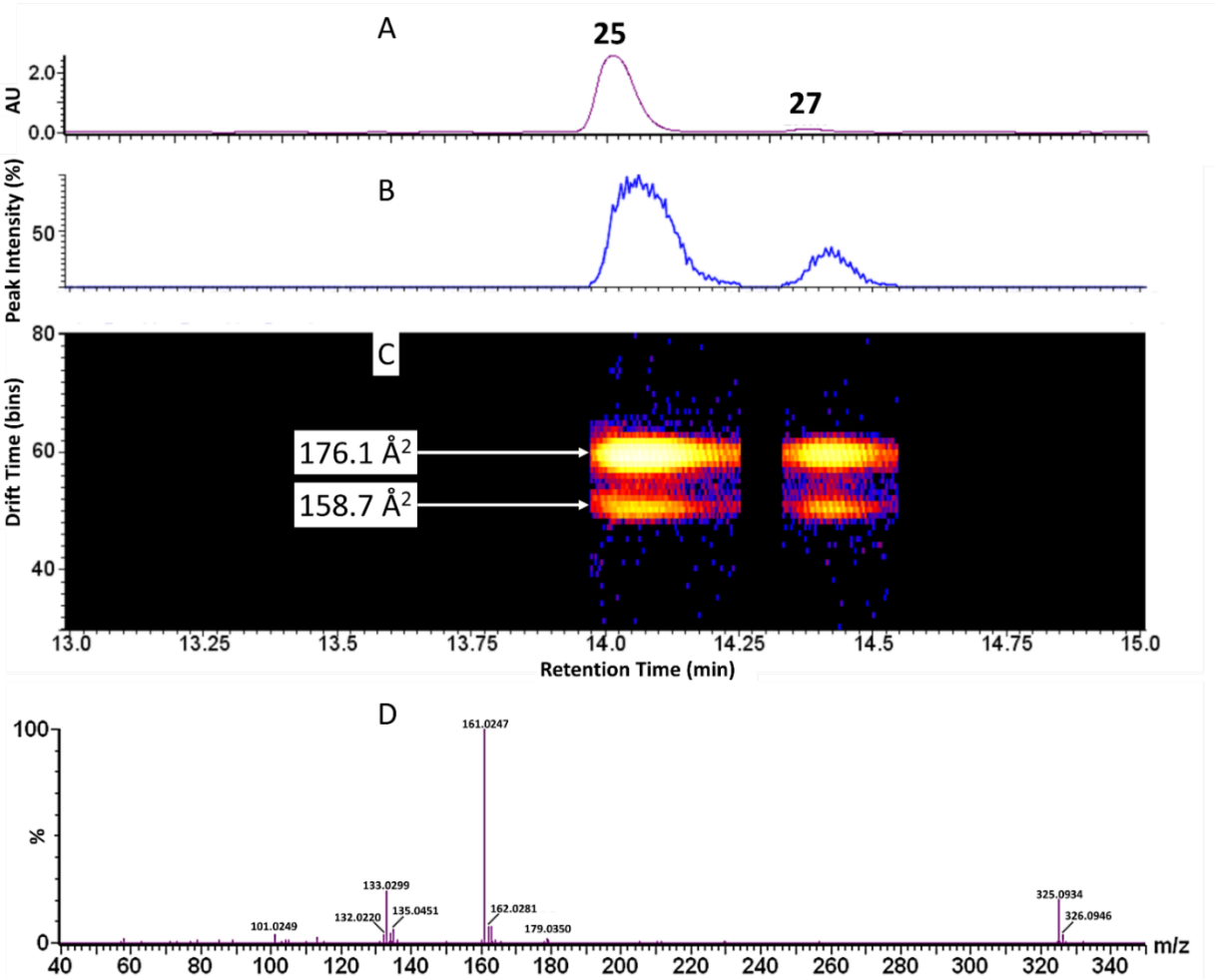

Figure 3.3: A) Chromatogram at 325 nm, **B**) extracted ion chromatogram at *m/z* 325, **C**) arrival time vs. retention time plots for *m/z* 325, and **D**) MS^E spectrum (identical for both species) showing the detection of the isomers of caffeoyl-*O*-polygalatol (1,5-anhydro-[6-*O*-caffeoyl]-sorbitol(glucitol)) (**25** and **27**).

Table 3.3: ^{1}H and ^{13}C chemical shifts (δ at 600 MHz) for compound **25** in DMSO-d_6 at 25˚C.

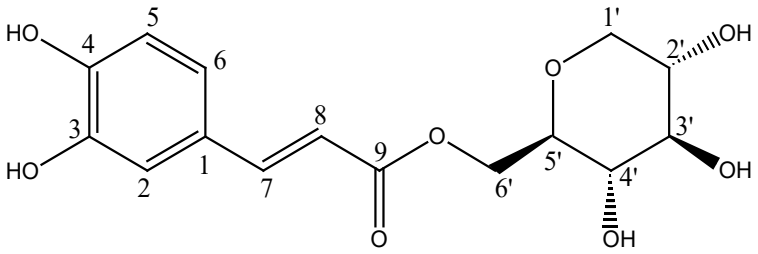

Compound **25**

Position	δ_H	δ_C	OH
1		125.47	
2	7.05 d (2.0)	114.96	
3		145.53	9.59 s
4		148.39	9.11 s
5	6.76 d (8.0)	115.73	
6	7.02 dd (8.0, 2.0)	121.30	
7	7.46 d (15.9)	145.25	
8	6.28 d (15.9)	113.80	
9		166.55	
1'a	3.73 dd (10.9, 5.3)	69.52	
1'b	3.02 t (10.7)		
2'	3.27 m	69.67	4.94 d (4.6)
3'	3.11 m	78.16	5.13 d (5.4)
4'	3.07 m	70.28	4.99 d (4.2)
5'	3.38 m	78.30	
6'a	4.39 dd (11.7, 1.3)	64.50	
6'b	4.07 dd (11.9, 6.7)		

The structure of **25** was elucidated in full utilising ^{1}H, ^{13}C, TOCSY, gHSQCAD and gHMBCAD NMR experiments recorded in DMSO-d_6. The tri-substituted aromatic ring is confirmed by the shared vicinal coupling constants and the TOCSY correlations (Figure 3.4) between H-6 (δ 7.02, dd, J = 8.0, 2.0 Hz) and H-5 (δ 6.76, d, J = 8.0 Hz), together with correlation between H-2 (δ 7.05, d, J = 2.0 Hz) and H-6 (δ 7.02, dd, J = 8.0, 2.0 Hz). The COSY spectrum couples H-7 (δ 7.46, d, J = 15.9 Hz) and H-8 (δ 6.28, d, J = 15.9 Hz) and their *trans* orientation is deduced from the large 15.9 Hz coupling constant measured. The UV spectrum of **25**, Supplementary Figure S3.5, confirms the presence of an hydroxycinnamic acid group. Isolated novel ferulic acid saccharides reported by Colquhoun *et al*. also affirms the caffeic acid moiety of **25** by almost identical ^{1}H NMR spectra in the aromatic region of the 6'-*O*-(*trans*-feruloyl) linked ester moeities.[69] Due to the

extensive overlap of the hexose ring protons, some of their TOCSY correlations shown in Figure 3.4 were only possible after their assignment via the HSQC and HMBC experiments.

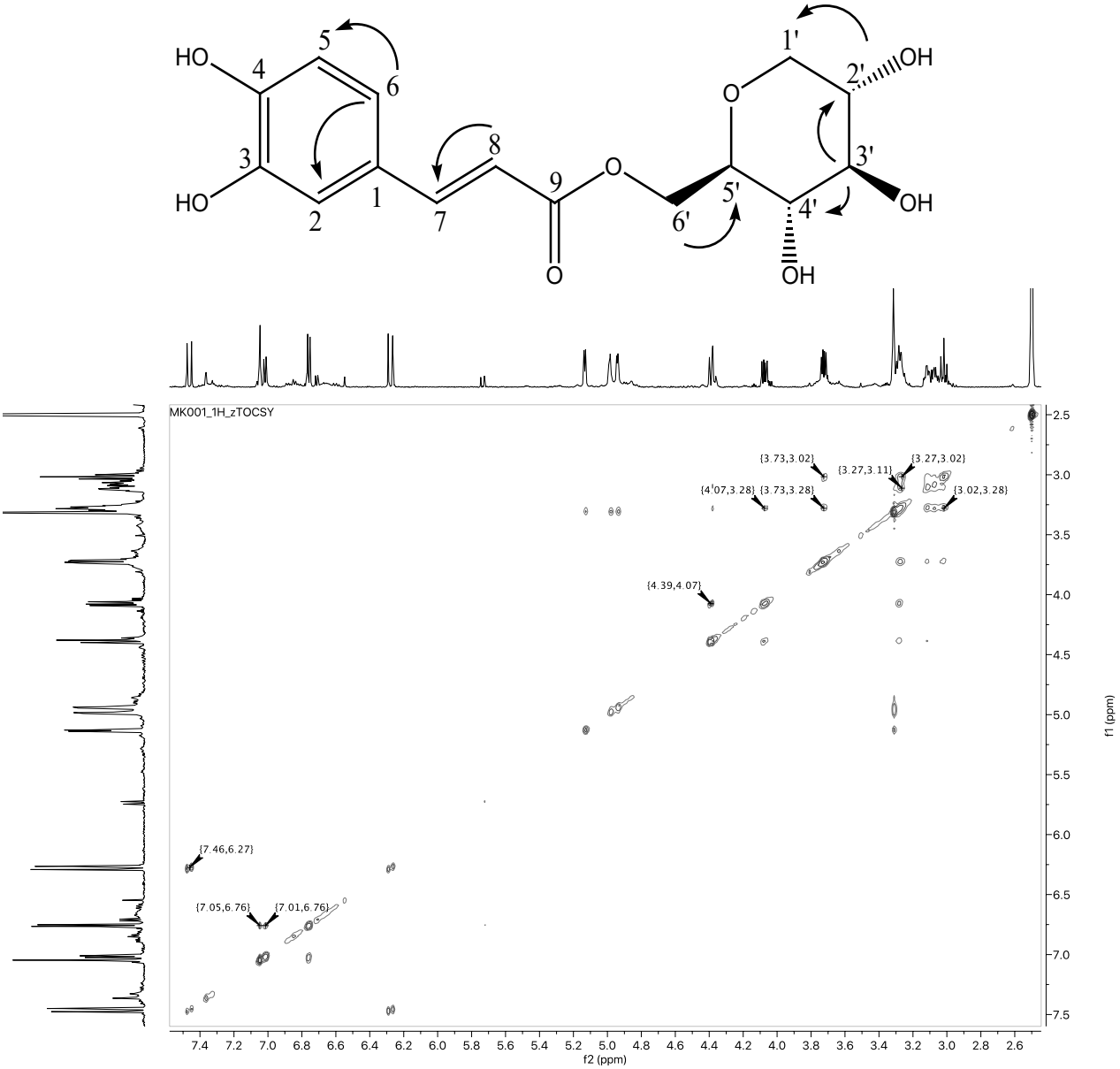

Figure 3.4: Key TOCSY plot and $^{2\text{-}4}J_{H\text{-}H}$ correlations for compound **25** in DMSO-d_6 at 25˚C.

The HSQC $^{1}J_{C\text{-}H}$ experiment confirmed all the protonated carbons as well as their multiplicity (Figure 3.5, Red = CH/CH_3, Blue = CH_2) (Table 3.3). The experiment displayed nine CH groups and two CH_2 groups, in line with the proposed structure of **25** and the molecular formula. This left four unprotonated carbons to be assigned via long range proton-carbon correlations in the HMBC $^{2,3}J_{C\text{-}H}$ experiment.

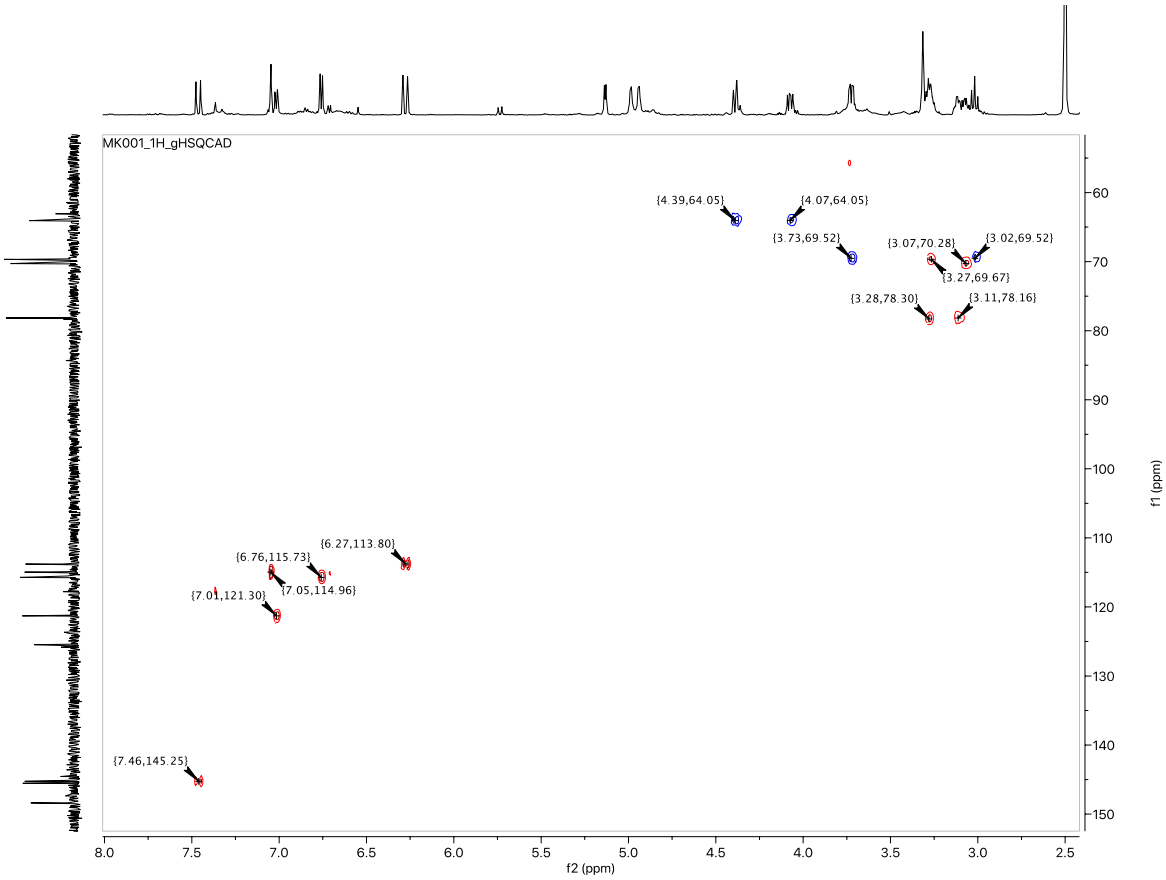

Figure 3.5: HSQC $^{1}J_{C\text{-}H}$ correlations for compound **25** in DMSO-d_6 at 25˚C. Red = CH/CH_3, Blue = CH_2.

The HMBC NMR experiment for **25** (Figure 3.6) establishes the position of the double bond linked directly to the aromatic ring on one side and, in turn, to the carbonyl functionality on the other side. H-7 (δ 7.46, d, J = 15.9 Hz) couples to both C-6 (δ 121.30 ppm) and C-2 (δ 114.96 ppm) on the aromatic ring, and H-8 (δ 6.28, d, J = 15.9 Hz) in turn correlates to C-1 (δ 125.47 ppm) and the carbonyl C-9 (δ 166.55 ppm).

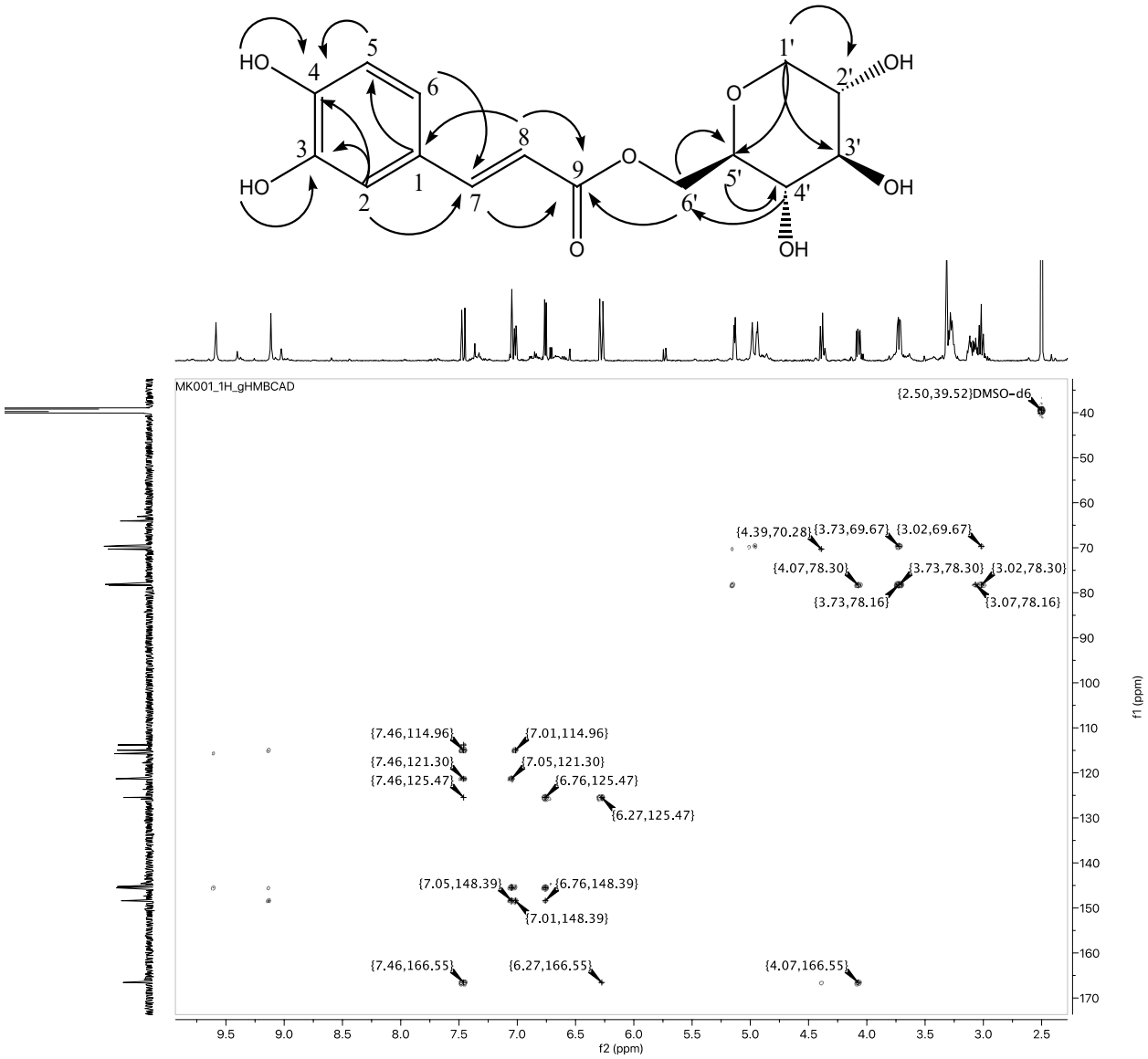

Figure 3.6: HMBC plot and key $^{2,3}J_{C\text{-}H}$ correlations for compound **25** in DMSO-d_6 at 25˚C.

Both H-6'a (δ 4.39, dd, J = 11.7, 1.3 Hz) and H-6'b (δ 4.07, dd, J = 11.9, 6.7 Hz) protons of the hexose moiety have long range correlations to the carbonyl carbon, thus confirming the ester linkage to the caffeic acid moiety via C-6' (δ 64.5 ppm).

Since the protons of the hexose moiety show extensive signal overlap in the ^{1}H NMR spectra (3.0-3.5 ppm), the NOESY NMR experiments were of limited use to solve and identify the type of anhydrohexose linked to the caffeoyl moiety (i.e., anhydroglucitol, anhydrogalactitol, anhydromannitol, etc.). These hexose moieties can be identified based on the specific NOE's

observed between their axial ring protons. Here the relative ^{13}C chemical shifts of our hexose unit were utilised and positively matched with 1,5-anhydroglucitol in literature.[70]

The nearest analogue of compound **25** found in literature is 1,5-anhydro-[6-*O*-(3,4,5-trimethoxycinnamoyl)]-D-glucitol (tenuifoliside D), published by Ikeya *et al*.[71] Only the aromatic ring of this molecule differs by having three methoxy groups on the 3,4,5-carbons, whereas compound **25** has two OH-groups on the C-3 and C-4 positions. The relative ^{1}H and ^{13}C chemical shifts of their 1,5-anhydro-glucitol (1,5-anhydro-sorbitol) moiety were found to closely match those of our hexose unit.

In addition to the anhydroglucitol moiety match in literature,[71,72] the sequential connectivity, as well as the cyclic nature of the anhydrohexose was then confirmed by the HMBC $^{2,3}J_{C\text{-}H}$ experiment (Figure 3.6). Coupling is observed from H-6'b (*δ* 4.07, dd, *J* = 11.9, 6.7 Hz), in the HMBC experiment, to C-5' (*δ* 78.3 ppm) and from H-6'a (*δ* 4.39, dd, *J* = 11.7, 1.3 Hz) to C-4' (*δ* 70.28 ppm). H-1'a (δ 3.73, dd, *J* = 10.9, 5.3 Hz) shows coupling to C-2' (*δ* 69.67 ppm) and C-3' (*δ* 78.16 ppm). The cyclical nature of the heterocyclic 1,5-anhydroglucitol is confirmed by the long-range coupling between H-1'a (*δ* 3.73, dd, *J* = 10.9, 5.3 Hz), H-1'b (*δ* 3.02, t, *J* = 10.7 Hz) and C-5' (*δ* 78.30 ppm).

In conclusion, the novel molecular structure of **25** was determined as 1,5-anhydro-[6-O-caffeoyl]-glucitol via 1D and 2D NMR experiments together with the use of analogue structures in literature.[69–72] With this information in hand, the fragmentation pattern of **25** is proposed in Supplementary Figure S3.6: the fragment at *m/z* 179.0350 (caffeic acid, $C_9H_8O_4$) resulted from the neutral loss of the dehydrated polygalatol moiety (blue route), and the ion at *m/z* 161.0247 results from the neutral loss of the polygalatol moiety from the precursor or the dehydration of the fragment at *m/z* 179.0350 (red route). The secondary fragments at *m/z* 135.0451 and 133.0299 are produced from the decarboxylation of the caffeoyl moiety (*m/z* 179.0350) and the loss of a carbonyl moiety (-28 Da) from the ion at *m/z* 161.0247, respectively. Bieleski and Briggs studied the distribution of polyol sugars across Proteaceae members, and polygalatol was observed to be present only in South African genera of this family.[10]

3.3.2. Flavonoid derivatives

3.3.2.1. Flavan-3-ols

At *m/z* 577.1327, two peaks (**42** and **45**) eluting at t_R's 11.25 and 13.37 min were detected, corresponding to molecular formulae of $C_{30}H_{26}O_{12}$ ($[M\text{-}H]^-$). UV maxima for these compounds were at ≈ 279 nm, and $^{TW}CCS_{N2}$ values of 220.1 Å^2 were calculated for both. The MS^E spectra showed

fragment ions at *m/z* 425.0819, 407.0695, 289.0684, 245.0798 and 125.0219 (bp). These data are characteristic of B-type procyanidins;[16,64] **42** and **45** were therefore identified as B-type procyanidins. Compounds **43** and **46** (*m/z* 289.0714, $C_{15}H_{14}O_6$, UV maxima at ≈279 nm and $^{TW}CCS_{N2}$ values 150.1 Å^2) were unambiguously identified as (+)-catechin and (-)-epicatechin, respectively, by co-injection of authentic standards.

3.3.2.2. Anthocyanins

Five peaks (**44, 47, 48, 49** and **53**) with UV maxima of ≈520 nm characteristic of anthocyanins, were detected in extracts from the bracts and beards (tufts) of black beauty and *P. neriifolia*. In positive ionisation, these five peaks showed precursor ions ([M]$^+$) at *m/z* 465.1032 ($C_{21}H_{21}O_{12}$), 449.1084 ($C_{21}H_{21}O_{11}$), 479.1181 ($C_{22}H_{23}O_{12}$), 463.1230 ($C_{22}H_{23}O_{11}$) and 493.1345 ($C_{23}H_{25}O_{12}$). All of these species showed the loss of a neutral hexoside moiety in their high collision energy spectra, with aglycones detected at *m/z* 303.0502 ($C_{15}H_{11}O_7$, **44**), *m/z* 287.0555 ($C_{15}H_{11}O_6$, **47**), *m/z* 317.0654 ($C_{16}H_{13}O_7$, **48**), 301.0703 ($C_{16}H_{13}O_6$, **49**) and *m/z* 331.0814 ($C_{17}H_{15}O_7$, **53**). These aglycone fragments and their molecular formulae are consistent with the anthocyanidins delphinidin (**44**), cyanidin (**47**), petunidin (**48**, with a secondary ion at *m/z* 302.0422 due to the loss of a methyl group), peonidin (**49**, with *m/z* 286.0462 due to demethylation), and malvidin (**53**, with a secondary ion at *m/z* 315.0495 due to loss of a methyl moiety), respectively. The five detected anthocyanins were therefore tentatively identified as delphinidin-*O*-hexoside (**44**), cyanidin-*O*-hexoside (**47**), petunidin-*O*-hexoside (**48**), peonidin-*O*-hexoside (**49**) and malvidin-*O*-hexoside (**53**).[14,65] The $^{TW}CCS_{N2}$ value measured for cyanidin-*O*-hexoside (201.3 Å^2) was close to that of cyanidin-3-*O*-galactoside reported by Yang *et al*. (201.6 Å^2),[49] and a $^{DT}CCS_{N2}$ value for the [M$^+$] ion in positive ion mode by Causon *et al*. (202.7 Å^2).[73] Similarly, comparable $^{TW}CCS_{N2}$ for **44**, **48, 49** and **53** were measured in the current work compared to $^{DT}CCS_{N2}$ values of the corresponding compounds in wine.[73] To the best of our knowledge this is the first scientific report of the anthocyanin distribution (**44, 47, 48, 49** and **53**) in *Protea* species.

3.3.2.3. Flavonols

Several compounds of this class were detected; all showed typical flavonol UV spectra with two absorbance maxima at ≈ 250 and 350 nm. Extracted ion chromatograms at *m/z* 609.456 ($C_{27}H_{30}O_{16}$, [M-H]$^-$), showed two peaks at t_R's 17.66 (**50**) and 17.86 (**51**) min. MS^E spectra showed fragment ions at *m/z* 301.0328, 300.0266, 271.0239, 255.0288, 243.0347, 178.9954 and 151.0012. These fragments are characteristic of quercetin, where the ion at *m/z* 301.0328 represents the aglycone resulting from the neutral loss of the disaccharide (hexoside-*O*-deoxy-hexose, -308 Da), and *m/z* 300.0266 the corresponding radical aglycone.[60,67] Compound **51** was

identified as rutin (quercetin-3-*O*-rutinoside (α-L-rhamnopyranosyl-(1→6)-β-D-glucopyranose)) using an authentic standard; **50** is tentatively identified as quercetin-*O*-hexoside-*O*-deoxy-hexose, possibly quercetin-neohesperidoside (α-L-rhamnopyranosyl-(1→2)-β-D-glucopyranose) based on its earlier elution. Yang *et al*. reported $^{TW}CCS_{N2}$ values of 230.6 Å^2 for both rutin and quercetin-3-*O*-neohesperidoside, which is comparable to the values of 232.2 and 231.0 Å^2 obtained for **50** and **51** in the present study.[49] Several related peaks with similar MS^E fragments indicative of the presence of quercetin derivatives were also detected. The isomeric compounds **52** and **54** were detected at *m/z* 463.0877 ($C_{21}H_{20}O_{21}$), with the aglycone at *m/z* 301.0328 resulting from the neutral loss of a hexose moiety indicating quercetin-*O*-hexoside isomers.[19,66] The calculated $^{TW}CCS_{N2}$ value was for 198.5 Å^2 for both peaks. Compound **52** was tentatively identified as quercetin-*O*-galactoside and compound **54** as isoquercetin (quercetin-3-*O*-glucoside) based on the known elution order of these compounds under reversed phase conditions;[66] **54** was subsequently unambiguously identified by the co-injection of an authentic standard. Compound **56** eluted at 19.46 min, with a molecular ion at *m/z* 433.0760 ($C_{20}H_{18}O_{11}$), a $^{TW}CCS_{N2}$ value of 193.0 Å^2 and an aglycone fragment at *m/z* 301.0328 in its MS^E spectrum indicating the neutral loss of a pentose moiety (-132 Da). Thus, this peak was tentatively annotated as quercetin-*O*-pentoside.[19] Similarly, the MS^E spectrum of **61** (precursor ion at *m/z* 447.0919, $C_{21}H_{20}O_{11}$, $^{TW}CCS_{N2}$ value of 192.8 Å^2) showed fragment ions characteristic of quercetin, corresponding to the neutral loss of the deoxy-hexose moiety (-146 Da), thus this peak was tentatively annotated as quercetin-*O*-deoxy-hexose.[19]

A precursor ion at *m/z* 593.1531 ($C_{27}H_{30}O_{15}$) was detected for compound **55**, with two UV maxima at ≈ 266 and 346 nm, and a $^{TW}CCS_{N2}$ value of 228.7 Å^2. MS^E fragment ions at *m/z* 285.0406, 284.0318, 255.0291 and 159.0294 are characteristic of kaempferol, with the ion at *m/z* 285.0406 ($C_{15}H_{10}O_6$) representing the aglycone and *m/z* 284.0318 the radical aglycone.[14,67] The aglycone resulted from the neutral loss of the hexoside-*O*-deoxy-hexose moiety (-308 Da), and this compound was therefore tentatively annotated as kaempferol-*O*-hexoside-*O*-deoxy-hexose. Compound **59** (*m/z* 447.0920 ($C_{21}H_{20}O_{11}$), $^{TW}CCS_{N2}$ values 197.3 Å^2) showed MS^E fragments at *m/z* 285.0374, 284.0322, 255.0288 and 159.0299 with the aglycone (*m/z* 285.0374) resulting from the loss of a hexose moiety. This peak was thus tentatively annotated as kaempferol-*O*-hexoside. The relative RP-LC retention of this compound compared to **55** and **58** is consistent with that of kaempferol-3-*O*-glucoside.[14] Compound **64** showed a precursor ion at *m/z* 431.0978 ($C_{21}H_{20}O_{10}$), $^{TW}CCS_{N2}$ value of 193.0 Å^2 and its MS^E spectrum showed fragments characteristic of kaempferol (*m/z* 285.0374 (bp), 284.0322, and 255.0288) following the neutral loss of a deoxy-hexose moiety (-146 Da). This peak was tentatively annotated as kaempferol-*O*-deoxy-hexoside.[15]

A final group of flavonols showed fragmentation data consistent with isorhamnetin.[47] Compounds **57** and **58** showed molecular ions at *m/z* 623.1597 ($C_{28}H_{32}O_{16}$) and fragment ions at *m/z* 315.0490 ($C_{16}H_{12}O_7$), 314.0417, 300.0262, 271.0233, 255.0296 and 243.0296. The aglycone (*m/z* 315.0490) and the radical aglycone (*m/z* 314.0417) fragments result from the neutral loss of the hexoside-*O*-deoxy-hexoside (-308 Da),[18] and the secondary ion at *m/z* 300.0262 is formed by the subsequent loss of the methyl group. Thus, these two peaks were identified as isorhamnetin-*O*-hexoside-*O*-deoxy-hexoside isomers. $^{TW}CCS_{N2}$ values of 234.5 and 235.7 Å^2 were measured, respectively. Compounds **60** and **62** were detected at *m/z* 477.1033 ($C_{22}H_{22}O_{12}$), with similar fragments (*m/z* 315.0490, 314.0417, 271.0233, 243.0296 and 159.0273) diagnostic of isorhamnetin and the aglycone resulting from the loss of the hexoside moiety. These isomers ($^{TW}CCS_{N2}$ value of 205.3 Å^2) were, considering their relative elution order, tentatively annotated as isorhamnetin-*O*-galactose (**60**) and isorhamnetin-*O*-glucose (**62**).[18] Similarly, the compound eluting at 21.76 min (**63**) showed fragment ions at *m/z* 315.0490, 314.0417, 271.0233 and 243.0296 following the neutral loss of a pentose moiety (-132 Da), and was tentatively annotated as isorhamnetin-*O*-pentose. The $^{TW}CCS_{N2}$ value was calculated as 198.7 Å^2. Finally, an aglycone compound eluting at 26.17 min (**65**) was characterised by MS data (precursor ion at *m/z* 315.0490 ($C_{16}H_{12}O_7$), $^{TW}CCS_{N2}$ value of 162.6 Å^2, product ions at *m/z* 300.0262, 271.0233, 255.0296, 243.0296 and 153.0183, with the diagnostic ion at *m/z* 300.0262 resulting from the loss of a methyl group from the precursor ion) as isorhamnetin.[47]

3.3.2.4. Flavone

Compound **66**, eluting at 29.40 min with a precursor at *m/z* 299.0557 ($C_{16}H_{12}O_6$), showed a UV spectrum typical of a flavone, with a maximum at ≈340 nm. The fragments observed for this peak were at *m/z* 284.0308, 255.0290, 227.0343 and 209.1178. These fragments, resulting from consecutive losses of methyl and CO moieties,[74] are characteristic of the flavone diosmetin,[47] as which this compound was tentatively identified.

3.3.3. Drift tube ion mobility spectrometry (DTIMS)

Comparison of the experimentally determined $^{TW}CCS_{N2}$ values with the CCS values determined on a low-field drift tube instrument ($^{DT}CCS_{N2}$) for selected compounds (Supplementary; Table S3.1), indicate that the CCS values determined using a travelling-wave instrument are often underestimated (~3-4 Å^2 lower) when compared with the $^{DT}CCS_{N2}$ values for compounds with CCS values below 200 Å^2. On the other hand, for higher CCS values, good agreement is obtained between both instruments (*cf.* compound **50**). Good agreement with literature CCS values was also observed for larger CCS values (see flavonoids above). We

suspect that the lower $^{TW}CCS_{N2}$ values for smaller ions is a consequence of poor calibration performance using poly-alanine in this region on the TWIMS instrument. However, recent progress in the theory of TWIMS-MS calibration may offer improvements for this type of comparison in the near future.[75]

3.4. Conclusion

This study reports the first detailed phytochemical investigation of pure and hybrid *Proteas*. By exploiting the latest technological developments, an untargeted UPLC-PDA-IM-HR-MS approach was used for the comprehensive, if mostly tentative, metabolite identification based on relative reversed phase chromatographic retention, UV-Vis spectral data, low- and high collision energy HR-MS data and gas-phase CCS values. We report the presence of 67 phenolic compounds, including 41 phenolic acid esters and 25 flavonoid derivatives (including 5 anthocyanins) in *Protea* species, and 27 of these compounds (**21**, **23**, **25**, **26**, **27**, **28**, **30**, **31**, **32**, **42**, **44**, **45**, **46**, **47**, **48**, **49**, **53**, **55**, **57**, **58**, **59**, **60**, **62**, **63**, **64**, **65** and **66**) are reported for the first time in these species. A new hydroxycinnamic acid derivative, a major constituent of the samples investigated here, was identified as caffeoyl-*O*-polygalatol (1,5-anhydro-[6-*O*-caffeoyl]-sorbitol(glucitol)) following isolation and 1D and 2D NMR characterization. This compound and its isomer (**25** and **27**) may serve as potential chemo-taxonomic markers, as previously polygalatol (1,5-anhydrosorbitol) was found only in South African indigenous Proteaceae species.[10] The results differ significantly from the only recent report on other Proteaceae members.[11,12] Significant differences in the levels of the compounds identified in the present work were also observed between the studied samples (Supplementary; Figure S3.3). Briefly, compounds like caffeoyl-*O*-polygalatol (**25**) were seen in varying levels in the plants studied, and (-)-epicatechin (**46**) was seen in high levels in the cultivar Black beauty and low in the rest of the plants. Anthocyanins are common in pigmented flowering plants,[14,20] in this study anthocyanins were found in the pink to deep-red pigmented flowers. This is, to the best of our knowledge, the first report of the anthocyanin (**44, 47, 48, 49** and **53**) composition in *Protea* species. There are many publications reporting on the presence of flavonoids in plants,[13–21,40,42,60,65,66,74,76] with an estimated number of 8000 flavonoids having been discussed,[76] however the combination of compounds (including the new compound) and the relative levels reported herein are unique. Current work on the detailed comparison of phytochemical profiles of a much larger set of *Protea* species will be reported elsewhere (Chapter 4).

3.5. References

(1) Barker, N. P.; Weston, P. H.; Rutschmann, F.; Sauquet, H. Molecular dating of the 'Gondwanan' plant family Proteaceae is only partially congruent with the timing of the break-up of Gondwana. *J. Biogeogr.* **2007**, *34* (12), 2012–2027. https://doi.org/10.1111/j.1365-2699.2007.01749.x.

(2) Collins, B. G.; Rebelo, T. Pollination biology of the Proteaceae in Australia and Southern Africa. *Aust. J. Ecol.* **1987**, *12* (4), 387–421. https://doi.org/10.1111/j.1442-9993.1987.tb00958.x.

(3) Statistics - Cape Flora http://www.capeflorasa.co.za/statistics/ (accessed Feb 25, 2021).

(4) Verotta, L.; Orsini, F.; Pelizzoni, F.; Torri, G.; Rogers, C. B. Polyphenolic glycosides from African Proteaceae. *J. Nat. Prod.* **1999**, *62* (11), 1526–1531. https://doi.org/10.1021/np9902237.

(5) Prunier, R.; Akman, M.; Kremer, C. T.; Aitken, N.; Chuah, A.; Borevitz, J.; Holsinger, K. E. Isolation by distance and isolation by environment contribute to population differentiation in *Protea repens* (Proteaceae L.), a widespread South African Species . *Am. J. Bot.* **2017**, *104* (5), 674–684. https://doi.org/10.3732/ajb.1600232.

(6) Prunier, R.; Holsinger, K. E. Was It an explosion? Using population genetics to explore the dynamics of a recent radiation within *Protea* (Proteaceae L.). *Mol. Ecol.* **2010**, *19* (18), 3968–3980. https://doi.org/10.1111/j.1365-294X.2010.04779.x.

(7) Akman, M.; Carlson, J. E.; Holsinger, K. E.; Latimer, A. M. Transcriptome sequencing reveals population differentiation in gene expression linked to functional traits and environmental gradients in the South African shrub *Protea repens*. *New Phytol.* **2016**, *210* (1), 295–309. https://doi.org/10.1111/nph.13761.

(8) León, F.; Alfayate, C.; Batista, C. V.; López, A.; Rico, M.; Brouard, I. Phenolic compounds, antioxidant activity and ultrastructural study from *Protea* hybrid "Susara." *Ind. Crops Prod.* **2014**, *55* (July), 230–237. https://doi.org/10.1016/j.indcrop.2014.02.024.

(9) Perold, G. W.; Carlton, L. Neriifolin, an ester glucoside of benzene-1,2,4-triol. *J. Chem. Soc. Perkin Trans. 1* **1989**, 1215–1217. https://doi.org/10.1039/P19890001215.

(10) Bieleski, R. L.; Briggs, B. G. Taxonomic Patterns in the distribution of polyols within the Proteaceae. *Aust. J. Bot.* **2005**, *53* (3), 205–217. https://doi.org/10.1071/BT04098.

(11) Deans, B. J.; Kilah, N. L.; Jordan, G. J.; Bissember, A. C.; Smith, J. A. Arbutin derivatives isolated from ancient Proteaceae: Potential phytochemical markers present in *Bellendena*, *Cenarrhenes*, and *Persoonia* Genera. *J. Nat. Prod.* **2018**, *81* (5), 1241–1251. https://doi.org/10.1021/acs.jnatprod.7b01038.

(12) Deans, B. J.; Tedone, L.; Bissember, A. C.; Smith, J. A. Phytochemical profile of the rare, ancient clone *Lomatia tasmanica* and comparison to other endemic Tasmanian species *L. tinctoria* and *L. polymorpha*. *Phytochemistry* **2018**, *153* (June), 74–78. https://doi.org/10.1016/j.phytochem.2018.05.019.

(13) Fang, N.; Yu, S.; Prior, R. L. LC/MS/MS characterization of phenolic constituents in dried plums. *J. Agric. Food Chem.* **2002**, *50* (12), 3579–3585. https://doi.org/10.1021/jf0201327.

(14) Yang, R. Z.; Wei, X. L.; Gao, F. F.; Wang, L. S.; Zhang, H. J.; Xu, Y. J.; Li, C. H.; Ge, Y. X.; Zhang, J. J.; Zhang, J. Simultaneous analysis of anthocyanins and flavonols in petals of Lotus (*Nelumbo*) cultivars by high-performance liquid chromatography-photodiode array detection/electrospray ionization mass spectrometry. *J. Chromatogr. A* **2009**, *1216* (1), 106–112. https://doi.org/10.1016/j.chroma.2008.11.046.

(15) Jaiswal, R.; Elsadig Karar, M. G.; Gadir, H. A.; Kuhnert, N. Identification and characterisation of phenolics from *Ixora coccinea* L. (Rubiaceae) by liquid chromatography multi-stage mass spectrometry. *Phytochem. Anal.* **2014**, *25* (6), 567–576. https://doi.org/10.1002/pca.2530.

(16) Rockenbach, I. I.; Jungfer, E.; Ritter, C.; Santiago-Schübel, B.; Thiele, B.; Fett, R.; Galensa, R. Characterization of flavan-3-ols in seeds of grape pomace by CE, HPLC-DAD-MS^n and LC-ESI-FTICR-MS. *Food Res. Int.* **2012**, *48* (2), 848–855. https://doi.org/10.1016/j.foodres.2012.07.001.

(17) Cádiz-Gurrea, M. de la L.; Fernández-Arroyo, S.; Joven, J.; Segura-Carretero, A. Comprehensive characterization by UHPLC-ESI-Q-TOF-MS from an *Eryngium bourgatii* extract and their antioxidant and anti-inflammatory activities. *Food Res. Int.* **2013**, *50* (1), 197–204. https://doi.org/10.1016/j.foodres.2012.09.038.

(18) Carazzone, C.; Mascherpa, D.; Gazzani, G.; Papetti, A. Identification of phenolic constituents in red chicory salads (*Cichorium intybus*) by high-performance liquid chromatography with diode array detection and electrospray ionisation tandem mass spectrometry. *Food Chem.* **2013**, *138* (2–3), 1062–1071.

https://doi.org/10.1016/j.foodchem.2012.11.060.

(19) Fromm, M.; Loos, H. M.; Bayha, S.; Carle, R.; Kammerer, D. R. Recovery and characterisation of coloured phenolic preparations from apple seeds. *Food Chem.* **2013**, *136* (3–4), 1277–1287. https://doi.org/10.1016/j.foodchem.2012.09.042.

(20) Xu, W.; Luo, G.; Yu, F.; Jia, Q.; Zheng, Y.; Bi, X.; Lei, J. Characterization of anthocyanins in the hybrid progenies derived from *Iris dichotoma* and *I. domestica* by HPLC-DAD-ESI/MS analysis. *Phytochemistry* **2018**, *150*, 60–74. https://doi.org/10.1016/j.phytochem.2018.03.003.

(21) Beelders, T.; de Beer, D.; Stander, M.; Joubert, E. Comprehensive phenolic profiling of *Cyclopia genistoides* (L.) Vent. by LC-DAD-MS and -MS/MS reveals novel xanthone and benzophenone constituents. *Molecules* **2014**, *19* (8), 11760–11790. https://doi.org/10.3390/molecules190811760.

(22) Ramirez-Ambrosi, M.; Abad-Garcia, B.; Viloria-Bernal, M.; Garmon-Lobato, S.; Berrueta, L. A.; Gallo, B. A New ultrahigh performance liquid chromatography with diode array detection coupled to electrospray ionization and quadrupole time-of-flight mass spectrometry analytical strategy for fast analysis and improved characterization of phenolic compounds in apple products. *J. Chromatogr. A* **2013**, *1316*, 78–91. https://doi.org/10.1016/j.chroma.2013.09.075.

(23) Gonzales, G. B.; Raes, K.; Coelus, S.; Struijs, K.; Smagghe, G.; Van Camp, J. Ultra(high)-pressure liquid chromatography–electrospray ionization-time-of-flight-ion mobility-high definition mass spectrometry for the rapid identification and structural characterization of flavonoid glycosides from cauliflower waste. *J. Chromatogr. A* **2014**, *1323*, 39–48. https://doi.org/10.1016/j.chroma.2013.10.077.

(24) Clifford, M. N.; Kirkpatrick, J.; Kuhnert, N.; Roozendaal, H.; Salgado, P. R. LC–MS^n Analysis of the *cis* isomers of chlorogenic acids. *Food Chem.* **2008**, *106* (1), 379–385. https://doi.org/10.1016/j.foodchem.2007.05.081.

(25) Masike, K.; Mhlongo, M. I.; Mudau, S. P.; Nobela, O.; Ncube, E. N.; Tugizimana, F.; George, M. J.; Madala, N. E. Highlighting mass spectrometric fragmentation differences and similarities between hydroxycinnamoyl-quinic acids and hydroxycinnamoyl-isocitric acids. *Chem. Cent. J.* **2017**, *11* (1), 29. https://doi.org/10.1186/s13065-017-0262-8.

(26) Masike, K.; Madala, N. Synchronized survey scan approach allows for efficient

discrimination of isomeric and isobaric compounds during LC-MS/MS analyses. *J. Anal. Methods Chem.* **2018**, *2018*, 1–8. https://doi.org/10.1155/2018/2046709.

(27) Fridén, M. E.; Sjöberg, P. J. R. Strategies for differentiation of isobaric flavonoids using liquid chromatography coupled to electrospray ionization mass spectrometry. *J. Mass Spectrom.* **2014**, *49* (7), 646–663. https://doi.org/10.1002/jms.3386.

(28) Makola, M. M.; Steenkamp, P. A.; Dubery, I. A.; Kabanda, M. M.; Madala, N. E. Preferential alkali metal adduct formation by *cis* geometrical isomers of dicaffeoylquinic acids allows for efficient discrimination from their *trans* isomers during ultra-high-performance liquid chromatography/quadrupole time-of-flight mass spectrometry. *Rapid Commun. Mass Spectrom.* **2016**, *30* (8), 1011–1018. https://doi.org/10.1002/rcm.7526.

(29) Paglia, G.; Williams, J. P.; Menikarachchi, L.; Thompson, J. W.; Tyldesley-Worster, R.; Halldórsson, S.; Rolfsson, O.; Moseley, A.; Grant, D.; Langridge, J.; Palsson, B. O.; Astarita, G. Ion mobility derived collision cross sections to support metabolomics applications. *Anal. Chem.* **2014**, *86* (8), 3985–3993. https://doi.org/10.1021/ac500405x.

(30) Paglia, G.; Angel, P.; Williams, J. P.; Richardson, K.; Olivos, H. J.; Thompson, J. W.; Menikarachchi, L.; Lai, S.; Walsh, C.; Moseley, A.; Plumb, R. S.; Grant, D. F.; Palsson, B. O.; Langridge, J.; Geromanos, S.; Astarita, G. Ion mobility-derived collision cross section as an additional measure for lipid fingerprinting and identification. *Anal. Chem.* **2015**, *87* (2), 1137–1144. https://doi.org/10.1021/ac503715v.

(31) Pacini, T.; Fu, W.; Gudmundsson, S.; Chiaravalle, A. E.; Brynjolfson, S.; Palsson, B. O.; Astarita, G.; Paglia, G. Multidimensional analytical approach based on UHPLC-UV-Ion Mobility-MS for the screening of natural pigments. *Anal. Chem.* **2015**, *87* (5), 2593–2599. https://doi.org/10.1021/ac504707n.

(32) Gonzales, G. B.; Smagghe, G.; Coelus, S.; Adriaenssens, D.; De Winter, K.; Desmet, T.; Raes, K.; Van Camp, J. Collision cross section prediction of deprotonated phenolics in a travelling-wave ion mobility spectrometer using molecular descriptors and chemometrics. *Anal. Chim. Acta* **2016**, *924*, 68–76. https://doi.org/10.1016/j.aca.2016.04.020.

(33) Zheng, X.; Renslow, R. S.; Makola, M. M.; Webb, I. K.; Deng, L.; Thomas, D. G.; Govind, N.; Ibrahim, Y. M.; Kabanda, M. M.; Dubery, I. A.; Heyman, H. M.; Smith, R. D.; Madala, N. E.; Baker, E. S. Structural elucidation of *cis*/*trans* dicaffeoylquinic acid photoisomerization using ion mobility spectrometry-mass spectrometry. *J. Phys. Chem. Lett.* **2017**, *8* (7),

1381–1388. https://doi.org/10.1021/acs.jpclett.6b03015.

(34) Kuhnert, N.; Yassin, G. H.; Jaiswal, R.; Matei, M. F.; Grün, C. H. Differentiation of prototropic ions in regioisomeric caffeoyl quinic acids by electrospray ion mobility mass spectrometry. *Rapid Commun. Mass Spectrom.* **2015**, *29* (7), 675–680. https://doi.org/10.1002/rcm.7151.

(35) Warnke, S.; Seo, J.; Boschmans, J.; Sobott, F.; Scrivens, J. H.; Bleiholder, C.; Bowers, M. T.; Gewinner, S.; Schöllkopf, W.; Pagel, K.; von Helden, G. Protomers of benzocaine: Solvent and permittivity dependence. *J. Am. Chem. Soc.* **2015**, *137* (12), 4236–4242. https://doi.org/10.1021/jacs.5b01338.

(36) Valentine, S. J.; Plasencia, M. D.; Liu, X.; Krishnan, M.; Naylor, S.; Udseth, H. R.; Smith, R. D.; Clemmer, D. E. Toward plasma proteome profiling with ion mobility-mass spectrometry. *J. Proteome Res.* **2006**, *5* (11), 2977–2984. https://doi.org/10.1021/pr060232i.

(37) Malan, G. *Protea cultivation: From concept to carton*, 1st ed.; Sun MeDIA publishers: Stellenbosch, 2012.

(38) Annual Report 2017/2018 - PPECB https://ppecb.com/document/annual-report-2017-2018/ (accessed Nov 29, 2019).

(39) De Villiers, A.; Cabooter, D.; Lynen, F.; Desmet, G.; Sandra, P. High performance liquid chromatography analysis of wine anthocyanins revisited: Effect of particle size and temperature. *J. Chromatogr. A* **2009**, *1216* (15), 3270–3279. https://doi.org/10.1016/j.chroma.2009.02.038.

(40) Díaz-García, M. C.; Obón, J. M.; Castellar, M. R.; Collado, J.; Alacid, M. Quantification by UHPLC of total individual polyphenols in fruit juices. *Food Chem.* **2013**, *138* (2–3), 938–949. https://doi.org/10.1016/j.foodchem.2012.11.061.

(41) Rautenbach, M.; Vlok, N. M.; Eyéghé-Bickong, H. A.; van der Merwe, M. J.; Stander, M. A. An electrospray ionization mass spectrometry study on the “in vacuo” hetero-oligomers formed by the antimicrobial peptides, surfactin and gramicidin. S. *J. Am. Soc. Mass Spectrom.* **2017**, *28* (8), 1623–1637. https://doi.org/10.1007/s13361-017-1685-0.

(42) Stander, M. A.; Van Wyk, B. E.; Taylor, M. J. C.; Long, H. S. Analysis of phenolic compounds in rooibos tea (*Aspalathus linearis*) with a comparison of flavonoid-based

compounds in natural populations of plants from different regions. *J. Agric. Food Chem.* **2017**, *65* (47), 10270–10281. https://doi.org/10.1021/acs.jafc.7b03942.

(43) Stow, S. M.; Causon, T. J.; Zheng, X.; Kurulugama, R. T.; Mairinger, T.; May, J. C.; Rennie, E. E.; Baker, E. S.; Smith, R. D.; McLean, J. A.; Hann, S.; Fjeldsted, J. C. An interlaboratory evaluation of drift tube ion mobility-mass spectrometry collision cross section measurements. *Anal. Chem.* **2017**, *89* (17), 9048–9055. https://doi.org/10.1021/acs.analchem.7b01729.

(44) Clifford, M. N.; Madala, N. E. Surrogate standards: A cost-effective strategy for identification of phytochemicals. *J. Agric. Food Chem.* **2017**, *65* (18), 3589–3590. https://doi.org/10.1021/acs.jafc.7b01588.

(45) Dictionary of Natural Products 29.2 Chemical Search http://dnp.chemnetbase.com/faces/chemical/ChemicalSearch.xhtml (accessed Nov 29, 2018).

(46) KNApSAcK Core System http://www.knapsackfamily.com/knapsack_core/top.php (accessed Nov 29, 2018).

(47) METLIN https://metlin.scripps.edu/landing_page.php?pgcontent=mainPage (accessed Nov 29, 2018).

(48) ChemSpider | Search and share chemistry http://www.chemspider.com/ (accessed Nov 29, 2018).

(49) Yang, X.; Wei, S.; Liu, B.; Guo, D.; Zheng, B.; Feng, L.; Liu, Y.; Tomás-Barberán, F. A.; Luo, L.; Huang, D. A novel integrated non-targeted metabolomic analysis reveals significant metabolite variations between different lettuce (*Lactuca sativa*. L) varieties. *Hortic. Res.* **2018**, *5* (1), 1–14. https://doi.org/10.1038/s41438-018-0050-1.

(50) McConchie, R.; Lang, N. S.; Lax, A. R.; Lang, G. A. Reexamining polyphenol oxidase, peroxidase, and leaf-blackening activity in *Protea*. *J. Am. Soc. Hortic. Sci.* **1994**, *119* (6), 1248–1254. https://doi.org/10.21273/JASHS.119.6.1248.

(51) Van Doorn, W. G. Leaf blackening in *Protea* flowers: Recent developments. *Acta Hortic.* **2001**, *545*, 197–204. https://doi.org/10.17660/ActaHortic.2001.545.27.

(52) Hoffman, E. W.; Windell, N. E.; Jacobs, G. Optimum time of harvest for the control of leaf blackening in *Protea* 'Sylvia.' *Acta Hortic.* **2014**, *1031* (1031), 125–133.

https://doi.org/10.17660/ActaHortic.2014.1031.14.

(53) Hoffman, E. W.; Vardien, W.; Jacobs, G.; Windell, N. E. Leaf blackening: A serious impediment to long-term cold storage, transport, and extended vase life in *Protea* cut flowers. In *Horticultural Reviews*; Warrington, I., Ed.; John Wiley & Sons, Inc.: Hoboken, NJ, USA, 2018; Vol. 45, pp 73–104. https://doi.org/10.1002/9781119431077.ch3.

(54) Abdel-Ghany, S. E.; Day, I.; Heuberger, A. L.; Broeckling, C. D.; Reddy, A. S. N. Production of phloroglucinol, a platform chemical, in arabidopsis using a bacterial gene. *Sci. Rep.* **2016**, *6* (1), 38483. https://doi.org/10.1038/srep38483.

(55) Louche, L. M. M.; Gaydou, E. M.; Lesage, J. C. Determination of phlorin as peel marker in orange (*Citrus sinensis*) fruits and juices. *J. Agric. Food Chem.* **1998**, *46* (10), 4193–4197. https://doi.org/10.1021/jf9803637.

(56) Garcia-Jimenez, A.; Teruel-Puche, J. A.; Berna, J.; Rodriguez-Lopez, J. N.; Tudela, J.; Garcia-Canovas, F. Action of tyrosinase on alpha and beta-arbutin: A kinetic study. *PLoS One* **2017**, *12* (5), 1–19. https://doi.org/10.1371/journal.pone.0177330.

(57) Cui, T.; Nakamura, K.; Ma, L.; Li, J. Z.; Kayahara, H. Analyses of arbutin and chlorogenic acid, the major phenolic constituents in oriental pear. *J. Agric. Food Chem.* **2005**, *53* (10), 3882–3887. https://doi.org/10.1021/jf047878k.

(58) Rychlińska, I.; Gudej, J. Qualitative and quantitative chromatographic investigation of hydroquinone derivatives in *Pyrus communis* L. flowers. *Acta Pol. Pharm.* **2003**, *60* (4), 309–312.

(59) Perold, G. W.; Beylis, P.; Howard, A. S. Metabolites of Proteaceae. Part VII. Lacticolorin, a phenolic glucoside ester, and other metabolites of *Protea lacticolor* Salisb. *J. Chem. Soc. Perkin Trans. 1* **1973**, No. 638, 638–643. https://doi.org/10.1039/P19730000638.

(60) Masike, K.; Khoza, B. S.; Steenkamp, P. A.; Smit, E.; Dubery, I. A.; Madala, N. E. A metabolomics-guided exploration of the phytochemical constituents of *Vernonia fastigiata* with the aid of pressurized hot water extraction and liquid chromatography-mass spectrometry. *Molecules* **2017**, *22* (8), 1–16. https://doi.org/10.3390/molecules22081200.

(61) Clifford, M. N.; Johnston, K. L.; Knight, S.; Kuhnert, N. Hierarchical scheme for LC-MS^n identification of chlorogenic acids. *J. Agric. Food Chem.* **2003**, *51* (10), 2900–2911. https://doi.org/10.1021/jf026187q.

(62) Perold, G. W.; Beylis, P.; Howard, A. S. Metabolites of Proteaceae. Part VIII. The occurrence of (+)-d-allose in nature: rubropilosin and pilorubrosin from *Protea rubropilosa* beard. *J. Chem. Soc. Perkin Trans. 1* **1973**, 643–649. https://doi.org/10.1039/P19730000643.

(63) Perold, G. W.; Rosenberg, M. E. K.; Howard, A. S.; Huddle, P. A. Metabolites of Proteaceae. Part 9. Eximin (6-*o*-benzoylarbutin) and the synthesis of aryl glycoside esters. *J. Chem. Soc. Perkin Trans. 1* **1979**, 239–243. https://doi.org/10.1039/p19790000239.

(64) Xiao, Y.; Hu, Z.; Yin, Z.; Zhou, Y.; Liu, T.; Zhou, X.; Chang, D. Profiling and distribution of metabolites of procyanidin B2 in mice by UPLC-DAD-ESI-IT-TOF-MS^n technique. *Front. Pharmacol.* **2017**, *8* (MAY), 1–12. https://doi.org/10.3389/fphar.2017.00231.

(65) Alberts, P.; Stander, M. A.; De Villiers, A. Advanced ultra high pressure liquid chromatography–tandem mass spectrometric methods for the screening of red wine anthocyanins and derived pigments. *J. Chromatogr. A* **2012**, *1235*, 92–102. https://doi.org/10.1016/j.chroma.2012.02.058.

(66) Schieber, A.; Keller, P.; Carle, R. Determination of phenolic acids and flavonoids of apple and pear by high-performance liquid chromatography. *J. Chromatogr. A* **2001**, *910* (2), 265–273. https://doi.org/10.1016/S0021-9673(00)01217-6.

(67) Ablajan, K.; Abliz, Z.; Shang, X. Y.; He, J. M.; Zhang, R. P.; Shi, J. G. Structural characterization of flavonol 3,7-di-*o*-glycosides and determination of the glycosylation position by using negative ion electrospray ionization tandem mass spectrometry. *J. Mass Spectrom.* **2006**, *41* (3), 352–360. https://doi.org/10.1002/jms.995.

(68) Wu, Z. J.; Ma, X. L.; Fang, D. M.; Qi, H. Y.; Ren, W. J.; Zhang, G. L. Analysis of caffeic acid derivatives from *Osmanthus yunnanensis* using electrospray ionization quadrupole time-of-flight mass spectrometry. *Eur. J. Mass Spectrom.* **2009**, *15* (3), 415–429. https://doi.org/10.1255/ejms.992.

(69) Colquhoun, I. J.; Ralet, M.-C.; Thibault, J.-F.; Faulds, C. B.; Williamson, G. Structure identification of feruloylated oligosaccharides from sugar-beet pulp by NMR spectroscopy. *Carbohydr. Res.* **1994**, *263* (2), 243–256. https://doi.org/10.1016/0008-6215(94)00176-6.

(70) Kametani, S.; Mizuno, H.; Shiga, Y.; Akanuma, H. NMR of all-carbon-13 sugars: An application in development of an analytical method for a novel natural sugar, 1,5-anhydrofructose. *J. Biochem.* **1996**, *119* (1), 180–185.

https://doi.org/10.1093/oxfordjournals.jbchem.a021206.

(71) Ikeya, Y.; Sugama, K.; Okada, M.; Mitsuhashi, H. Four new phenolic glycosides from *Polygala tenuifolia*. *Chem. Pharm. Bull. (Tokyo).* **1991**, *39* (10), 2600–2605. https://doi.org/10.1248/cpb.39.2600.

(72) Kamori, A.; Kato, A.; Miyawaki, S.; Koyama, J.; Nash, R. J.; Fleet, G. W. J.; Miura, D.; Ishikawa, F.; Adachi, I. Dual action of acertannins as potential regulators of intracellular ceramide levels. *Tetrahedron: Asymmetry* **2016**, *27* (22–23), 1177–1185. https://doi.org/10.1016/j.tetasy.2016.09.006.

(73) Causon, T. J.; Ivanova-Petropulos, V.; Petrusheva, D.; Bogeva, E.; Hann, S. Fingerprinting of traditionally produced red wines using liquid chromatography combined with drift tube ion mobility-mass spectrometry. *Anal. Chim. Acta* **2019**, *1052*, 179–189. https://doi.org/10.1016/j.aca.2018.11.040.

(74) Abad-García, B.; Berrueta, L. A.; Garmón-Lobato, S.; Gallo, B.; Vicente, F. A general analytical strategy for the characterization of phenolic compounds in fruit juices by high-performance liquid chromatography with diode array detection coupled to electrospray ionization and triple quadrupole mass spectrometry. *J. Chromatogr. A* **2009**, *1216* (28), 5398–5415. https://doi.org/10.1016/j.chroma.2009.05.039.

(75) Richardson, K.; Langridge, D.; Dixit, S. M.; Ruotolo, B. T. An improved calibration approach for traveling wave ion mobility spectrometry: Robust, high-precision collision cross sections. *Anal. Chem.* **2021**. https://doi.org/10.1021/acs.analchem.0c04948.

(76) Iwashina, T. Contribution to flower colors of flavonoids including anthocyanins: A review. *Nat. Prod. Commun.* **2015**, *10* (3), 529–544. https://doi.org/10.1177/1934578X1501000335.

Supplementary information for: Detailed Phenolic Characterization of *Protea* Pure and Hybrid Cultivars by Liquid Chromatography−Ion Mobility−High Resolution Mass Spectrometry (LC-IM-HR-MS)

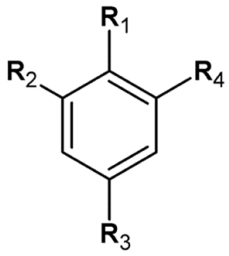

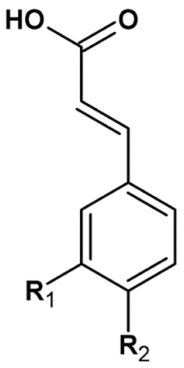

Hydroquinone: R_1=R_3=OH; R_2=R_4=H
Benzene-1,2,4-triol: R_1=R_2=R_3=OH; R_4=H
Benzene-1,3,5-triol: R_1=H; R_2=R_3=R_4=OH
Benzoic acid: R_1=R_2=R_4=H; R_3=COOH
***p*-Hydroxybenzoic acid:** R_1=OH; R_2=R_4=H; R_3=COOH
Protocatechuic acid: R_1=R_2=OH; R_3=COOH; R_4=H
Protocatechuic alcohol: R_1=R_2=OH; R_3=CH_2OH; R_4=H
Vanillic acid: R_1=OCH_3; R_2=OH; R_3=COOH; R_4=H

***p*-Coumaric acid:** R_1=H; R_2=OH
Caffeic acid: R_1=R_2=OH
Ferulic acid: R_1=OCH_3; R_2=OH

Figure S3.1: Chemical structures of phenol, phenolic acid and hydroxycinnamic acid derivatives (tentatively) identified in the four studied *Protea* plants (pure species and hybrid cultivars).

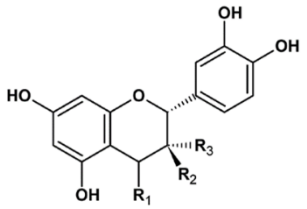

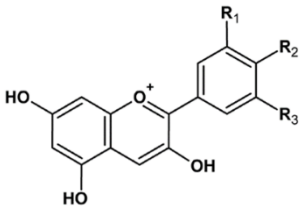

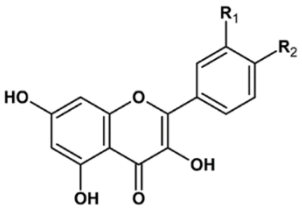

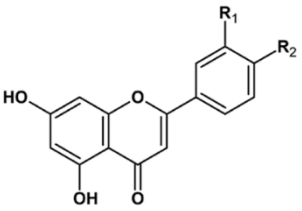

(+)-Catechin: R_1=H; R_2=OH; R_3=H
(-)-Epicatechin: R_1=H; R_2=H; R_3=OH
Procyanidin B: R_1=(Epi)catechin; R_2 or R_3=OH

Delphinidin: R_1=R_2=R_3=OH
Cyanidin: R_1=R_2=OH; R_3=H
Petunidin: R_1=R_2=OH; R_3=OCH_3
Peonidin: R_1=OCH_3; R_2=OH; R_3=H
Malvidin: R_1=OCH_3; R_2=OH; R_3=OCH_3

Quercetin: R_1=R_2=OH
Kaempferol: R_1=H; R_2=OH
Isorhamnetin: R_1=OCH_3; R_2=OH

Diosmetin: R_1=OH; R_2=OCH_3

Figure S3.2: Chemical structures of the flavan-3-ols, anthocyanidins, flavonols and flavone (tentatively) identified in the four studied *Protea* plants (pure species and hybrid cultivars).

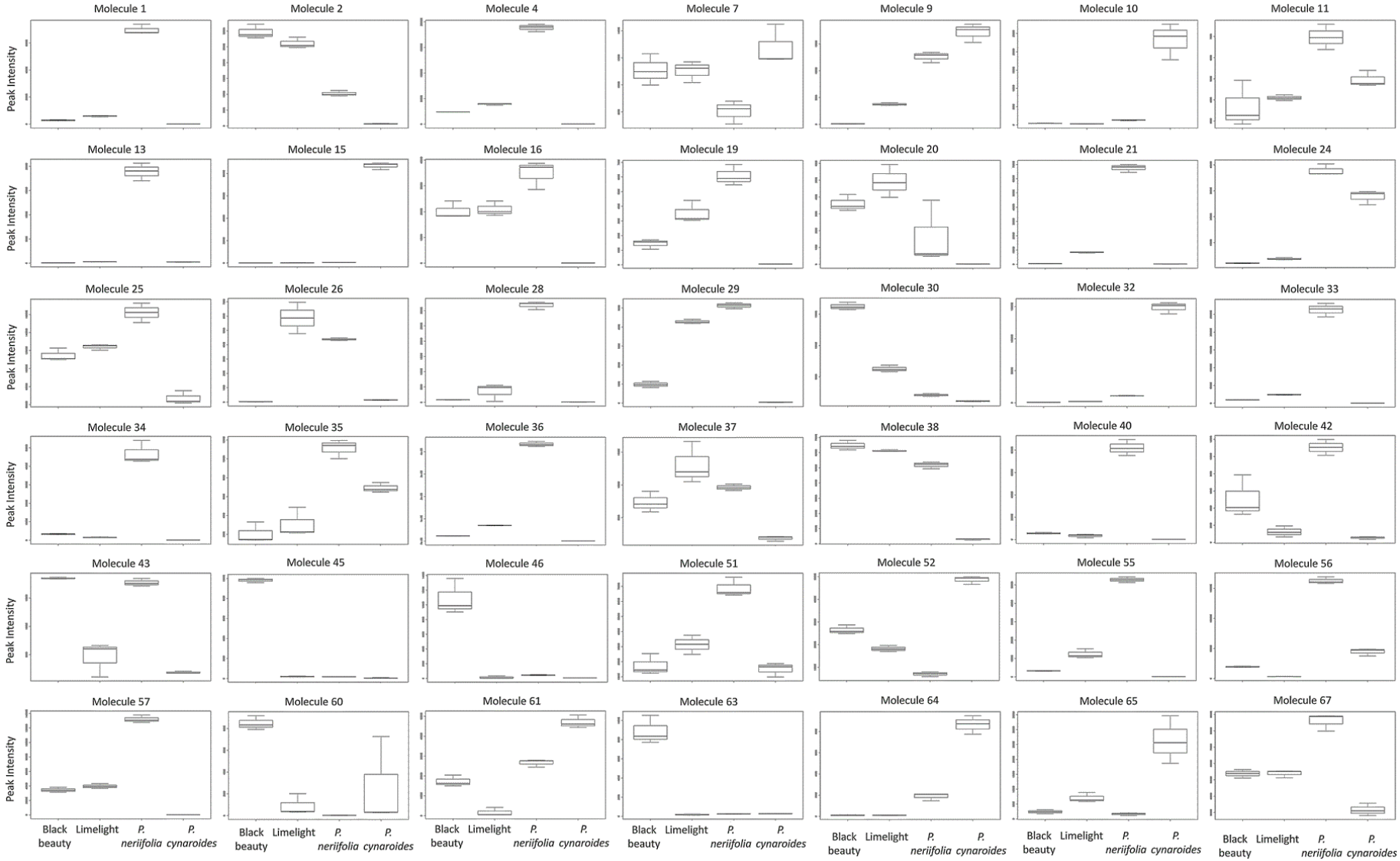

Figure S3.3: Box-and-whiskers plots showing the distribution of 42 different metabolites across two hybrid cultivars (Black beauty and limelight) and two pure species (*P. neriifolia* and *P. cynaroides*) in Table 3.1 (phenol and phenolic acid derivatives) and Table 3.2 (flavonoid derivatives). All significant differences are based on ANOVA with $p \leq 0.01$.

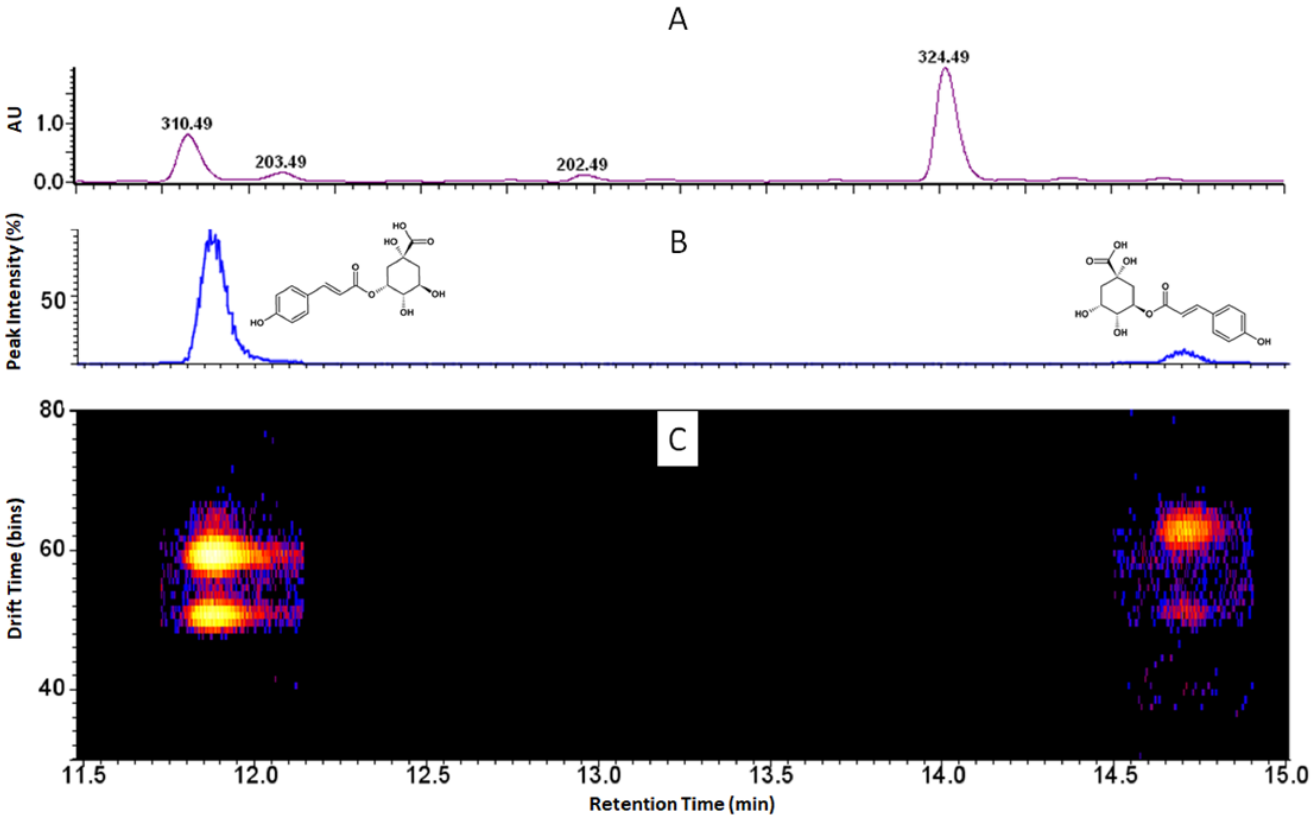

Figure S3.4: Selected UPLC-PDA-IM-HR-MS data showing separation of 3-*p*-coumaroyl-*O*-quinic acid (**16**) and 5-*p*-coumaroyl-*O*-quinic acid (**29**). **A**) shows the RP-LC chromatograms recorded at 310 nm, **B**) the extracted ion chromatogram (EIC) at *m/z* 337, and **C**) two distinct arrival time distributions for **16** (175.9 and 160.3 Å^2) and **29** (180.8 and 162.1 Å^2) likely corresponding to prototropic species for each compound.

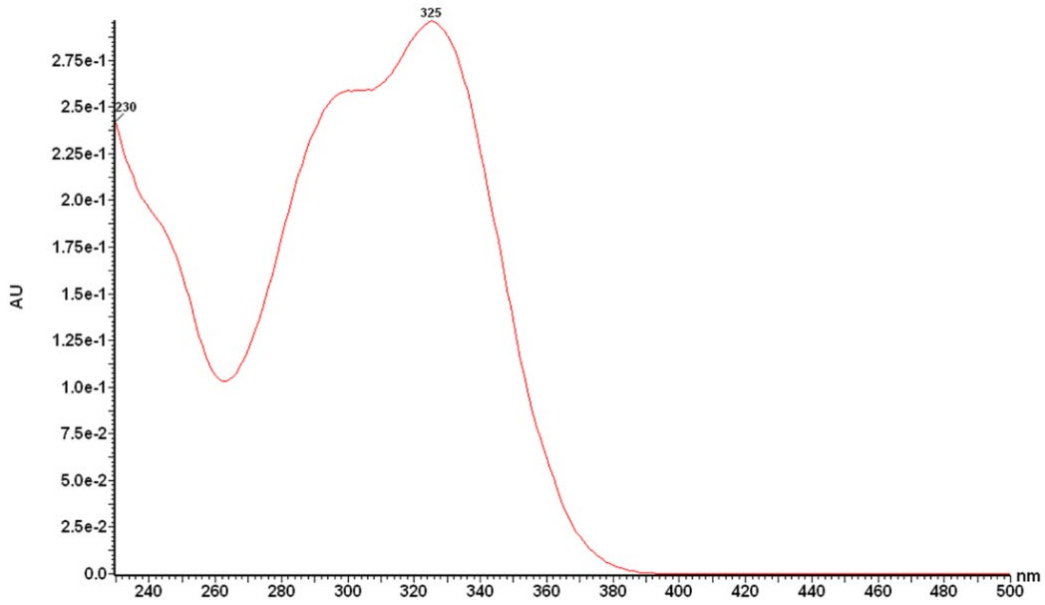

Figure S3.5: UV spectrum of compound **25.**

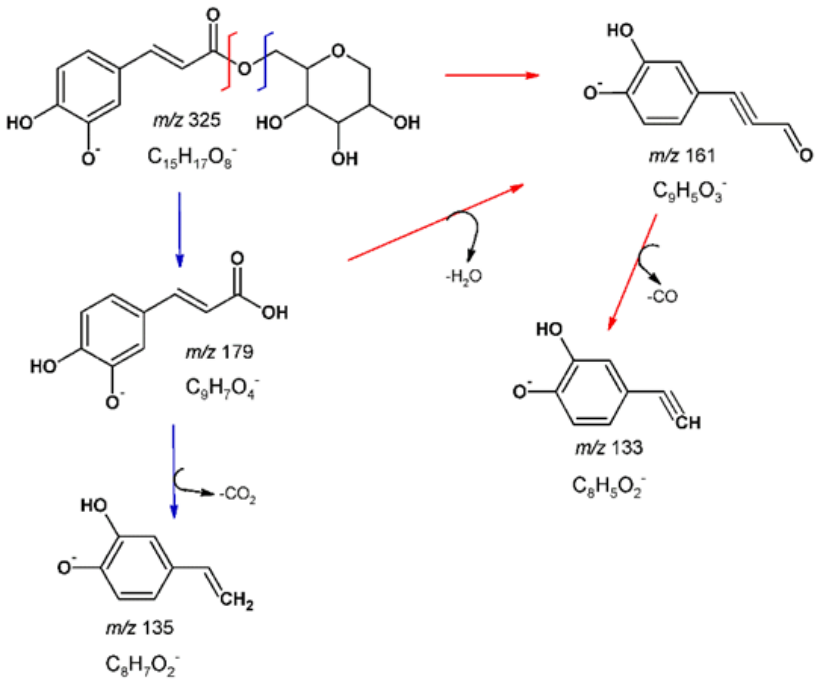

Figure S3.6: Schematic representation of the proposed fragmentation of caffeoyl-*O*-polygalatol (1,5-anhydro-[6-*O*-caffeoyl]-sorbitol(glucitol)) (**25**) and caffeoyl-*O*-polygalatol (1,5-anhydrosorbitol(glucitol)) (**27**).

Table S3.1: Comparison of CCS values measured for selected metabolites identified in *Protea* on a low-field drift tube instrument ($^{DT}CCS_{N2}$) and on a travelling wave instrument ($^{TW}CCS_{N2}$). Compound numbers correspond to Tables 3.1 and 3.2.

Number	Compound	Adduct	t_R (min)[a]	$^{DT}CCS_{N2}$ (Å^2)	$^{TW}CCS_{N2}$ (Å^2)
32	Protocatechuic acid-*O*-hexoside-*O*-protocatechuic alcohol isomer 2	$[M-H]^-$	18.12	185.8	182.4
33	Neriifolin (benzyl-*O*-hexoside-*O*-hydroxyquinol) isomer 1	$[M-H]^-$	20.33	187.7	184.6
35	Lacticolorin/Pilorubrosin (benzyl-*O*-hexoside-*O*-protocatechuic alcohol) isomer 1	$[M-H]^-$	21.78	195.1	191.9
36	Neriifolin isomer 2	$[M-H]^-$	22.00	190.0	186.0
37	Lacticolorin/Pilorubrosin isomer 2	$[M-H]^-$	22.22	196.2	193.4
38	Eximin (6-*O*-benzyl-*O*-arbutin)	$[M-H]^-$	22.25	186.9	183.3
50	Quercetin-*O*-hexoside-*O*-deoxy-hexose	$[M-H]^-$	17.66	232.9	232.2
52	Quercetin-*O*-galactoside	$[M-H]^-$	18.29	201.9	198.5
54	Isoquercetin (Quercetin-3-*O*-glucoside)	$[M-H]^-$	18.61	202.2	198.5
59	Kaempferol-3-*O*-glucoside	$[M-H]^-$	20.26	201.7	197.3
61	Quercetin-*O*-deoxy-hexose	$[M-H]^-$	20.53	196.6	192.8
63	Isorhamnetin-*O*-pentoside	$[M-H]^-$	21.93	203.2	198.7
64	Kaempferol-*O*-deoxy-hexose	$[M-H]^-$	22.52	195.6	193.0

[a] Retention times on the drift tube instrument (refer to section 3.2.3.4 for experimental details).

Declaration with signatures in possession of candidate and supervisor.

Declaration by the candidate:

Regarding **Chapter 4**, the nature and scope of my contribution were as follows:

Nature of contribution	**Extent of contribution (%)**
Performed the experiments, data analysis, co-wrote paper	88

The following co-authors have contributed to **Chapter 4**:

Name	**E-mail address**	**Nature of contribution**	**Extent of contribution (%)**
Marietjie A. Stander	lcms@sun.ac.za	Co-conceptualised the idea, editing of the paper	5
André de Villiers	ajdevill@sun.ac.za	Co-conceptualised the idea, editing of the paper	5
Eleanor W. Hoffman	ewh@sun.ac.za	Co-conceptualised the idea, editing of the paper	2

Signature of candidate: …… 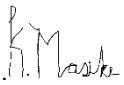 ……

Date: …25 February 2021……

Declaration by co-authors:

The undersigned confirm that:

The declaration above accurately reflects the nature and extent of the contributions of the candidate and the co-authors to **Chapter 4**,
No other authors contributed to **Chapter 4** besides those specified above, and
Potential conflicts of interest have been revealed to all interested parties and that the necessary changes have been made to use the material in Chapter 4 of this thesis.

Signature	**Institutional affiliation**	**Date**
	Stellenbosch University	17 February 2021
	Stellenbosch University	17 February 2021

Chapter 4: Application of Metabolomics Tools to Determine Possible Biomarker Metabolites Linked to Leaf Blackening in *Protea*

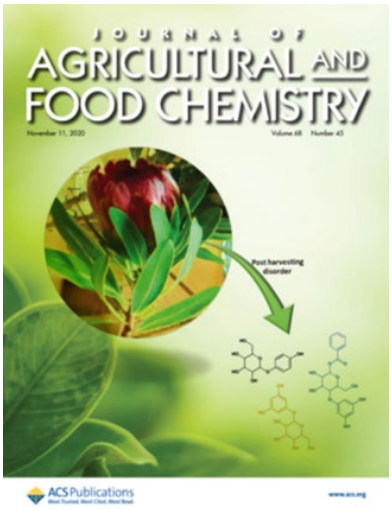

Abstract

The post harvesting disorder leaf blackening is the main cause of product rejection in *Protea* during export. In this study we report an investigation into metabolites associated with leaf blackening in *Protea* species. Methanol extracts of leaf and involucral bract tissue were analysed by liquid-chromatography hyphenated to photodiode array and high-resolution mass spectrometry (LC-PDA-HR-MS), where 116 features were annotated. Analytical data obtained from 37 *Protea* species, selections and hybrids were investigated using metabolomics tools, which showed that stems susceptible to leaf blackening cluster together and contained features identified as benzenetriol and/or hydroquinone derived metabolites. On the other hand, species, selections and cultivars not prone to blackening were linked to metabolites with known protective properties against biotic and abiotic stressors. During the browning process, susceptible cultivars also produce these protective metabolites, yet at innately low levels, which may render these species and cultivars more vulnerable to blackening. Metabolites that were found to be correlated to the instigation of the browning process, all comprising of benzenetriol- and hydroquinone-glycoside derivatives, are highlighted. The study provides preliminary insights to guide the development of new *Protea* cultivars not susceptible to leaf blackening.

4.1. Introduction

Protea, an international floricultural crop originating from the Cape Floristic Kingdom, are sought after for their large, striking inflorescence and perceived long vase life. Yet, most species, selections and cultivars of current commercial importance are prone, to varying extents, to the postharvesting disorder called leaf blackening, whereby the foliage develops distinct, dark brown to black discolorations.[1] Blackening presents itself in four different ways: on the leaf-tip, mid-rib area, leaf-base, or lateral leaf margins.[2] The manifestation of leaf blackening varies significantly between species[3–5] and also between cultivars derived from these species.[6–9] Leaf blackening can occur at any point of the postharvest marketing chain, resulting in the reduction of product quality and consignment rejection by importers.[10] For this reason, causes of blackening have been studied extensively.[3,6–8,11–13] The phenomenon has mostly been linked to a reduction in carbohydrate content,[3,7,8,11–13] particularly a decline in sucrose levels in the leaves in response to a demand by the developing inflorescence.[6] In the cultivar `Sylvia' (*P. eximia* x *P. susannae*), on the other hand, a reduction in glucose content was considered the main link to blackening.[7] Enzymatic activity of polyphenol oxidases (PPOs)[14–16] as well as non-enzymatic processes (such as the oxidation of phenolic compounds)[17] are also understood as possible instigators of the blackening process. Despite previous research, the causes of blackening in *Protea* species, selections and cultivars are still not clearly understood. Most of the above mentioned studies looked at changes during the browning process at a physiological level,[3,5,11–13,17] whereas changes at a metabolic level have yet to be studied.

Untargeted metabolomics approaches can be used to obtain a detailed understanding of the intricate differences and similarities between biological samples.[18–20] The untargeted approach allows the detection of a wide range of metabolites obtained from a single extract (or treatment), thus providing insight into an organism's metabolome at different physiological and pathological states. Metabolomics has been discussed as a relevant approach to accelerate plant improvement in crop science.[21] Plant metabolomics can aid in the selection of trait-specific markers to improve commercially important traits.[20–23] For instance, commercially important apple cultivars have been differentiated based on their metabolite content;[24] while metabolites linked to the resistance, tolerance and susceptibility of different tomato cultivars to microbial infections,[20] and the susceptibility of lettuce cultivars to browning[22] have been identified. A metabolomics study on stored apples showed that increased levels of the primary metabolites (i.e. mannose and xylose) during postharvest enhanced the occurrence of the internal browning disorder.[25] Such studies enhance the plant breeder's ability to make informed decisions.

In the present study, insight into the metabolic changes occurring during the leaf blackening process was acquired. Using an untargeted metabolomics approach, we report the metabolite distribution in 37 *Protea* plants (12 pure species, 10 species selections and 15 hybrid cultivars) obtained by the analytical platform ultra-high performance liquid chromatography-photodiode array-ion mobility-high resolution mass spectrometry (UPLC-PDA-IM-HR-MS) in combination with multivariate data analysis methods.

4.2. Materials and methods

4.2.1. Materials

Authentic standards of vanillic acid (97%), caffeic acid (98%), (+)-catechin (99%), (-)-epicatechin (99%), rutin (94%), 5-caffeoylquinic acid (95%) and isoquercitrin (90%) were purchased from Sigma-Aldrich (MO, USA). LC-grade acetonitrile (99.9%) and methanol (99.9%) were obtained from Romil (Cambridge, UK). Formic acid (98-100%) was obtained from Merck (MO, USA). Analytical-grade (Milli-Q) water was prepared from a Millipore water purification system and used in all assays and solutions.

4.2.2. Samples

One pure *Protea* species (*Protea mundii*) together with seven hybrid cultivars, namely 'Sharonette' (*P. eximia* x *P. susannae), '*Black Beauty*'* (Sheila (*P. magnifica* x *P. burchellii*) cross)*,* 'Sylvia' (*P. eximia* x *P. susannae*), 'Susara' (*P. magnifica* x *P. susannae*), 'Carnival' (*P. compacta* x *P. neriifolia*), 'Limelight' (*P. neriifolia* x *P. burchellii*) and 'Pink Ice' (*P. compacta* x *P. susannae*) were collected from the commercial farm "FynBloem" (34°09′01″S 19°54′52″E); seven *Protea* pure species (*P. susannae, P. compacta, P. neriifolia*, *P. burchellii*, *P. obtusifolia*, *P. repens* and *P. cynaroides*) were collected from the Harold Porter National Botanical Garden (34°21′06″S 18°55′37″E), whilst 22 *Protea* pure species, selections and hybrids including *P. nitida*, *P. grandiceps*, *P. laurifolia*, *P. cordata*, 'Barbigera' (*P. magnifica* selection), 'Ice Queen' (*P. magnifica* selection), 'Venus' (*P. repens* x *P. aristata*), 'Brenda' (*P. compacta* x *P. burchellii*), 'Cerise' (*P. magnifica* x *P. obtusifolia*), 'Robyn' (*P. glabra* x *P. laurifolia*), 'Liamarie' (*P. magnifica* selection), 'Red Magic' (*P. magnifica* selection), 'Suzanne' (*P. magnifica* selection), 'Lady Di' (*P. compacta* x *P. magnifica*), 'Chelsea' (*P. magnifica* selection), 'Crinkle Cut' (*P. magnifica* selection), 'Niobe' (*P. laurifolia* x *P. magnifica*), 'Maria' (*P. magnifica* selection), 'Didi' (*P. laurifolia* x *P. magnifica*), 'Sheila' (*P. magnifica* x *P. burchellii*), 'White Night' (*P. longifolia* x *P. repens*) and 'Carli' (*P. magnifica* selection) were collected from the Berghoff-fynbos farm (33°00′S 18°59′E).

Standard cultivation practices for irrigation and nutrition were followed at Fynbloem and Berghoff-fynbos, as recommended for Cape Flora production on nutrient poor soils under Mediterranean-like climatic conditions,[26] whereas inflorescences collected from the Harold Porter National Botanical Garden were obtained from a wild population. A list of the samples is included in the supplementary information (Table S4.1, Supplementary Information). At harvest, the plants were hydrated for one hour in tap water. The inflorescences were then stored as dry stems at 4°C as stipulated by the South African Perishable Products Export Control Board (PPECB) (https://ppecb.com/document/annual-report-2017-2018) until extractions were performed. Due to the susceptibility of *Protea* leaf and stem material to blackening upon damage or cutting, fresh tissue (unless otherwise stated) was used in this study (Figure S4.1, Supplementary Information).[10,17] This precautionary measure also prevented the possibility of metabolite decomposition and blackening.

4.2.3. Methods

4.2.3.1. Sample preparation

For each authentic standard, a 0.500 mg/mL solution was prepared with 50% methanol in water containing 2% formic acid. The resulting solutions were placed in glass vials and analysed by UPLC-PDA-HR-MS.

4.2.3.2. Vase life evaluation study

The onset and development of leaf blackening on the foliage of flowering stems (n=3) of 'Pink Ice', 'Carnival', 'Susara' and 'Sylvia', cut at the commercial harvesting maturity of the flowerhead, were evaluated under standard vase life conditions of 20±2°C, 60% relative humidity and light levels of 20 µmol.m^{-2}/s in 1 L tap water as vase solution. Light levels in the vase life room were maintained as recommended by Reid and Kofranek for standardized vase life evaluations,[27] where 20 µmol.m^{-2}/s PPFD (photosynthetic photo flux density) is converted to 1080 lux. Tap water was replaced daily to eliminate possible leachates from cut wounds on flowering stems as these have been reported to block xylem vessels, resulting in water stress and possibly the induction of blackening.[28] Leaf material was sampled weekly randomly from three individual flowering stems in preparation for extraction. Whereby, the first week (28th March 2018) of sampling fresh-green leaves were sampled, the second week (04th April 2018) slightly blackened leaves were obtained and by the third week (11th April 2018) all the collected leaves had blackened.

4.2.3.3. Metabolite extraction

For extraction, 1.00 g of fresh plant tissue (leaves or involucral bracts) was crushed in a mortar and pestle and mixed with 15 mL methanol/water/formic acid (50:48:2). Samples were prepared

in triplicate for each plant tissue per *Protea* species, selection or cultivar. The samples were subjected to sonication in an ultrasonic bath (250 W, 40 kHz, Lasec Group, RSA) for 60 min at room temperature. Post-sonication, samples were centrifuged (Hermle Z 160 M, LaborTechnik, Germany) at 15 994 x*g* for 60 min. The resulting supernatants were placed in glass vials and analysed by UPLC-PDA-IM-HR-MS.

4.2.3.4. UPLC-PDA-IM-HR-MS analyses

Extracts were analysed as previously reported (section 3.2.3.3).[29] Briefly, 2 µL of extract was injected into an Acquity UPLC system coupled to a Synapt G2 quadrupole-time-of-flight (q-TOF) instrument (Waters Corporation, Manchester, UK) equipped with an Acquity HSS T3 C_{18} column (2.1 mm × 150 mm, 1.8 µm, Waters). The mobile phase for the chromatographic analysis consisted of 0.1% formic acid in MilliQ water (solvent A) and 0.1% formic acid in acetonitrile (solvent B), at a flow rate of 0.25 mL.min^{-1}. The initial conditions were 0% B, maintained for 1 min, increased to 28% B at 22 min and subsequently to 40% B at 30 min and 100% B at 31 min, kept for 1 min before returning to the initial conditions after 1 min. The gradient was followed by 4 min isocratic wash at 0% B to re-equilibrate the column. The column temperature was maintained at 60°C. This 37 min chromatographic run was monitored by both PDA and MS detectors. The Acquity PDA detector (Waters) scanning range was set from 230 to 650 nm, with 1.2 nm bandwidth resolution and a sampling rate of 20 points/s.

For IMS analysis, travelling-wave IM spectrometry (TWIMS) was performed as previously reported (section 3.2.3.3).[29] Briefly, extraction cone 4 V, helium cell gas flow 180 mL/min, IM buffer gas (N_2) flow 110 mL/min, IM wave velocity 650 m/s and IM wave height 40 V. Polyalanine (PolyA) was used as calibrant to determine $^{TW}CCS_{N2}$ values from the measured arrival time distributions (ATD) in ESI$^-$ modes and was prepared in H_2O/MeOH (50:50, v:v) at a concentration of 277 mg/mL. Calibration was performed using singly charged PolyA oligomers (n = 3 to 14) covering a mass range 231 to 1012 Da and CCS values ranging from 150 to 308 Å^2 in ESI$^-$. For data acquisition and processing, MassLynx™ 4.1 and Driftscope 2.9 software (Waters) were utilised.

For MS detection, electrospray ionisation in negative or positive modes (ESI$^-$ or ESI$^+$) were used; optimised settings were presented elsewhere.[29] Briefly, the source conditions were: cone voltage 15 V, nitrogen (N_2) as desolvation gas and a desolvation temperature of 275°C and a flow rate of 650 L/h. Sodium formate was used for the calibration of the TOF-MS instrument and leucine enkaphalin was used as the lock mass to obtain accurate mass data. Data was acquired across a mass range of 150-1500 Da in resolution-mode at a rate of 0.2 scans/s. For compound

identification, MS^E mode was utilised, where data was acquired using two channels: at low collision energy (4 V) and with a collision energy ramped from 20 to 60 V (mass range 40-1500 Da) to obtain MS fragmentation data.

For the separation of anthocyanins, an acidic mobile phase comprising MilliQ water containing 7.5% formic acid (solvent A) and acetonitrile containing 7.5% formic acid (solvent B) was used,[29] with an Acquity BEH C18 column (2.1 mm × 100 mm, 1.7 µm particle size, Waters). The injection volume was 2 µL, the column oven temperature was maintained at 50°C and a flow rate of 0.20 $mL.min^{-1}$ was used. The initial conditions were 1% B maintained for 0.50 min, followed by an increase to 22% B at 20 min and 100% B at 20.10 min. These conditions were kept for 1.40 min before returning to the initial conditions after 10 s, followed by 3.4 min re-equilibration step. The total chromatographic run time was 25 min. The peaks were monitored at a wavelength range of 500-520 nm. MS detection was performed in ESI^+ using the settings outlined above.

4.2.3.5. Data processing and multivariate data analyses (MVDA)

UPLC-HR-MS raw data (converted to mzML format) were uploaded and analysed using the cloud-based informatics software XCMS Online (https://xcmsonline.scripps.edu). Briefly, the XCMS processing parameters were as follows: centWave for feature detection (with $\Delta m/z$ = 15 ppm, minimum peak width 10 s and maximum peak width 120 s), and obiwarp for retention time (t_R) correction. The chromatogram alignment parameters were: bw 10 s (allowable t_R deviations), minifrac 0.5 (minimum fraction of samples necessary in at least one of the sample groups for it to be a valid group) and *m/z* width of 0.25 (width of overlapping *m/z* slices to use for peak density chromatograms and grouping peaks across samples). To perform multivariate data analysis and for visualization, MetaboAnalyst 4.0 (www.metaboanalyst.ca) was used. The data were normalised using the sample median, transformed by log normalization and data scaling was performed using the pareto scaling algorithm. The statistical significance was calculated by ANOVA for multi-group comparisons. The distribution of each annotated metabolite (feature) was visualised using box-and-whiskers plots (boxplots). For pathway analyses in MetPA (Metabolomics Pathway Analysis), a list of selected metabolites were uploaded and processed using the '*Arabidopsis*' library, where algorithms 'GlobalAncova' and the 'Out-degree centrality' were selected for pathway enrichment analysis and for pathway topological analysis, respectively.[30]

4.2.3.6. Metabolite annotation

Compound annotation and identification was performed as previously discussed by Masike *et al*.[29] (sections 3.3.1 and 3.3.2). Briefly, MS^E fragmentation patterns, standards, surrogate

standards,[31] and online databases such as Dictionary of Natural Products (dnp.chemnetbase.com), KNApSAck (http://kanaya.naist.jp/knapsack), METLIN (http://metlin.scripps.edu) and ChemSpider (www.chemspider.com) were used. The level of identification used for the annotated compounds is indicated in Table S4.2 (Supplementary Information) as set out by the COSMOS Metabolomics Standards Initiative and indicated previously.[29]

4.3. Results and discussion

4.3.1. Metabolite identification by UPLC-PDA-IM-HR-MS

UPLC-PDA-HR-MS analysis was used to study the phytochemical composition of 37 distinct *Protea* genetic lines: 12 pure species, 10 selections and 15 hybrid cultivars. Figure 4.1 shows representative UPLC-MS chromatograms for five selected *Protea* pure species that showed overt chromatographic differences. We recently reported the characterization of the phenolic profiles of the leaf and involucral bract tissue of two *Protea* pure species and two hybrid cultivars (Chapter 3),[29] where 66 metabolites were identified (41 phenolic acid esters and 25 flavonoids, including five anthocyanins). The distribution of metabolites identified in the present work in pure species and hybrid cultivars (including species selections) are indicated in Tables 4.1 and 4.2, respectively. In addition to the 67 phenolic metabolites previously reported (66 identified (**9-17**, **19-21**, **23**, **24**, **26**, **30-35**, **37-40**, **42-44**, **46**, **51**, **53**, **54**, **59-65**, **67-93**), one unknown (**102**)), five organic acids (**1-5**), three sugars (**6-8**) and 22 prominent unknown compounds (**94-101**, **103-116**) were also included in the present work. Furthermore, several polyphenols not detected in our previous study (**18**, **22**, **25**, **27-29**, **36**, **41**, **45**, **47-50**, **52**, **55-58**, **66**) were tentatively identified and included in the dataset subjected to multivariate data analysis. Since this is not the focus of the present work, a detailed discussion on the identification of metabolites is not included; detailed chromatographic, UV-Vis, MS, and IMS data used for this purpose is however presented in Table S4.2 (Supplementary Information). To align the chromatograms and construct the data matrix, peaks were extracted from the converted data (mzML) using the cloud-based informatics software XCMS Online (https://xcmsonline.scripps.edu). The data matrix contained a total of 1733 aligned features. Features that did not correspond to molecular ions (i.e., formic acid adducts, dimers, fragment ions etc.) were removed, resulting in 116 annotated features. Multivariate data analyses were conducted using the MetaboAnalyst 4.0 tool.

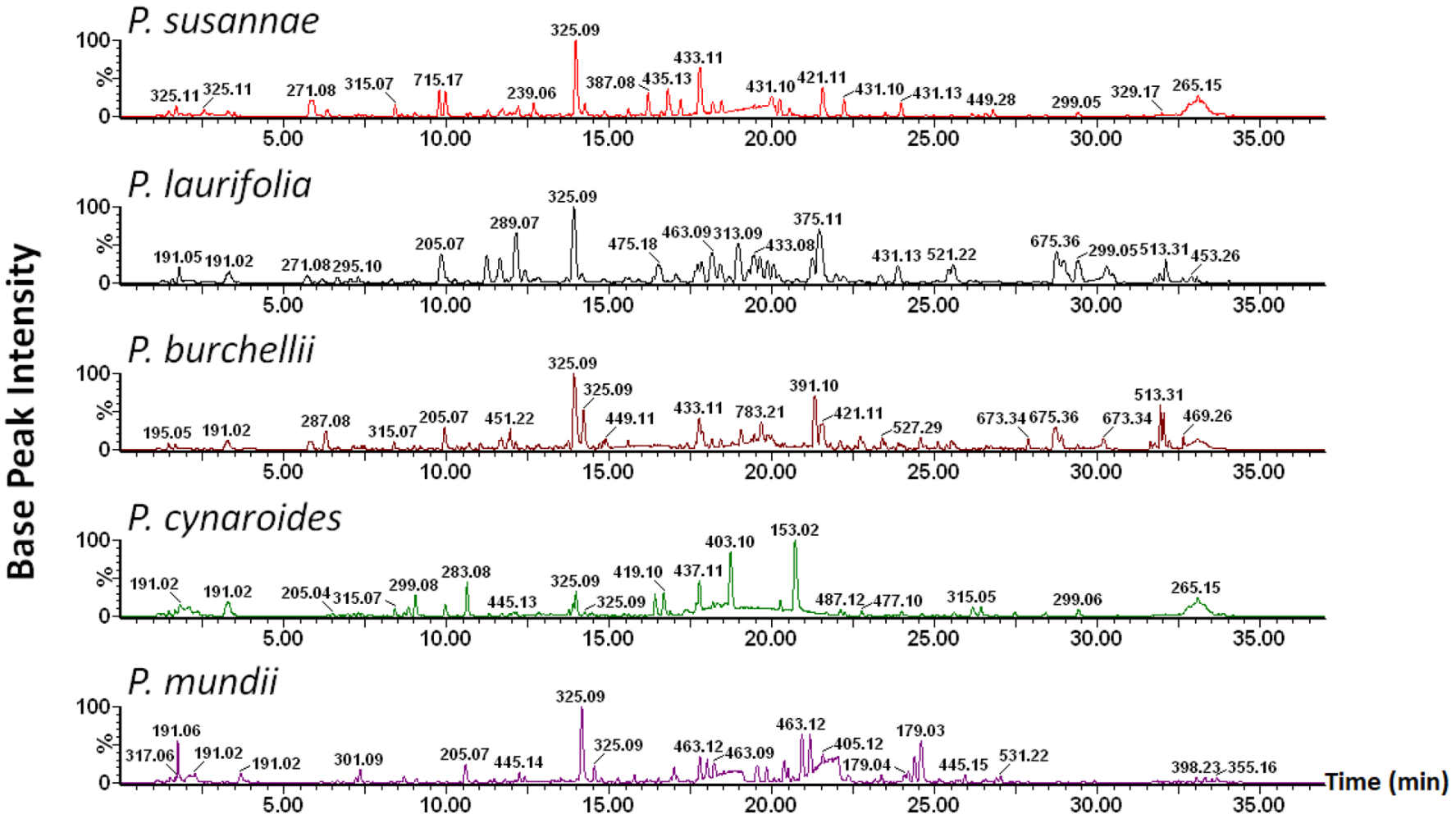

Figure 4.1: Stacked UPLC-HR-MS base peak intensity (BPI) chromatograms illustrating the different chromatographic profiles between extracts obtained from leaf tissues of *Protea susannae*, *P. laurifolia*, *P. burchellii*, *P. cynaroides* and *P. mundii*. Chromatograms were obtained using the 0.1% formic acid (FA), in the mobile phase, method mentioned in section 4.2.3.4.

Table 4.1: The distribution of 116 features in 12 *Protea* pure species.

Molecule number	Identified and Annotated metabolites	*m/z*	t_R (mins)	A	B	C	D	E	F	G	H	I	J	K	L
Organic and Sugar acids															
1	Gluconic acid	195.0505	1.58	√	√	√	√	√	√	√	√	√	√	√	√
2	Xylonic acid	165.0401	1.60	√	√	√	√	√	×	√	√	√	√	√	√
3	Quinic acid	191.0544	1.78	×	×	√	√	√	√	√	×	×	√	√	√
4	Isocitric acid	191.0201	2.15	√	√	×	√	√	√	√	√	√	√	√	√
5	Citric acid	191.0187	3.33	√	√	√	√	√	√	√	√	√	√	√	√
Sugars															
6	Hexose	179.0556	1.58	√	×	×	√	×	√	×	√	×	√	√	×
7	Hexoside-*O*-deoxy-hexose isomer 1	325.1135	1.94	√	√	√	√	√	×	√	√	√	√	√	√
8	Hexoside-*O*-deoxy-hexose isomer 2	325.1130	2.97	√	√	√	√	√	×	√	√	√	√	√	√
Phenolic acids															
9	Phlorin (benzene-1,3,5-triol)-*O*-hexoside)	287.0771	4.14	√	×	√	√	√	×	×	×	×	×	×	×
10	β-Arbutin (hydroquinone-*O*-hexoside) isomer	271.0794	5.71	√	√	√	√	√	×	√	×	×	×	√	×
11	α-Arbutin (hydroquinone-*O*-hexoside) isomer	271.0800	5.89	×	√	×	×	×	×	√	×	×	×	√	×
12	Hydroxyquinol (benzene-1,2,4-triol)-*O*-hexoside	287.0754	6.26	√	×	√	√	√	×	×	×	×	×	√	×
13	Protocatechuic alcohol (3,4-dihydroxybenzoyl alcohol)-*O*-hexoside isomer 1	301.0915	7.11	√	√	√	√	√	√	√	√	√	√	√	√
14	Protocatechuic alcohol-*O*-hexoside isomer 2	301.0904	7.23	√	√	√	√	√	√	√	√	√	√	√	√
15	Protocatechuic alcohol-*O*-hexoside isomer 3	301.0925	7.43	√	×	√	√	√	×	√	×	×	×	√	×
16	Protocatechuic acid (3,4-dihydroxybenzoic acid)-*O*-hexoside isomer 1	315.0803	8.32	√	√	√	√	√	×	√	√	√	√	√	√
17	Protocatechuic acid-O-hexoside isomer 2	315.0702	8.43	×	√	×	×	×	√	×	√	√	√	×	√
18	Piscidic acid	255.0505	8.49	√	√	×	×	×	×	×	×	×	×	×	×
19	Protocatechuic acid	153.0203	8.81	×	√	×	×	×	√	√	√	√	√	×	×
20	Vanillic acid (4-hydroxy-3-methoxybenzoic acid)-*O*-hexoside	329.0862	8.98	√	√	√	√	√	×	√	√	×	√	√	√
21	Protocatechuic acid-*O*-hexoside isomer 3	315.0702	9.39	√	√	×	√	√	×	√	√	√	√	√	√
22	*p*-Hydroxybenzoic acid-*O*-hexoside isomer 1	299.0761	9.48	×	×	×	×	×	×	×	√	×	×	×	√
23	Hydroxyquinol-*O*-hexoside-*O*-acetyl	329.0872	9.53	×	×	√	√	×	×	×	×	×	×	×	×
24	3-Caffeoyl-*O*-quinic acid	353.0873	10.01	√	√	×	√	√	×	√	×	×	×	×	√
25	Protocatechuic acid-*O*-rhamnoside isomer 1	299.0758	10.33	×	×	×	√	×	×	×	×	×	×	×	×
26	*p*-Hydroxybenzoic acid-*O*-deoxy-hexose isomer 1	283.0808	10.60	×	×	×	×	×	×	×	×	√	×	×	×
27	Protocatechuic acid-*O*-rhamnoside isomer 2	299.0770	10.65	√	√	√	√	√	√	√	√	√	√	√	×
28	*p*-Hydroxybenzoic acid-*O*-hexoside isomer 2	299.0773	11.19	×	×	×	√	×	×	×	√	×	×	×	×
29	Caffeoyl-*O*-hexoside	341.0869	11.50	√	√	√	√	×	×	×	×	√	×	√	√
30	3-*p*-Coumaroyl-*O*-quinic acid	337.0898	11.69	√	√	√	√	√	×	√	√	×	×	√	√
31	Feruloyl-*O*-hexoside isomer 1	355.1039	11.96	×	×	×	×	×	×	×	√	√	√	×	×
32	*p*-Hydroxybenzoic acid-*O*-deoxy-hexose isomer 2	283.0800	12.48	√	√	×	×	×	×	×	√	×	√	√	×
33	5-Caffeoyl-*O*-quinic acid	353.0862	12.54	×	√	×	×	×	×	×	×	×	×	×	×
34	3-Feruloyl-*O*-quinic acid	367.1043	12.83	√	√	√	√	√	×	√	√	×	×	×	√
35	Protocatechuic acid-*O*-hexoside-*O*-hydroxyquinol isomer 1	423.0989	13.34	×	×	√	√	×	×	×	×	×	×	√	×
36	Protocatechuic acid-*O*-arbutin isomer 1	407.0962	13.45	×	√	×	×	×	×	×	×	×	×	×	×
37	Feruloyl-*O*-hexoside isomer 2	355.1041	13.51	×	×	×	×	×	×	×	√	√	√	√	×
38	Protocatechuic acid-*O*-hexoside-*O*-hydroxyquinol isomer 2	423.0989	13.66	×	×	√	√	×	×	×	×	×	×	×	×
39	*p*-Hydroxybenzoic acid derivative	423.0923	13.89	√	√	√	√	×	√	√	√	√	√	√	√

40	Caffeoyl-*O*-polygalatol (1,5-anhydro-[6-*O*-caffeoyl]- sorbitol(glucitol)) isomer 1	325.0934	14.05	√	√	√	√	√	√	√	√	√	√	√	√
41	Protocatechuic acid-*O*-arbutin isomer 2	407.0978	14.12	×	√	×	×	×	×	×	×	×	×	√	×
42	Protocatechuic acid-*O*-hexoside-*O*-protocatechuic alcohol isomer 1	437.1074	14.25	×	√	√	×	×	×	×	√	×	×	×	×
43	Caffeoyl-*O*-polygalatol isomer 2	325.0911	14.42	√	√	√	√	√	√	×	×	×	×	×	×
44	Protocatechuic acid-*O*-hexoside-*O*-hydroxyquinol isomer 3	423.0923	14.64	×	×	√	√	×	×	×	×	×	×	√	×
45	*p*-Hydroxybenzoic acid-*O*-deoxy-hexose isomer 3	283.0818	14.65	×	×	×	×	×	×	×	×	×	×	×	×
46	5-*p*-Coumaroyl-*O*-quinic acid	337.0918	14.76	×	×	×	√	√	√	√	×	×	×	×	×
47	Protocatechuic acid-*O*-arbutin isomer 3	407.0981	14.79	√	√	×	√	×	×	×	×	×	×	√	×
48	Protocatechuic acid-*O*-hexoside-*O*-protocatechuic alcohol isomer 2	437.1083	14.99	×	×	×	×	×	√	×	×	×	×	×	×
49	Protocatechuic acid-*O*-arbutin isomer 4	407.0976	15.19	×	√	×	×	×	×	×	×	×	×	√	×
50	Protocatechuic acid derivative isomer 1	405.0823	17.03	√	√	×	√	×	×	×	×	×	×	√	×
51	*p*-Hydroxybenzoyl-*O*-arbutin isomer 1	391.1029	17.16	√	√	×	√	√	×	×	√	×	×	√	×
52	Hydroxyquinol-*O*-hexoside-*O*-acetyl derivative isomer 1	435.1288	17.37	×	×	√	√	√	×	×	×	×	×	×	×
53	*p*-Hydroxybenzoyl-*O*-arbutin isomer 2	391.1030	17.58	×	√	×	×	×	×	×	×	×	×	√	×
54	Protocatechuic acid-*O*-hexoside-*O*-protocatechuic alcohol isomer 3	437.1083	17.68	×	×	×	√	×	×	×	√	√	√	×	√
55	Caffeoyl-*O*-polygalatol-*O*-hydroxyquinol isomer 1	433.1136	17.76	√	√	√	√	√	×	√	×	×	×	×	×
56	Caffeoyl-*O*-polygalatol-*O*-hydroxyquinol isomer 2	433.1139	18.14	√	√	√	√	√	×	×	×	×	×	√	×
57	Hydroxyquinol-*O*-hexoside-*O*-acetyl derivative isomer 2	435.1278	18.71	×	×	√	√	√	×	×	×	×	×	×	×
58	Hydroxyquinol-*O*-hexoside-*O*-acetyl derivative isomer 3	435.1289	18.96	×	×	√	√	√	×	×	×	×	×	×	×
59	Benzoylhexoside of hydroxyquinol (benzoyl-*O*-hexoside-*O*-hydroxyquinol, previously referred to as neriifolin) isomer 1	391.1036	19.63	×	×	√	√	√	×	×	×	×	×	√	×
60	Hydroxyquinol-*O*-hexoside derivative isomer 1	405.1214	20.37	×	×	√	√	√	×	×	×	×	×	×	×
61	Lacticolorin/Pilorubrosin (benzoyl-*O*-hexoside-*O*-protocatechuic alcohol) isomer 1	405.1182	21.17	√	×	√	√	√	×	×	√	√	√	√	√
62	Benzoylhexoside of hydroxyquinol isomer 2	391.1034	21.29	√	×	√	×	×	×	×	×	×	×	√	×
63	Lacticolorin/Pilorubrosin isomer 2	405.1181	21.49	×	×	√	√	√	√	×	√	√	√	√	√
64	Eximin (6-*O*-benzoyl-*O*-arbutin) isomer 1	375.1069	21.51	√	√	√	×	×	×	×	×	×	×	√	×
65	Benzoylhexoside of hydroxyquinol isomer 3	391.1024	21.75	×	×	√	×	×	×	×	×	×	×	√	×
66	Eximin isomer 2	375.1080	22.05	×	√	×	×	×	×	×	×	×	×	×	×
67	Hydroxyquinol-*O*-hexoside derivative isomer 2	405.1192	22.08	×	×	√	√	√	×	×	×	×	×	×	×
68	Hydroxyquinol-*O*-hexoside derivative isomer 3	405.1193	22.54	√	×	√	√	√	×	×	×	×	×	×	√
Flavonoids															
69	B-type procyanidin	577.1327	11.25	√	×	√	×	√	×	×	×	×	×	×	×
70	(+)-Catechin	289.0714	12.17	√	×	√	×	√	×	×	×	×	×	×	√
71	Delphinidin-3-*O*-glucoside	465.1032	12.86	×	×	√	√	√	×	×	×	×	×	×	×
72	B-type procyanidin	577.1327	13.37	×	×	×	×	√	×	×	×	×	×	×	×
73	(-)-Epicatechin	289.0717	14.21	×	×	×	×	×	×	×	×	×	×	×	×
74	Cyanidin-3-*O*-glucoside	449.1084	14.91	√	√	√	√	√	×	×	√	√	×	×	×
75	Petunidin-3-*O*-glucoside	479.1181	16.42	×	×	√	√	√	×	×	×	×	×	×	×
76	Peonidin-*O*-hexoside	463.1230	17.64	×	×	×	×	×	×	×	×	×	×	×	×
77	Quercetin-*O*-hexoside-*O*-deoxy-hexose	609.1456	17.66	×	×	√	√	√	√	×	×	√	×	×	×
78	Rutin (quercetin-3-*O*-rutinoside (α-L-rhamnopyranosyl-(1→6)-β-D-glucopyranose))	609.1456	17.86	×	×	√	√	√	√	√	×	√	×	×	×
79	Quercetin-*O*-galactoside	463.0877	18.16	√	√	√	√	√	√	×	√	√	√	√	√
80	Malvidin-*O*-hexoside	493.1345	18.37	×	×	√	√	√	×	×	×	×	×	×	×

81	Isoquercitrin (Quercetin-3-*O*-glucoside)	463.0878	18.42	√	√	√	√	√	√	√	√	√	√	√	√
82	Kaempferol-*O*- hexoside-*O*-deoxy-hexose	593.1531	19.45	×	×	√	√	×	×	√	×	×	×	×	×
83	Quercetin-*O*-pentoside	433.0760	19.46	√	√	×	×	√	√	×	√	×	√	√	√
84	Isorhamnetin-*O*-hexoside-*O*-deoxy-hexose isomer 1	623.1597	19.63	×	×	×	×	√	×	×	√	×	×	×	×
85	Isorhamnetin-*O*-hexoside-*O*-deoxy-hexose isomer 2	623.1601	19.87	×	×	√	√	√	×	×	√	×	×	×	×
86	Kaempferol-*O*-glucoside	447.0920	20.20	√	×	√	√	√	√	√	×	×	×	×	√
87	Isorhamnetin-*O*-galactoside	477.1033	20.32	√	×	×	√	√	×	×	×	×	×	×	×
88	Quercetin-*O*-deoxy-hexose	447.0919	20.37	√	√	×	×	×	√	√	√	√	√	√	√
89	Isorhamnetin-*O*-glucoside	477.1033	20.67	√	×	√	√	√	×	×	×	×	×	×	×
90	Isorhamnetin-*O*-pentoside	447.0927	21.76	√	×	×	×	√	×	×	√	×	×	×	×
91	Kaempferol-*O*-deoxy-hexose	431.0978	22.37	√	√	×	×	√	√	×	√	√	√	√	√
92	Isorhamnetin	315.0503	26.17	×	×	×	×	×	×	×	×	×	×	×	×
93	Diosmetin	299.0557	29.40	√	√	√	√	√	×	√	√	√	√	√	×
Unknowns															
94	237_1.79	237.0595	1.79	√	√	√	√	√	√	√	√	√	√	√	√
95	317_1.83	317.0521	1.83	√	√	√	√	√	√	√	√	√	√	√	√
96	267_1.93	267.0717	1.93	√	√	√	√	√	√	√	√	√	√	√	√
97	209_1.95	209.0661	1.95	√	√	√	√	√	√	√	√	√	√	√	√
98	203_4.28	203.0191	4.28	√	√	√	√	×	×	√	√	√	√	×	×
99	329_6.66	329.0867	6.66	×	×	×	×	√	×	√	√	√	√	×	×
100	295_7.84	295.1036	7.84	√	√	√	√	√	√	√	√	√	√	√	√
101	417_8.09	417.1397	8.09	×	√	×	×	×	×	√	×	×	×	×	×
102	205_9.87	205.0711	9.87	√	√	√	√	√	√	×	√	√	√	√	√
103	451_12.62	451.2179	12.62	×	×	×	×	×	×	×	×	×	×	×	×
104	239_12.98	239.0548	12.98	√	√	×	×	×	×	×	×	×	×	×	×
105	487_13.22	487.1452	13.22	√	√	×	√	×	×	×	×	×	×	×	√
106	431_15.12	431.1917	15.12	√	√	×	×	×	×	×	×	×	×	×	√
107	465_15.73	465.1033	15.73	×	×	√	√	×	×	×	×	×	×	×	√
108	449_15.89	449.1096	15.89	×	√	√	√	×	×	×	×	×	×	√	×
109	399_16.18	399.1291	16.18	√	×	×	×	×	×	×	×	×	×	×	√
110	475_17.39	475.1811	17.39	×	×	√	√	√	×	×	×	×	×	×	×
111	337_17.42	337.0570	17.42	×	×	√	√	×	×	×	×	×	×	√	×
112	407_17.62	407.0978	17.62	×	×	√	√	√	×	×	×	×	×	√	×
113	449_18.01	449.1080	18.01	×	×	√	√	×	×	×	×	×	×	√	×
114	313_19.01	313.0919	19.01	×	×	×	√	√	×	×	×	×	×	×	×
115	313_19.32	313.0921	19.32	×	×	×	√	√	×	×	×	×	×	×	×
116	431_20.63	431.0978	20.63	√	√	×	√	×	×	√	×	×	×	√	×

A: *P. susannae*, **B**: *P. compacta*, **C**: *P. neriifolia*, **D**: *P. burchellii*, **E**: *P. laurifolia*, **F**: *P. mundii*, **G**: *P. repens*, **H**: *P. obtusifolia*, **I**: *P. cynaroides*, **J**: *P. grandiceps*, **K**: *P. cordata* and **L**: *P. nitida*

√= present

×= not detected

Table 4.2: The distribution of 116 features in 25 *Protea* species selections and cultivars.

Molecule number	Identified and Annotated metabolites	*m/z*	t_R (mins)	A	B	C	D	E	F	G	H	I	J	K	L	M	N	O	P	Q	R	S	T	U	V	W	X	Y
Organic and Sugar acids																												
1	Gluconic acid	195.0505	1.58	√	√	√	√	√	√	√	√	√	√	√	√	√	√	√	√	√	√	√	√	√	√	√	√	√
2	Xylonic acid	165.0401	1.60	√	√	√	√	√	√	√	√	√	√	√	√	√	√	√	√	√	√	√	√	√	√	√	√	√
3	Quinic acid	191.0544	1.78	√	√	√	√	√	√	√	√	√	√	√	√	√	√	√	√	√	×	√	×	√	×	×	√	√
4	Isocitric acid	191.0201	2.15	√	√	√	√	√	√	√	√	√	√	√	√	√	√	√	√	√	√	√	√	√	√	√	√	√
5	Citric acid	191.0187	3.33	√	√	√	√	√	√	√	√	√	√	√	√	√	√	√	√	√	√	√	√	√	√	√	√	√
Sugars																												
6	Hexose	179.0556	1.58	√	√	√	√	√	√	√	×	×	×	×	×	×	×	×	×	×	×	×	×	×	√	×	×	×
7	Hexoside-*O*-deoxy-hexose isomer 1	325.1135	1.94	√	√	√	√	√	√	√	√	√	√	√	√	√	√	√	√	√	√	√	√	√	√	√	√	√
8	Hexoside-*O*-deoxy-hexose isomer 2	325.1130	2.97	√	√	√	√	√	√	√	√	√	√	√	√	√	√	√	√	√	√	√	√	√	√	√	√	√
Phenolic acids																												
9	Phlorin (benzene-1,3,5-triol)-*O*-hexoside)	287.0771	4.14	×	×	×	×	×	×	×	×	×	×	×	×	×	×	×	√	×	×	×	×	×	×	×	×	×
10	β-Arbutin (hydroquinone-*O*-hexoside) isomer	271.0794	5.71	√	√	√	√	√	√	√	×	√	√	√	√	√	√	√	√	√	√	√	√	√	×	×	√	√	√
11	α-Arbutin (hydroquinone-*O*-hexoside) isomer	271.0800	5.89	×	√	×	×	×	×	×	×	×	√	√	×	×	×	×	×	×	×	×	√	×	×	×	√	√
12	Hydroxyquinol (benzene-1,2,4-triol)-*O*-hexoside	287.0754	6.26	√	√	√	√	√	√	√	×	×	√	√	√	×	×	×	√	√	√	√	√	√	√	√	×	√
13	Protocatechuic alcohol (3,4-dihydroxybenzoyl alcohol)-*O*-hexoside isomer 1	301.0915	7.11	√	√	√	√	×	×	×	×	√	√	×	√	√	√	√	√	×	√	√	√	√	×	√	√	√
14	Protocatechuic alcohol-*O*-hexoside isomer 2	301.0904	7.23	√	√	×	×	√	√	×	√	√	√	√	√	√	√	√	√	√	√	√	√	√	√	×	√	√	√
15	Protocatechuic alcohol-*O*-hexoside isomer 3	301.0925	7.43	√	√	√	√	√	√	×	×	√	√	×	√	√	√	√	√	√	√	√	√	√	√	×	√	×	×
16	Protocatechuic acid (3,4-dihydroxybenzoic acid)-*O*-hexoside isomer 1	315.0803	8.32	√	√	√	√	√	√	√	√	√	√	√	×	√	√	√	√	×	√	√	√	√	√	√	√	√	√
17	Protocatechuic acid-O-hexoside isomer 2	315.0702	8.43	√	√	√	√	×	×	×	×	×	×	×	×	×	×	×	×	×	×	×	×	×	×	×	×	×	×
18	Piscidic acid	255.0505	8.49	√	√	×	×	×	×	×	×	×	×	×	×	×	×	×	×	×	×	×	×	×	×	×	×	×	×
19	Protocatechuic acid	153.0203	8.81	×	×	×	×	×	×	×	√	×	×	×	×	×	×	×	×	×	×	×	×	×	×	×	×	×	×
20	Vanillic acid (4-hydroxy-3-methoxybenzoic acid)-*O*-hexoside	329.0862	8.98	√	√	√	√	√	√	√	√	√	√	√	√	√	√	√	√	√	√	√	√	√	√	√	√	√	√
21	Protocatechuic acid-*O*-hexoside isomer 3	315.0702	9.39	×	×	×	×	√	×	√	×	×	√	×	×	×	×	×	×	×	×	×	√	×	×	×	√	√	√
22	*p*-Hydroxybenzoic acid-*O*-hexoside isomer 1	299.0761	9.48	√	×	×	×	×	×	×	×	√	√	√	√	√	×	×	×	×	×	×	×	×	×	×	×	√
23	Hydroxyquinol-*O*-hexoside-*O*-acetyl	329.0872	9.53	√	×	×	×	×	×	×	×	×	×	×	×	×	×	×	√	×	×	×	×	√	√	×	×	×
24	3-Caffeoyl-*O*-quinic acid	353.0873	10.01	√	√	√	√	√	√	×	×	√	×	×	×	√	×	×	×	√	×	×	×	√	×	×	√	√
25	Protocatechuic acid-*O*-rhamnoside isomer 1	299.0758	10.33	×	×	×	×	×	×	×	×	×	×	×	√	√	×	×	×	×	×	×	×	×	×	×	×	√	×
26	*p*-Hydroxybenzoic acid-*O*-deoxy-hexose isomer 1	283.0808	10.60	√		×	×	×	×	×	×	×	×	×	×	×	×	×	×	√	×	×	×	×	×	×	×	×	×
27	Protocatechuic acid-*O*-rhamnoside isomer 2	299.0770	10.65	√	√	√	√	√	√	√	×	√	√	√	√	√	√	√	√	√	√	√	√	√	√	√	×	×	√
28	*p*-Hydroxybenzoic acid-*O*-hexoside isomer 2	299.0773	11.19	×	×	√	×	√	×	×	×	√	√	×	×	×	×	√	×	×	×	×	×	×	×	×	×	×	×
29	Caffeoyl-*O*-hexoside	341.0869	11.50	√	×	×	×	×	×	√	√	×	×	×	×	×	×	√	√	√	√	√	×	×	×	×	×	×	×
30	3-*p*-Coumaroyl-*O*-quinic acid	337.0898	11.69	√	√	√	√	√	√	√	×	√	√	√	√	√	√	√	√	√	√	√	√	√	√	√	√	√	√
31	Feruloyl-*O*-hexoside isomer 1	355.1039	11.96	×	×	×	×	×	×	×	×	×	×	×	×	×	×	×	×	×	×	×	×	×	×	×	×	×	×
32	*p*-Hydroxybenzoic acid-*O*-deoxy-hexose isomer 2	283.0800	12.48	√	√	√	√	√	√	×	×	×	√	√	√	√	√	√	×	√	√	√	√	×	×	√	√	√
33	5-Caffeoyl-*O*-quinic acid	353.0862	12.54	√	√	√	√	√	×	×	×	×	×	×	×	×	×	×	×	×	×	×	×	×	×	×	×	×	×
34	3-Feruloyl-*O*-quinic acid	367.1043	12.83		√	√	√	√	√	√	×	√	√	√	√	√	√	√	√	√	√	√	√	√	√	×	×	×	√	√
35	Protocatechuic acid-*O*-hexoside-*O*-hydroxyquinol isomer 1	423.0989	13.34	√	√	×	√	×	√	×	×	×	×	×	√	×	×	×	√	×	×	×	×	√	√	×	×	×

36	Protocatechuic acid-*O*-arbutin isomer 1	407.0962	13.45	×	×	×	√	×	×	×	×	×	×	×	×	×	×	×	×	×	×	×	×	×	×	×
37	Feruloyl-*O*-hexoside isomer 2	355.1041	13.51	×	×	×		×	×	×	×	×	×	×	×	×	×	×	×	×	×	×	×	×	×	×
38	Protocatechuic acid-*O*-hexoside-*O*-hydroxyquinol isomer 2	423.0989	13.66	×	×	×	√	×	×	×	×	×	×	×	×	×	×	×	×	√	×	×	×	×	×	×
39	*p*-hydroxybenzoic acid derivative	423.0923	13.89	×	×	√	×	√	√	√	√	√	√	√	√	√	√	√	√	√	√	√	×	×	√	√	√
40	Caffeoyl-*O*-polygalatol (1,5-anhydro-[6-*O*-caffeoyl]-sorbitol(glucitol)) isomer 1	325.0934	14.05	√	√	√	√	√	√	√	√	√	√	√	√	√	√	√	√	√	√	√	√	√	√	√	√
41	Protocatechuic acid-*O*-arbutin isomer 2	407.0978	14.12	×	×	×	×	×	×	×	×	×	×	×	×	×	×	×	×	×	×	×	×	×	×	×	×
42	Protocatechuic acid-*O*-hexoside-*O*-protocatechuic alcohol isomer 1	437.1074	14.25	√	×	×	√	×	×	×	×	×	×	×	×	×	×	×	×	√	×	×	×	×	×	×	×
43	Caffeoyl-*O*-polygalatol isomer 2	325.0911	14.42	√	√	√	√	√	√	√	×	×	×	×	√	×	√	√	√	√	√	√	√	√	√	×	×
44	Protocatechuic acid-*O*-hexoside-*O*-hydroxyquinol isomer 3	423.0923	14.64	√	√	√	√	√	√	×	×	×	×	×	√	×	×	×	√	×	×	×	×	√	√	×	×	×
45	*p*-Hydroxybenzoic acid-*O*-deoxy-hexose isomer 3	283.0818	14.65	√	×	×	×	×	×	×	×	×	×	×	×	×	×	×	×	×	×	×	×	×	×	×	×
46	5-*p*-Coumaroyl-*O*-quinic acid	337.0918	14.76	×	×	×	×	×	×	√	√	√	×	√	√	×	×	×	×	×	×	×	×	×	×	×	√	√
47	Protocatechuic acid-*O*-arbutin isomer 3	407.0981	14.79	√	√	√	√	√	√	√		√	√	√	√	√	√	√	√	√	√	√	√	√	√	√	√	√
48	Protocatechuic acid-*O*-hexoside-*O*-protocatechuic alcohol isomer 2	437.1083	14.99	√	×	×	×	×	×	×	√	×	×	×	×	×	×	×	×	×	×	×	×	×	×	×	×	×
49	Protocatechuic acid-*O*-arbutin isomer 4	407.0976	15.19	×	√	×	×	×	×	×	×	×	√	√	×	√	×	×	×	√	×	×	×	×	×	×	×	×
50	Protocatechuic acid derivative isomer 1	405.0823	17.03	√	√	√	√	√	√	√	√	×	√	√	√	√	√	√	√	√	×	√	√	√	√	√	√	√
51	*p*-Hydroxybenzoyl-*O*-arbutin isomer 1	391.1029	17.16	√	√	√	√	√	√	√	×	√	√	√	√	√	√	√	√	√	√	√	√	×	×	√	√	√
52	Hydroxyquinol-*O*-hexoside-*O*-acetyl derivative isomer 1	435.1288	17.37	×	×	√	√	√	√	×	×	×	×	×	×	×	×	×	√	×	×	√	×	×	×	×	×	×
53	*p*-Hydroxybenzoyl-*O*-arbutin isomer 2	391.1030	17.58	×	√	√	×	×	×	√	×	×	√	√	√	√	√	×	×	√	×	√	√	×	×	√	√	√
54	Protocatechuic acid-*O*-hexoside-*O*-protocatechuic alcohol isomer 3	437.1083	17.68	×	×	×	×	√	√	×	√	√	×	×	×	×	×	×	×	×	×	×	×	√	×	×	×	×	×
55	Caffeoyl-*O*-polygalatol-*O*-hydroxyquinol isomer 1	433.1136	17.76	√	√	√	√	√	√	√	×	√	√	√	√	√	√	√	√	√	√	√	√	√	√	√	√	√
56	Caffeoyl-*O*-polygalatol-*O*-hydroxyquinol isomer 2	433.1139	18.14	√	√	√	√	√	√	√	×	√	√	√	√	√	√	√	√	√	√	√	√	√	√	√	√	√
57	Hydroxyquinol-*O*-hexoside-*O*-acetyl derivative isomer 2	435.1278	18.71	×	×	×	×	×	×	×	×	×	×	×	×	×	×	×	√	×	√	×	×	√	√	×	×	×
58	Hydroxyquinol-*O*-hexoside-*O*-acetyl derivative isomer 3	435.1289	18.96	√	×	√	√	×	×	×	×	×	×	×	×	×	×	×	√	×	√	×	×	√	√	×	×	×
59	Benzoylhexoside of hydroxyquinol (benzoyl-*O*-hexoside-*O*-hydroxyquinol, previously referred to as neriifolin) isomer 1	391.1036	19.63	√	√	√	√	×	×	×	×	×	×	×	√	×	×	×	√	√	√	×	×	√	√	×	×	×
60	Hydroxyquinol-*O*-hexoside derivative isomer 1	405.1214	20.37	√	√	√	√	×	×	×	×	×	×	×	×	×	×	×	√	√	×	√	×	×	√	×	×	×
61	Lacticolorin/Pilorubrosin (benzoyl-*O*-hexoside-*O*-protocatechuic alcohol) isomer 1	405.1182	21.17	√	√	√	√	√	√	×	√	√	√	×	×	√	×	√	√	×	√	×	×	√	√	√	×	√
62	Benzoylhexoside of hydroxyquinol isomer 2	391.1034	21.29	√	√	√	√	√	√	×	×	×	×	×	×	×	×	√	√	√	√	×	×	√	√	√	×	×
63	Lacticolorin/Pilorubrosin isomer 2	405.1181	21.49	√	√	√	√	√	√	×	√	√	√	√	√	√	√	√	√	√	√	√	√	√	√	√	√	√
64	Eximin (6-*O*-benzoyl-*O*-arbutin) isomer 1	375.1069	21.51	√	√	√	√	√	√	×	×	×	×	×	×	√	√	√	√	√	√	√	√	√	√	√	×	×
65	Benzoylhexoside of hydroxyquinol isomer 3	391.1024	21.75	×	√	√	×	×	×	×	×	×	×	×	×	×	×	×	√	√	√	×	×	√	√	×	×	×
66	Eximin isomer 2	375.1080	22.05	×	√	√	×	×	×	×	×	×	×	√	√	√	×	×	×	×	×	√	√	×	×	√	√	√
67	Hydroxyquinol-*O*-hexoside derivative isomer 2	405.1192	22.08	√	√	√	√	×	×	×	×	×	×	×	√	×	×	×	√	×	√	×	×	√	√	×	×	×
68	Hydroxyquinol-*O*-hexoside derivative isomer 3	405.1193	22.54	×	×	×	×	×	√	×	×	√	×	×	√	√	√	√	√	√	×	√	√	√	√	√	√	√
Flavonoids																												
69	B-type procyanidin	577.1327	11.25	√	√	√	√	√	√	√	×	√	√	√	√	√	√	√	√	√	√	×	√	√	×	×	×	×	×

70	(+)-Catechin	289.0714	12.17	√	√	√	√	√	√	√	×	×	√	√	√	√	√	√	√	√	√	×	×	×	×	×	×	×
71	Delphinidin-3-*O*-glucoside	465.1032	12.86	×	×	√	×	×	×	×	×	×	×	×	√	√		√	√	√	√	×	×	×	×	×	×	×
72	B-type procyanidin	577.1327	13.37	×	×	√	×	×	×	×	×	×	×	×	×	×	×	×	×	×	×	×	×	×	×	×	×	×
73	(-)-Epicatechin	289.0717	14.21	×	×	√	×	×	×	×	×	×	×	×	×	×	×	×	×	×	×	×	×	×	×	×	×	×
74	Cyanidin-3-*O*-glucoside	449.1084	14.91	√	√	√	×	√	√	×	√	√	√	√	√	√	√	√	√	√	√	√	√	√	√	×	×	√	×
75	Petunidin-3-*O*-glucoside	479.1181	16.42	×	×	√	×	×	×	×	×	×	×	×	√	√	×	×	√	√	√	×	×	×	×	×	×	×	×
76	Peonidin-*O*-hexoside	463.1230	17.64	×	×	×	×	×	×	×	×	×	×	×	×	×	×	×	×	×	×	×	×	×	×	×	×	×	×
77	Quercetin-*O*-hexoside-*O*-deoxy-hexose	609.1456	17.66	√	√	√	√	√	√	√	√	√	√	√	√	√	√	√	√	√	√	√	√	√	√	×	√	√	√
78	Rutin (quercetin-3-*O*-rutinoside (α-L-rhamnopyranosyl-(1→6)-β-D-glucopyranose))	609.1456	17.86	√	√	√	√	√	√	√	√	√	√	√	√	√	√	√	√	√	√	√	√	√	√	√	√	√	√
79	Quercetin-*O*-galactoside	463.0877	18.16	√	√	√	√	√	√	√	×	√	√	√	√	√	√	√	√	√	√	√	√	√	√	√	√	√	√
80	Malvidin-*O*-hexoside	493.1345	18.37	×	×	√	×	×	×	×	×	×	×	×	√	√	×	×	×	×	√	×	×	×	×	×	×	×	×
81	Isoquercitrin (Quercetin-3-*O*-glucoside)	463.0878	18.42	√	√	√	√	√	√	√	×	√	√	√	√	√	√	√	√	√	√	√	√	√	√	√	√	√	√
82	Kaempferol-*O*- hexoside-*O*-deoxy-hexose	593.1531	19.45	×	×	×	√	×	×	×	√	√	√	√	√	√	√	√	√	√	√	√	√	√	√	√	√	×	×
83	Quercetin-*O*-pentoside	433.0760	19.46	√	√	√	×	√	√	√	√	√	√	√	√	√	√	√	√	×	×	√	√	√	×	×	√	√	√
84	Isorhamnetin-*O*-hexoside-*O*-deoxy-hexose isomer 1	623.1597	19.63	√	√	√	√	×	×	×	×	√	×	√	√	√	√	√	√	√	×	√	√	×	×	√	√	√	√
85	Isorhamnetin-*O*-hexoside-*O*-deoxy-hexose isomer 2	623.1601	19.87	√	√	√	√	×	×	×	×	√	×	√	√	√	√	√	√	√	√	√	√	√	√	√	√	√	√
86	Kaempferol-*O*-glucoside	447.0920	20.20	√	√	√	√	√	√	√	×	√	√	√	√	√	√	√	√	√	√	√	√	√	√	×	√	√	√
87	Isorhamnetin-*O*-galactoside	477.1033	20.32	√	√	×	√	√	√	√	×	√	×	√	√	√	√	×	×	√	×	×	√	√	×	×	×	√	√
88	Quercetin-*O*-deoxy-hexose	447.0919	20.37	√	√	×	×	√	√	√	√	√	√	√	×	×	×	×	×	×	×	×	√	√	√	×	×	×	×
89	Isorhamnetin-*O*-glucoside	477.1033	20.67	√	√	×	√	√	√	√	×	√	×	√	√	√	√	√	√	√	√	√	√	√	√	×	×	√	√
90	Isorhamnetin-*O*-pentoside	447.0927	21.76	√	√	√	×	√	√	√	×	√	×	√	√	√	√	√	√	√	×	√	√	×	×	√	√	√	√
91	Kaempferol-*O*-deoxy-hexose	431.0978	22.37	√	×	×	×	√	√	√	√	√	√	√	×	×	×	×	×	×	×	×	√	√	√	√	×	×	×
92	Isorhamnetin	315.0503	26.17	×	×	×	×	×	×	×	×	×	×	×	×	×	×	×	×	×	×	×	×	×	×	×	×	×	×
93	Diosmetin	299.0557	29.40	√	√	√	√	√	√	√	√	√	√	√	√	√	√	√	√	√	√	√	√	√	√	√	×	×	√	√
Unknowns																													
94	237_1.79	237.0595	1.79	×	×	×	×	×	×	×	×	×	×	×	×	×	×	×	×	×	×	×	×	×	×	×	×	√	√
95	317_1.83	317.0521	1.83	√	√	√	√	√	√	√	√	√	√	√	√	√	√	√	√	√	√	√	√	√	√	√	√	√	√
96	267_1.93	267.0717	1.93	√	√	√	√	√	√	√	√	√	√	√	√	√	√	√	√	√	√	√	√	√	√	√	√	√	√
97	209_1.95	209.0661	1.95	√	√	√	√	√	√	√	√	√	√	√	√	√	√	√	√	√	√	√	√	√	√	√	√	√	√
98	203_4.28	203.0191	4.28	×	×	√	√	√	√	√	√	×	×	×	×	×	×	×	√	√	√	√	√	√	×	√	√	×	
99	329_6.66	329.0867	6.66	×	×	√	×	×	×	√	√	√	√	×	√	√	√	√	√	√	√	×	×	×	×	×	×	×	
100	295_7.84	295.1036	7.84	√	√	√	√	√	√	√	√	√	√	√	√	√	√	√	√	√	√	√	√	√	×	√	√	√	
101	417_8.09	417.1397	8.09	×	×	√	×	×	×	√	×	√	×	√	√	√	×	×	√	×	×	√	×	×	×	×	√	√	
102	205_9.87	205.0711	9.87	√	√	√	√	√	√	√	√	√	√	√	√	√	√	√	√	√	√	√	√	√	√	√	√	√	
103	451_12.62	451.2179	12.62	√	√	×	×	√	√	×	×	×	√	√	×	×	×	√	√	√	√	√	√	√	√	√	×	×	
104	239_12.98	239.0548	12.98	√	√	×	×	√	×	√	×	×	√	√	×	×	×	×	×	×	×	×	√	√	×	×	×		
105	487_13.22	487.1452	13.22	√	√	×	×	×	×	×	√	√	√	√	√	√	√	√	√	√	√	√	√	√	√	×	√		
106	431_15.12	431.1917	15.12	×	√	×	√	√	√	×	×	×	√	√	×	×	×	√	√	√	√	√	×	√	√	√	×	×	
107	465_15.73	465.1033	15.73	×	√	×	×	×	×	×	×	×	×	×	×	×	×	×	√	×	×	×	×	√	√	×	×	√	
108	449_15.89	449.1096	15.89	√	√	√	√	√	√	√	×	×	×	×	×	×	×	√	√	√	√	√	√	√	×	√	×	×	
109	399_16.18	399.1291	16.18	×	×	×	×	×	×	√	×	×	×	×	×	×	×	×	×	×	×	×	×	×	×	×	√	√	
110	475_17.39	475.1811	17.39	√	√	√	√	×	×	√	×	√	√	√	√	√	√	√	√	√	√	√	√	√	√	√	√	√	
111	337_17.42	337.0570	17.42	×	√	×	√	√	×	×	×	×	×	×	×	×	×	×	×	×	×	×	×	×	×	×	√	√	

112	407_17.62	407.0978	17.62	×	×	×	×	×	×	×	×	×	×	×	×	×	×	×	√	×	×	×	×	×	×	√	√
113	449_18.01	449.1080	18.01	√	√	×	√	×	×	×	×	×	×	×	×	×	×	×	√	×	×	×	×	√	√	×	√	√
114	313_19.01	313.0919	19.01	√	√	√	√	×	×	×	×	√	×	×	√	√	√	√	√	√	√	√	×	√	√	√	√	√
115	313_19.32	313.0921	19.32	×	√	√	√	×	×	×	×	√	×	×	√	√	√	√	√	√	√	√	√	×	×	×	√	√	√
116	431_20.63	431.0978	20.63	√	√	√	√	√	√	√	×	×	√	√	√	√	√	√	√	√	√	√	√	√	×	√	√	√	√

A: 'Pink Ice', **B**: 'Carnival', **C**: 'Black Beauty', **D**: 'Limelight', **E**: 'Sylvia', **F**: 'Sharonette', **G**: 'Susara', **H**: 'Venus', **I**: 'Robyn', **J**: 'Brenda', **K**: 'Lady Di,' **L**: 'Niobe', **M**: 'Didi', **N**:'Sheila', **O**: 'Carli', **P**: 'Crinkle Cut', **Q**: 'Red Magic', **R**: 'Liamarie', **S**: 'Chelsea', **T**: 'Cerise', **U**: 'Suzanne', **V**: 'White Night', **W**: 'Maria', **X**: 'Barbigera' and **Y**: 'Ice Queen'

√**=** present

×= not detected

4.3.2. Multivariate data analyses (MVDA)

4.3.2.1. Pure Protea species

For the sake of simplicity, metabolite profiles of only the 12 *Protea* pure species, rather than the species selections and hybrid cultivars, were initially subjected to multivariate analysis. To uncover the major, as well as the subtle, differences and similarities (variance) between the 12 *Protea* pure species, a 2D principal component analysis (PCA) scores plot and hierarchical cluster analysis (HCA) dendrogram were generated (Figure 4.2A and 4.2B, respectively). The scores plot was constructed between Component 1 and Component 2, accounting for 51.6% of the variance of the data set. The HCA output using Pearson's distance metric is projected as a Ward's linkage dendrogram and outlines the clustering observed from the PCA model. From the scores plot (Figure 4.2A), three distinguishable groupings are evident: Group I made up of *P. neriifolia*, *P. burchellii* and *P. laurifolia*; Group II made up of *P. compacta*, *P. cordata*, *P. repens* and *P. susannae*; and Group III made up of *P. cynaroides*, *P. grandiceps*, *P. mundii*, *P. nitida* and *P. obtusifolia*. To identify the features responsible for the clustering patterns illustrated on the scores plot and dendrogram, a biplot was generated (Supplementary Information, Figure S4.2,). The biplot, based on the PCA, illustrates which features (shown as vector arrows specifying the accurate mass/retention time) are responsible for the differences in the spatial distribution observed in the PCA scores plot. A simplified biplot generated by removing features that do not contribute significantly to the variance explained by PC1 and PC2 is shown in Figure 4.3, and the distribution of the features associated with the PCA scores plot and the HCA dendrogram are tabulated in Table S4.3 (Supplementary Information).

The compounds associated with Group I are mostly benzenetriol derivatives, namely phlorin (benzene-1,3,5-triol)-*O*-hexoside) (**9**), hydroxyquinol (benzene-1,2,4-triol)-*O*-hexoside derivatives (**12**, **60**, **67**) and benzoylhexoside of hydroxyquinol (benzoyl-*O*-hexoside-*O*-hydroxyquinol, previously referred to as neriifolin) isomers (**59**, **62**, **65**). Benzenetriol derivatives have been noted to undergo oxidation reactions to produce black insoluble products.[32] Compounds associated with Group II were identified as the glycosylated hydroquinone (*p*-diphenol), arbutin (**10**) and its derivatives **51** and **53**. Hydroquinone derivatives are known to produce black insoluble polymers through a series of enzymatic and non-enzymatic reactions upon oxidation.[33]

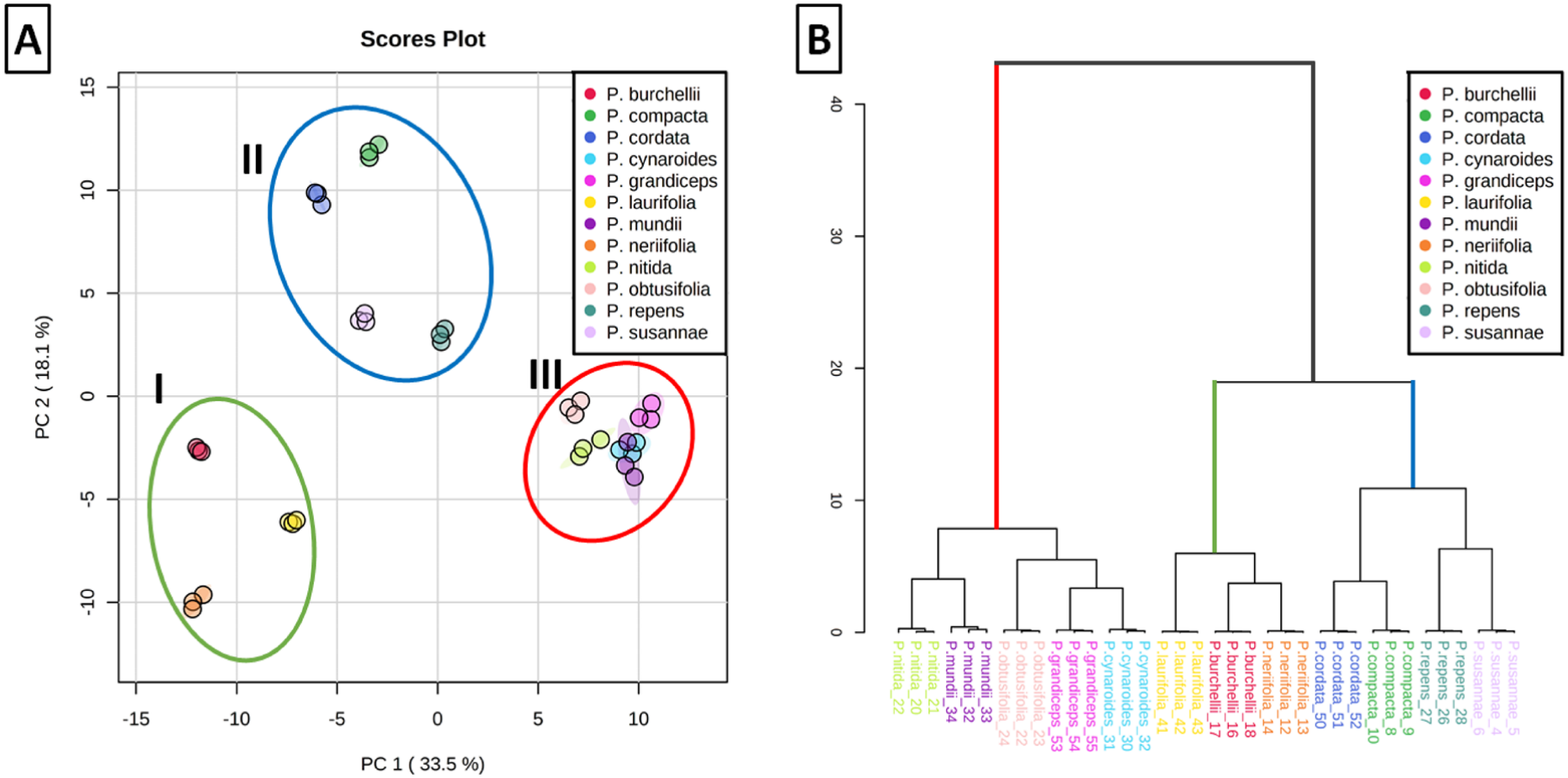

Figure 4.2: Principal component analysis (PCA) scores plot **(A)** and a hierarchical analysis component (HCA) dendrogram **(B)** showing the grouping of 12 pure *Protea* species based on metabolite data. The scores plot **(A)** and dendrogram **(B)** suggests that these species segregate into three groups. **Group I** (green circle) is made up of *P. burchellii*, *P. laurifolia* and *P. neriifolia*; **Group II** (blue circle) contains *P. susannae*, *P. compacta*, *P. cordata* and *P. repens*; and **Group III** (red circle) is made up of *P. mundii*, *P. nitida*, *P. grandiceps*, *P. cynaroides* and *P. obtusifolia*.

Recently, six novel arbutin-derived metabolites were identified in other Proteaceae members,[34] which were hypothesised to be potential markers for ancient Proteaceae species. Group III was associated with features characterised as organic acids (**1, 3-5**), protocatechuic alcohol derivatives (**14**, **54**, **61**), protocatechuic acid derivatives (**17**, **19**, **54**), vanillic acid-*O*-hexoside (**20**), *p*-hydroxybenzoic acid derivatives (**26, 39**), feruloyl-*O*-hexoside isomers (**31**, **37**) and flavonol derivatives (**79**, **86, 91**, **92**). The levels of the metabolites that are responsible for the clustering observed to produce Group III on the PCA scores plot (Figure 4.2A) are often enhanced in plants as a protective response against biotic and abiotic stressors.[35–41] The prominence of these protective metabolites in the species forming the cluster in Group III (such as *P. grandiceps* and *P. cynaroides*) might explain why these particular species are not particularly susceptible to blackening.

Previously, Proteaceae members not prone to blackening were noted to contain *C*-glycoside esters, like the diastereoisomers leucodrin and conocarpin, typically found in the species of the genera *Leucadendron* and *Leucospermum.*[42] These diastereoisomers which have been hypothesised to protect these species against blackening, were not detected in the *Protea* plant samples inspected in this study, nor were they reported in a previous study.[42]

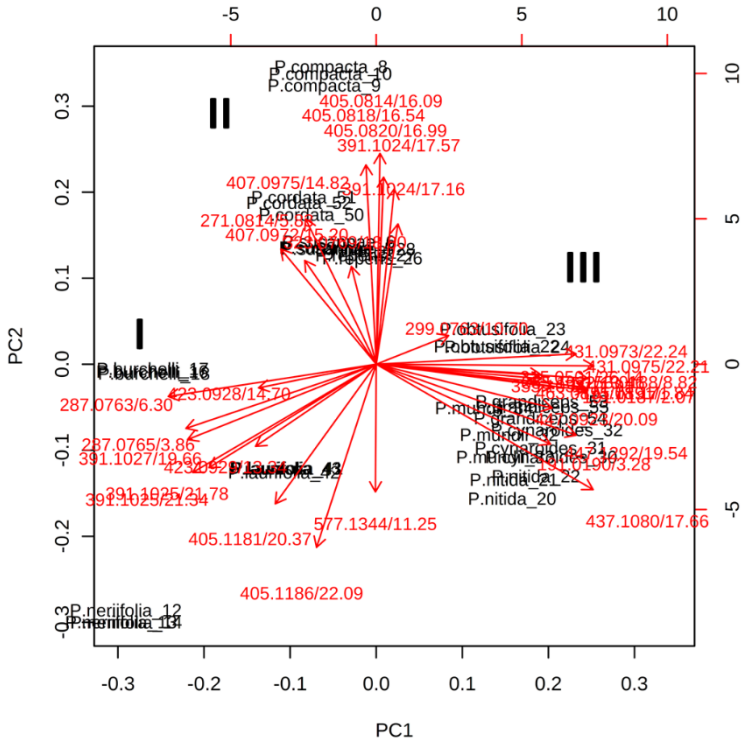

Figure 4.3: A simplified PCA biplot showing the potential biomarkers linked to the 12 *Protea* pure species comprising Group **I**, **II** and **III** in Figure 4.2. For a complete biplot, the reader is referred to Figure S4.2 in the Supplementary Information.

To visualize the above discussion, boxplots representing the three groupings were generated (Figure 4.4) to show how the selected metabolites from Table S4.3 (Supplementary Information) are distributed across the different species and how the levels of these metabolites contributed to the clustering patterns and hierarchical arrangements observed in Figure 4.2. This figure may provide insight into which metabolites may play a synergistic role in, or may serve as markers for, the susceptibility of some *Protea* species, selections and cultivars to leaf blackening.[10,17,43,44]

4.3.2.2. Protea cultivars

A vase life study was conducted using four *Protea* cultivars: 'Pink Ice' (*P. compacta* x *P. susannae*), 'Carnival' (*P. compacta* x *P. neriifolia*), 'Susara' (*P. susannae* x *P. magnifica*) and 'Sylvia' (*P. eximia* x *P. susannae*). The cultivars evaluated are considered to be susceptible to leaf blackening as they are derived from species with known susceptibility.[6–9] The leaves of *P. neriifolia* and *P. compacta* (among other species), for example, have been shown to blacken 3 to 7 days post-harvest.[45] *P. neriifolia* and *P. compacta* occurred in Groups I and II, respectively, in Figure 4.2, as such in this section 'Carnival', a hybrid of *P. neriifolia* and *P. compacta*, will be discussed as a representative example of the cultivars studied in the vase life study. The cultivars were studied to analyze metabolite differences over a three-week period in order to determine the biomarkers linked to leaf blackening. Sample differences are shown in the PCA scores plot (Figure S4.3, Supplementary Information), which confirm clear differentiation of metabolite profiles as a function of time.

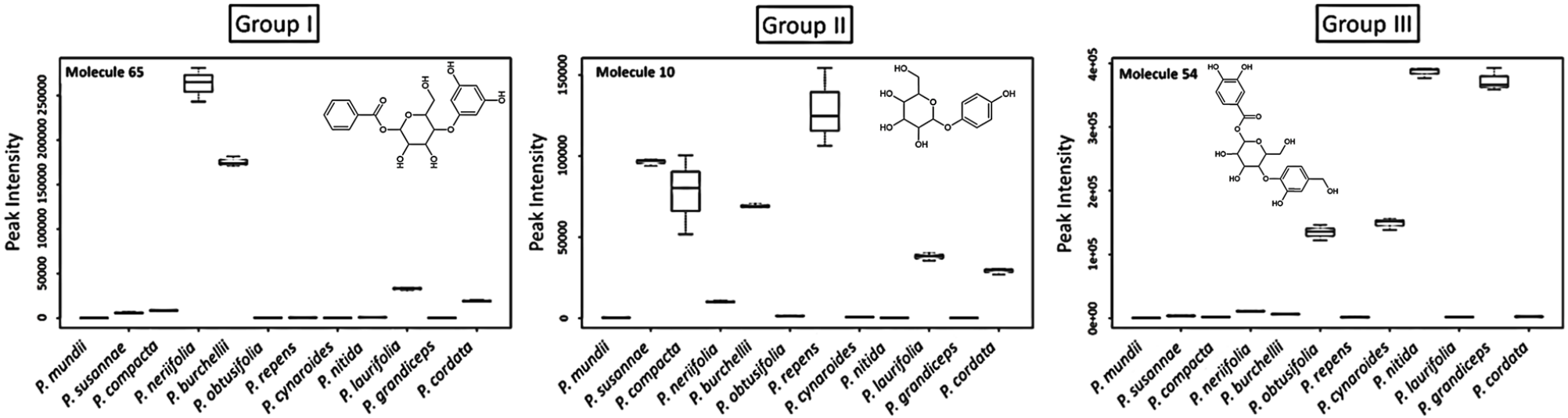

Figure 4.4: Boxplots showing the distribution of compounds **10**, **54** and **65** and how their peak intensities contributed to the clustering and hierarchical patterns observed for Groups **I**, **II** and **III** in Figure 4.2. Group **I** (*P. neriifolia, P. burchellii* and *P. laurifolia*) was characterized by metabolites derived from benzenetriol, such as **65** (benzoylhexoside of hydroxyquinol (benzoyl-*O*-hexoside-*O*-hydroxyquinol, previously referred to as neriifolin) isomer 3). Group **II** (*P. susannae, P. compacta, P. repens* and *P. cordata*) was characterised by hydroquinone derivatives such as **10** (arbutin (hydroquinone-*O*-hexoside)) and Group **III** (*P. mundii, P. obtusifolia, P. cynaroides, P. nitida* and *P. grandiceps)* by metabolites derived from protocatechuic acid such as **54** (protocatechuic acid-*O*-hexoside-*O*-protocatechuic alcohol isomer 2). All significant differences are based on ANOVA with $p \leq 0.01$.

For further analysis of the significant metabolites, a 'variable importance in projection' (VIP) plot was constructed for `Carnival' (Figure 4.5). The VIP plot for the other three cultivars ('Pink Ice', 'Susara' and 'Sylvia') are included in Figure S4.4 (Supplementary Information). The VIP plot summarizes the overall contribution of the features across all samples, allowing the selection of statistically important metabolites.[46] The VIP score of each feature is directly proportional to its significance: the higher the VIP score (≥ 1), the more significant a feature is in explaining differences between two or more treatments. The 30 most significant metabolites are shown in Figure 4.5. As expected, a decrease in metabolite levels over the three-week period was observed, suggesting a reduction in the overall phenolic content. However, an increase in metabolites such as organic acid derivatives (**1, 5**), sugars (**8**), hydroxycinnamic acid derivative (**24**), *p*-hydroxybenzoic acid derivatives (**26, 53**), protocatechuic acid derivatives (**50**), and unknowns of significant importance (**95**, **96**, **98**, **100**, **101**, **103**, **104**, **106**) were observed (Figure 4.5). Interestingly, most of these metabolites (**1, 24, 26, 50, 53**) were associated with Group III species with low susceptibility to leaf blackening in section 4.3.2.1, suggesting that a stress response triggers an increase in the production of these metabolites. Notably, this observation further suggests that the propensity to produce these stress response metabolites biologically at low levels is the possible cause for the susceptibility of some *Protea* species and cultivars to leaf blackening.

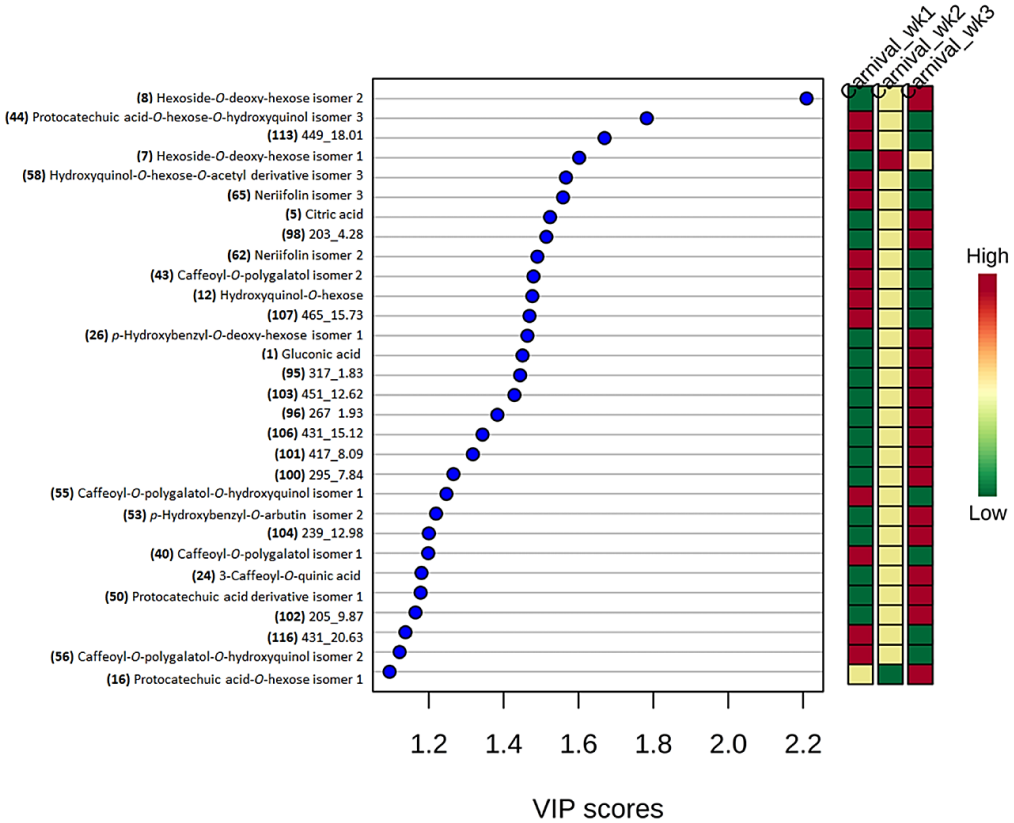

Figure 4.5: 'Variable importance in projection' (VIP) plot showing the 30 most statistically significant metabolites linked to the leaf tissue blackening of 'Carnival' (*P. compacta* x *P. neriifolia*) over a three week period.

4.3.2.3. Metabolic pathways affected by the onset of leaf blackening in 'Carnival'

The metabolome view of the progression of leaf blackening over a three-week period are summarised in Figure 4.6. Unlike most pathway analysis tools, Metaboanalyst, the online software used in the present work, integrates two analysis approaches: pathway (or metabolite set) enrichment analysis (shown on the y-axis) and pathway topology analysis (shown on the x-axis).[30] Pathway enrichment analysis identifies metabolic pathways that are affected as a result of significant perturbations to metabolite concentrations, due to a response to treatment.[30] Pathway topological analysis calculates the importance of the metabolite in a given metabolic network.[30] From Figure 4.6, we are able to visualise specific metabolic pathways that the uploaded list of metabolites matched, as well as gather the importance of the metabolite(s) in a given metabolic network. Based on the metabolomic pathway analysis, the matched metabolites primarily participated in the following pathways: 1) the pentose phosphate pathway, 2) fructose and mannose metabolism, 3) amino sugar and nucleoside sugar metabolism, 4) ascorbate and aldarate metabolism, 5) galactose metabolism, 6) the citrate (TCA) cycle, 7) glyoxylate and dicarboxylate metabolism, 8) starch and sucrose metabolism, 9) stilbenoid, diarylheptanoid and gingerol biosynthesis, 10) flavonoid biosynthesis, 11) phenylpropanoid biosynthesis, and 12) flavone and flavonol biosynthesis. The metabolic pathways most impacted (impact factor ≥ 0.1) were pathways 11 and 12 (larger circles), whereas pathways significantly affected (-log(*p*) ≥2.99) were pathways 1-4 (circles highlighted in a dark red shade), the majority of which are linked to the sugar metabolism. These results support the theory that the cause of blackening in *Protea* species, selections and cultivars is linked to a reduction in the carbohydrate content,[3,7,8,11–13] and might explain why sugar pulsing after harvesting is currently the most effective treatment to delay the onset of leaf blackening in susceptible species and cultivars.[4,5,8,47] The author acknowledge that the majority of the metabolites studied were phenolic compounds and this, thus, affects the resulting pathways enriched, the selection of extraction solvents is also biased towards certain compounds (i.e. pathways 11 and 12).

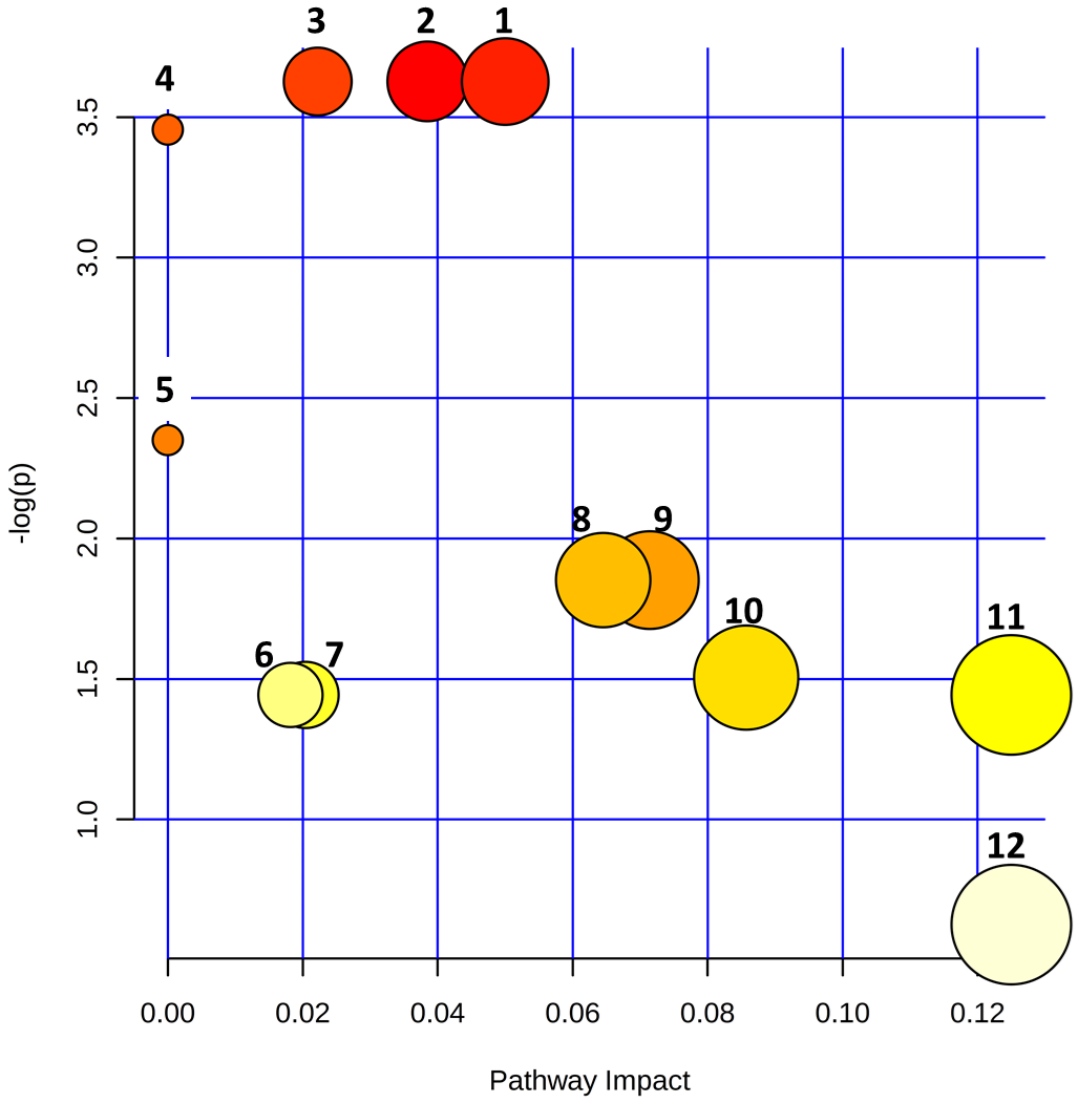

Figure 4.6: Summary of the pathway analysis showing the metabolic pathways arranged based on the scores from the enrichment analysis (y-axis) and from the topology analysis (x-axis). The colour of each circle is based on the *p*-value (-log(*p*) ≥2.99) and the size of the circle is based on the pathway impact value (impact factor ≥ 0.1). The darker colour (dark red) denotes the most affected pathway and the bigger the size of the circle the more significantly impacted the pathway is. Metabolic pathways affected or impacted during the leaf-blackening process include: **1**) the pentose phosphate pathway, **2**) fructose and mannose metabolism, **3**) amino sugar and nucleoside sugar metabolism, **4**) ascorbate and aldarate metabolism, **5**) galactose metabolism, **6**) the citrate (TCA) cycle, **7**) glyoxylate and dicarboxylate metabolism, **8**) starch and sucrose metabolism, **9**) stilbenoid, diarylheptanoid and gingerol biosynthesis, **10**) flavonoid biosynthesis, **11**) phenylpropanoid biosynthesis, and **12**) flavone and flavonol biosynthesis.

4.3.3. Anthocyanin distribution in *Protea* inflorescences

Protea species are acclaimed for their striking flowerheads, which contain pigments ranging from white, pink to red.[26] White and pale-yellow colours are associated with the presence of flavonols, while pink and red (as well as blue-purple) colours are indicative of the presence of anthocyanins (anthocyanidin-*O*-glycosides) in plants.[48,49] Until recently, the anthocyanin pigments responsible for *Protea* colours were undescribed;[50] we recently

characterised five anthocyanins present in two *Protea* species and two cultivars as delphinidin-*O*-hexoside (**71**), cyanidin-*O*-hexoside (**74**), petunidin-*O*-hexoside (**75**), peonidin-*O*-hexoside (**76**) and malvidin-*O*-hexoside (**80**) (Chapter 3).[29] In the present work, which involved a much larger sample set comprising pure species, selections and hybrids, the same five anthocyanins were detected. As summarised in Tables 4.1 and 4.2, cyanidin-*O*-hexoside (**74**) was found to be the most prevalent anthocyanin. This pigment was detected in 27 pink to red coloured flower-heads of the pure species (*P. susannae, P. compacta, P. neriifolia*, *P. burchellii*, *P. laurifolia*, *P. obtusifolia* and *P. cyanaroides*), as well as the selections ('Barbigera', 'Carli', 'Crinkle Cut', 'Red Magic', 'Liamarie', 'Chelsea' and 'Suzanne') and the cultivars ('Pink Ice', 'Carnival', 'Black Beauty', 'Sylvia', 'Sharonette', 'Venus', 'Robyn', 'Brenda', 'Lady Di', 'Niobe', 'Didi', 'Sheila' and 'Cerise'). Notably, the other four detected anthocyanins (**71**, **75**, **76** and **80**) were distributed only in pure species, selections and cultivars with black-bearded (tufted) flowerheads (*P. neriifolia, P. burchellii, P. laurifolia,* 'Black Beauty', 'Niobe', 'Didi', 'Carli', 'Crinkle Cut', 'Red Magic' and 'Liamarie', Figure S4.5, Supplementary Information). These plants all have pink to deep red coloured flowerheads, except for 'Niobe' which has a white/lime coloured flowerhead (Figure S4.5, Supplementary Information) suggesting the anthocyanins detected are expressed in the tufts of the flowerhead. Thus, the tufts were separated from the remaining parts of the involucral bracts and analysed, confirming that the five anthocyanins were present solely in the beards and not the bracts of the flowerheads (Figure S4.6, Supplementary Information). During flavonoid biosynthesis, precursors such as leuco-anthocyanins form part of the intermediates in the production of anthocyanins (or anthocyanidins).[51] Browning studies have hypothesised that the leaching out of leuco-anthocyanins from the *Protea* stems into the vase water is associated with the blockage of the xylem vessels, which causes water stress and may contribute to blackening.[28]

4.4. Conclusion

In conclusion, untargeted metabolomics guided tools were used in the present study to investigate differences in metabolite levels between *Protea* species, selections and cultivars. Our findings point to the levels of benzenetriol (**9**, **12**, **59**, **62**, **64**), anthocyanins (**71**, **74-76**, **80**) and/or hydroquinone (**10**, **51**, **53**) derivatives being linked to the susceptibility of *Proteas* to leaf blackening. On the other hand, organic acids (**1, 3-5**), protocatechuic alcohol derivatives (**14**, **54**, **61**), protocatechuic acid derivatives (**17**, **19**, **54**), vanillic acid-*O*-hexoside (**20**), *p*-hydroxybenzoic acid derivatives (**26**, **39**), feruloyl-*O*-hexoside isomers (**31**, **37**) and flavonol derivatives (**79**, **86**, **91**, **92**) were linked to the *Protea* species not prone to blackening. A vase life study indicated that these protective metabolites are released as a stress response during

the browning process in the susceptible cultivars. The innate production of these protective metabolites at lower levels in susceptible species and cultivars may be the reason for the manifestation of the blackening process upon stress. Our findings confirm that the progression of blackening impacts the sugar metabolism pathways, as has been previously reported.[3,7,8,11–13] Finally, metabolites that could be of phenotypic/physiological importance in the browning process were highlighted (notably the benzenetriol and hydroquinone derivatives **9**, **10**, **12**, **51**, **53**, **59**, **62**, **64**, **65**). These metabolites could be used as potential biomarkers of browning susceptibility in *Protea* species, selections and cultivars. Such observations serve as preliminary insights relevant to the development of new cultivars that are not/less susceptible to blackening.

4.5. References

(1) Ferreira, D. I. Prevention of browning of leaves of *Protea neriifolia* R. Br. *Acta Hortic.* **1982**, *XXI IHC 138*, 273–276. https://doi.org/10.17660/actahortic.1983.138.31.

(2) Windell, N. E. Leaf blackening and the control thereof in selected *Protea* species and cultivars. M. Sc. Agric. Thesis, Stellenbosch University, South Africa, **2012**, page 5.

(3) Bieleski, R. L.; Ripperda, J.; Newman, J. P.; Reid, M. S. Carbohydrate changes and leaf blackening in cut flower stems of *Protea eximia*. *J. Am. Soc. Hortic. Sci.* **1992**, *117*, 124–127. https://doi.org/10.21273/JASHS.117.1.124.

(4) McConchie, R.; Lang, N. S. Carbohydrate metabolism and possible mechanisms of leaf blackening in *Protea neriifolia* under dark postharvest conditions. *J. Am. Soc. Hortic. Sci.* **1993**, *118*, 355–361. https://doi.org/10.21273/JASHS.118.3.355.

(5) McConchie, R.; Lang, N. S. Postharvest leaf blackening and preharvest carbohydrate status in three *Protea* species. *HortScience* **1993**, *28*, 313–316. https://doi.org/10.21273/HORTSCI.28.4.313.

(6) Paull, R. E.; Dai, J. *Protea* postharvest black leaf a problem in search of a solution. *Acta Hortic.* **1990**, *264*, 93–102. https://doi.org/10.17660/ActaHortic.1990.264.11.

(7) Stephens, I. A.; Jacobs, G.; Holcroft, D. M. Glucose prevents leaf blackening in 'Sylvia' Proteas. *Postharvest Biol. Technol.* **2001**, *23*, 237–240. https://doi.org/10.1016/S0925-5214(01)00167-3.

(8) Stephens, I. A.; Meyer, C.; Holcroft, D. M.; Jacobs, G. Carbohydrates and postharvest leaf blackening of Proteas. *HortScience* **2005**, *40*, 181–184. https://doi.org/10.21273/hortsci.40.1.181.

(9) Windell, N. E.; Stephens, I. A.; Jacobs, G.; Hoffman, L. Effect of ethanol vapour on leaf blackening of selected *Protea* species. *Acta Hortic.* **2010**, *869*, 135–140.

(10) Hoffman, E. W.; Vardien, W.; Jacobs, G.; Windell, N. E. Leaf blackening: A serious impediment to long-term cold storage, transport, and extended vase life in *Protea* cut flowers. *Hortic. Rev*. **2018**, *45*, 73–104. https://doi.org/10.1002/9781119431077.ch3.

(11) Reid, M. S.; Doorn, W.; Newman, J. P. Leaf blackening in Proteas. *Acta Hortic.* **1988**, *261*, 81–84. https://doi.org/10.17660/ActaHortic.1989.261.9.

(12) McConchie, R.; Lang, N. S.; Gross, K. C. Carbohydrate depletion and leaf blackening in *Protea neriljiolia*. *J. Am. Soc. Hortic. Sci.* **1991**, *116*, 1019–1024. https://doi.org/10.21273/JASHS.116.6.1019.

(13) Dai, J.; Paull, R. E. Source-sink relationship and *Protea* postharvest leaf blackening. *J. Am. Soc. Hortic. Sci.* **1995**, *120*, 475–480. https://doi.org/10.21273/JASHS.120.3.475.

(14) Whitehead, C. S.; de Swardt, G. H. Extraction and activity of polyphenoloxidase and peroxidase from senescing leaves of *Protea neriifolia*. *S. Afr. J. Bot.* **1982**, *1*, 127–130. https://doi.org/10.1016/S0022-4618(16)30161-9.

(15) Dai, J.; Paull, R. E. Comparison of leaf susceptibility to enzymatic blackening in *Protea neriifolia* R. Br. and *Leucospermum* "Rachel". *Postharvest Biol. Technol.* **1997**, *11*, 101–106. https://doi.org/10.1016/S0925-5214(97)01418-X.

(16) Hernández, M.; Álvarez, C. E.; Fernández-Falcón, M.; Fernández-García, N.; Olmos, E. Ascorbic acid antioxidant activity against leaf blackening of *Protea*. *Acta Hortic.* **2012**, *1031*, 135–140. https://doi.org/10.17660/ActaHortic.2014.1031.15.

(17) McConchie, R.; Lang, N. S.; Lax, A. R.; Lang, G. A. Reexamining polyphenol oxidase, peroxidase, and leaf-blackening activity in *Protea*. *J. Am. Soc. Hortic. Sci.* **1994**, *119*, 1248–1254. https://doi.org/10.21273/jashs.119.6.1248.

(18) De Vos, R. C. H.; Moco, S.; Lommen, A.; Keurentjes, J. J. B.; Bino, R. J.; Hall, R. D. Untargeted large-scale plant metabolomics using liquid chromatography coupled to mass spectrometry. *Nat. Protoc.* **2007**, *2*, 778–791. https://doi.org/10.1038/nprot.2007.95.

(19) Keurentjes, J. J. B.; Fu, J.; De Vos, C. H. R.; Lommen, A.; Hall, R. D.; Bino, R. J.; Van Der Plas, L. H. W.; Jansen, R. C.; Vreugdenhil, D.; Koornneef, M. The genetics of plant metabolism. *Nat. Genet.* **2006**, *38*, 842–849. https://doi.org/10.1038/ng1815.

(20) Zeiss, D.; Mhlongo, M.; Tugizimana, F.; Steenkamp, P.; Dubery, I. Comparative metabolic phenotyping of tomato (*Solanum lycopersicum*) for the identification of metabolic signatures in cultivars differing in resistance to *Ralstonia solanacearum*. *Int. J. Mol. Sci.* **2018**, *19*, 1–17. https://doi.org/10.3390/ijms19092558.

(21) Kumar, R.; Bohra, A.; Pandey, A. K.; Pandey, M. K.; Kumar, A. Metabolomics for plant improvement: Status and prospects. *Front. Plant Sci.* **2017**, *8*, 1–27. https://doi.org/10.3389/fpls.2017.01302.

(22) García, C. J.; García-Villalba, R.; Gil, M. I.; Tomas-Barberan, F. A. LC-MS untargeted metabolomics to explain the signal metabolites inducing browning in fresh-cut lettuce. *J. Agric. Food Chem.* **2017**, *65*, 4526–4535. https://doi.org/10.1021/acs.jafc.7b01667.

(23) Mareya, C. R.; Tugizimana, F.; Piater, L. A.; Madala, N. E.; Steenkamp, P. A.; Dubery,

I. A. Untargeted metabolomics reveal defensome-related metabolic reprogramming in *Sorghum bicolor* against infection by *Burkholderia andropogonis*. *Metabolites* **2019**, *9*, 1–23. https://doi.org/10.3390/metabo9010008.

(24) Cuthbertson, D.; Andrews, P. K.; Reganold, J. P.; Davies, N. M.; Lange, B. M. Utility of metabolomics toward assessing the metabolic basis of quality traits in apple fruit with an emphasis on antioxidants. *J. Agric. Food Chem.* **2012**, *60*, 8552–8560. https://doi.org/10.1021/jf3031088.

(25) Hatoum, D.; Annaratone, C.; Hertog, M. L. A. T. M.; Geeraerd, A. H.; Nicolai, B. M. Targeted metabolomics study of “Braeburn” apples during long-term storage. *Postharvest Biol. Technol.* **2014**, *96*, 33–41. https://doi.org/10.1016/j.postharvbio.2014.05.004.

(26) Malan, G. *Protea Cultivation: From Concept to Carton*, 1st ed.; Sun MeDIA publishers, Stellenbosch, **2012**.

(27) Reid, M. S.; Kofranek, A. M. Recommendations for standardized vase life evaluations. *Acta Hortic.* **1981**, *113*, 171–173. https://doi.org/10.17660/ActaHortic.1981.113.25.

(28) De Swardt, G. H.; Pretorius, J.; Burger, L. The browning of foliage leaves in Proteas-A review. *Protea News* **1987**, *6*, 4–9.

(29) Masike, K.; De Villiers, A.; Hoffman, E. W.; Brand, D. J.; Causon, T.; Stander, M. A. Detailed phenolic characterization of *Protea* pure and hybrid cultivars by liquid chromatography-ion mobility-high resolution mass spectrometry (LC-IM-HR-MS). *J. Agric. Food Chem.* **2020**, *68*, 485–502. https://doi.org/10.1021/acs.jafc.9b06361.

(30) Xia, J.; Wishart, D. S. Web-based inference of biological patterns, functions and pathways from metabolomic data using Metaboanalyst. *Nat. Protoc.* **2011**, *6*, 743–760. https://doi.org/10.1038/nprot.2011.319.

(31) Clifford, M. N.; Madala, N. E. Surrogate standards: A cost-effective strategy for identification of phytochemicals. *J. Agric. Food Chem.* **2017**, *65*, 3589–3590. https://doi.org/10.1021/acs.jafc.7b01588.

(32) Fiege, H.; Voges, H.-W.; Hamamoto, T.; Umemura, S.; Iwata, T.; Miki, H.; Fujita, Y.; Buysch, H.-J.; Garbe, D.; Paulus, W. Phenol derivatives. In *Ullmann’s Encyclopedia of Industrial Chemistry*; Wiley-VCH Verlag GmbH & Co. KGaA: Weinheim, Germany, **2000**, pp 503–519. https://doi.org/10.1002/14356007.a19_313.

(33) Walker, J. R. L.; Ferrar, P. H. Diphenol oxidases, enzyme-catalysed browning and plant

disease resistance. *Biotechnol. Genet. Eng. Rev.* **1998**, *15*, 457–498. https://doi.org/10.1080/02648725.1998.10647966.

(34) Deans, B. J.; Kilah, N. L.; Jordan, G. J.; Bissember, A. C.; Smith, J. A. Arbutin derivatives isolated from ancient Proteaceae: Potential phytochemical markers present in *Bellendena*, *Cenarrhenes*, and *Persoonia* Genera. *J. Nat. Prod.* **2018**, *81*, 1241–1251. https://doi.org/10.1021/acs.jnatprod.7b01038.

(35) Parrott, D. L.; Anderson, A. J.; Carman, J. G. Agrobacterium induces plant cell death in wheat (*Triticum aestivum* L.). *Physiol. Mol. Plant Pathol.* **2002**, *60*, 59–69. https://doi.org/10.1006/pmpp.2002.0378.

(36) Ryan, K. G.; Markham, K. R.; Bloor, S. J.; Bradley, J. M.; Mitchell, K. A.; Jordan, B. R. UVB radiation induced increase in quercetin:kaempferol ratio in wild-type and transgenic lines of *Petunia*. *Photochem. Photobiol.* **1998**, *68*, 323–330. https://doi.org/10.1111/j.1751-1097.1998.tb09689.x.

(37) Vasquez-Robinet, C.; Mane, S. P.; Ulanov, A. V.; Watkinson, J. I.; Stromberg, V. K.; De Koeyer, D.; Schafleitner, R.; Willmot, D. B.; Bonierbale, M.; Bohnert, H. J.; Grene, R. Physiological and molecular adaptations to drought in Andean potato genotypes. *J. Exp. Bot.* **2008**, *59*, 2109–2123. https://doi.org/10.1093/jxb/ern073.

(38) Agati, G.; Biricolti, S.; Guidi, L.; Ferrini, F.; Fini, A.; Tattini, M. The biosynthesis of flavonoids is enhanced similarly by UV radiation and root zone salinity in *L. vulgare* leaves. *J. Plant Physiol.* **2011**, *168*, 204–212. https://doi.org/10.1016/j.jplph.2010.07.016.

(39) Quan, N. T.; Anh, L. H.; Khang, D. T.; Tuyen, P. T.; Toan, N. P.; Minh, T. N.; The Minh, L.; Bach, D. T.; Thu Ha, P. T.; Elzaawely, A. A.; Khanh, T. D.; Trung, K. H.; Xuan, T. D. Involvement of secondary metabolites in response to drought stress of rice (*Oryza sativa* L.). *Agriculture* **2016**, *6*, 1–14. https://doi.org/10.3390/agriculture6020023.

(40) Quan, N. T.; Xuan, T. D. Foliar application of vanillic and *p*-hydroxybenzoic acids enhanced drought tolerance and formation of phytoalexin momilactones in rice. *Arch. Agron. Soil Sci.* **2018**, *64* (13), 1831–1846. https://doi.org/10.1080/03650340.2018.1463520.

(41) Xuan, T. D.; Khang, D. T. Effects of exogenous application of protocatechuic acid and vanillic acid to chlorophylls, phenolics and antioxidant enzymes of rice (*Oryza sativa* L.) in submergence. *Molecules* **2018**, *23*, 1–14. https://doi.org/10.3390/molecules23030620.

(42) Perold, G. W. Consistency and variation in metabolite patterns of South African Proteaceae: A chemical perspective. *S. Afr. J. Sci.* **1993**, *89*, 90–93.

(43) Van Doorn, W. G. Leaf blackening in *Protea* flowers: Recent developments. *Acta Hortic.* **2001**, *545*, 197–204. https://doi.org/10.17660/ActaHortic.2001.545.27.

(44) Hoffman, E. W.; Windell, N. E.; Jacobs, G. Optimum time of harvest for the control of leaf blackening in *Protea* "Sylvia". *Acta Hortic.* **2012**, *1031*, 125–133. https://doi.org/10.17660/ActaHortic.2014.1031.14.

(45) Crick, S. G.; McConchie, R. Ethanol vapour reduces leaf blackening in cut flower *Protea* "Pink Ice" stems. *Postharvest Biol. Technol.* **1999**, *17*, 227–231. https://doi.org/10.1016/S0925-5214(99)00049-6.

(46) Trivedi, K., D.; Iles, K., R. The application of SIMCA P+ in shotgun metabolomics analysis of ZIC® HILIC-MS spectra of human urine-experience with the Shimadzu IT-TOF and Profiling Solutions data extraction software. *J. Chromatogr. Sep. Tech.* **2012**, *3*, 1–5. https://doi.org/10.4172/2157-7064.1000145.

(47) Jones, R. B. Understanding and controlling leaf blackening in *Protea* leaves: The use of high concentrations of sucrose. In *Proc. Int. Protea Assoc. 6th Biennial Conf., Perth, Western Australia*; 1991; pp 313–322.

(48) Castañeda-Ovando, A.; Pacheco-Hernández, M. de L.; Páez-Hernández, M. E.; Rodríguez, J. A.; Galán-Vidal, C. A. Chemical studies of anthocyanins: A Review. *Food Chem.* **2009**, *113*, 859–871. https://doi.org/10.1016/j.foodchem.2008.09.001.

(49) Tanaka, Y.; Sasaki, N.; Ohmiya, A. Biosynthesis of plant pigments: Anthocyanins, betalains and carotenoids. *Plant J.* **2008**, *54* (4), 733–749. https://doi.org/10.1111/j.1365-313X.2008.03447.x.

(50) Carlson, J. E.; Holsinger, K. E. Extrapolating from local ecological processes to genus-wide patterns in colour polymorphism in South African *Protea*. *Proc. R. Soc. B Biol. Sci.* **2015**, *282*, 1–10. https://doi.org/10.1098/rspb.2015.0583.

(51) Heller, W.; Britsch, L.; Forkmann, G.; Grisebach, H. Leucoanthocyanidins as intermediates in anthocyanidin biosynthesis in flowers of *Matthiola incana* R. Br. *Planta* **1985**, *163*, 191–196. https://doi.org/10.1007/BF00393505.

Supplementary information for: Application of Metabolomics Tools to Determine Possible Biomarker Metabolites Linked to Leaf Blackening in *Protea*

Table S4.1: List of *Protea* species, cultivars and selections obtained from different suppliers and grown in different locations and under different conditions.

Plant name	Plant type	Supplier	Locality	Growing conditions
P. susannae	Pure species	Harold Porter National Botanical Garden	34°21′06″S 18°55′37″E	Wild population conditions
P. compacta	Pure species	Harold Porter National Botanical Garden	34°21′06″S 18°55′37″E	Wild population conditions
P. neriifolia	Pure species	Harold Porter National Botanical Garden	34°21′06″S 18°55′37″E	Wild population conditions
P. burchellii	Pure species	Harold Porter National Botanical Garden	34°21′06″S 18°55′37″E	Wild population conditions
P. obtusifolia	Pure species	Harold Porter National Botanical Garden	34°21′06″S 18°55′37″E	Wild population conditions
P. repens	Pure species	Harold Porter National Botanical Garden	34°21′06″S 18°55′37″E	Wild population conditions
P. cynaroides	Pure species	Harold Porter National Botanical Garden	34°21′06″S 18°55′37″E	Wild population conditions
P. nitida	Pure species	Berghoff-fynbos farm	33°00′S 18°59′E	Standard cultivation practices
P. grandiceps	Pure species	Berghoff-fynbos farm	33°00′S 18°59′E	Standard cultivation practices
P. laurifolia	Pure species	Berghoff-fynbos farm	33°00′S 18°59′E	Standard cultivation practices
P. cordata	Pure species	Berghoff-fynbos farm	33°00′S 18°59′E	Standard cultivation practices
‘Barbigera’ (*P. magnifica* selection)	Selection	Berghoff-fynbos farm	33°00′S 18°59′E	Standard cultivation practices
‘Ice Queen’ (*P. magnifica* selection)	Selection	Berghoff-fynbos farm	33°00′S 18°59′E	Standard cultivation practices
‘Venus’ (*P. repens* x *P. aristata*)	Cultivars	Berghoff-fynbos farm	33°00′S 18°59′E	Standard cultivation practices
‘Brenda’ (*P. compacta* x *P. burchellii*)	Cultivars	Berghoff-fynbos farm	33°00′S 18°59′E	Standard cultivation practices
‘Cerise’ (*P. magnifica* x *P. obtusifolia*)	Cultivars	Berghoff-fynbos farm	33°00′S 18°59′E	Standard cultivation practices
‘Robyn’ (*P. glabra* x *P. laurifolia*)	Cultivars	Berghoff-fynbos farm	33°00′S 18°59′E	Standard cultivation practices
‘Liamarie’ (*P. magnifica* selection)	Selection	Berghoff-fynbos farm	33°00′S 18°59′E	Standard cultivation practices
‘Red Magic’ (*P. magnifica* selection)	Selection	Berghoff-fynbos farm	33°00′S 18°59′E	Standard cultivation practices
‘Suzanne’ (*P. magnifica* selection)	Selection	Berghoff-fynbos farm	33°00′S 18°59′E	Standard cultivation practices
‘Lady Di’ (*P. compacta* x *P. magnifica*)	Cultivars	Berghoff-fynbos farm	33°00′S 18°59′E	Standard cultivation practices
‘Chelsea’ (*P. magnifica* selection)	Selection	Berghoff-fynbos farm	33°00′S 18°59′E	Standard cultivation practices
‘Crinkle Cut’ (*P. magnifica* selection)	Selection	Berghoff-fynbos farm	33°00′S 18°59′E	Standard cultivation practices
‘Niobe’ (*P. laurifolia* x *P. magnifica*)	Cultivars	Berghoff-fynbos farm	33°00′S 18°59′E	Standard cultivation practices
‘Maria’ (*P. magnifica* selection)	Selection	Berghoff-fynbos farm	33°00′S 18°59′E	Standard cultivation practices
‘Didi’ (*P. laurifolia* x *P. magnifica*)	Cultivars	Berghoff-fynbos farm	33°00′S 18°59′E	Standard cultivation practices
‘Sheila’ (*P. magnifica* x *P. burchellii*)	Cultivars	Berghoff-fynbos farm	33°00′S 18°59′E	Standard cultivation practices
‘White Night’ (*P. longifolia* x *P. repens*)	Cultivars	Berghoff-fynbos farm	33°00′S 18°59′E	Standard cultivation practices
‘Carli’ (*P. magnifica* selection)	Selection	Berghoff-fynbos farm	33°00′S 18°59′E	Standard cultivation practices
Sharonette’ (*P. eximia* x *P. susannae)*	Cultivars	FynBloem	34°09′01″S 19°54′52″E	Standard cultivation practices
‘Black Beauty’ (Sheila (*P. magnifica* x *P. burchellii*) cross)	Cultivars	FynBloem	34°09′01″S 19°54′52″E	Standard cultivation practices
‘Sylvia’ (*P. eximia* x *P. susannae*)	Cultivars	FynBloem	34°09′01″S 19°54′52″E	Standard cultivation practices
‘Susara’ (*P. magnifica* x *P. susannae*)	Cultivars	FynBloem	34°09′01″S 19°54′52″E	Standard cultivation practices
‘Carnival’ (*P. compacta* x *P. neriifolia*)	Cultivars	FynBloem	34°09′01″S 19°54′52″E	Standard cultivation practices
‘Limelight’ (*P. neriifolia* x *P. burchellii*)	Cultivars	FynBloem	34°09′01″S 19°54′52″E	Standard cultivation practices
‘Pink Ice’ (*P. compacta* x *P. susannae*)	Cultivars	FynBloem	34°09′01″S 19°54′52″E	Standard cultivation practices
P. mundii	Pure species	FynBloem	34°09′01″S 19°54′52″E	Standard cultivation practices

Figure S4.1: The manifestation of leaf blackening in the cultivar 'Pink Ice' (*P. susannae* x *P. compacta*) seven days post-harvest, expressed on the lateral leaf margins.

Table S4.2: Summary of the analytical data for the `new' compounds identified in the studied *Protea* plants by UPLC-PDA-HR-MS.

Number	Compound	Adduct	t_R (min)	*m/z*	Mass Error (ppm)	Fragments	Chemical Formula	UV-Vis max (nm)	$^{TW}CCS_{N2}$ (Å^2)	Level of Identification	Reference(s)
Organic and Sugar acids											
1	Gluconic acid	$[M-H]^-$	1.58	195.0505 (bp)	-0.5	195-> 177.0380; 159.0350; 99.0029; 89.0231; 75.0099; 71.0114; 59.0133; 57.0362	$C_6H_{12}O_7$	-	116.3	2	[1]
2	Xylonic acid	$[M-H]^-$	1.60	165.0401	-1.2	165-> 153.0001; 126.8284; 105.0192; 75.0090 (bp)	$C_5H_{10}O_6$	-	-	2	[2]
3	Quinic acid	$[M-H]^-$	1.78	191.0544	-3.1	191-> 173.0373; 171.0340; 127.0379; 111.0423; 109.0284; 93.0349; 87.0097; 85.0298 (bp)	$C_7H_{12}O_6$	-	116.5	2	[1]
4	Isocitric acid	$[M-H]^-$	2.15	191.0201 (bp)	2.6	191-> 173.0117; 154.9945; 129.0173; 117.0193; 111.0103; 85.0313; 73.0118	$C_6H_8O_7$	-	-	2	[1]
5	Citric acid	$[M-H]^-$	3.33	191.0187 (bp)	-4.2	191-> 154.9363; 129.0007; 116.9656; 111.0079; 87.0086; 85.0268	$C_6H_8O_7$	-	-	2	[1]
Sugars											
6	Hexose	$[M-H]^-$	1.58	179.0556 (bp)	2.2	179-> 142.9642; 131.0438; 96.9618; 89.0223	$C_6H_{12}O_6$	-	117.0	3	[1]
7	Hexoside-*O*-deoxy-hexose isomer 1	$[M-H]^-$	1.94	325.1135 (bp)	-2.2	325-> 179.0541; 163.0524	$C_{12}H_{22}O_{10}$	-	160.0	3	MS^E
8	Hexoside-*O*-deoxy-hexose isomer 2	$[M-H]^-$	2.97	325.1130 (bp)	-3.1	325-> 179.0484; 163.0590	$C_{12}H_{22}O_{10}$	-	160.0	3	MS^E
Phenolic acids											
18	Piscidic acid	$[M-H]^-$	8.49	255.0505 (bp)	-1.2	255-> 211.0297; 193.0415; 179.0359; 165.0554; 149.1361	$C_{11}H_{12}O_7$	275	143.0	2	[1,3]
22	*p*-Hydroxybenzoic acid-*O*-hexoside isomer 1	$[M-H]^-$	9.48	299.0761 (bp)	2.3	299-> 137.0343; 93.0408	$C_{13}H_{16}O_8$	260	164.2	3	MS^E
25	Protocatechuic acid-*O*-rhamnoside isomer 1	$[M-H]^-$	10.33	299.0758	-2.3	299-> 153.0179 (bp); 109.0287; 108.0194	$C_{13}H_{16}O_8$	260	164.2	3	MS^E
27	Protocatechuic acid-*O*-rhamnoside isomer 2	$[M-H]^-$	10.65	299.0770 (bp)	0.7	299-> 153.0179; 109.0287; 108.0194	$C_{13}H_{16}O_8$	261	164.2	3	MS^E
28	*p*-Hydroxybenzoic acid-*O*-hexoside isomer 2	$[M-H]^-$	11.19	299.0767	1.0	299-> 137.0343; 93.0408 (bp)	$C_{13}H_{16}O_8$	260	164.2	3	MS^E
29	Caffeoyl-*O*-hexoside	$[M-H]^-$	11.50	341.0869 (bp)	2.6	341-> 179.0378; 135.0457	$C_{15}H_{18}O_9$	290, 326	163.2	3	MS^E
36	Protocatechuic acid-*O*-arbutin isomer 1	$[M-H]^-$	13.45	407.0962	2.2	407-> 153.0186 (bp); 109.0262; 108.0283	$C_{19}H_{20}O_{10}$	266	181.6	3	MS^E
41	Protocatechuic acid-*O*-arbutin isomer 2	$[M-H]^-$	14.12	407.0978 (bp)	0.0	407-> 153.0228; 109.0272; 108.0283	$C_{19}H_{20}O_{10}$	262	181.6	3	MS^E
45	*p*-Hydroxybenzoic acid-*O*-deoxy-hexose isomer 3	$[M-H]^-$	14.65	283.0818	-2.1	283-> 137.0216 (bp); 93.0318	$C_{13}H_{16}O_7$	260	157.9	3	[4,5]

47	Protocatechuic acid-*O*-arbutin isomer 3	$[M-H]^-$	14.79	407.0981 (bp)	-1.0	407-> 297.0605; 153.0187; 109.0293; 108.0234	$C_{19}H_{20}O_{10}$	262	181.6	3	MS^E
48	Protocatechuic acid-*O*-hexoside-*O*-protocatechuic alcohol isomer 2	$[M-H]^-$	14.99	437.1083	-0.5	437-> 153.0194; 139.0388 (bp); 121.0281; 109.0293	$C_{20}H_{22}O_{11}$	263	181.1	3	[1]
49	Protocatechuic acid-*O*-arbutin isomer 4	$[M-H]^-$	15.19	407.0976 (bp)	-0.5	407-> 297.0588; 153.0189; 109.0299; 108.0252	$C_{19}H_{20}O_{10}$	263	181.6	3	MS^E
50	Protocatechuic acid derivative isomer 1	$[M-H]^-$	17.03	405.0823	1.5	405-> 295.0457; 159.0301; 153.0205 (bp); 109.0287	$C_{19}H_{18}O_{10}$	262	178.5	3	MS^E
52	Hydroxyquinol-*O*-hexoside-*O*-acetyl derivative isomer 1	$[M-H]^-$	17.37	435.1288 (bp)	3.7	435-> 417.1245; 329.0907; 287.0659; 269.0443; 125.0241	$C_{21}H_{24}O_{10}$	284	195.0	3	MS^E
55	Caffeoyl-*O*-polygalatol-*O*-hydroxyquinol isomer 1	$[M-H]^-$	17.76	433.1136 (bp)	0.2	433-> 323.0791; 179.0352; 161.0264; 135.0465; 133.0303; 109.0288; 108.0251	$C_{21}H_{22}O_{10}$	294, 326	192.5	3	MS^E
56	Caffeoyl-*O*-polygalatol-*O*-hydroxyquinol isomer 2	$[M-H]^-$	18.14	433.1136 (bp)	-3.2	433-> 323.0791; 179.0352; 161.0264; 135.0465; 133.0303; 109.0288; 108.0251	$C_{21}H_{22}O_{10}$	294, 326	192.5	3	MS^E
57	Hydroxyquinol-*O*-hexoside-*O*-acetyl derivative isomer 2	$[M-H]^-$	18.71	435.1278	4.1	435-> 417.1166; 329.0867; 287.0761; 269.0657; 125.0239 (bp)	$C_{21}H_{24}O_{10}$	284	195.2	3	MS^E
58	Hydroxyquinol-*O*-hexoside-*O*-acetyl derivative isomer 3	$[M-H]^-$	18.96	435.1289	0.0	435-> 417.1379; 329.0863; 287.0772; 125.0242 (bp)	$C_{21}H_{24}O_{10}$	284	195.2	3	MS^E
66	Eximin isomer 2	$[M-H]^-$	22.05	375.1080	1.6	375-> 121.0338; 109.0289 (bp); 108.0199	$C_{19}H_{20}O_8$	282	182.1	3	[6,7]
Unknowns											
94	237_1.79	$[M-H]^-$	1.79	237.0595	-3.4	237->129.0183; 113.0152; 87.0106 (bp)	$C_8H_{14}O_8$	-	139.3	4	MS^E
95	317_1.83	$[M-H]^-$	1.83	317.0521 (bp)	4.1	317>225.0044	$C_{12}H_{14}O_{10}$	-	153.35	4	MS^E
96	267_1.93	$[M-H]^-$	1.93	267.0717 (bp)	-3.0	267->149.0450; 119.0341; 113.0238; 101.0239; 89.0242; 85.0238	$C_9H_{16}O_9$	-	332.8	4	MS^E
97	209_1.95	$[M-H]^-$	1.95	209.0661 (bp)	2.9	209->179.0606; 149.0423; 71.0122; 59.0128	$C_7H_{14}O_7$	-	126.3	4	MS^E
98	203_4.28	$[M-H]^-$	4.28	203.0191 (bp)	-2.5	203->113.0359; 111.0079; 97.0107; 79.0189	$C_7H_8O_7$	-	116.0	4	MS^E
99	329_6.66	$[M-H]^-$	6.66	329.0867	-0.9	329->153.0215; 139.0361; 135.0356; 123.0466; 122.0335 (bp)	$C_{14}H_{18}O_9$	283	176.8	4	MS^E
100	295_7.84	$[M-H]^-$	7.84	295.1036 (bp)	0.0	295->217.0560; 119.0378	$C_{11}H_{20}O_9$	-	157.6	4	MS^E
101	417_8.09	$[M-H]^-$	8.09	417.1397 (bp)	-1.0	417->371.0962; 307.1109; 137.0225; 125.0249; 119.0342; 103.0403; 89.0229; 71.0135	$C_{18}H_{26}O_{11}$	-	195.5	4	MS^E
102	205_9.87	$[M-H]^-$	9.87	205.0711	-0.5	205->143.0699; 129.0556; 115.0760 (bp)	$C_8H_{14}O_6$	279	126.4	4	MS^E
103	451_12.62	$[M-H]^-$	12.62	451.2179	2.7	451->325.0979; 179.0363; 161.0303 (bp); 135.0442; 133.0296	$C_{20}H_{36}O_{11}$	294, 326	205.6	4	MS^E
104	239_12.98	$[M-H]^-$	12.98	239.0548 (bp)	-3.3	239->149.0607; 91.0558	$C_{11}H_{12}O_6$	-	138.6	4	MS^E
105	487_13.22	$[M-H]^-$	13.22	487.1452	0.2	487->325.0919; 179.0411; 161.0257 (bp); 135.0642; 133.0147	$C_{21}H_{28}O_{13}$	-	210.3	4	MS^E
106	431_15.12	$[M-H]^-$	15.12	431.1917	-1.4	431->153.0737 (bp); 161.0243; 109.0262	$C_{20}H_{32}O_{10}$	295	198.0	4	MS^E
107	465_15.73	$[M-H]^-$	15.73	465.1033	-3.7	465->177.0166; 133.0298 (bp)	$C_{21}H_{22}O_{12}$	283	192.0	4	MS^E
108	449_15.89	$[M-H]^-$	15.89	449.1096 (bp)	0.7	449->295.0463; 177.0190; 153.0189; 133.0286; 109.0301	$C_{21}H_{22}O_{11}$	-	195.0	4	MS^E
109	399_16.18	$[M-H]^-$	16.18	399.1291	-2.3	399->325.0960; 161.0429 (bp); 109.0286	$C_{18}H_{24}O_{10}$	285, 326	201.3	4	MS^E
110	475_17.39	$[M-H]^-$	17.39	475.1811	-2.1	475->177.0184; 163.0601 (bp); 125.0229; 103.0387	$C_{21}H_{32}O_{12}$	-	210.5	4	MS^E
111	337_17.42	$[M-H]^-$	17.42	337.0570	-1.2	337->159.0300 (bp); 151.0401; 133.0289; 125.0239	$C_{15}H_{14}O_9$	280	159.8	4	MS^E
112	407_17.62	$[M-H]^-$	17.62	407.0978	2.7	407->281.0655; 137.0238; 125.0251 (bp)	$C_{19}H_{20}O_{10}$	280	181.6	4	MS^E
113	449_18.01	$[M-H]^-$	18.01	449.1080	-1.1	449->221.0469; 271.0249; 179.0375; 161.0259; 133.0295; 125.02422 (bp)	$C_{21}H_{22}O_{11}$	293, 326	195.0	4	MS^E
114	313_19.01	$[M-H]^-$	19.01	313.0919	-1.3	313->287.0800; 253.0723; 179.0327; 161.0351; 159.0317 (bp); 135.0441; 125.0236; 109.0289	$C_{14}H_{18}O_8$	285	170.7	4	MS^E
115	313_19.32	$[M-H]^-$	19.32	313.0921	-1.3	313->271.0841; 179.0326; 161.0415 (bp); 159.0415; 135.0442; 125.0238; 109.0297	$C_{14}H_{18}O_8$	285	170.7	4	MS^E
116	431_20.63	$[M-H]^-$	20.63	431.0978	-1.4	431->321.0569; 179.0365; 161.0339; 159.0292 (bp); 135.0421; 73.0236	$C_{21}H_{20}O_{10}$	315	189.6	4	MS^E

bp = Base Peak

Levels of identification: **1**= Identified compound (reference standard available), **2**= Tentatively annotated (MS spectra compared with reference standard in literature), **3**= Putatively characterised (compared to compound class or isomers) and **4**= Unknown compound

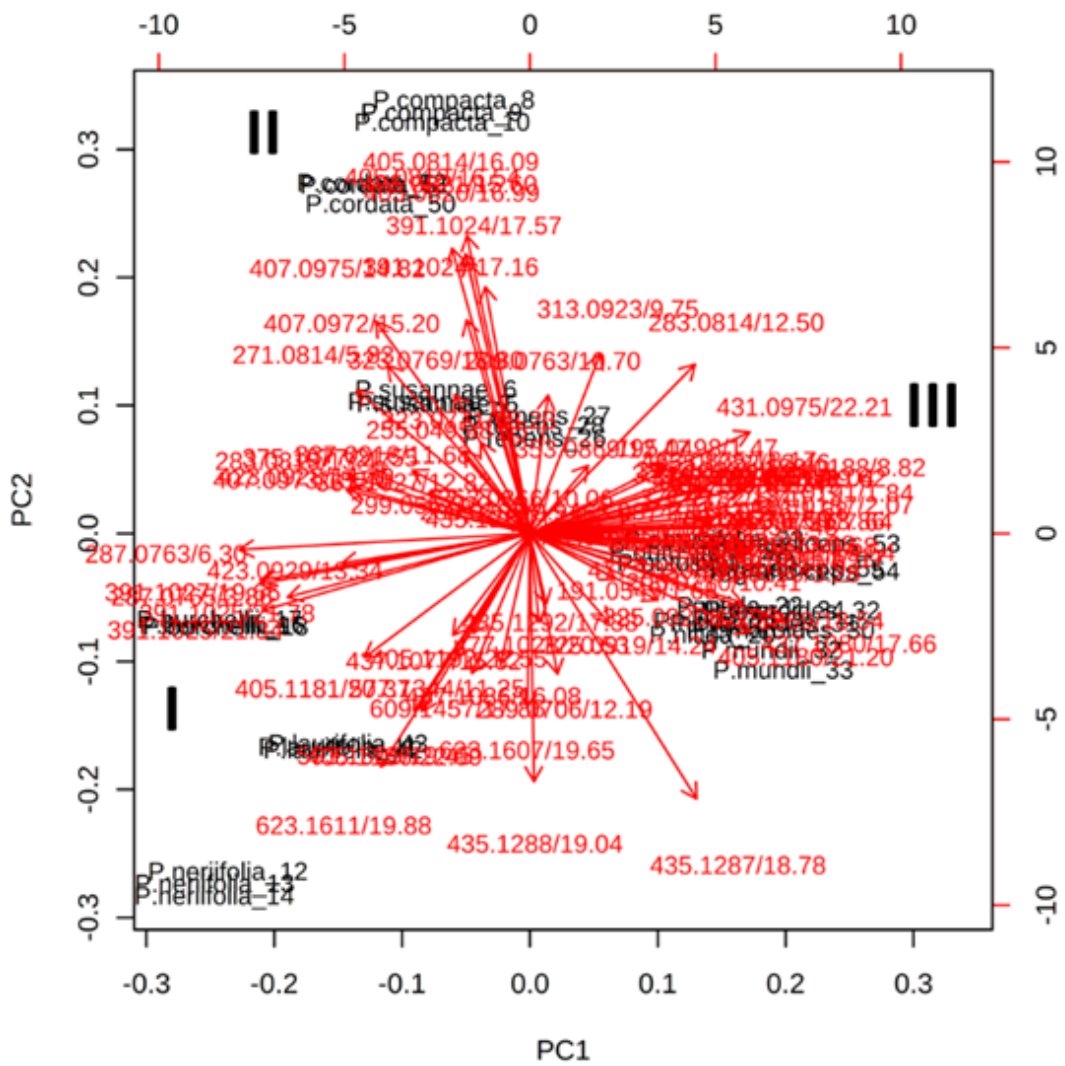

Figure S4.2: Principal component analysis (PCA) biplot of the potential biomarkers linked to the *Protea* species making up Group **I**, **II** and **III** in Figure 4.2. The variables are represented by the first (33.5%) and second (18.1%) components.

Table S4.3: Summary of the features associated with the clustering patterns observed on the 2D scores plot and HCA dendrogram (Figure 4.2) resulting in three groups. Refer to section 4.3.2.1 for further details and discussion.

Molecule number	Feature (*mz*/t_R)	Metabolite	Group I	Group II	Group III
1	195/1.58	Gluconic Acid			√
3	191/1.68	Quinic acid			√
4	191/2.15	Isocitric acid			√
5	191/3.33	Citric acid			√
6	179/1.58	Hexose			√
9	287/4.14	Phlorin (phloroglucinol-*O*-hexoside)	√		
10	271/5.71	β-Arbutin (hydroquinone-*O*-hexoside)		√	
12	287/6.26	Hydroxyquinol-*O*-hexoside	√		
14	301/7.23	Protocatechuic alcohol-*O*-hexoside isomer 2			√
17	315/8.43	Protocatechuic acid-*O*-hexoside isomer 2			√
19	153/8.82	Protocatechuic acid			√
20	329/8.98	Vanillic-*O*-hexoside			√
26	283/10.60	*p*-hydroxybenzoic acid-*O*-deoxy-hexose isomer 1			√
31	355/11.96	Feruloyl-*O*-hexoside isomer 1			√
37	355/13.51	Feruloyl-*O*-hexoside isomer 2			√
39	423/13.89	*p*-hydroxybenzoic acid derivative			√
51	391/17.16	*p*-hydroxybenzoic acid-*O*-arbutin isomer 1		√	
53	391/17.58	*p*-hydroxybenzoic acid-*O*-arbutin isomer 2		√	
54	437/17.68	Protocatechuic acid-*O*-hexoside-*O*-protocatechuic alcohol isomer 3			√
59	391/19.63	Benzoylhexoside of hydroxyquinol (benzoyl-*O*-hexoside-*O*-hydroxyquinol, previously referred to as neriifolin) isomer 1	√		
60	405/20.37	Hydroxyquinol-*O*-hexoside derivative isomer 1	√		
61	405/21.17	Lacticolorin/Pilorubrosin (benzoyl-*O*-hexoside-*O*-protocatechuic alcohol) isomer 1			√
62	391/21.29	Benzoylhexoside of hydroxyquinol isomer 2	√		
64	375/21.51	Eximin (6-*O*-benzoyl-*O*-arbutin) isomer 1		√	
65	391/21.75	Benzoylhexoside of hydroxyquinol isomer 3	√		
67	405/22.08	Hydroxyquinol-*O*-hexoside derivative isomer 2	√		
79	463/18.16	Quercetin-*O*-galactoside			√
86	447/20.20	Kaempferol-*O*-glucoside			√
91	431/22.37	Kaempferol-*O*-deoxy-hexose			√
92	315/26.17	Isorhamnetin			√

Group I comprise of *P. neriifolia*, *P. burchellii* and *P. laurifolia*; **Group II** *P. compacta*, *P. cordata*, *P. repens* and *P. susannae*; and **Group III** *P. cynaroides*, *P. grandiceps*, *P. mundii*, *P. nitida* and *P. obtusifolia*.

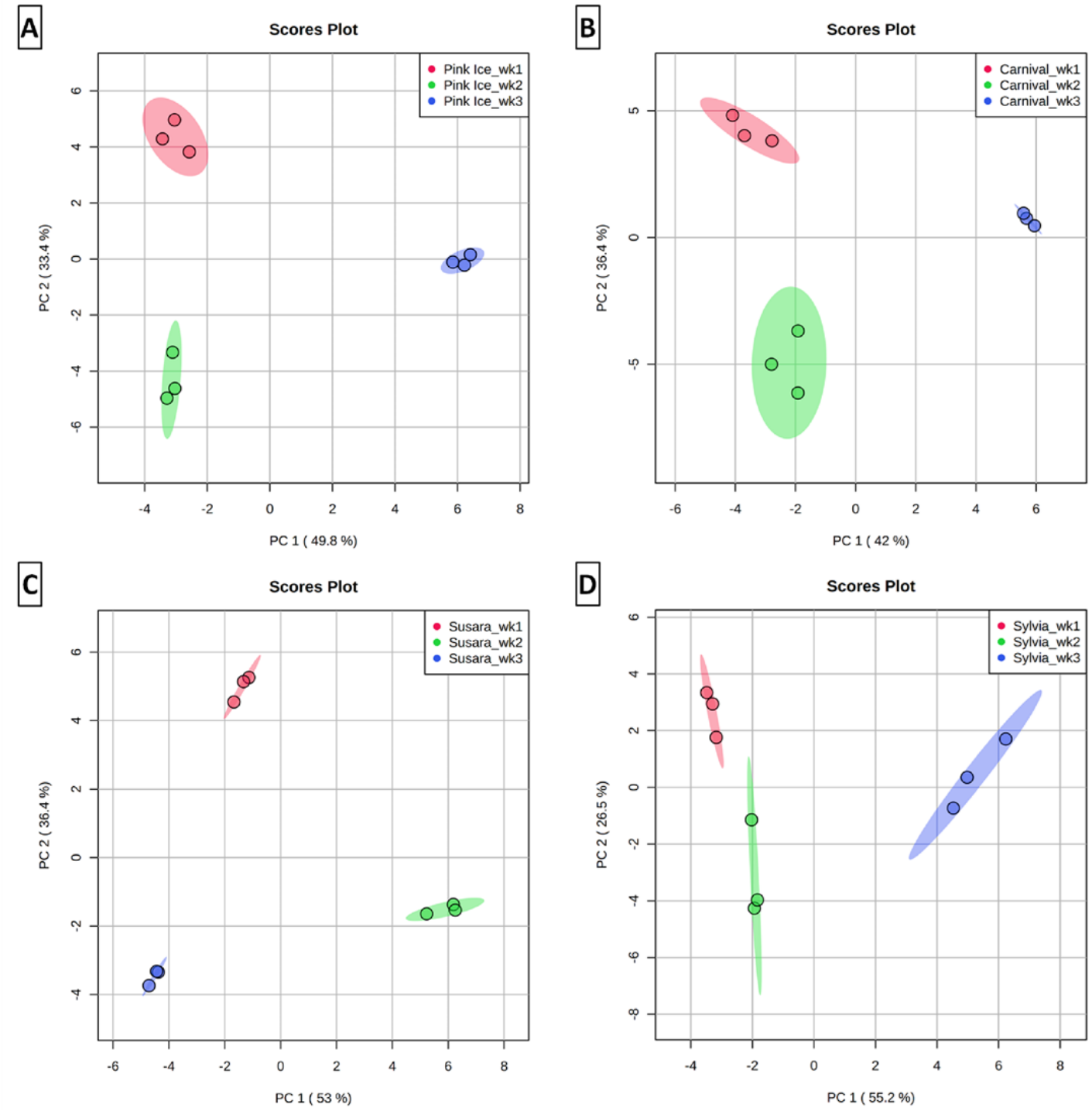

Figure S4.3: Principal component analysis (PCA) scores plot showing similarities and differences between the leaf tissue samples of the cultivar (**A**) 'Pink Ice' (*P. compacta* x *P. susannae*), (**B**) 'Carnival' (*P. compacta* x *P. neriifolia*), (**C**) 'Susara' (*P. susannae* x *P. magnifica*) and (**D**) 'Sylvia' (*P. eximia* x *P. susannae*) sampled over a three-week period post-harvest. The scores plot was constructed between Component 1 and Component 2, accounting for 83.2%, 78.4%, 89.4% and 81.7% of the variation, respectively.

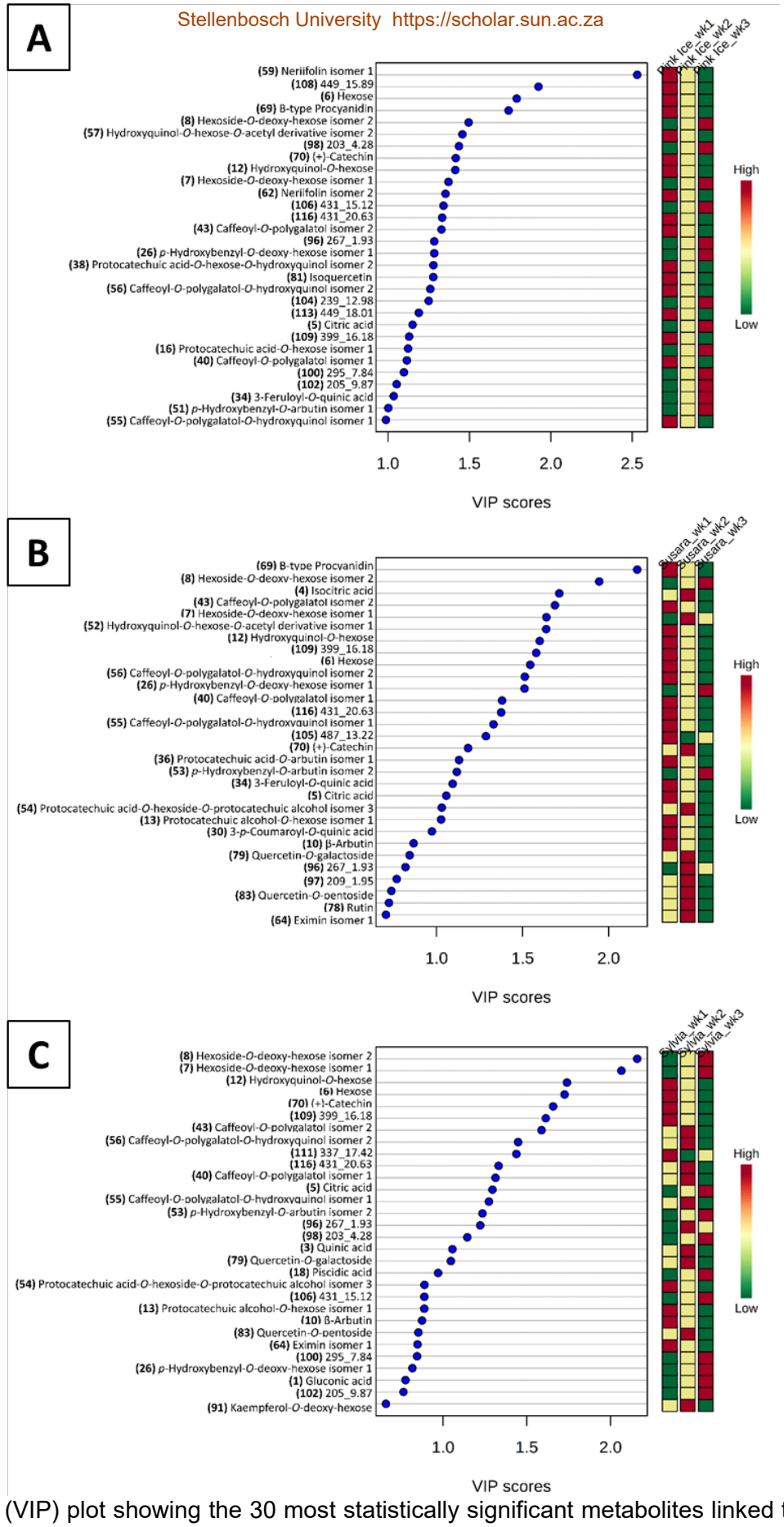

Figure S4.4: 'Variable importance' in projection (VIP) plot showing the 30 most statistically significant metabolites linked to the leaf tissue blackening of (**A**) 'Pink Ice' (*P. compacta* x *P. susannae*), (**B**) 'Susara' (*P. susannae* x *P. magnifica*) and (**C**) 'Sylvia' (*P. eximia* x *P. susannae*) over a three-week period.

Figure S4.5: Examples of the bearded *Protea* cultivars 'Didi' (*P. magnifica* x *P. laurifolia*), 'Black Beauty' (Sheila (*P. magnifica* x *P. burchellii*) cross) and 'Niobe' (*P. magnifica* x *P. laurifolia*).

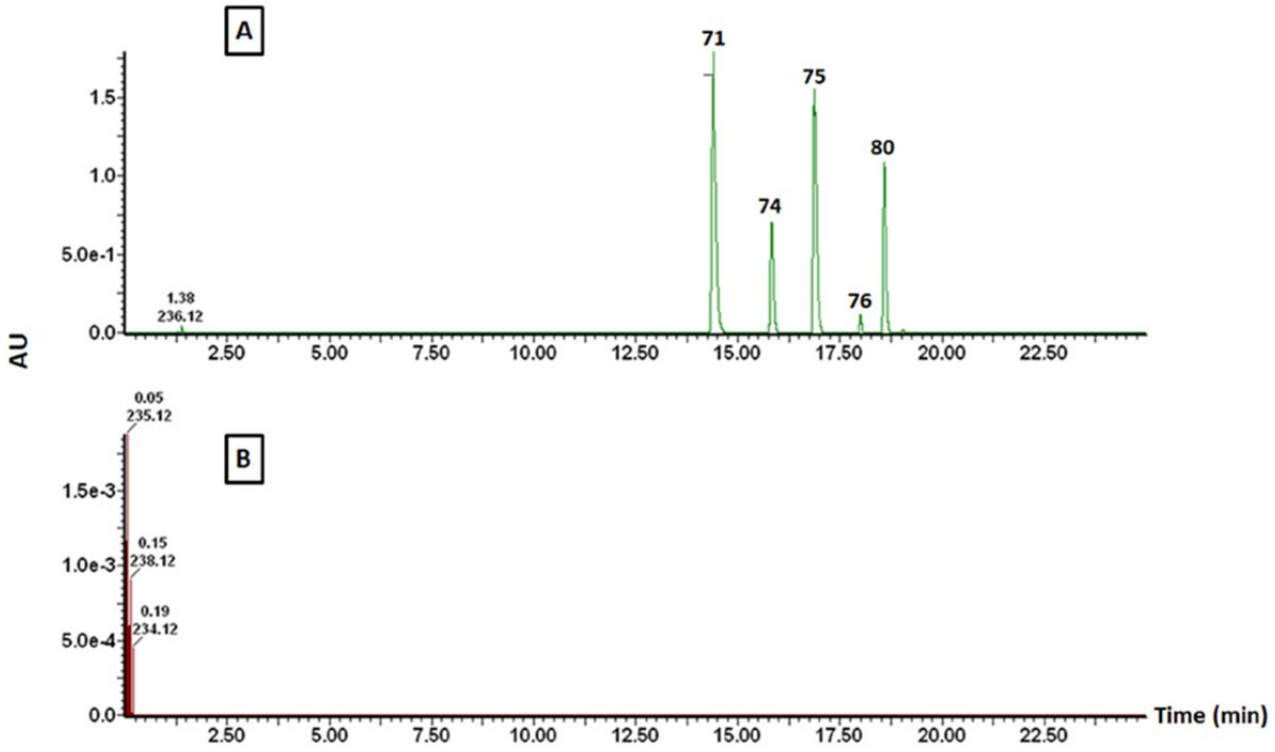

Figure S4.6: UV chromatogram at 500 nm showing the detection of five anthocyanins, namely delphinidin-*O*-hexoside (**71**), cyanidin-*O*-hexoside (**74**), petunidin-*O*-hexoside (**75**), peonidin-*O*-hexoside (**76**) and malvidin-*O*-hexoside (**80**), in the bearded part **(A)** and not in the bract part **(B)** of the inflorescences of the cultivar 'Niobe' (*P. magnifica* x *P. laurifolia*).

4.6. References

(1) METLIN https://metlin.scripps.edu/landing_page.php?pgcontent=mainPage (accessed Nov 29, 2018).

(2) Maulidiani, M.; Abdul-Hamid, N. A.; Abas, F.; Park, Y. S.; Park, Y.-K.; Kim, Y. M.; Gorinstein, S. Detection of bioactive compounds in persimmon (*Diospyros kaki*) using uplc-esi-orbitrap-ms/ms and fluorescence analyses. *Microchem. J.* **2019**, *149*, 1–8. https://doi.org/10.1016/j.microc.2019.103978.

(3) Touati, R.; Santos, S. A. O.; Rocha, S. M.; Belhamel, K.; Silvestre, A. J. D. Phenolic composition and biological prospecting of grains and stems of *Retama sphaerocarpa*. *Ind. Crops Prod.* **2017**, *95*, 244–255. https://doi.org/10.1016/j.indcrop.2016.10.027.

(4) Fang, N.; Yu, S.; Prior, R. L. LC/MS/MS characterization of phenolic constituents in dried plums. *J. Agric. Food Chem.* **2002**, *50* (12), 3579–3585. https://doi.org/10.1021/jf0201327.

(5) Perold, G. W.; Beylis, P.; Howard, A. S. Metabolites of Proteaceae. Part VII. Lacticolorin, a phenolic glucoside ester, and other metabolites of *Protea lacticolor* Salisb. *J. Chem. Soc. Perkin Trans. 1* **1973**, No. 638, 638–643. https://doi.org/10.1039/P19730000638.

(6) Perold, G. W.; Rosenberg, M. E. K.; Howard, A. S.; Huddle, P. A. Metabolites of Proteaceae. Part 9. Eximin (6-*o*-benzoylarbutin) and the synthesis of aryl glycoside esters. *J. Chem. Soc. Perkin Trans. 1* **1979**, 239–243. https://doi.org/10.1039/p19790000239.

(7) Verotta, L.; Orsini, F.; Pelizzoni, F.; Torri, G.; Rogers, C. B. Polyphenolic glycosides from African Proteaceae. *J. Nat. Prod.* **1999**, *62* (11), 1526–1531. https://doi.org/10.1021/np9902237.

Declaration with signatures in possession of candidate and supervisor.

Declaration by the candidate:

Regarding **Chapter 5**, the nature and scope of my contribution were as follows:

Nature of contribution	**Extent of contribution (%)**
Performed the experiments, data analysis, co-wrote paper	88

The following co-authors have contributed to **Chapter 5**:

Name	**E-mail address**	**Nature of contribution**	**Extent of contribution (%)**
Marietjie A. Stander	lcms@sun.ac.za	Assisted with experimental set-up and data manipulation; editorial input	5
André de Villiers	ajdevill@sun.ac.za	Co-wrote paper	1
Dalene de Beer	DBeerD@arc.agric.za	Co-conceptualised the idea, collected the samples and applied for the funding. Wrote part of the introduction.	5
Lizette Joubert	joubertL@arc.agric.za	Co-wrote paper	1

Signature of candidate: …… 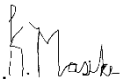 ……

Date: …25 February 2021……

Declaration by co-authors:

The undersigned confirm that:

The declaration above accurately reflects the nature and extent of the contributions of the candidate and the co-authors to **Chapter 5**,
No other authors contributed to **Chapter 5** besides those specified above, and
Potential conflicts of interest have been revealed to all interested parties and that the necessary changes have been made to use the material in Chapter 5 of this thesis.

Signature	**Institutional affiliation**	**Date**
	Stellenbosch University	17 February 2021
	Stellenbosch University	17 February 2021

Chapter 5: Application of direct injection-ion mobility mass spectrometry (DI-IM-MS) for the analysis of Honeybush and Rooibos tea samples

Abstract

Consumer awareness of the health benefits of herbal teas (i.e., rooibos and honeybush tea) lead to an increase in production demand and to inevitable accidental or deliberate adulterations. In this study, direct injection-ion mobility mass spectrometry (DI-IM-MS) is proposed as a rapid methodology for the differentiation of rooibos and honeybush blends (adulterations). Analytical data was obtained from 100 rooibos, 130 honeybush and 7 blend samples. Quantitative data was acquired with the aid of DI-IM-MS and compared with data obtained using traditional ultra-high performance liquid chromatography mass spectrometry (UPLC-MS). For DI-IM-MS analyses, descriptive chemometrics showed differences between samples of rooibos and honeybush blends (adulterations), and further showed the diagnostic value of marker compounds in distinguishing the three commercialised honeybush species (*Cyclopia intermedia*, *C. genistoides* and *C. subternata*). Markers such as eriodictyol-*C*-hexose isomers (**4-6**), orientin (**9**), aspalathin (**10**), and vitexin (**13**) were characteristic of blends containing more than 80% of rooibos plant material, and quinic acid (**22**), iriflophenone-3-*C*-glucoside-4-*O*-glucoside (**24**), *C*-glycosylxanthones isomers (mangiferin (**29**) and isomangiferin (**30**)), and eriodictyol (**39**) were characteristic of blends containing more than 80% of *C. intermedia* plant material. Furthermore, the *C*-glycosylxanthones isomers (mangiferin (**29**) and isomangiferin (**30**)) were prominent in *C. genistoides*, quinic acid (**22**) was prominent in *C. subternata* and piscidic acid (**1**) was prominent in *C. intermedia* plant material. The traditional UPLC-MS method showed more linear calibration curves (R^2 > 0.995) than the DI-IM-MS method (R^2 > 0.955) during quantification. Lastly, phenolic compounds in the herbal teas were characterised based on an array of complementary descriptors (e.g., retention time, drift time, accurate mass information, tandem MS, and $^{TW}CCS_{N2}$) to aid in compound identification.

5.1. Introduction

Rooibos (*Aspalathus linearis*) and honeybush (*Cyclopia* spp) tea are proudly South African products and are protected as geographical indications (GI).[1] These herbal teas are exported internationally and have health-promoting properties such as anti-diabetic, anti-obesity, anti-cancer, amongst others.[2,3]

There are more than 20 known *Cyclopia* species that can be used for tea, but the bulk of production comprises of wild-harvested *Cyclopia intermedia*.[3–5] The *C*-glycosylxanthone mangiferin and its isomer isomangiferin occur in high concentration in all the commercial honeybush tea,[3] but are absent in rooibos and black tea. Aspalathin is one of the main phenolic compounds in rooibos,[2] but not present in honeybush or black tea. Most of the phenolic compounds are oxidised during fermentation of rooibos (low temperature oxidation process involving polyphenol oxidase enzyme), especially aspalathin and nothofagin,[6,7] and honeybush (high-temperature oxidation process).[3] These compounds in conjunction with caffeine, which is absent in these teas,[8] are markers that can be easily used to distinguish the teas. The flavones, orientin, isoorientin, vitexin and isovitexin are other main constituents in rooibos, while honeybush contains benzophenones (iriflophenone-3-*C*-glucoside and iriflophenone-3-*C*-glucoside-4-*O*-glucoside), flavanones (e.g., hesperidin) and flavones (e.g., vicenin-2). Blends of rooibos and honeybush are also prevalent on the market, but no regulations exist that specify the minimum content of each for labelling purposes. Furthermore, *Cyclopia* species can be pooled together before or after processing due to a limited amount of available product per species.[9] To control product authenticity for GI purposes, differentiation of the species and blends is important, thus necessitating analytical methodologies. High performance liquid chromatography (HPLC) with diode-array detection and ultra-high pressure liquid chromatography (UHPLC)-mass spectrometry (MS) methods for the analysis of major phenolic compounds in different *Cyclopia* species[9–15] and rooibos teas[6,16,17] have been documented, however these often require long chromatographic runs due to the complexity of phenolic compounds (i.e. the presence of multiple isomers).

Ion mobility spectrometry (IMS) is an emergent technique whose efficiency in the characterization and analysis of compounds from different matrices, such as food samples, has been determined.[18,19] IMS has become an appealing technology for the separation and detection of structurally similar metabolites, while also reducing the need for LC separation. During analysis, gas-phase ions are separated based on their different migrations through a region filled with a buffer gas submitted to an electric field maintained at atmospheric pressure.[20,21] Separation is

based on the ion's physical properties, such as size, charge, and conformation (collision cross section, CCS). CCS values (measured in square Ångström, Å^2) are characteristic for each ion and describe the physicochemical properties of the ion as it interacts with the neutral buffer gas, thus providing information of the ion's shape which helps increase molecular information content and specificity for structural identification. IMS is revered for its rapidity and sensitivity, however when hyphenated to MS: 1) the possible separation of isomers,[22] 2) enhanced detection of low abundance metabolites,[23,24] 3) improved signal-to-noise (S/N) ratios,[24] and 4) enhanced compound coverage,[25] can be achieved. The potential applicability of IMS in the adulteration of honey,[26–29] and olive oil[29,30] have been demonstrated.

In this study, the use of direct injection-ion mobility mass spectrometry (DI-IM-MS) as a simple and rapid test for the screening of major phenolic compounds in 100 rooibos, different *Cyclopia* species (100 *C*. *intermedia*, 15 *C*. *genistoides* and 15 *C*. *subternata*), and 7 blends of rooibos and honeybush was demonstrated. A DI-IM-MS method was developed and compared with the traditional UPLC-MS method for the separation and quantitation of 11 polyphenolic standards common in rooibos and honeybush extracts. Lastly, the extracted phenolics were further characterized based on an array of analytical molecular descriptors, particularly their $^{TW}CCS_{N2}$ values.

5.2. Materials and methods

5.2.1. Materials

Authentic standards were analytical grade (purity ≥ 95%) and purchased from Sigma-Aldrich (MO, USA) unless otherwise stated [isoorientin (luteolin-6-*C*-glucoside), orientin (luteolin-8-*C*-glucoside), neoponcirin (isosakuranetin-7-*O*-rutinoside), scolymoside (luteolin-7-O-rutinoside), isovitexin (apigenin-6-*C*-glucoside), vitexin (apigenin-8-*C*-glucoside), rutin (quercetin-3-*O*-rutinoside), hesperidin (hesperetin-7-*O*-rutinoside), hesperetin, quercetin, iriflophenone-3-*C*-glucoside, eriodictyol-7-*O*-glucopyranoside, quercetin-3'-*O*-glucopyranoside, hyperoside, luteolin-7-*O*-glucopyranoside, apigenin, eriodictyol]. Iriflophenone-3-*C*-glucoside-4-*O*-glucoside (99% purity by LC–MS) was isolated from *C. genistoides* as described by Beelders *et al*.[31] and phloretin-3',5'-*C*-diglucopyranoside was isolated from *C*. *subternata* was obtained from Agricultural Research Council (ARC-Infruitec, Stellenbosch, South Africa). The rest of the authentic standards (purity ≥ 95%) were purchased from Phytolab (Vestenbergsgreuth, Germany; vicenin-2), Extrasynthese (Genay, France; narirutin, eriocitrin (eriodictyol-7-*O*-rutinoside), neoeriocitrin (eriodictyol-7-*O*-neohesperidoside), mangiferin (norathyriol-2-*C*-glucoside), luteolin), and Chemos (Regenstauf, Germany; isomangiferin (norathyriol-4-*C*-glucoside)). Aspalathin (3-

hydroxyphloretin-3'-*C*-glucoside) (>95%) and nothofagin (phloretin-3'-*C*-glucoside) (>95%) were obtained from PROMEC (Medical Research Council of South Africa, Tygerberg, South Africa). The phenolic standard stock solutions were prepared in dimethyl sulphoxide (DMSO) at concentrations of ca. 1.000 mg/mL and diluted with 50% (*v/v*) methanol in water containing 2% formic acid to 0.500 mg/mL.

5.2.2. Samples

Commercial herbal teas (100 rooibos (*Aspalathus linearis*) and 130 honeybush (100 *Cyclopia intermedia*, 15 *C. genistoides*, and 15 *C. intermedia*) were obtained during the period 2011, 2016 to 2018 in the harvest seasons for rooibos (quality grades, A to D) and during the harvest seasons of honeybush (2016-2018). "Fermented" rooibos samples, sampled from different production batches, were obtained from different producers and/or plantations, and collected from Rooibos Ltd (Clanwilliam, Western Cape), the largest rooibos processing and marketing company. For honeybush, "fermented" samples were obtained from major producers in the Langkloof (Eastern Cape) for *C. intermedia*, Overberg region (Western Cape) for *C. genistoides*, and the Southern Cape and Langkloof for *C. subternata*.

5.2.3. Methods

5.2.3.1. Preparation of the calibration curve

To distinguish between co-eluting isomers, two sets of standard mixtures were prepared. For calibration purposes, the following concentrations were prepared from the composite mixtures at concentrations of 0.500 mg/mL: 125, 62.5, 31.3, 15.6, 7.81, 3.91, 1.95, 0.980, 0.490, 0.240, 0.12, 0.06 µg/mL with methanol/water/formic acid (50:48:2).

5.2.3.2. Preparation of plant material

Plant material were prepared as previously described by Małyjurek *et al*. [32] Briefly, 10.0 grams of dried "fermented" rooibos and honeybush plant material was finely milled using a Retsch mill with a 0.25 mm sieve (Retsch GmbH, Haan, Germany).

5.2.3.3. Metabolite extraction

For extraction, 1.00 g of powder was mixed with 15 mL of methanol/water/formic acid (50:48:2). After two hours, samples were subjected to sonication in an ultrasonic bath (0.5 Hz, Integral Systems, RSA) for one hour at room temperature. Post-sonication, samples were centrifuged (Hermle Z 160 M, LaborTechnik, Germany) at 15 994 x*g* for one hour to remove the cell debris.

The resulting supernatants were placed in glass vials for analysis. Blends of rooibos and *C. intermedia* were prepared at varying concentrations (1, 5, 20, 50, 80, 95 and 99% of *C. intermedia*).

5.2.3.4. Direct injection-ion mobility mass spectrometry (DI-IM-MS) and ultra-high performance liquid chromatography-mass spectrometry (UPLC-MS) analyses

Samples (3 µL) were injected directly into a solvent stream (50% acetonitrile, 0.1% formic acid, isocratic elution) at a flow rate of 0.25 mL/min, using a Waters Acquity UPLC system coupled to a Synapt G2 quadrupole-time-of-flight (q-TOF) instrument (Waters Corporation, Manchester, U.K.). For MS detection, ESI^- was used. Mass calibration was performed using a sodium formate solution and leucine enkephalin was used as the lock spray solution (*m/z* = 554.2771 reference mass). Operating conditions were as follows: capillary voltage 2.5 kV, sampling cone voltage 15 V, source temperature 120°C, N_2 was used as desolvation gas at 275˚C, desolvation gas flow 650 L/hr, cone gas flow (N_2) 50 L/hr. Data were acquired in the ion mobility scan mode (100–1500 amu). Each sample was injected three times (3 technical replicates).

(TWIMS was performed using the following settings: extraction cone 4 V, helium cell gas flow 180 mL/min, and IM buffer gas (N_2) flow 110 mL/min. The wave velocity for ion mobility was set at 650 m/s and wave height at 40 V.[33] Poly-DL-alanine[34] and poly-L-malic acid[35] were used as calibrants to determine $^{TW}CCS_{N2}$ values from the measured arrival time distributions in ESI^- modes. Poly-DL-alanine was prepared in H_2O/MeOH (50:50, *v:v*) at a concentration of 1.00 mg/mL and poly-L-malic acid was prepared at 0.50 mM in MilliQ water as proposed by Forsythe *et al.*,[35] 5 µL of calibrants were injected in triplicate. Calibration was performed using singly charged poly-DL-alanine oligomers (n = 3 to 14) covering a mass range of 231 to 1012 Da and CCS values ranging from 150 to 308 $Å^2$ in ESI^-, and singly charged poly-L-malic acid oligomers (n = 1 to 8) covering a mass range of 134 to 946 Da and CCS values ranging from 113 to 260 $Å^2$ in ESI^-. For data acquisition and processing, MassLynx™ 4.1 was utilized.

The samples were also analysed with a short chromatographic run (7 min) to aid in compound identification. Briefly, 2 µL of extract was injected into UPLC-MS instrument equipped with an Acquity HSS T3 C_{18} column (2.1 mm × 50 mm, 1.8 µm, Waters). The mobile phase for the chromatographic analysis consisted of 0.1% formic acid in Milli-Q water (solvent A) and 0.1% formic acid in acetonitrile (solvent B), at a flow rate of 0.5 mL/min. The initial conditions were 5% B, maintained for 0.2 min, increased to 40% B at 5 min, and subsequently to 100% B at 5.10 min and returned to the initial conditions after 0.1 min. The gradient was followed by a 1.8 min isocratic wash at 5% B to re-equilibrate the column. The column temperature was maintained at 60 °C.

This chromatographic run was monitored by MS conditions discussed above; whereby in MS^E mode the collision energy ramped from 20 to 60 V (for mass range 40-1500 Da).

5.2.3.5. Quantitative DI-IM-MS and UPLC-MS analyses and preliminary method validation

For both DI-IM-MS and UPLC-MS, preliminary method validation included evaluation of linearity, intra-day repeatability (6 repeat injections). The limits of detection (LOD) and quantification (LOQ) were determined as 3.3 σ/S and 10 σ/S, respectively.[36] Where σ the standard deviation of y-intercepts from 6 calibration curves and S is the slope of the calibration curve.[36] For compounds unique to the respective herbal teas, the linear regression was performed to determine the slope, y-intercept and correlation coefficient (R^2) using Microsoft Excel 2013 (Microsoft Corporation, Redmond, WA, USA). Samples used for method validation were randomly chosen and included one *C. genistoides*, *C. intermedia*, *C. subternata* and *A. linearis*. Averaged concentrations of the 11 phenolics (iriflophenone-3-*C*-glucoside-4-*O*-glucoside, iriflophenone-3-*C*-glucoside, (iso- and mangiferin), (iso- and orientin), aspalathin, eriocitrin, rutin, scolymoside, phloretin-3',5'-*C*-diglucoside, nothofagin and quercetin) in the respective herbal tea samples were determined using UPLC-MS (Supplementary information, Figure S1).

5.2.3.6. Metabolite annotation

For compound annotation and identification, MS^E fragmentation patterns, standards, and online databases such as Dictionary of Natural Products, KNApSAck, METLIN and ChemSpider were used. Experimental $^{TW}CCS_{N2}$ values ($Å^2$) were compared to available literature.[16,37–42]

5.2.3.7. Data processing and Multivariate data analyses (MVDA)

All DI-IM-MS raw data (converted to mzML format) were processed using XCMS Online (https://xcmsonline.scripps.edu) to yield a data matrix containing drift times, accurate masses and peak intensities. Briefly, the XCMS processing parameters were as follows: matchedFilter for feature detection (with 30 FWHM, 0.01 minimum difference in *m/z* for peaks with overlapping drift times and 10 signal to noise ratio cutoff), and obiwarp for drift time (t_D) correction. The chromatogram alignment parameters were: bandwidth of 5 sec (allowable t_D deviations), minifrac of 0.5 (minimum fraction of samples necessary in at least one of the sample groups for it to be a valid group) and *m/z* width of 0.05 (width of overlapping *m/z* slices to use for peak density chromatograms and grouping peaks across samples). For multivariate data analysis and for visualization, MetaboAnalyst 4.0 (www.metaboanalyst.ca) was used. The data were normalized using the sample median and transformed by log normalization, and data scaling was performed using the Pareto scaling algorithm. The statistical significance was calculated by analysis of

variance (ANOVA) for multigroup comparisons. The distribution of a select few annotated/identified metabolites (features) were visualized using box-and whiskers plots (boxplots).

5.3. Results and discussion

In this study, direct injection-ion mobility mass spectrometry (DI-IM-MS) with the aid of UPLC-MS and descriptive chemometrics was used to profile marker compounds in complex extracts of rooibos, honeybush (*C. intermedia*, *C. genistoides* and *C. subternata*) and the blends thereof. Samples of the herbal teas were concurrently ran with the available standards and the drift times were compared to aid in compound identification of the herbal teas (Table 5.1 and 5.2). Retention times and MS/MS data for the respective compounds and standards are also included in Table 5.1 and 5.2. Thus, phenolic compounds in the herbal teas were characterized based on an array of complementary descriptors, such retention time, drift time, accurate mass information, tandem MS, and $^{TW}CCS_{N2}$.

Table 5.1: List of compounds identified in Rooibos samples, showing retention time, drift time, precursor ion, elemental composition, MS^E fragments, $^{TW}CCS_{N2}$ values, and literature references from which the compounds were previously detected.

Compound number	Compound Name	Adduct	*m/z*	Chemical formulae	t_R (min)	t_D (ms)	$^{TW}CCS_{N2}$ (Å^2) Poly-DL-alanine calibrant	$^{TW}CCS_{N2}$ (Å^2) Poly-L-malic acid calibrant	$^{TW}CCS_{N2}$ (Å^2) in Literature	Fragments	References
1	Piscidic acid	$[M-H]^-$	255.0499	$C_{11}H_{12}O_7$	1.48	1.66	145.2	151.7	145.7 ($^{TW}CCS_{N2}$)	255-> 165.0522; 72.9512	[16]
2	Caffeoyl-*O*-hexose	$[M-H]^-$	341.0885	$C_{15}H_{18}O_9$	2.00	2.14	165.5	170.0	174.5 ($^{TW}CCS_{N2}$)	341-> 179.0357; 135.0343	[16]
3	Phenylpyruvic acid-*O*-glucoside (PPAG) isomer 1	$[M-H]^-$	325.0909	$C_{15}H_{18}O_8$	2.19	2.21	164.8	173.1	173.7 or 169.0 ($^{TW}CCS_{N2}$)	325-> 163.0219; 119.0592	[43]
4	Eriodictyol-*C*-hexose	$[M-H]^-$	449.1080	$C_{21}H_{22}O_{11}$	2.60	2.90	193.1	194.5	191.6 or 193.6 or 193.0 ($^{TW}CCS_{N2}$)	449-> 329.0560; 193.0125; 135.0348	[16]
5	Eriodictyol-*C*-hexose	$[M-H]^-$	449.1085	$C_{21}H_{22}O_{11}$	2.70	2.90	193.1	194.5	191.6 or 193.6 or 193.0 ($^{TW}CCS_{N2}$)	449-> 329.0577; 193.0125; 135.0434	[16]
6	Eriodictyol-*C*-hexose	$[M-H]^-$	449.1080	$C_{21}H_{22}O_{11}$	2.83	2.90	193.1	194.5	191.6 or 193.6 or 193.0 ($^{TW}CCS_{N2}$)	449-> 329.0676; 193.0177; 135.0679	[16]
7	Phenylpyruvic acid-*O*-glucoside (PPAG) isomer 2	$[M-H]^-$	325.0920	$C_{15}H_{18}O_8$	2.90	2.21	164.8	173.1	173.7 or 169.0 ($^{TW}CCS_{N2}$)	325-> 163.0427; 119.0514	[43]
8	Isoorientin (Luteolin-6-*C*-glucoside)	$[M-H]^-$	447.0911	$C_{21}H_{20}O_{11}$	2.98	3.11	200.3	201.0	198.1 ($^{TW}CCS_{N2}$)	447-> 357.0606; 327.0253; 297.0404	Standard; [42]
9	Orientin (Luteolin-8-*C*-glucoside)	$[M-H]^-$	447.0916	$C_{21}H_{20}O_{11}$	3.02	2.83	190.6	192.4	187.7 ($^{TW}CCS_{N2}$)	447-> 357.0787; 327.0487; 299.0526	Standard; [42]
10	Aspalathin (3-hydroxyphloretin-3'-*C*-glucoside)	$[M-H]^-$	451.1238	$C_{21}H_{24}O_{11}$	3.08	2.90	193.1	194.6	191.6 ($^{TW}CCS_{N2}$)	451-> 361.0958; 331.0844; 209.0578; 167.0308	Standard; [6,16]
11	PPAG derivative isomer 1	$[M-H]^-$	469.1320	$C_{21}H_{26}O_{12}$	3.14	2.97	195.3	196.5	194.4 ($^{TW}CCS_{N2}$)	469-> 325.0920; 163.427; 119.0514	[43]
12	Rutin (Quercetin-3-*O*-rutinoside)	$[M-H]^-$	609.1434	$C_{27}H_{30}O_{16}$	3.23	4.21	231.9	228.6	230.6 ($^{TW}CCS_{N2}$) 230.8 ($^{TW}CCS_{N2}$)	609-> 301.0325; 300.0436; 271.0160	Standard; [16,37,39]

									230.6 ($^{TW}CCS_{N2}$)		
13	Vitexin (Apigenin-8-*C*-glucoside)	$[M-H]^-$	431.0928	$C_{21}H_{20}O_{10}$	3.25	2.83	190.9	192.7	188.8 ($^{TW}CCS_{N2}$)	431-> 311.0550; 283.0457	Standard; [42]
14	Isovitexin (Apigenin-6-*C*-glucoside)	$[M-H]^-$	431.0981	$C_{21}H_{20}O_{10}$	3.34	3.04	198.2	199.2	195.5 ($^{TW}CCS_{N2}$)	431-> 341.0662; 311.0594; 283.0714	Standard; [42]
15	Hyperoside (Quercetin-3-*O*-galactoside)	$[M-H]^-$	463.0870	$C_{21}H_{20}O_{12}$	3.37	3.11	200.1	200.8	201.9 ($^{TW}CCS_{N2}$)	463-> 301.0448; 300.0172; 271.0574; 255.0330	Standard; [38]
16	Isoquercitrin (Quercetin-3-*O*-glucoside)	$[M-H]^-$	463.0884	$C_{21}H_{20}O_{12}$	3.42	3.11	200.1	200.8	200.9 ($^{TW}CCS_{N2}$)	463-> 301.0329; 300.0240; 271.0167; 255.0647	Standard; [37]
17	Luteolin-7-*O*-glucoside	$[M-H]^-$	447.0943	$C_{21}H_{20}O_{11}$	3.44	3.31	206.9	206.9	209.3 ($^{TW}CCS_{N2}$)	447-> 285.0420; 284.0193	Standard; [39]
18	PPAG derivative isomer 2	$[M-H]^-$	469.1349	$C_{21}H_{26}O_{12}$	3.54	2.97	195.3	196.5	194.4 ($^{TW}CCS_{N2}$)	469-> 325.0920; 163.0427; 119.0514	[16]
19	Nothofagin (Phloretin-3'-*C*-glucoside)	$[M-H]^-$	435.1365	$C_{21}H_{24}O_{10}$	3.57	3.04	198.12	199.10	190.3 ($^{TW}CCS_{N2}$)	435-> 345.1138; 315.1065; 167.0629	[6,16]
20	Quercetin	$[M-H]^-$	301.0374	$C_{15}H_{10}O_7$	4.72	1.93	157.1	162.44	158.6 ($^{TW}CCS_{N2}$) 156.0 ($^{TW}CCS_{N2}$) 165.5 ($^{DT}CCS_{N2}$)	301-> 179.0226; 151.0227	Standard; [16,37,40]
21	Diosmetin	$[M-H]^-$	299.0561	$C_{16}H_{12}O_6$	5.48	2.07	163.43	168.24	161.1 ($^{TW}CCS_{N2}$)	299-> 284.0233	[41]

Table 5.2: List of compounds tentatively identified in *Cyclopia* samples, showing retention time, drift time, precursor ion, elemental composition, MS^E fragments, $^{TW}CCS_{N2}$ values, and literature references from which the compounds were previously detected.

Compound number	**Compound Name**	**Adduct**	***m/z***	**Chemical formulae**	**t_R (min)**	**t_D (ms)**	**$^{TW}CCS_{N2}$ (Å^2) Poly-DL-alanine calibrant**	**$^{TW}CCS_{N2}$ (Å^2) Poly-L-malic acid calibrant**	**CCS_{N2} (Å^2) in Literature**	**Fragments**	**References**

22	Quinic acid	$[M-H]^-$	191.0545	$C_7H_{12}O_6$	0.50	1.24	123.5	131.7	-	191-> 173.0362; 111.0246	-
23	(Iso)citric acid	$[M-H]^-$	191.0188	$C_6H_8O_7$	0.75	1.10	119.1	122.8	-	191-> 173.0214; 154.9474; 111.0240	-
1	Piscidic acid	$[M-H]^-$	255.0499	$C_{11}H_{12}O_7$	1.48	1.66	143.0	151.7	145.7 ($^{TW}CCS_{N2}$)	255-> 165.0522; 72.9512	[16]
24	Iriflophenone-3-*C*-glucoside-4-*O*-glucoside	$[M-H]^-$	569.1556	$C_{25}H_{30}O_{15}$	1.50	4.42	238.1	234.0	-	569-> 479.1248; 449.1089; 317.0569; 287.0550; 167.0361; 125.0262	Standard
25	Dihydroxybenzoic acid	$[M-H]^-$	153.0182	$C_7H_6O_4$	1.66	1.10	116.0	124.8	118.6 ($^{TW}CCS_{N2}$)	153-> 109.0242	[37]
26	Iriflophenone-3-*C*-glucoside	$[M-H]^-$	407.0991	$C_{19}H_{20}O_{10}$	2.11	2.76	188.7	190.8	-	407-> 317.0648; 287.0566; 245.0443; 125.0217	Standard
27	Dihydroxybenzoic acid-di-pentose	$[M-H]^-$	417.1012	$C_{17}H_{22}O_{12}$	2.13	2.55	180.8	183.6	-	417-> 153.0048; 152.0031; 108.0418	[14]
3	Phenylpyruvic acid-*O*-glucoside (PPAG) isomer 1	$[M-H]^-$	325.0923	$C_{15}H_{18}O_8$	2.19	2.21	164.8	173.1	173.7 or 169.0 ($^{TW}CCS_{N2}$)	325-> 163.0389; 119.0499	[43]
28	PPAG derivative	$[M-H]^-$	457.1352	$C_{20}H_{26}O_{12}$	2.33	2.83	190.5	192.3	-	457-> 163.0473; 119.0575	[14]
29	Mangiferin (Norathyriol-2-*C*-glucoside)	$[M-H]^-$	421.0770	$C_{19}H_{18}O_{11}$	2.58	2.76	188.5	190.6	-	421-> 331.0475; 301.0356; 271.0263; 243.0292	Standard
30	Isomangiferin (Norathyriol-4-*C*-glucoside)	$[M-H]^-$	421.0764	$C_{19}H_{18}O_{11}$	2.67	2.83	191.0	192.8	-	421-> 331.0475; 301.0356	Standard
31	Naringenin-5-*O*-neohesperidoside isomer 1	$[M-H]^-$	579.1703	$C_{27}H_{32}O_{14}$	2.84	3.80 and 4.35	220.5 and 236.1*	218.6 and 232.2*	-	579-> 271.0547; 151.0075; 119.0488	[44]
32	Naringenin-5-*O*-neohesperidoside isomer 2	$[M-H]^-$	579.1724	$C_{27}H_{32}O_{14}$	2.92	3.80 and 4.35	220.5 and 236.1*	218.6 and 232.2*	-	579-> 271.0514; 151.0106; 119.0454	[44]

33	Eriocitrin (Eriodictyol-7-*O*-rutinoside)	$[M-H]^-$	595.1653	$C_{27}H_{32}O_{15}$	3.14	4.07	228.1	225.3	-	595-> 433.1095; 287.0552; 151.0027;135.0417	Standard
34	Naringenin-*O*-hexoside	$[M-H]^-$	433.1122	$C_{21}H_{22}O_{10}$	3.25	2.69	200.5	201.2	-	433-> 271.0538; 151.0134; 119.0492	[14]
35	Scolymoside (Luteolin-7-*O*-rutinoside)	$[M-H]^-$	593.1523	$C_{27}H_{30}O_{15}$	3.30	4.07	228.2	225.3	-	593-> 285.0393	Standard
36	Phloretin-3',5'-di-*C*-glucoside	$[M-H]^-$	597.1813	$C_{27}H_{34}O_{15}$	3.32	4.07	228.1	225.3	-	597-> 477.1129; 417.1434; 387.1098; 357.0869; 209.0663	Standard
37	Hesperidin (Hesperetin-7-*O*-rutinoside)	$[M-H]^-$	609.1797	$C_{28}H_{34}O_{15}$	3.77	4.21 and 4.55	231.9 and 241.2*	228.6 and 236.6*	233.1 ($^{TW}CCS_{N2}$)	609-> 301.0699	Standard; [37]
38	Apigenin	$[M-H]^-$	269.0472	$C_{15}H_{10}O_5$	3.89	1.79	151.3	157.2	151.0 ($^{TW}CCS_{N2}$)	269-> 201.0330; 151.0083	Standard; [37]
39	Eriodictyol	$[M-H]^-$	287.0553	$C_{15}H_{12}O_6$	4.53	1.93	157.4	162.8	-	287-> 151.0018; 135.0490; 125.1184; 107.0123	Standard
40	Neoponcirin (Isosakuranetin-7-*O*-rutinoside)	$[M-H]^-$	593.1779	$C_{28}H_{34}O_{14}$	4.58	4.55	241.3	236.7	-	593-> 285.0940; 270.0738	Standard
41	Luteolin	$[M-H]^-$	285.0388	$C_{15}H_{10}O_6$	4.71	1.86	154.2	159.9	154.0 ($^{TW}CCS_{N2}$)	285-> 243.0426; 151.0200; 133.0291; 121.1107; 107.0107	Standard; [37]
20	Quercetin	$[M-H]^-$	301.0374	$C_{15}H_{10}O_7$	4.72	1.93	157.1	162.44	158.6 ($^{TW}CCS_{N2}$) 156.0 ($^{TW}CCS_{N2}$) 165.5 ($^{DT}CCS_{N2}$)	301-> 179.0226; 151.0227	Standard; [16,37,40]
42	Naringenin	$[M-H]^-$	271.0616	$C_{15}H_{12}O_5$	5.14	1.86	154.6	160.3	164.9 ($^{DT}CCS_{N2}$)	271-> 177.0217; 151.0051; 119.0499; 107.0157	[40]

43	Hesperetin	$[M-H]^-$	301.0708	$C_{16}H_{14}O_6$	5.44	2.14	166.4	171.0	166.1 ($^{TW}CCS_{N2}$)	301-> 286.0517; 257.0722; 242.0540; 199.0467; 174.0360; 164.0103; 151.0026; 136.0261	Standard; [37]

*prototropic ions

5.3.1. DI-IM-MS application in the authentication of herbal teas

DI-IM-MS mobilograms (Figure 5.1) show that the overall phenolic profile of these teas are overtly different, where the presence of the isomeric *C*-glycosylxanthones (at *m/z* 421 $[M - H]^-$, ($C_{19}H_{18}O_{11}$) drifting at drift time (t_D) 2.76 (millisecond) ms for mangiferin (**29**) and t_D 2.83 ms for isomangiferin (**30**)) is characteristic of the three honeybush species[3,14] and the presence of isomeric *C*-glycosylflavones (at *m/z* 447 $[M - H]^-$, ($C_{21}H_{20}O_{11}$) drifting at t_D 2.83 ms for orientin (**9**) and t_D 3.11 ms for isoorientin (**8**)) is characteristic of rooibos tea.[16] However, rapid strategies to authenticate products of these herbal teas and prevent counterfeits are required. Recently, energy-dispersive X-ray fluorescence spectrometry (EDXRF) for elemental analysis and a one-class classification approach was applied for the authentication of rooibos and honeybush based on the elemental composition.[32] The authors note the potential use of EDXRF analysis combined with one-class classification approach for the routine authentication of honeybush and rooibos teas, as well as in the differentiation of *Cyclopia* spp. based on their elemental composition.

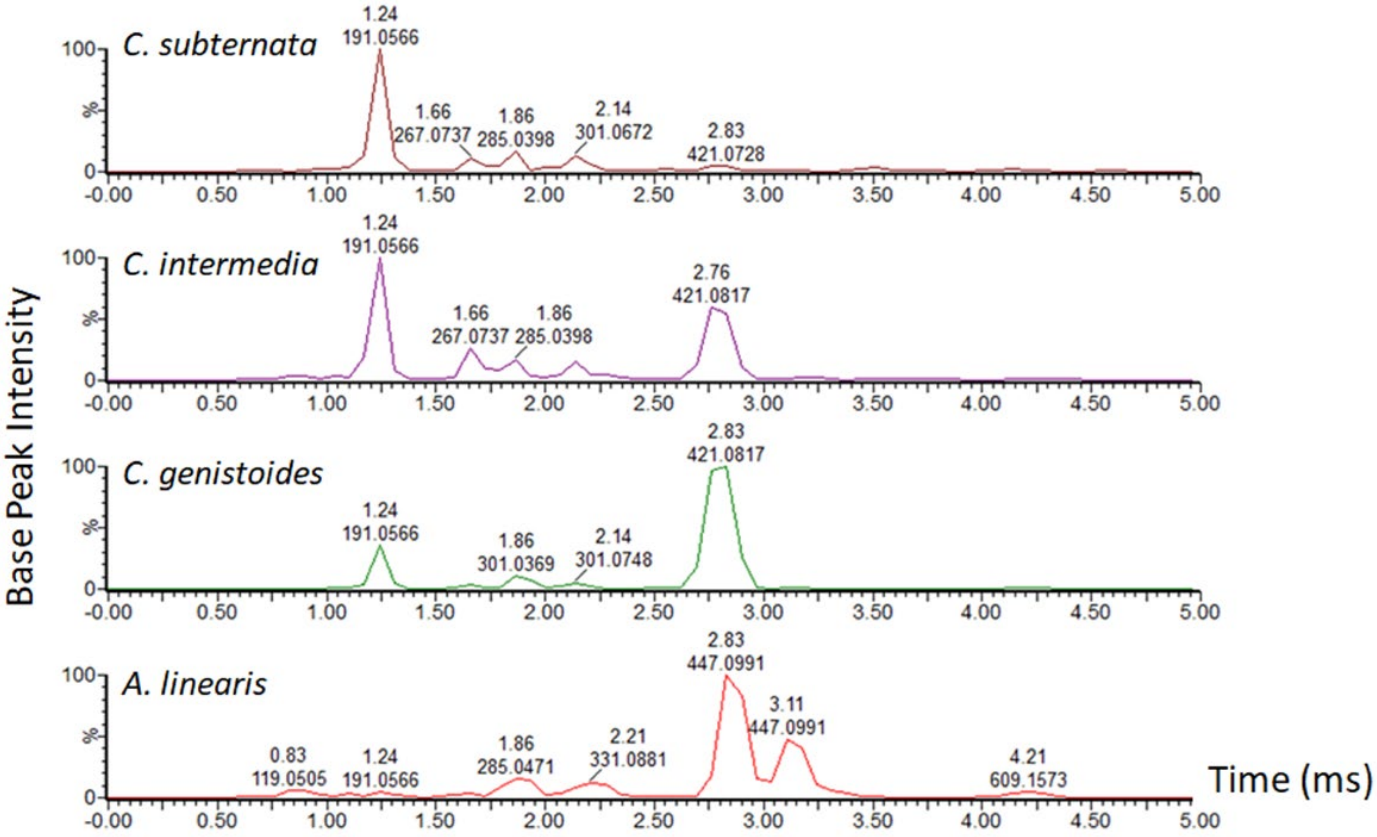

Figure 5.1: Stacked DI-IM-MS base peak ion (BPI) mobilograms illustrating the different profiles between the studied extracts of rooibos (*Aspalathus linearis*) and the three commercialized *Cyclopia* species (*C. genistoides, C. intermedia and C. subternata*).

In this study, based on the phenolic composition analysed by DI-IM-MS, a principal component analysis scores plot of 100 rooibos and the 130 honeybush (100 *C. intermedia*, 15 *C. genistoides* and 15 *C. subternata*) samples was constructed (data not shown), and the rooibos samples were observed to be completely different from the honeybush samples, as is evident in Figure 5.1. In the adulteration study, for simplicity pooled samples (with technical replicates) of the respective teas were compared with the blend samples. Blends of rooibos and *C. intermedia* at varying concentrations (1, 5, 20, 50, 80, 95 and 99% HB) were prepared. The PCA scores plot (Figure 5.2) was constructed between component 1 and component 2 (78.2% of the variance of the data set).

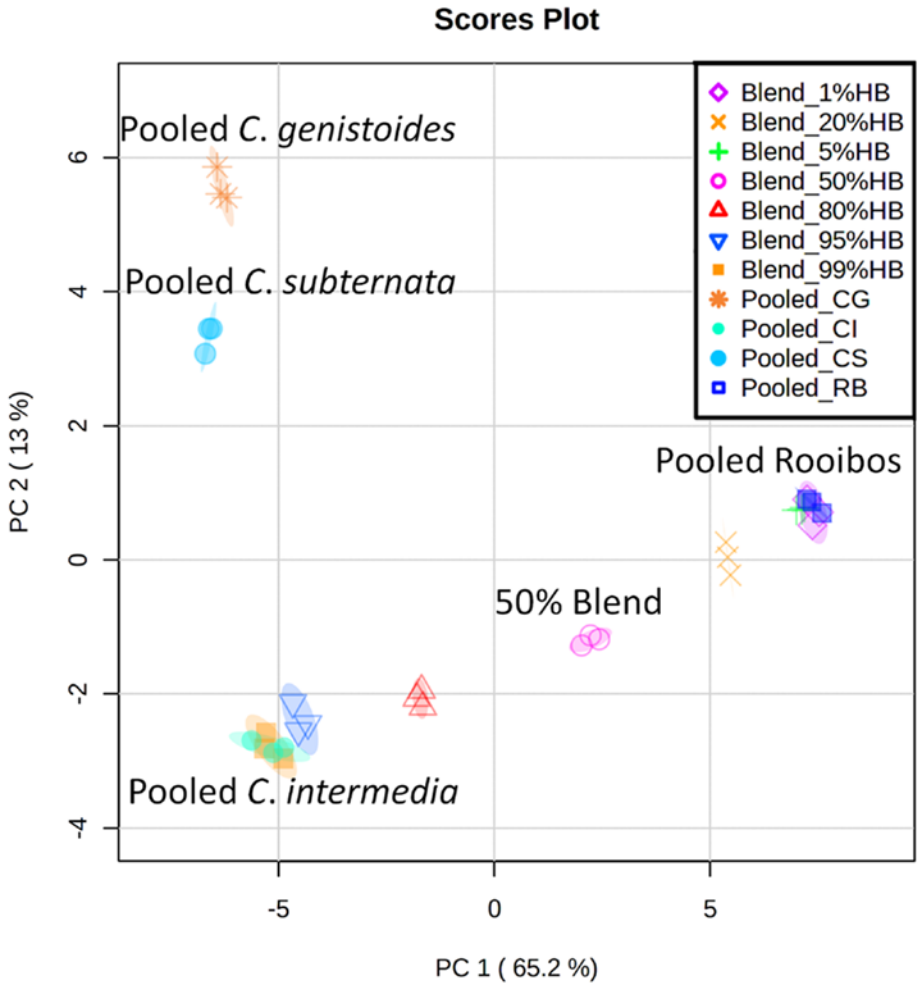

Figure 5.2*:* Principal component analysis (PCA) score plot showing the groupings of the pooled samples of *C. genistoides* (Pooled_CG), *C. intermedia* (Pooled_CI), *C. subternata* (Pooled_CS), rooibos (Pooled_RB) and prepared blend samples of 1, 5, 20, 50, 80, 95 and 99% honeybush (HB). Samples were analyzed by DI-IM-MS.

The scores plot shows no distinguishable differences between the blends at 1% and 5% to the respective authentic herbal teas (rooibos or *C. intermedia*). Whereby 1% HB represents

rooibos/*C. intermedia* (99:1), 5% HB refers to rooibos/*C. intermedia* (95:5), 95% HB refers to rooibos/*C. intermedia* (5:95), and 99% HB represents rooibos/*C. intermedia* (1:99). However, 50% and 80% blends are distinguishable from the respective authentic teas. In the context of the geographical indication (GI) for rooibos, a product should contain a minimum of 80% rooibos for it to be described as a rooibos product on the label. For the 80% rooibos blends (labelled 20% HB representing rooibos/*C. intermedia* (80:20)), markers such as eriodictyol-*C*-hexose isomers (**4-6**), orientin (**9**), aspalathin (**10**), and vitexin (**13**) are characteristic (Figure 5.3). Furthermore, marker compounds for 80% *C. intermedia* (80% HB) blends were observed to be quinic acid (**22**), iriflophenone-3-*C*-glucoside-4-*O*-glucoside (**24**), *C*-glycosylxanthones isomers (mangiferin (**29**) and isomangiferin (**30**)), and eriodictyol (**39**) (Figure 5.3).

5.3.2. DI-IM-MS application in species discrimination in the genus *Cyclopia*

Of the 23 known *Cyclopia* species, commercialized crop and product development is mainly focused on the three species *C. genistoides*, *C. intermedia* and *C. subternata*.[5,14,43] *Cyclopia* species are sometimes pooled together to produce honeybush products,[9] a problem for quality control purposes. Previously, Stander *et al.*[14] utilized UPLC-HR-MS for the analysis of the phenolic variation in 15 *Cyclopia* species, where the three commercialized species (*C. genistoides*, *C. intermedia* and *C. subternata*) required the exclusion of mangiferin and citric acid from the data set to aid in differentiation on the PCA scores plot. A run time of 38 minutes was required to chromatographically separate all the important isomers. However, analysis using DI-IM-MS shows that there are phenolic variations between the three commercialized species (Figure 5.1). The mobilograms for the three species with the respective three technical replicates per sample (15 samples of C. *genistoides*, 100 *C. intermedia* and 15 *C. subternata*) were aligned to allow for multivariate data analysis (MVDA).

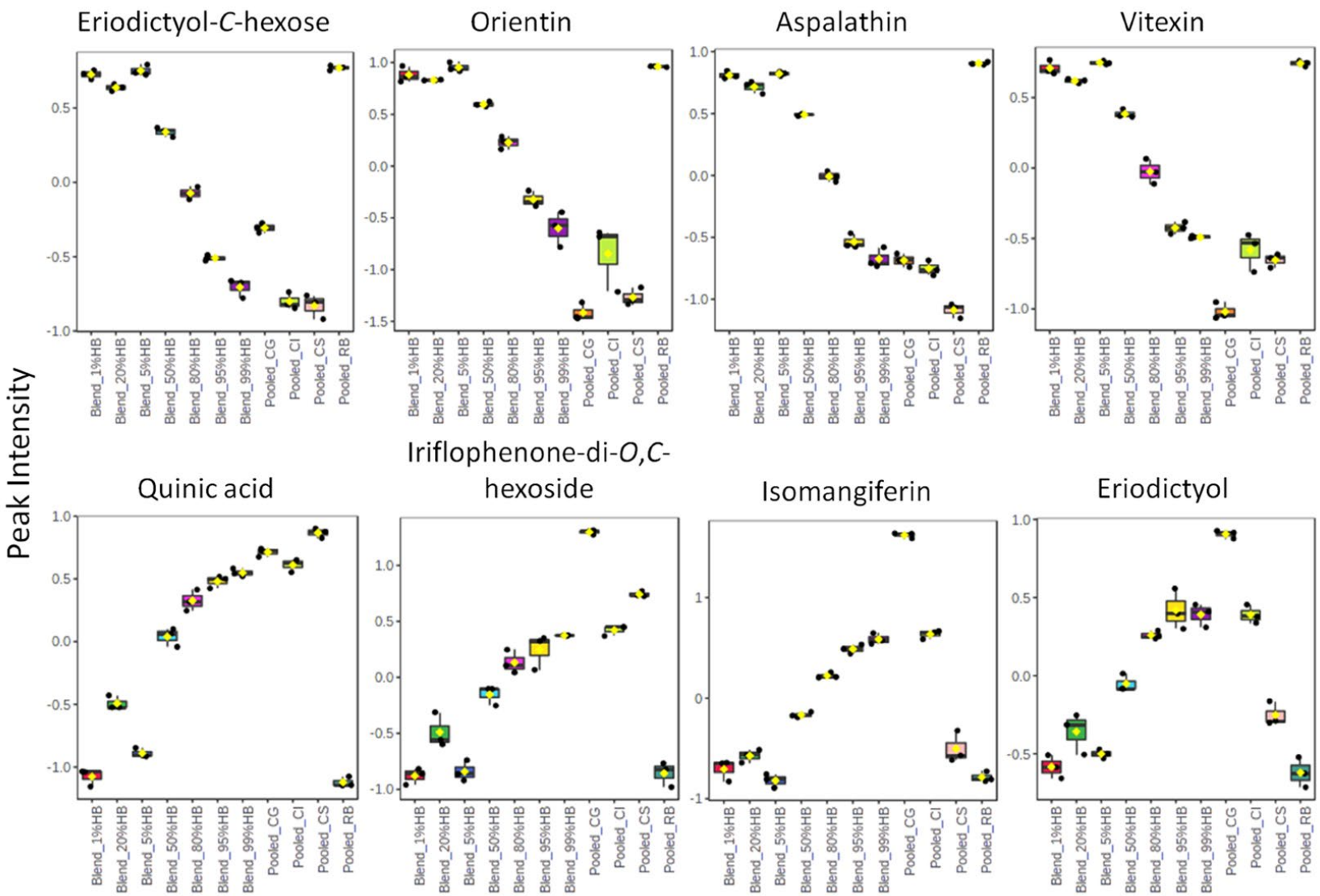

Figure 5.3*:* Boxplots showing marker compounds that can be targeted to authenticate 80% rooibos products (eriodictyol-*C*-hexose isomers (**4-6**), orientin (**9**), aspalathin (**10**), and vitexin (**13**)) and 80% *C. intermedia* products (quinic acid (**22**), iriflophenone-3-*C*-glucoside-4-*O*-glucoside (**24**), *C*-glycosylxanthones isomers (mangiferin (**29**) and isomangiferin (**30**)), and eriodictyol (**39**). All significant differences are based on ANOVA with $p \leq 0.01$.

From the data matrix, features that did not correspond to molecular ions (i.e., formic acid adducts, dimers, fragment ions, etc.) were removed for further MVDA (Figure 5.4A and 5.4B). The PCA scores plot (Figure 5.4A) was constructed, 51.2% of the variance of the data set. From scores plot, the *C. intermedia* samples show intermediate differences when compared to the other two species studied.[3] With some *C. intermedia* samples showing similarities to the *C. genistoides* and *C. subternata* samples. To observe the diagnostic value of using phenolic compounds to distinguish between these species, particularly between *C. genistoides* and *C. subternata*, a heatmap was constructed (Figure 5.4B).

The heatmap reiterated the some observations discussed in Stander *et al*.[14] Simply, quercetin (**20**), iriflophenone-3-*C*-glucoside-4-*O*-glucoside (**24**), iriflophenone-3-*C*-glucoside (**26**), the *C*-glycosylxanthones isomers (mangiferin (**29**) and isomangiferin (**30**)),[14] and hesperetin (**43**) are prominent in *C. genistoides* samples, quinic acid (**22**), scolymoside (**35**), and hesperidin (**37**) are prominent in *C. subternata* samples, and piscidic acid (**1**) and a PPAG derivative (**28**) are prominent in *C. intermedia* samples. These observations show IMS' ability to rapidly distinguish between the three species for quality control purposes without the need for long chromatographic runs.

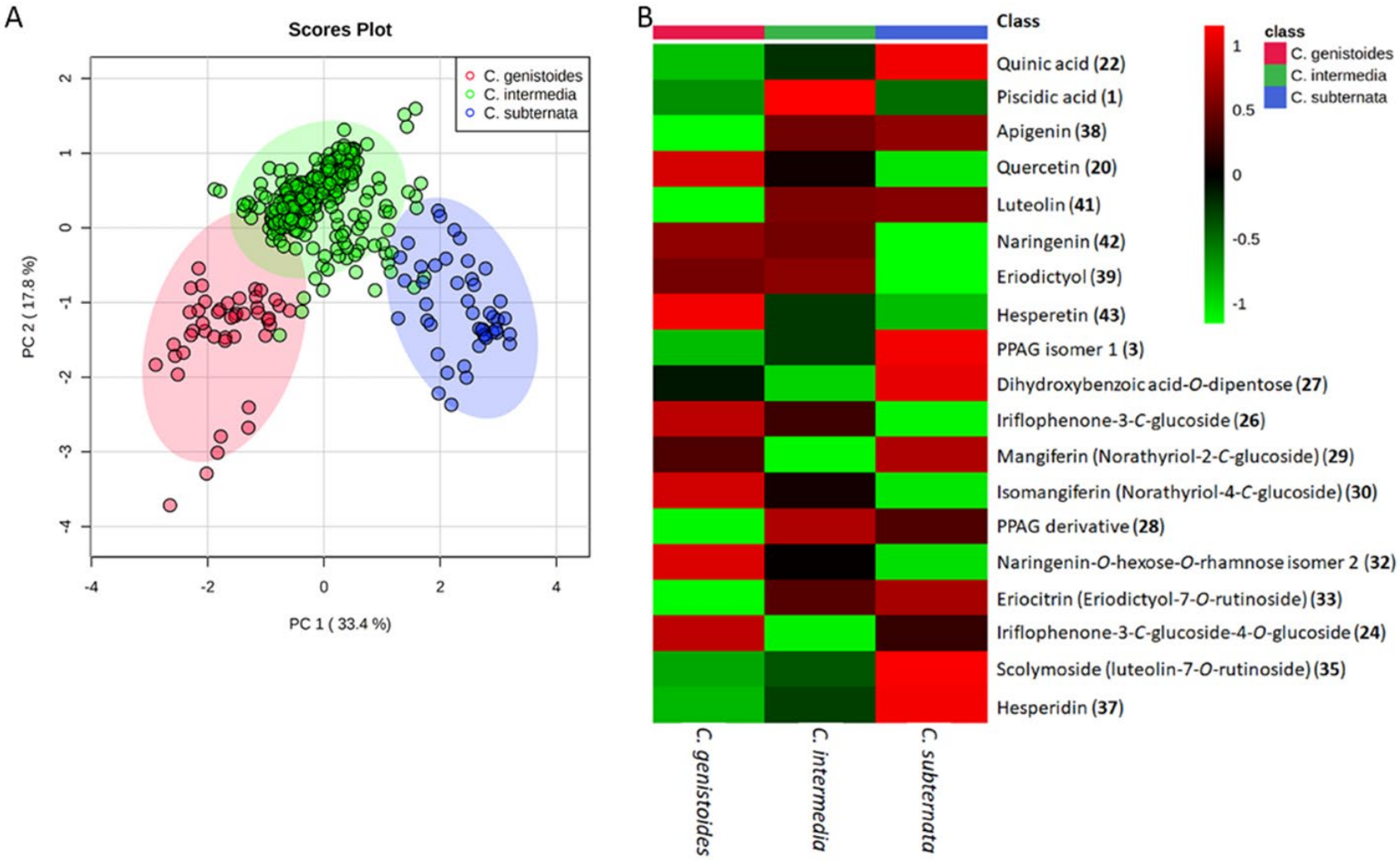

Figure 5.4: PCA scores plots (**A**), and a heatmap (**B**) showing the phenolic differences between three *Cyclopia* species (*C. genistoides*, *C. intermedia* and *C. subternata*). Simply, the *C*-glycosylxanthones isomers (mangiferin (**29**) and isomangiferin (**30**)) are prominent in *C. genistoides* samples, quinic acid (**22**) is prominent in *C. subternata* samples, and piscidic acid (**1**) is prominent in *C. intermedia* samples.

5.3.3. Quantitation of phenolics and flavonoids in the rooibos and honeybush extracts

Due to the purported benefits of polyphenolic compounds in these herbal teas, the analytical characterization of their proportions (concentration) in a mixture can assist in identifying tea counterfeits. LC-MS is the go-to analytical technique, however longer chromatographic runs are often required for the separation of the polyphenols, such as isomeric compounds. Therefore, direct and rapid analyses, such DI-IM-MS, is an intriguing approach. In this study, two approaches were evaluated (using DI-IM-MS and UPLC-MS), whereby a standard mixture made of 11 target phenolics, unique to rooibos and honeybush, were analysed. External calibration was performed, and 12 concentration points were used to quantify the 11 unique phenolics in the respective 230 herbal teas. When compared, the calibration curves in the standard solutions obtained through UPLC-MS were linear (regression coefficient $R^2 > 0.995$). However, a nonlinear (sigmoidal) calibration curve (regression coefficient $R^2 > 0.955$) was observed for analyses obtained through DI-IM-MS. At a higher concentration (125 µg/mL), during DI-IM-MS analyses, signal suppression is observed for all the standard solutions, suggesting matrix effects or detector saturation.[46,47] Due to the lack of chromatographic separation during direct injection (DI-IM-MS), "co-eluting" analytes negatively affect the ionisation efficiency of each respective analyte,[47–49] thus impairing quantification.[47] To improve the shape of the curve, Zabell *et al*. suggests adding data points at the point (inflection point) at which the curve deviates from linearity (62.5 µg/mL).[50]

Due to the nonlinear calibration curve and matrix suppression observed during DI-IM-MS analyses, quantification of the 11 compounds in the respective 230 herbal tea samples were determined using UPLC-MS, as shown by the bar graphs with the concentration presented as mean±standard deviation (Supplementary information, Figure S1). The concentration ranges of iriflophenone-3-*C*-glucoside-4-*O*-glucoside, iriflophenone-3-*C*-glucoside, iso- and mangiferin, iso- and orientin, aspalathin, eriocitrin, rutin, scolymoside, phloretin-3',5'-*C*-diglucoside, nothofagin and quercetin in the herbal teas are summarized in Table 5.3. Due to lack of chromatographic separation, isomangiferin and mangiferin, as well as isoorientin and orientin were quantified together. From Table 5.3, iriflophenone-3-*C*-glucoside-4-*O*-glucoside (**24**), iriflophenone-3-*C*-glucoside (**26**), iso- and mangifern (**29** and **30**), erioctrin (**33**), scolymoside (**35**), and phloretin-3',5'-*C*-diglucoside (**36**) were exclusively quantified in the honeybush samples, whereas iso- and orientin (**8** and **9**), aspalathin (**10**), rutin (**12**), nothofagin (**19**), and quercetin (**20**) were exclusively quantified in rooibos samples. Previously, a HPLC-diode-array detection method was used for quantitation of phenolic compounds in rooibos plant material extracted with hot water and 40% acetonitrile.[17]

Table 5.2: Linear range, regression equations and correlaton coefficients of phenolics in herbal teas

Compound Name	Formula	*m/z*	t_R (min)	Regression equation (y= ax + b)	R^2	MLOQ (g/100g)	MLOD (g/100g)	Concentration range (g/100g)				Reproduciblity (%RSD, n=3)			
								CS	CI	CG	RB	CS	CI	CG	RB
Iriflophenone-3-*C*-glucoside-4-*O*-glucoside	$C_{25}H_{30}O_{15}$	569.1718	1.50	y = 0.9891x + 0.1915	0.999	0.022	0.0072	0.1-0.30	0.33-1.51	0.3-0.74	nd	4	6	1	nd
Iriflophenone-3-*C*-glucoside	$C_{19}H_{20}O_{10}$	407.1076	2.11	y = 0.9345x + 1.3306	0.999	0.021	0.007	nd	0.1-0.78	0.1-0.26	nd	nd	3	6	nd
Iso- and Mangiferin	$C_{19}H_{18}O_{11}$	421.0770	2.58	y = 0.9789x + 0.3526	0.999	0.022	0.007	0.03-0.30	0.36-1.46	0.85-1.62	nd	4	5	2	nd
Iso- and Orientin	$C_{21}H_{20}O_{11}$	447.0991	3.02	y = 0.9682x + 0.6296	0.996	0.042	0.014	nd	nd	nd	0.38-0.74	nd	nd	nd	1
Aspalathin	$C_{21}H_{24}O_{11}$	451.1288	3.08	y = 0.9814x + 0.3617	0.997	0.035	0.011	nd	nd	nd	0.30-1.23	nd	nd	nd	1
Eriocitrin	$C_{27}H_{32}O_{15}$	595.1805	3.14	y = 0.9157x + 1.7218	0.998	0.031	0.010	nd-0.13	0.03-0.35	nd-0.13	nd	29	1	8	nd
Rutin	$C_{27}H_{30}O_{16}$	609.1434	3.23	y = 0.903x + 1.988	0.997	0.038	0.013	nd	nd	nd	0.21-0.60	nd	nd	nd	5
Scolymoside	$C_{27}H_{30}O_{15}$	593.1667	3.30	y = 0.952x + 0.9673	0.999	0.012	0.004	0.02-0.27	nd-0.19	0.01-0.18	nd	2	2	2	nd
Phloretin-3',5'-*C*-diglucoside	$C_{27}H_{34}O_{15}$	597.1813	3.32	y = 0.9722x + 0.5447	0.999	0.010	0.003	nd-0.04	0.01-0.15	0.01-0.17	nd	2	25	7	nd
Nothofagin	$C_{21}H_{24}O_{10}$	435.1365	3.57	y = 0.9839x + 0.3062	0.998	0.034	0.011	nd	nd	nd	0.08-0.41	nd	nd	nd	5
Quercetin	$C_{15}H_{10}O_7$	301.0575	4.72	y = 1.0113x - 0.2663	0.999	0.018	0.006	nd	nd	nd	0.35-1.05	nd	nd	nd	5

CS refers to *C. subternata*, CI refers to *C. intermedia*, CG refers to *C. genistoides*, and RB refers to *A. linearis* samples, nd - Not detected, MLOQ – method limit of quantitation, MLOD method limit of detection.

When the results obtained by Walters *et al*.[17] were compared with those obtained in this study, an intermediate concentration range for iso- and orientin, aspalathin, rutin, and nothofagin was observed (Table 5.3) and this is due to the methanol/water/formic acid (50:48:2) extracton solvent used. The repeatability of the method was tested by reinjecting the same samples three times and the relative standard deviatons (RSDs) between 1 and 29% were observed (the two very high values were for compounds that occur in low concentrations) (Table 5.3).

A direct and rapid analyses, such as DI-IM-MS, would be ideal for quantification however as stated above a nonlinear calibration curve was observed. However future intentions involve the use of previously quantified extracts as reference materials for the quantification of other phenolics in plant extracts, as this will account for the matrix effects. This approach can also help in situations whereby standards are unavailable. In an ideal world one would prefer to use labelled internal standards or do standard addition, but it is not practical or viable for such a complex mixture. Recently, Fenclova *et al*. studied silymarin flavonolignans in milk thistle extracts and noted that compared to the UPLC-MS quantitative data, the addition of ion mobility (UPLC-IMS-MS) to the quantitative approach demonstrated an extended linear range, lower detection limits and total separation of analytes of interest from interferences.[51] Thus, highlighting the applicability and benefits of ion mobility in quantitation, specifically when coupled with chromatographic separation.

5.3.4. Collision cross-section (CCS) as a complimentary identification metric

The main application of IMS is to eventually use CCS values, in addition to MS data, as a descriptor for the identification of unknown compounds. Where adding the IM dimension to LC-MS/MS workflows, allows species to be characterized based on an array of complementary descriptors (e.g. retention time, accurate mass information, tandem MS, and drift time) which helps increase molecular information content and specificity in structural identification.[16,38–42,52–56] The rooibos and honeybush samples were analysed using DI-TWIMS-MS and UPLC-MS^E and the phenolic compounds were characterized based on the above-mentioned descriptors (Table 5.1 and 5.2). To derive CCS values using a TWIMS instrument calibrants are required,[34] poly-DL-alanine is a common calibrant however calibration errors have been noted when the analyte under study is structurally and chemically different from that of the calibrant.[57,58] Poly-DL-alanine covers a mass range 231 to 1012 Da, this makes the determination of the CCS values for smaller compounds (< 231 Da) subject to higher CCS errors. For the analysis of negatively charged analytes under 1 kDa (such as phenolics), poly-L-malic acid (n=1 to n=8, mass range 134 to 946 Da) as a calibrant was proposed.[35] In this study, CCS values were determine using both poly-DL-

alanine and poly-L-malic acid as calibrants (Table 5.1 and 5.2) and these were further compared to CCS values obtained from literature. Most of the available CCS values in literature were obtained using a TWIMS instrument and poly-DL-alanine as a calibrant for the studied phenolic compounds,[16,37–39,41,42] making comparisons between the two calibrants difficult. Poly-DL-malic acid does seem to improve the underestimation of CCS values below 200 Å^2, as previously discussed[41] when compared to poly-DL-alanine obtained $^{TW}CCS_{N2}$ values.

Furthermore, an interesting drift time profile was observed for the flavonoid isomer pairs (6-*C* and 8-*C*-glycosylflavone isomer pairs (orientin (**9**)/isoorientin (**8**) and vitexin (**13**)/isovitexin (**14**)) and the 2-*C* and 4-*C*-glycosylxanthone pair (mangiferin (**29**)/isomangiferin (**30**))). The respective pairs of the 8-*C* glycosylflavone[42] (orientin (**9**) (t_D 2.83 ms) and vitexin (**13**) (t_D 2.83 ms)) and the 2-*C*-glycosylxanthone (mangiferin (**29**) (t_D 2.76 ms)) showed earlier drift times relative to their respective isomer pairs (isoorientin (**8**) (t_D 3.11 ms), isovitexin (**14**) (t_D 3.04 ms) and isomangiferin (**30**) (t_D 2.83 ms)), a distinguishing characteristic as these isomers are known to chromatographically co-elute (as observed in this study) unless longer chromatographic runs and/or columns are used. Thus, highlighting the beneficial use of the drift time (specifically the concommitant $^{TW}CCS_{N2}$ values) to distinguish between these isomer pairs, and expediting compound identification.

5.4. Conclusion

This study demonstrates the potential use of direct injection-ion mobility mass spectrometry (DI-IM-MS) for the rapid assessment of adulterated herbal teas. Whereby, markers such as eriodictyol-*C*-hexose isomers (**4-6**), orientin (**9**), aspalathin (**10**), and vitexin (**13**) were characteristic of blends containing more than 80% of rooibos plant material, and quinic acid (**22**), iriflophenone-3-*C*-glucoside-4-*O*-glucoside (**24**), *C*-glycosylxanthones isomers (mangiferin (**29**) and isomangiferin (**30**)), and eriodictyol (**39**) were characteristic of blends containing more than 80% of *C. intermedia* plant material. The diagnostic value of using phenolic compounds to distinguish between the three commercialized honeybush species (*C. genistoides*, *C. intermedia* and *C. subternata*) for the quality control assessment of pooled *Cyclopia* products was observed. The quantitation of phenolic compounds using DI-IM-MS is not ideal as it is subject to matrix effects, however coupling with chromatographic separation shows potential advantage.[51] Using UPLC-HR-MS and DI-IM-MS, phenolic compounds of rooibos and honeybush were characterized based on their retention time, drift time, accurate mass information, MS^E and $^{TW}CCS_{N2}$ values.

Lastly, DI-IM-MS proved to be a useful tool for quality control purposes, particularly considering the analysis time is 1 minute per sample.

5.5. References

(1) Biénabe, E.; Marie-Vivien, D. Institutionalizing geographical indications in southern countries: Lessons learned from basmati and rooibos. *World Dev.* **2017**, *98*, 58–67. https://doi.org/10.1016/j.worlddev.2015.04.004.

(2) Joubert, E.; de Beer, D. Rooibos (*Aspalathus linearis*) beyond the farm gate: From herbal tea to potential phytopharmaceutical. *South African J. Bot.* **2011**, *77* (4), 869–886. https://doi.org/10.1016/j.sajb.2011.07.004.

(3) Joubert, E.; de Beer, D.; Malherbe, C. J.; Muller, M.; Louw, A.; Gelderblom, W. C. A. Formal honeybush tea industry reaches 20-year milestone – progress of product research targeting phenolic composition, quality and bioactivity. *South African J. Bot.* **2019**, *127*, 58–79. https://doi.org/10.1016/j.sajb.2019.08.027.

(4) Bester, C.; Joubert, M. E.; Joubert, E. A Breeding strategy for south african indigenous herbal teas. *Acta Hortic.* **2016**, *1127* (1127), 15–22. https://doi.org/10.17660/ActaHortic.2016.1127.3.

(5) Joubert, E.; Joubert, M. E.; Bester, C.; de Beer, D.; De Lange, J. H. Honeybush (*Cyclopia* Spp.): From local cottage industry to global markets — the catalytic and supporting role of research. *South African J. Bot.* **2011**, *77* (4), 887–907. https://doi.org/10.1016/j.sajb.2011.05.014.

(6) de Beer, D.; Malherbe, C. J.; Beelders, T.; Willenburg, E. L.; Brand, D. J.; Joubert, E. Isolation of aspalathin and nothofagin from rooibos (*Aspalathus linearis*) using high-performance countercurrent chromatography: Sample loading and compound stability considerations. *J. Chromatogr. A* **2015**, *1381*, 29–36. https://doi.org/10.1016/j.chroma.2014.12.078.

(7) de Beer, D.; Tobin, J.; Walczak, B.; Van Der Rijst, M.; Joubert, E. Phenolic composition of rooibos changes during simulated fermentation: Effect of endogenous enzymes and fermentation temperature on reaction kinetics. *Food Res. Int.* **2019**, *121* (December 2018), 185–196. https://doi.org/10.1016/j.foodres.2019.03.041.

(8) Stander, M. A.; Joubert, E.; de Beer, D. Revisiting the caffeine-free status of rooibos and honeybush herbal teas using specific MRM and high resolution LC-MS methods. *J. Food Compos. Anal.* **2019**, *76* (November 2018), 39–43. https://doi.org/10.1016/j.jfca.2018.12.002.

(9) Schulze, A. E.; Beelders, T.; Koch, I. S.; Erasmus, L. M.; de Beer, D.; Joubert, E. Honeybush herbal teas (*Cyclopia* Spp.) contribute to high levels of dietary exposure to xanthones, benzophenones, dihydrochalcones and other bioactive phenolics. *J. Food Compos. Anal.* **2015**, *44*, 139–148. https://doi.org/10.1016/j.jfca.2015.08.002.

(10) de Beer, D.; Schulze, A.; Joubert, E.; de Villiers, A.; Malherbe, C.; Stander, M. Food ingredient extracts of *Cyclopia subternata* (honeybush): Variation in phenolic composition and antioxidant capacity. *Molecules* **2012**, *17* (12), 14602–14624. https://doi.org/10.3390/molecules171214602.

(11) Beelders, T.; de Beer, D.; Stander, M.; Joubert, E. Comprehensive phenolic profiling of *Cyclopia genistoides* (L.) Vent. by LC-DAD-MS and -MS/MS reveals novel xanthone and benzophenone constituents. *Molecules* **2014**, *19* (8), 11760–11790. https://doi.org/10.3390/molecules190811760.

(12) Schulze, A. E.; de Beer, D.; de Villiers, A.; Manley, M.; Joubert, E. Chemometric analysis of chromatographic fingerprints shows potential of *Cyclopia maculata* (Andrews) kies for production of standardized extracts with high xanthone content. *J. Agric. Food Chem.* **2014**, *62* (43), 10542–10551. https://doi.org/10.1021/jf5028735.

(13) Jack, B. U.; Malherbe, C. J.; Huisamen, B.; Gabuza, K.; Mazibuko-Mbeje, S.; Schulze, A. E.; Joubert, E.; Muller, C. J. F.; Louw, J.; Pheiffer, C. A polyphenol-enriched fraction of *cyclopia intermedia* decreases lipid content in 3T3-L1 adipocytes and reduces body weight gain of obese Db/Db mice. *South African J. Bot.* **2017**, *110*, 216–229. https://doi.org/10.1016/j.sajb.2016.08.007.

(14) Stander, M. A.; Redelinghuys, H.; Masike, K.; Long, H.; Van Wyk, B.-E. Patterns of variation and chemosystematic significance of phenolic compounds in the genus *Cyclopia* (Fabaceae, Podalyrieae). *Molecules* **2019**, *24* (13), 2352. https://doi.org/10.3390/molecules24132352.

(15) Walters, N. A.; de Beer, D.; de Villiers, A.; Walczak, B.; Joubert, E. Genotypic variation in phenolic composition of *Cyclopia pubescens* (honeybush tea) seedling plants. *J. Food Compos. Anal.* **2019**, *78* (August 2018), 129–137. https://doi.org/10.1016/j.jfca.2019.02.006.

(16) Stander, M. A.; Van Wyk, B.-E.; Taylor, M. J. C.; Long, H. S. Analysis of phenolic compounds in rooibos tea (*Aspalathus linearis*) with a comparison of flavonoid-based

compounds in natural populations of plants from different regions. *J. Agric. Food Chem.* **2017**, *65* (47), 10270–10281. https://doi.org/10.1021/acs.jafc.7b03942.

(17) Walters, N. A.; de Villiers, A.; Joubert, E.; de Beer, D. Improved HPLC method for rooibos phenolics targeting changes due to fermentation. *J. Food Compos. Anal.* **2017**, *55*, 20–29. https://doi.org/10.1016/j.jfca.2016.11.003.

(18) Karpas, Z. Applications of ion mobility spectrometry (IMS) in the field of foodomics. *Food Res. Int.* **2013**, *54* (1), 1146–1151. https://doi.org/10.1016/j.foodres.2012.11.029.

(19) Hernández-Mesa, M.; Ropartz, D.; García-Campaña, A. M.; Rogniaux, H.; Dervilly-Pinel, G.; Le Bizec, B. Ion mobility spectrometry in food analysis: Principles, current applications and future trends. *Molecules* **2019**, *24* (15), 1–28. https://doi.org/10.3390/molecules24152706.

(20) Burnum-Johnson, K. E.; Zheng, X.; Dodds, J. N.; Ash, J.; Fourches, D.; Nicora, C. D.; Wendler, J. P.; Metz, T. O.; Waters, K. M.; Jansson, J. K.; Smith, R. D.; Baker, E. S. Ion mobility spectrometry and the omics: Distinguishing isomers, molecular classes and contaminant ions in complex samples. *TrAC - Trends Anal. Chem.* **2019**, *116*, 292–299. https://doi.org/10.1016/j.trac.2019.04.022.

(21) Dodds, J. N.; Baker, E. S. Ion Mobility Spectrometry: Fundamental Concepts, Instrumentation, Applications, and the Road Ahead. *J. Am. Soc. Mass Spectrom.* **2019**, *30* (11), 2185–2195. https://doi.org/10.1007/s13361-019-02288-2.

(22) Werres, T.; Leonhardt, J.; Jäger, M.; Teutenberg, T. Critical comparison of liquid chromatography coupled to mass spectrometry and three different ion mobility spectrometry systems on their separation capability for small isomeric compounds. *Chromatographia* **2019**, *82* (1), 251–260. https://doi.org/10.1007/s10337-018-3640-z.

(23) Dwivedi, P.; Schultz, A. J.; Hill, H. H. Metabolic profiling of human blood by high-resolution ion mobility mass spectrometry (IM-MS). *Int. J. Mass Spectrom.* **2010**, *298* (1–3), 78–90. https://doi.org/10.1016/j.ijms.2010.02.007.

(24) Räsänen, R. M.; Dwivedi, P.; Fernández, F. M.; Kauppila, T. J. Desorption atmospheric pressure photoionization and direct analysis in real time coupled with travelling wave ion mobility mass spectrometry. *Rapid Commun. Mass Spectrom.* **2014**, *28* (21), 2325–2336. https://doi.org/10.1002/rcm.7028.

(25) Shrestha, B.; Vertes, A. High-throughput cell and tissue analysis with enhanced molecular coverage by laser ablation electrospray ionization mass spectrometry using ion mobility separation. *Anal. Chem.* **2014**, *86* (9), 4308–4315. https://doi.org/10.1021/ac500007t.

(26) Arroyo-Manzanares, N.; García-Nicolás, M.; Castell, A.; Campillo, N.; Viñas, P.; López-García, I.; Hernández-Córdoba, M. Untargeted headspace gas chromatography – ion mobility spectrometry analysis for detection of adulterated honey. *Talanta* **2019**, *205* (July), 120123. https://doi.org/10.1016/j.talanta.2019.120123.

(27) Wang, X.; Rogers, K. M.; Li, Y.; Yang, S.; Chen, L.; Zhou, J. Untargeted and targeted discrimination of honey collected by *Apis cerana* and *Apis mellifera* based on volatiles using HS-GC-IMS and HS-SPME-GC–MS. *J. Agric. Food Chem.* **2019**, *67* (43), 12144–12152. https://doi.org/10.1021/acs.jafc.9b04438.

(28) Wang, X.; Yang, S.; He, J.; Chen, L.; Zhang, J.; Jin, Y.; Zhou, J.; Zhang, Y. A green triple-locked strategy based on volatile-compound imaging, chemometrics, and markers to discriminate winter honey and sapium honey using headspace gas chromatography-ion mobility spectrometry. *Food Res. Int.* **2019**, *119* (January), 960–967. https://doi.org/10.1016/j.foodres.2019.01.004.

(29) Schwolow, S.; Gerhardt, N.; Rohn, S.; Weller, P. Data fusion of GC-IMS data and FT-MIR spectra for the authentication of olive oils and honeys—is it worth to go the extra mile? *Anal. Bioanal. Chem.* **2019**, *411* (23), 6005–6019. https://doi.org/10.1007/s00216-019-01978-w.

(30) Liu, L.; Hu, C.; Liu, L.; Zhang, S.; Chen, K.; He, D. Rapid detection and separation of olive oil and camellia oil based on ion mobility spectrometry fingerprints and chemometric models. *Eur. J. Lipid Sci. Technol.* **2017**, *119* (3), 1–9. https://doi.org/10.1002/ejlt.201500463.

(31) Beelders, T.; Brand, D. J.; de Beer, D.; Malherbe, C. J.; Mazibuko, S. E.; Muller, C. J. F.; Joubert, E. Benzophenone *C*- and *O*-glucosides from *Cyclopia genistoides* (Honeybush) inhibit mammalian α-glucosidase. *J. Nat. Prod.* **2014**, *77* (12), 2694–2699. https://doi.org/10.1021/np5007247.

(32) Małyjurek, Z.; Zawisza, B.; de Beer, D.; Joubert, E.; Walczak, B. Authentication of honeybush and rooibos herbal teas based on their elemental composition. *Food Control* **2020**, September, 107757. https://doi.org/10.1016/j.foodcont.2020.107757.

(33) Paglia, G.; Williams, J. P.; Menikarachchi, L.; Thompson, J. W.; Tyldesley-Worster, R.; Halldórsson, S.; Rolfsson, O.; Moseley, A.; Grant, D.; Langridge, J.; Palsson, B. O.; Astarita, G. Ion mobility derived collision cross sections to support metabolomics applications. *Anal. Chem.* **2014**, *86* (8), 3985–3993. https://doi.org/10.1021/ac500405x.

(34) Ruotolo, B. T.; Benesch, J. L. P.; Sandercock, A. M.; Hyung, S. J.; Robinson, C. V. Ion mobility-mass spectrometry analysis of large protein complexes. *Nat. Protoc.* **2008**, *3* (7), 1139–1152. https://doi.org/10.1038/nprot.2008.78.

(35) Forsythe, J. G.; Petrov, A. S.; Walker, C. A.; Allen, S. J.; Pellissier, J. S.; Bush, M. F.; Hud, N. V.; Fernández, F. M. Collision cross section calibrants for negative ion mode traveling wave ion mobility-mass spectrometry. *Analyst* **2015**, *140* (20), 6853–6861. https://doi.org/10.1039/c5an00946d.

(36) Araujo, P. Key aspects of analytical method validation and linearity evaluation. *J. Chromatogr. B* **2009**, *877* (23), 2224–2234. https://doi.org/10.1016/j.jchromb.2008.09.030.

(37) Gonzales, G. B.; Smagghe, G.; Coelus, S.; Adriaenssens, D.; De Winter, K.; Desmet, T.; Raes, K.; Van Camp, J. Collision Cross section prediction of deprotonated phenolics in a travelling-wave ion mobility spectrometer using molecular descriptors and chemometrics. *Anal. Chim. Acta* **2016**, *924*, 68–76. https://doi.org/10.1016/j.aca.2016.04.020.

(38) Wang, Y.; Vorsa, N.; Harrington, P. D. B.; Chen, P. Nontargeted metabolomic study on variation of phenolics in different cranberry cultivars using UPLC-IM-HRMS. *J. Agric. Food Chem.* **2018**, *66* (46), 12206–12216. https://doi.org/10.1021/acs.jafc.8b05029.

(39) Yang, X.; Wei, S.; Liu, B.; Guo, D.; Zheng, B.; Feng, L.; Liu, Y.; Tomás-Barberán, F. A.; Luo, L.; Huang, D. A novel integrated non-targeted metabolomic analysis reveals significant metabolite variations between different lettuce (*Lactuca sativa*. L) varieties. *Hortic. Res.* **2018**, *5* (1), 1–14. https://doi.org/10.1038/s41438-018-0050-1.

(40) Causon, T. J.; Ivanova-Petropulos, V.; Petrusheva, D.; Bogeva, E.; Hann, S. Fingerprinting of traditionally produced red wines using liquid chromatography combined with drift tube ion mobility-mass spectrometry. *Anal. Chim. Acta* **2019**, *1052*, 179–189. https://doi.org/10.1016/j.aca.2018.11.040.

(41) Masike, K.; De Villiers, A.; Hoffman, E. W.; Brand, D. J.; Causon, T.; Stander, M. A. Detailed phenolic characterization of *Protea* pure and hybrid cultivars by liquid chromatography-ion mobility-high resolution mass spectrometry (LC-IM-HR-MS). *J. Agric. Food Chem.* **2020**,

68 (2), 485–502. https://doi.org/10.1021/acs.jafc.9b06361.

(42) McCullagh, M.; Pereira, C. A. M.; Yariwake, J. H. Use of ion mobility mass spectrometry to enhance cumulative analytical specificity and separation to profile 6-*C*/8-*C*-glycosylflavone critical isomer pairs and known–unknowns in medicinal plants. *Phytochem. Anal.* **2019**, *30* (4), 424–436. https://doi.org/10.1002/pca.2825.

(43) Joubert, E.; de Beer, D.; Malherbe, C. J.; Muller, N.; Bonnet, S. L.; van der Westhuizen, J. H.; Ferreira, D. Occurrence and sensory perception of Z-2-(β-d-glucopyranosyloxy)-3-phenylpropenoic acid in rooibos (*Aspalathus linearis*). *Food Chem.* **2013**, *136* (2), 1078–1085. https://doi.org/10.1016/j.foodchem.2012.09.014.

(44) Danton, O.; Alexander, L.; Hunlun, C.; de Beer, D.; Hamburger, M.; Joubert, E. Bitter taste impact and thermal conversion of a naringenin glycoside from *Cyclopia genistoides*. *J. Nat. Prod.* **2018**, *81* (12), 2743–2749. https://doi.org/10.1021/acs.jnatprod.8b00710.

(45) Joubert, E.; Gelderblom, W. C. A.; Louw, A.; de Beer, D. South African herbal teas: *Aspalathus linearis*, *Cyclopia* Spp. and *Athrixia phylicoides*—A review. *J. Ethnopharmacol.* **2008**, *119* (3), 376–412. https://doi.org/10.1016/j.jep.2008.06.014.

(46) Kebarle, P.; Tang, L. From ions in solution to ions in the gas phase - the mechanism of electrospray mass spectrometry. *Anal. Chem.* **1993**, *65* (22), 972A-986A. https://doi.org/10.1021/ac00070a001.

(47) Villagrasa, M.; Guillamón, M.; Eljarrat, E.; Barceló, D. Matrix effect in liquid chromatography–electrospray ionization mass spectrometry analysis of benzoxazinoid derivatives in plant material. *J. Chromatogr. A* **2007**, *1157* (1–2), 108–114. https://doi.org/10.1016/j.chroma.2007.04.040.

(48) Matuszewski, B. K.; Constanzer, M. L.; Chavez-Eng, C. M. Matrix effect in quantitative lc/ms/ms analyses of biological fluids: A method for determination of finasteride in human plasma at picogram per milliliter concentrations. *Anal. Chem.* **1998**, *70* (5), 882–889. https://doi.org/10.1021/ac971078+.

(49) Kruve, A. Strategies for drawing quantitative conclusions from nontargeted liquid chromatography–high-resolution mass spectrometry analysis. *Anal. Chem.* **2020**, *92* (7), 4691–4699. https://doi.org/10.1021/acs.analchem.9b03481.

(50) Zabell, A. P. R.; Lytle, F. E.; Julian, R. K. A Proposal to improve calibration and outlier

detection in high-throughput mass spectrometry. *Clin. Mass Spectrom.* **2016**, *2* (2016), 25–33. https://doi.org/10.1016/j.clinms.2016.12.003.

(51) Fenclova, M.; Stranska-Zachariasova, M.; Benes, F.; Novakova, A.; Jonatova, P.; Kren, V.; Vitek, L.; Hajslova, J. Liquid chromatography–drift tube ion mobility–mass spectrometry as a new challenging tool for the separation and characterization of silymarin flavonolignans. *Anal. Bioanal. Chem.* **2020**, *412* (4), 819–832. https://doi.org/10.1007/s00216-019-02274-3.

(52) Wang, Y.; de B. Harrington, P.; Chang, T.; Wu, X.; Chen, P. Analysis of cranberry proanthocyanidins using UPLC–ion mobility–high-resolution mass spectrometry. *Anal. Bioanal. Chem.* **2020**, *412* (15), 3653–3662. https://doi.org/10.1007/s00216-020-02601-z.

(53) Pacini, T.; Fu, W.; Gudmundsson, S.; Chiaravalle, A. E.; Brynjolfson, S.; Palsson, B. O.; Astarita, G.; Paglia, G. Multidimensional analytical approach based on UHPLC-UV-ion mobility-ms for the screening of natural pigments. *Anal. Chem.* **2015**, *87* (5), 2593–2599. https://doi.org/10.1021/ac504707n.

(54) Jia, L.; Zuo, T.; Zhang, C.; Li, W.; Wang, H.; Hu, Y.; Wang, X.; Qian, Y.; Yang, W.; Yu, H. Simultaneous profiling and holistic comparison of the metabolomes among the flower buds of *Panax ginseng*, *Panax quinquefolius*, and *Panax notoginseng* by UHPLC/IM-QTOF-HDMS^{E}-based metabolomics analysis. *Molecules* **2019**, *24* (11), 2188. https://doi.org/10.3390/molecules24112188.

(55) Venter, P.; Causon, T.; Pasch, H.; de Villiers, A. Comprehensive analysis of chestnut tannins by reversed phase and hydrophilic interaction chromatography coupled to ion mobility and high resolution mass spectrometry. *Anal. Chim. Acta* **2019**, *1088*, 150–167. https://doi.org/10.1016/j.aca.2019.08.037.

(56) Venter, P.; Pasch, H.; de Villiers, A. Comprehensive analysis of tara tannins by reversed-phase and hydrophilic interaction chromatography coupled to ion mobility and high-resolution mass spectrometry. *Anal. Bioanal. Chem.* **2019**, *411*, 6329–6341. https://doi.org/10.1016/j.aca.2019.08.037.

(57) Hines, K. M.; May, J. C.; McLean, J. A.; Xu, L. Evaluation of collision cross section calibrants for structural analysis of lipids by traveling wave ion mobility-mass spectrometry. *Anal. Chem.* **2016**, *88* (14), 7329–7336. https://doi.org/10.1021/acs.analchem.6b01728.

(58) Hines, K. M.; Ross, D. H.; Davidson, K. L.; Bush, M. F.; Xu, L. Large-scale structural

characterization of drug and drug-like compounds by high-throughput ion mobility-mass spectrometry. *Anal. Chem.* **2017**, *89* (17), 9023–9030. https://doi.org/10.1021/acs.analchem.7b01709.

Supplementary information for: Application of direct injection-ion mobility mass spectrometry (DI-IM-MS) for the analysis of Honeybush and Rooibos tea samples

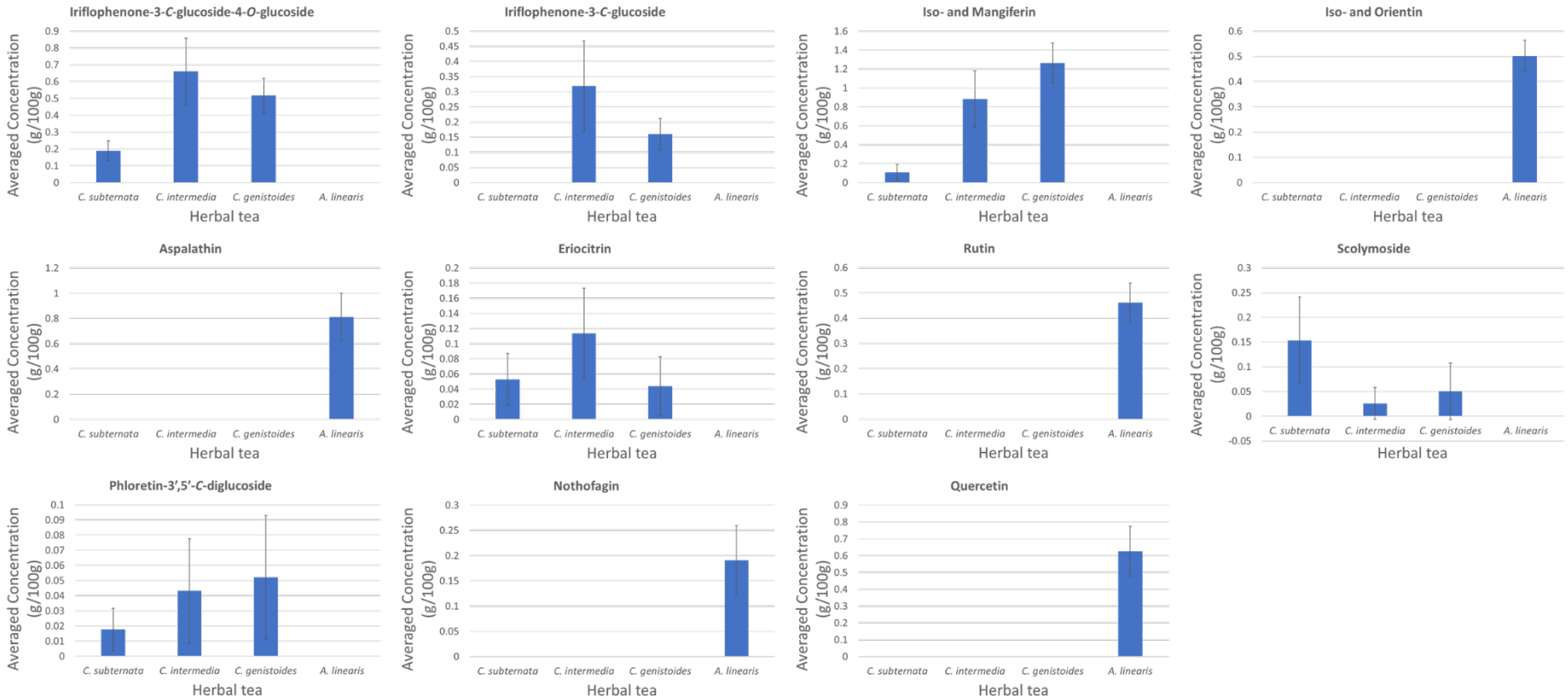

Figure S1: Bar graphs of iriflophenone-3-*C*-glucoside-4-*O*-glucoside (**24**), iriflophenone-3-*C*-glucoside (**26**), iso- and mangifern (**29** and **30**), eriocitrin (**33**), scolymoside (**35**), and phloretin-3',5'-*C*-diglucoside (**36**) were exclusively quantified in the honeybush samples, whereas iso- and orientin (**8** and **9**), aspalathin (**10**), rutin (**12**), nothofagin (**19**), and quercetin (**20**) were exclusively quantified in rooibos samples. Data are presented as mean ±standard deviation, n= 3.

Chapter 6: Conclusions and Future Recommendations

6.1. Conclusions

The combination of ion mobility spectrometry (IMS) with traditional liquid chromatography-photodiode array-ion mobility-high resolution mass spectrometry (LC-PDA-IM-HR-MS) -based analytical approaches, is shown to provide major advantages and opportunities for future analysis of complex samples. IMS allows the calculation of the collision cross sections (CCS's), which describes the unique rotationally averaged surface area of the ion, which can support phenolic compound identification across analytical laboratories, such as in plant metabolomics and food science.

Therefore, the goal of this study was to design improved LC-PDA-IM-HR-MS methods capable of structurally characterizing plant phenolics based on these analytical profiles. Using travelling wave IMS (TWIMS) hyphenated to LC-PDA-HR-MS, phenolic compounds of *Protea* species and hybrid cultivars were characterised based on their retention time (t_R), spectroscopic data, mass spectral information (including high resolution and tandem MS (MS/MS) data), and CCS value. A total of 67 phenolic compounds, including 41 phenolic acid esters and 25 flavonoid derivatives (including 5 anthocyanins) were characterised. To complement structural identification, a new hydroxycinnamic acid derivative, a possible chemo-taxonomic marker, was identified as caffeoyl-*O*-polygalatol (1,5-anhydro-[6-*O*-caffeoyl]-sorbitol(glucitol)) following 1D and 2D NMR characterization. For LC-PDA-TWIMS-HR-MS analysis, positional isomers with similar MS/MS profiles were resolved by the IMS-dimension and consequently could be distinguished by their differences in $^{TW}CCS_{N2}$ values. The accuracy of $^{TW}CCS_{N2}$ values were validated by comparative low-field $^{DT}CCS_{N2}$ values, showing that $^{TW}CCS_{N2}$ values were often underestimated for compounds with CCS values below 200 Å^2.

The experimentally derived $^{TW}CCS_{N2}$ values, from the previous study, were extended to a plant metabolomics approach designed to investigate metabolites linked to leaf blackening susceptibility of *Protea* species, selections and cultivars. Metabolites that could be of phenotypic/physiological importance in the browning process were highlighted (notably the benzenetriol and hydroquinone derivatives). These metabolites could be used as potential biomarkers of browning susceptibility in *Protea* species, selections and cultivars; thus, allowing plant breeders to select trait-specific markers to improve commercially important traits.

Finally, direct injection-IM-MS (DI-IM-MS) along with UPLC-HR-MS^E were used to characterize the phenolic compounds in herbal teas and related blends. Isomeric flavone pairs (orientin/isoorientin and vitexin/isovitexin) characteristic of rooibos tea and the xanthone isomer pair (mangiferin/isomangiferin) characteristic of honeybush teas were distinguished

based on their difference in $^{TW}CCS_{N2}$ values. These isomers are known to chromatographically co-elute, making identification difficult, however the study shows that these isomers could be differentiated using the IMS dimension. Orientin, vitexin and mangiferin had earlier drift times relative to their respective to their isomer pairs, an analytical observation that may be helpful for identification. During quantitation, the DI-IM-MS method was prone to matrix effects and/or detector saturation, while the traditional UPLC-MS method showed more linear calibration curves (R^2 > 0.995). Lastly, $^{TW}CCS_{N2}$ values obtained using poly-L-malic acid as calibrant showed an improvement in the underestimation of CCSs below 200 Å^2, when compared to those obtained using poly-DL-alanine, the commonly used calibrant.

6.2. Future recommendations

The addition of CCS values to databases and in-house libraries will help expedite the characterization of phenolic compounds in a variety of fields, such as in natural product research, food science, and plant metabolomics.

For an IMS instrument to be considered as a HR instrument, the resolving power (R_p) value should be between ~300 and up to 1000. However, commercially available IMS instruments- DTIMS and TWIMS- have relatively low R_p, between 40-60, and this is insufficient for resolving ions differing in CCS values by <1%, such stereoisomers and enantiomers. It has been announced that a 6th IMS technology hyphenated to existing MS instruments will be commercialised in 2021, that is Structures for Lossless Ion Manipulation (SLIM) IMS.[1,2] SLIM-IMS is a TWIMS-based technology and has been demonstrated to achieve ultra-high resolution.[1,3–5] Lastly, the expectation is that a collective participation of researchers in establishing CCS databases, together with the continued development in new software and hardware tools, will further accelerate the integration of IMS into routine LC-MS workflows.

6.3. References

(1) Deng, L.; Ibrahim, Y. M.; Hamid, A. M.; Garimella, S. V. B.; Webb, I. K.; Zheng, X.; Prost, S. A.; Sandoval, J. A.; Norheim, R. V.; Anderson, G. A.; Tolmachev, A. V.; Baker, E. S.; Smith, R. D. Ultra-High Resolution Ion Mobility Separations Utilizing Traveling Waves in a 13 m Serpentine Path Length Structures for Lossless Ion Manipulations Module. *Anal. Chem.* **2016**, *88* (18), 8957–8964. https://doi.org/10.1021/acs.analchem.6b01915.

(2) Paglia, G.; Smith, A. J.; Astarita, G. Ion Mobility Mass Spectrometry in the Omics Era: Challenges and Opportunities for Metabolomics and Lipidomics. *Mass Spectrom. Rev.* **2021**, *22* (8), mas.21686. https://doi.org/10.1002/mas.21686.

(3) Deng, L.; Webb, I. K.; Garimella, S. V. B.; Hamid, A. M.; Zheng, X.; Norheim, R. V.; Prost, S. A.; Anderson, G. A.; Sandoval, J. A.; Baker, E. S.; Ibrahim, Y. M.; Smith, R. D. Serpentine Ultralong Path with Extended Routing (SUPER) High Resolution Traveling Wave Ion Mobility-MS Using Structures for Lossless Ion Manipulations. *Anal. Chem.* **2017**, *89* (8), 4628–4634. https://doi.org/10.1021/acs.analchem.7b00185.

(4) Tolmachev, A. V.; Webb, I. K.; Ibrahim, Y. M.; Garimella, S. V. B.; Zhang, X.; Anderson, G. A.; Smith, R. D. Characterization of Ion Dynamics in Structures for Lossless Ion Manipulations. *Anal. Chem.* **2014**, *86* (18), 9162–9168. https://doi.org/10.1021/ac502054p.

(5) Hollerbach, A. L.; Li, A.; Prabhakaran, A.; Nagy, G.; Harrilal, C. P.; Conant, C. R.; Norheim, R. V.; Schimelfenig, C. E.; Anderson, G. A.; Garimella, S. V. B.; Smith, R. D.; Ibrahim, Y. M. Ultra-High-Resolution Ion Mobility Separations Over Extended Path Lengths and Mobility Ranges Achieved Using a Multilevel Structures for Lossless Ion Manipulations Module. *Anal. Chem.* **2020**, *92* (11), 7972–7979. https://doi.org/10.1021/acs.analchem.0c01397.

Appendix A: Recent applications of ion mobility spectrometry in natural product research

Journal of Pharmaceutical and Biomedical Analysis 195 (2021) 113846

Contents lists available at ScienceDirect

Journal of Pharmaceutical and Biomedical Analysis

journal homepage: www.elsevier.com/locate/jpba

Recent applications of ion mobility spectrometry in natural product research

Keabetswe Masike[a], Maria A. Stander[a,b], André de Villiers[c,*]

[a] Department of Biochemistry, Stellenbosch University, Private Bag X1, Matieland, 7602, South Africa
[b] Central Analytical Facility, Stellenbosch University, Private Bag X1, Matieland, 7602, South Africa
[c] Department of Chemistry and Polymer Science, Stellenbosch University, Private Bag X1, Matieland, 7602, South Africa

ARTICLE INFO

Article history:
Received 4 August 2020
Received in revised form 8 December 2020
Accepted 8 December 2020
Available online 7 January 2021

Keywords:
Natural products
Secondary metabolites
Ion mobility spectrometry (IMS)
Mass spectrometry
Liquid chromatography (LC)
Gas chromatography (GC)

ABSTRACT

Ion mobility spectrometry (IMS) is a rapid separation technique capable of extracting complementary structural information to chromatography and mass spectrometry (MS). IMS, especially in combination with MS, has experienced inordinate growth in recent years as an analytical technique, and elicited intense interest in many research fields. In natural product analysis, IMS shows promise as an additional tool to enhance the performance of analytical methods used to identify promising drug candidates. Potential benefits of the incorporation of IMS into analytical workflows currently used in natural product analysis include the discrimination of structurally similar secondary metabolites, improving the quality of mass spectral data, and the use of mobility-derived collision cross-section (CCS) values as an additional identification criterion in targeted and untargeted analyses. This review aims to provide an overview of the application of IMS to natural product analysis over the last six years. Instrumental aspects and the fundamental background of IMS will be briefly covered, and recent applications of the technique for natural product analysis will be discussed to demonstrate the utility of the technique in this field.

Contents

* Corresponding author.
E-mail address: ajdevill@sun.ac.za (A. de Villiers).

https://doi.org/10.1016/j.jpba.2020.113846
0731-7085/

1. Introduction

Natural products have been used by humanity for centuries, and since the first isolation of morphine more than 200 years ago, isolated natural products have been a consistent source of new drug molecules [1]. Indeed, based on the criteria of Newman et al., therapeutic agents based on natural products have consistently comprised ~40 % of all first-approved drugs since 1981 [1–6]. The relative success of natural products in drug discovery stems from their versatile chemical structures and physiological targets, allowing them to be effective for a range of potential clinical uses [6]. The use of natural products in drug discovery has however declined somewhat in recent years. Among the reasons for this are technical challenges associated with the identification of natural product drug leads, the advent of high throughput screening and combinatorial chemistry methods and the concomitant reduced emphasis on natural products by the pharmaceutical industry [7,8], and more recently by the rapid development of biopharmaceuticals [9]. Nevertheless, natural products continue to serve as inspiration for many new small molecule drugs [1,10], and interest in the their pharmaceutical application has been bolstered in recent years by developments in analytical technology supporting the identification of promising candidates [11].

According to a narrow but commonly accepted definition [8,12], natural products are secondary metabolites[1] . Secondary metabolites are compounds produced by both terrestrial and marine sources, including bacteria, fungi, animals and plants, that are not directly linked to the development, normal growth and the reproduction of an organism, but are produced as a response to the organism's interaction with the environment [12]. Based on their biosynthetic origin, plant secondary metabolites include phenolics (flavonoid and non-flavonoids), alkaloids and terpenoids (such as saponins, steviol glycosides, etc.) [12–15], whereas microbial secondary metabolites include peptides, polyketides, alkaloids, lipids, and terpenes [16–19]. Some secondary metabolites, such as terpenoid derivatives, carotenoids [20] and saponins [21–23], are found both in terrestrial and marine sources.

Due to their vital role in the discovery of drug candidates [24,25], the identification of secondary metabolites in what are often highly complex matrices is of paramount importance in the search for new biologically active compounds. In this endeavour, advanced analytical methods based on high resolution liquid- or gas chromatographic separation and/or mass spectrometric detection are playing an increasingly important role, especially in screening analyses prior to isolation and structural elucidation by nuclear magnetic resonance (NMR) [26].

Modern GC on high-efficiency capillary columns offers excellent performance for complex samples, with noteworthy developments in sample preparation, comprehensive two-dimensional GC (GC × GC) [27] and detectors [28,29]. On the other hand, significant recent developments in HPLC, including the use of ultra-high pressures [30], core-shell particles [31] and comprehensive two-dimensional LC (LC × LC) [32] have revolutionised the field and have played an important role in improving the performance of the technique for complex samples.

In the field of natural product analysis, however, advances in MS have arguably overshadowed those in chromatographic separations. Nowadays, exceptionally powerful high resolution and multi-stage MS instruments capable of a range of acquisition modes for different analysis goals are commercially available, and indeed are essential tools in any natural product laboratory [26,33]. Considering that the majority of natural products are non-volatile, state-of-the-art LC–MS has played an important role in the improvement of screening analyses of natural products [34–38].

The availability of high resolution (HR) MS data allows determination of analyte molecular formulae, whereas tandem MS instruments deliver fragmentation information essential for tentative identification purposes, the latter often acquired in data dependent acquisition (DDA) mode for complex unknown samples. Moreover, data-independent acquisition (DIA) strategies can be used to acquire both low- and high collision energy data in a single chromatographic run [39,40] at the expense of selectivity. These technologies greatly facilitate the tentative assignment of compounds in complex natural product extracts.

Nevertheless, chromatographic methods hyphenated to MS also show some limitations for natural product analysis. The complexity of biological matrices means that chromatographic resolution of all compounds is virtually impossible to attain, an important consideration especially in LC–MS, where mass spectra of natural products are often very similar for a given compound class, and in light of the susceptibility of electrospray ionisation (ESI) to matrix effects. Further analysis challenges include isomerisation encountered in biological samples [41,42]. HR-MS instruments can mostly resolve isobaric compounds, but cannot differentiate isomers in most cases, necessitating long chromatographic runs to aid in their separation. This has driven efforts aimed at developing analytical methods capable of rapidly separating and detecting isomeric secondary metabolites [43,44].

It is partially in the context of these limitations that the integration of ion mobility spectrometry (IMS) with MS has become such an appealing technology for the separation and detection of such structurally similar compounds [45–47]. IMS can be thought of as a form of gas-phase electrophoresis, whereby ions are separated based on their mobilities through a region filled with a buffer gas (typically either helium or nitrogen) under the influence of an electric field. The mobility of the ions is based on their physical properties (charge, size, and shape), with ions of lower masses (m/z) and/or more compact structures characterised by faster mobilities than larger and/or bulkier ions. A range of different IMS instruments have been developed based on different principles (refer to Section 2 below for a brief overview) [48–51], which may be operated as standalone or even portable instruments, or, more often, are combined with MS (IMS-MS) [52–54], and recently with gas- [48,55,56] or liquid-phase separation methods [57–61].

Due to its operational principles, IMS offers rapid (millisecond timescale) analysis of relatively simple gaseous mixtures, and indeed has been used for this purpose for many years. Hyphenation to MS represents an important adaptation that allows the identification of the separated ions based on their mass spectra, with the MS providing additional selectivity, while maintaining the high throughput benefit. In this hyphenation, IMS offers a potentially complementary separation, including possible separation of isomeric species pairs [62] which cannot be differentiated by MS, improved signal-to-noise (S/N) ratios by filtering chemical noise [63], improved MS data quality by filtering according to arrival time [45,46,64], enhanced detection of low abundance metabolites [63,65] and improved compound coverage [66]. For highly complex mixtures, though, the trend is to hyphenate IMS-MS to front-end separation techniques such as GC and HPLC. The millisecond timescale of IMS ensures that the technique is ideally suited for incorporation into such workflows, while offering the same benefits alluded to above due to the additional post-ionisation gas phase separation prior to MS detection [67–69]. A further benefit of IMS is that an ion's mobility can be converted to its collision cross section (CCS), a measure of an ion's average surface area. Measured CCS values have been shown to be exceptionally reproducible [70]. Hyphenated chromatography-IMS-MS methods allow species to be characterised based on an array of complementary descriptors (e.g.

[1] It is in this sense that the term is used in the present review

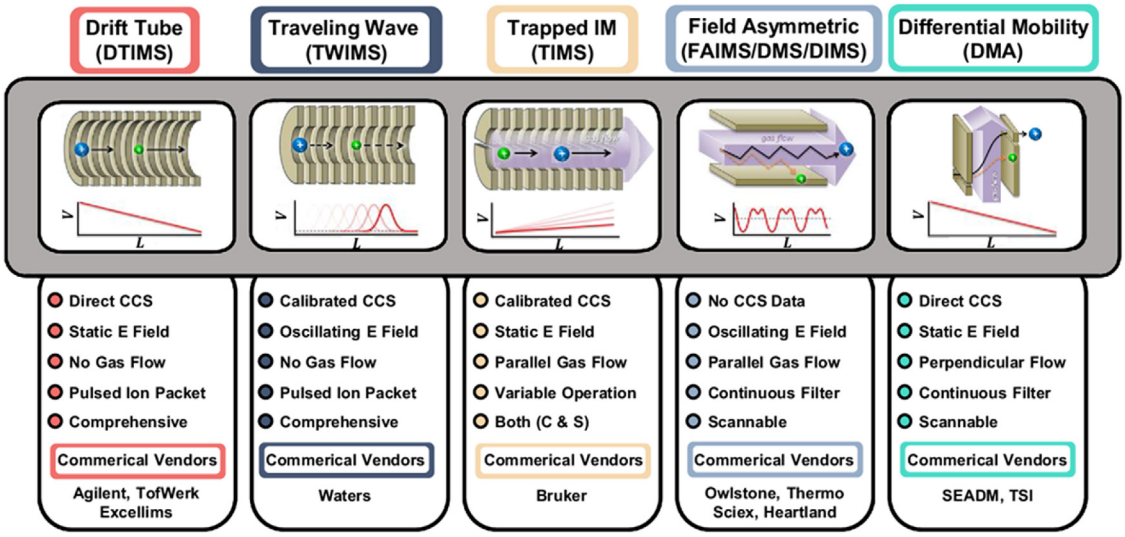

Fig. 1. The five most common IMS platforms, which separate ions either in a time-dispersive (DTIMS and TWIMS), space-dispersive (FAIMS and DMA) or ion confinement with selective release (TIMS) manner. Reprinted with permission from [50].

retention time, mass spectral information (including high resolution and tandem MS data), spectroscopic data and CCS value), which increases molecular information content and specificity in structural identification, particularly in untargeted workflows [71–74]. It is therefore not surprising that IMS has found widespread application in the analysis of complex biological samples, including most notably in the fields of proteomics [45,75–77] and lipidomics [45,78–81], but also in steroid [82] and carbohydrate [83] analysis, as well as in metabolomic studies [45,46,73,74,84–86], food analysis [87–89], and indeed in natural product analysis [26,33,90,91].

Considering the inordinate growth in the number of applications of IMS in recent years, the goal of the present review is to provide a recent update of the applications of the technique in natural product analysis. As such, this work compliments a recent overview article on the topic [91] by providing a synopsis of application papers of IMS in this area over the last six years. Related reviews focusing on natural product analysis in general [26] and by LC–MS [33] place the present contribution in context of the broader field. Furthermore, background on IMS fundamentals and instrumentation will be discussed only briefly here; readers interested in further details are referred to a number of recent dedicated reviews [48–51,56,58,92–94].

To limit the scope of the present work, we will focus on the narrow definition of natural products as secondary metabolites, and include only papers published since 2015 on the analysis of these species in samples of natural origin and foods derived from these. Special emphasis is placed on the benefits offered by IMS for secondary metabolite annotation in combination with chromatographic separation, including the potential differentiation of isomeric species. We aim to highlight the emerging benefits of IMS in the identification of natural product secondary metabolites, and discuss the advantages, limitations, and future developments in the field.

2. Ion mobility spectrometry (IMS) techniques and instrumentation

The origins of IMS can be traced back to the late 19th century [49]. The technique, referred to as plasma chromatography [95,96] and ion chromatography [97] in early literature, only found extensive analytical application since the 1970s following instrumental developments, including the hyphenation of IMS to MS from the early 1960s [98]. A major application area of IMS was (and remains) in security analyses, such as for the detection of chemical warfare agents, explosives, and drugs [51,90]. IMS was explored in biological research in the mid-1980s [99], but it was only from the 1990s, when significant advances in both IMS and MS instrumentation coincided to drastically improve performance, that a resurgence in IMS applications occurred, mostly focusing on the analysis of biomolecules [100–103]. The next decade saw the genesis of home-built IMS-MS instruments [104,105] (a process still continuing [106–115]), followed by the commercial availability of instrumentation based on travelling wave IMS-TOF in 2006 [116], drift tube IMS-TOF in 2014 [49], trapped IMS-TOF in 2016 [117] and in 2019 a cyclic IMS instrument [118]. The present work will provide a brief overview of the main IMS platforms currently in use.

2.1. IMS platforms

According to the classification introduced by May and McLean, IMS-MS instruments can be grouped based on their operational principles into time-dispersive, space-dispersive or ion confinement with selective release systems (Fig. 1) [49]. Time-dispersive techniques generate an arrival time spectrum reflecting the flow of ions past a specific location in the instrument. Drift tube IMS (DTIMS) and travelling wave IMS (TWIMS) devices are common time-dispersive platforms, where ions are directed through a stationary buffer gas. These techniques primarily differ in the applied electric field, which is a weak constant field in the case of DTIMS [95] and an oscillating electric field in the case of TWIMS [106]. Time-dispersive instruments allow all ions to be analysed simultaneously, and have found widespread application in untargeted omics approaches [49,67,72–74] as well as for targeted analyses in food and natural product research [42,69,119–124]. In ion confinement and selective release methods, such as trapped ion mobility spectrometry (TIMS), ions are trapped in position against a flow of buffer gas using an electric field, and released according to their mobilities as the electric field is incrementally decreased [50,94]. In space-dispersive platforms such as field asymmetric IMS (FAIMS; also known as differential mobility spectrometry (DMS) or differential IMS (DIMS)) and the differential mobility analyser (DMA), an electric field and carrier gas flow are used to direct ions of different mobilities along different drift paths, resulting in their separation in space [50,51].

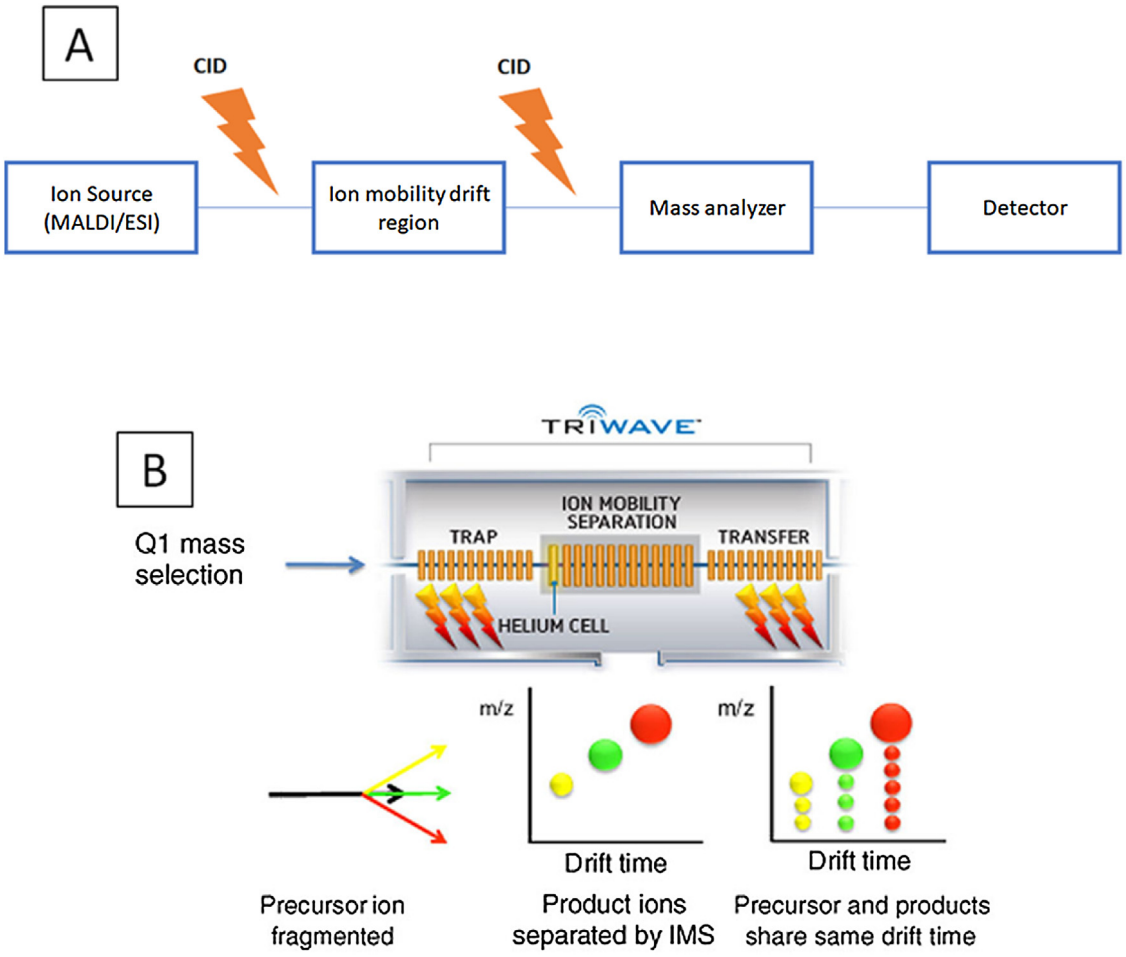

Fig. 2. (A) A simplified schematic of an IMS-MS instrumental configuration. Depending on manufacturer design, fragmentation can occur before or after IMS separation. (B) On a commercial TWIMS instrument, fragmentation can occur before and/or after IMS separation; the time-aligned-parallel (TAP) procedure is illustrated where fragmentation occurs in both trap and transfer ion guides. (B) is reprinted with permission from [126].

2.2. IMS-MS instrument configurations

Commercial instrumentation from different manufacturers, and ranging from portable devices to MS imaging instruments and systems incorporated in high-end mass spectrometers [48,50], are available nowadays. A simplified generic schematic of an IMS-MS instrument is shown in Fig. 2A. Most ionisation sources, as well as ambient ionisation techniques, can be used in combination with IMS, with the most common being ESI and matrix-assisted laser desorption/ionisation (MALDI). Similarly, most mass analysers have been combined with IMS, although time-of-flight based mass spectrometers (TOF and quadrupole-TOF, Q-TOF) are mostly employed due to their fast duty cycles [60]. For tandem MS systems incorporating IMS, three configurations are possible, depending on the relative positions of the collision and IMS cells, i.e. where collision induced dissociation (CID) is performed [90,125]. Firstly, if the collision cell is located before the IMS cell, fragmentation can precede IMS separation, and mobility measurements are acquired for fragment ions (and unfragmented precursor ions). Secondly, in post-mobility fragmentation, fragmentation occurs after IMS separation and fragment ions have arrival times that align with their parent ions. This mode of operation is common in DTIMS-MS instruments due to manufacturer's design [60]. Lastly, a combination of both modes of operation, termed time-aligned-parallel (TAP) fragmentation, is possible using commercial TWIMS-MS instruments [35,79]. Here fragmentation occurs both before (in the trap ion guide) and after (in the transfer ion guide) the IMS separation (i.e. CID-IMS-CID) to produce 'MS^3' data [126] (Fig. 2B). First generation fragment ions are separated by IMS, while second generation ions share their arrival times. Incorporation of in-source fragmentation may be used to produce 'MS^4' spectra to discriminate between co-eluting isobaric compounds [127].

For data independent acquisition (DIA) methods such as 'MS^E', where low and high collision energy data are alternately measured without pre-selecting particular parent ions, IMS allows the separation of co-eluting precursor ions prior to their fragmentation, thereby greatly increasing the performance [79]. Alternative data acquisition strategies have been developed for different IMS instruments, parallel accumulation–serial fragmentation (PASEF) for TIMS being a notable example, where the quadrupole is rapidly scanned to allow large numbers of MS/MS experiments [128].

2.3. IMS separation performance

The separation performance of IMS is typically evaluated by means of the resolving power (R_p). However, comparing R_p values between different platforms is complicated by the fact that their separation principles differ [49,129]. For example, for DTIMS instruments a time-based definition of R_p, $(t/\Delta t)$, is used [130], whereas for TWIMS devices, a definition of R_p in terms of the ions collision cross section is preferred $(CCS/\Delta CCS)$ [129,131]. In TIMS, R_p is defined in terms of mobility $(K/\Delta K)$ [93,132], and for the filtering devices, FAIMS/DMS/DIMS, a definition for R_p in terms of the compensation field $(E_c/\Delta E_c)$ is used [133,134]. DMA platforms can be

used to measure K [50], such that R_p can be defined in terms of the CCS-based definition [128,134].

Due to these differences, Dodds and colleagues suggested using a CCS-based definition of R_p to enable the cross-platform comparison of instruments (with the exception of FAIMS/DMS/DIMS, since CCS values cannot be determined) [129]. According to this definition, R_p values for commercial DTIMS devices are ~60 [129,135], for TWIMS instruments ~40–50, and for TIMS systems between ~170–180 and as high as ~400 [136]. For this reason, TIMS devices are considered ultra-high resolution instruments [51].

The above rough comparison highlights that the most used commercial IMS instruments (DTIMS and TWIMS) are characterized by relatively low resolving power (40–60), which is typically sufficient to resolve ions differing in CCS values by ~1.5–3%, but not for the resolution of most stereoisomers (ΔCCS <1%) and enantiomers (ΔCCS ~0.1 %). Recent instrumental advances in TIMS [132,136] and TWIMS-based technologies, such as cyclic ion mobility (cIM) [118] and structures for lossless ion manipulations (SLIM) [113,137,138], as well as high pressure DTIMS instruments [104,110,111,139] and cyclic DTIMS [107,140] show promising improvement in IMS performance (R_p > 300, and up to 1000) for such demanding separations.

2.4. CCS values and their determination

The primary measured variable in IMS is an ion's mobility, K, which reflects the interactions between the ion and buffer gas molecules under conditions prevalent in the IMS cell. Measured mobilities are normalised to standard temperature and pressure conditions (STP, 273.15 K and 760 Torr), providing the reduced mobility, K_0, for comparison purposes. An ion's reduced mobility can be converted to the collision cross section (CCS or Ω) via the Mason-Schamp equation [96,141]:

$$CCS = \frac{3}{16}\sqrt{\frac{2\pi}{\mu k_B T}}\frac{ze}{N_0 K_0} \quad (1)$$

Where μ is the reduced mass of the ion-neutral collision complex ($=m_i m_g/(m_i+m_g)$, with m_i and m_g the mass of the ion and the buffer gas, respectively), k_B is Boltzmann's constant, T is the temperature of the gas in Kelvin, z is the ion's charge, e the elementary charge, and N_0 is the number density of the drift gas at STP.

The CCS value, in units of square Ångström (Å^2), describes the number of collisions the molecular species' 3-dimensional structure encounters with the neutral buffer gas – a momentum transfer cross section [50,92] - which provides information about the ion's conformation. The CCS value therefore provides a potentially important descriptor of the ion, which is characteristic under defined conditions. It is for this reason that CCS values are increasingly being used as an additional identification criterion in compound assignment; it is therefore relevant to discuss briefly how CCS values can be determined in a reliable manner.

An important condition for the use of the Mason-Schamp equation is that measurements be performed under low-field conditions. A consequence of this is that FAIMS cannot be used to determine CCS values. If this condition is met, and provided a constant field is used, Eq. 1 can be used to derive CCS values from measured mobilities. This scenario applies to DTIMS instruments, where single-field (calibrant-dependent) [70,142] or stepped-field (calibrant-independent) [70,130] approaches may be used. The stepped-field method is considered the gold standard, as CCS values can be calculated directly from the drift time (derived from the measured arrival time) [70,130], provided all other parameters in Eq. 1 are known to a high degree of accuracy. This method uses multiple measurements at different field strengths to derive the drift time used to calculate K. The stepped field method is not compatible with chromatographic separation due to its long cycle times. In contrast, the single-field approach uses a single drift voltage to measure arrival times [70,142], and CCS values of unknowns are derived from regression analysis of arrival times vs. CCS values measured for calibrants with known, standardized CCS values under identical conditions. Agilent's ESI-L Low Concentration Tune Mix, which contains betaine, trifluoroacetic acid ammonium salt, and a series of fluorinated phosphazenes and triazines, is commonly used as calibrant. Stow et al. showed in a recent inter-laboratory study that CCS values obtained using the stepped field method are exceptionally reproducible [70]. Comparison of the two methods showed an average error of 0.54 % attributed to the single-field measured CCS values, compared to a 0.34 % for the stepped-field values [70].

TWIMS uses low but variable fields, and as such requires calibration to derive experimental CCS values. Similar to the single-field DTIMS method, CCS values of unknowns are obtained from calibration using molecules with known CCS values under defined conditions [143,144]; a detailed procedure for the calibration protocol in TWIMS may be found in Ruotolo et al. [145]. The most used calibrant is poly-DL-alanine, for which CCS reference values were measured by DTIMS. Clearly, the accuracy of CCS values derived using calibration depends on the suitability of the calibrant. Calibration errors have been noted when using calibrants structurally and chemically unrelated to the target molecules, as when peptide calibrants were used for the determination of lipid [143] and small drug-like compound [146] CCS values. Poly-DL-alanine (n = 3 to n = 14) covers the mass range 231–1012 Da (CCS values of 150-308 Å^2 in ESI$^-$ and 151–306 Å^2 in ESI$^+$ with nitrogen as drift gas) [71,147,148], and compounds outside this mass range are subject to higher CCS errors [146]. Such issues can be circumvented by the judicious selection of suitable calibrants, such as a mixture of poly-DL-alanine and drug-like molecules used by Hines et al. [146]. It is worth noting that calibration strategies using negative ion mode have received relatively little attention, despite the fact that many secondary metabolites for instance are acidic in nature. Dextran has been used as calibrant to measure CCS values of oligosaccharides in negative ionisation mode [144], and poly-L-malic acid (n = 1 to n = 8, mass range 134–946 Da) as calibrant for the analysis of negatively-charged analytes under 1 kDa [149].

Although CCS measurements using TIMS is in theory possible from first principles, in practice calibration procedures are often used as outlined in [94,132,150]. Schroeder et al. used the Agilent Tune Mix as calibrant to generate a CCS library for 146 plant secondary products [151]. DMA can be used to measure K directly, although DTIMS is more commonly used as reference method for CCS determination since DMA is primarily applied for very large molecules. In practice, calibration approaches are also used to derive CCS in DMA [152].

Inconsistencies in how IMS data was reported, especially in earlier work, prompted Gabelica and co-workers to report a comprehensive set of recommendations for IMS measurements [92]. These authors called for the standardisation of the manner in which CCS values are measured and reported on particular platforms [70,71], and highlighted considerations for comparing CCS data obtained on different platforms [92]. A notable consideration is that the drift gas composition should always be specified, as calibrant CCS values obtained using nitrogen are often larger compared to those obtained using helium [147,153]. The nomenclature $^{TW}CCS_{N2}$ was suggested, where the subscript specifies the buffer gas composition and the superscript denotes the IMS technique used to derive the CCS value [154,155]; this nomenclature is also used in the present work.

CCS values can be used to study gas-phase phenomena, and as such are useful in physical chemistry [156,157] and in the study of biological molecules' conformations [158]. From an analytical

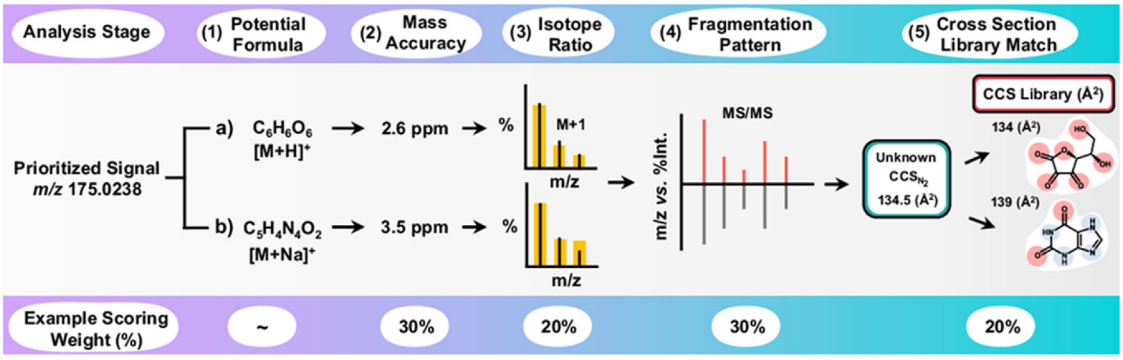

Fig. 3. Example of a workflow used in the identification of a "known-unknown" analyte using both *m/z* and CCS data to increase confidence in annotation. Reprinted with permission from [50].

chemistry perspective, though, the main application of CCS values is as a complementary descriptor to chromatographic, spectroscopic and MS data for the identification of compounds. Databases such as HMDB [159] and METLIN [160] often suggest multiple potential metabolite hits based on HR-MS data, thus using CCS values to assist with identity confirmation is of analytical interest. One of the attractive features of CCS values in this context is their precision. For example, in inter-laboratory studies Paglia et al. found $^{TW}CCS_{N2}$ values to be more reproducible (97 % of compounds within 2% RSD) than retention times (80 % within 2% RSD) for 125 common metabolites [71], while the stepped-field method using DTIMS demonstrated a 0.29 % RSD for CCS measurements [70].

Experimental CCS searchable databases have been created for lipids [148,161,162], peptides [108,163], N-glycans [144], toxins [164], pesticides [165], drug-like compounds [146,165], metabolites [71,166] and various biomolecules [130,167]. Furthermore, prediction of CCS values using computation methods is a fast-growing field [168–173].

While it is essential to consider the requirements of accuracy in reported CCS values as discussed above, the availability of reliable CCS databases clearly shows promise for the incorporation of IMS into hyphenated chromatography-MS workflows for the identification of unknown compounds (Fig. 3). In this endeavour, a distinction between "known-unknowns" (i.e. an analyte for which MS and CCS data determined for the standard are available online) and "unknown-unknowns" (representing analytes without a database hit, no *m/z* or CCS value) can be made. In the case of "unknown-unknowns", mass-mobility trendlines (CCS values vs *m/z*) can be used to assign the chemical class of the analyte [146,166,167].

2.5. IMS data format and analysis

Incorporating IMS into chromatography-MS workflows increases data dimensionality (Fig. 4): in principle, a hyphenated chromatography-IMS-MS methods produces three-dimensional data, whereas comprehensive two-dimensional chromatographic analysis adds a further dimension [69,174,175]. IMS also greatly increases datafile size, such that data storage and analyses of large datasets as are common in the omics fields are of concern [176]. Kaufmann and co-workers have noted that the hyphenation of IMS to MS is beneficial for the reduction of false detects, although due to the low resolution of currently available time-dispersive IMS platforms this comes at a cost of missing detects, particularly for the analysis of trace analytes [64]. The addition of CCS filters as an identification criterion to a < 5 ppm mass window also decreased the number of false positive results [64], thus increasing identification reliability [64,177].

While a range of commercial software packages are available for the analysis of IMS data, these are mostly instrument specific. However, 2D IMS-MS data can also be exported and processed (peak alignment and picking) using different pre-processing and pattern recognition techniques [176], and online tools such as XCMS [178,179] can be used for alignment to yield a data matrix containing mobility/drift time, *m/z* data and peak intensity. Depending on the goal of the analyses, unsupervised or supervised pattern recognition techniques can be used for data interpretation. Higher dimensional IMS data is compatible with open source packages, as demonstrated by the incorporation of LC-IMS-CID-MS data into Skyline [180] and *ORIGAMI* [181], and freely available software for visualisation and interpretation of comprehensive two-dimensional LC × LC × IMS-MS data (Fig. 4D) [69]. Indeed, chemometric methods are increasingly being used for the analysis of IMS data, also in natural product analysis [69,182–202].

3. Applications of IMS in the analysis of natural products

The inordinate growth in the number of applications of IMS-MS in recent years, particularly in biomolecule analysis, is mirrored to a lesser extent also in natural product analysis. In this section we provide an overview of the applications of IMS in natural product analysis since 2015. Table 1 summarises the relevant reports according to plant and microbial sources, while the following discussion will highlight significant findings in the field. Note that although the focus is on natural products, specifically secondary metabolites, we have included studies on foods containing these compounds and studies utilising standard natural product mixtures where relevant.

3.1. Plant secondary metabolites

Plant secondary metabolites are an important source of drug leads [10], and are increasingly being used in nutraceutical, functional food and herbal medicine industries [15]. Plant secondary metabolites can broadly be grouped into phenolic compounds (including flavonoids), terpenoids and nitrogen- and sulphur-containing compounds (the former including the important alkaloids). Crude plant extracts typically used to screen for natural product constituents are often highly complex mixtures, and it is in the screening analysis of these extracts that IMS has found extensive application in the last six years in combination with MS and often chromatographic separation.

Phenolic compounds are the class of plant secondary metabolites most represented in the studies cited in Table 1. This is not surprising considering the intense interest these compounds have elicited as bioactive natural products. The rapid growth in the use of IMS is evident from a comparison of the number of applications of the technique to flavonoid analysis at the end of 2015 [34] and those listed in Table 1 since 2015. Indeed, IMS has found application

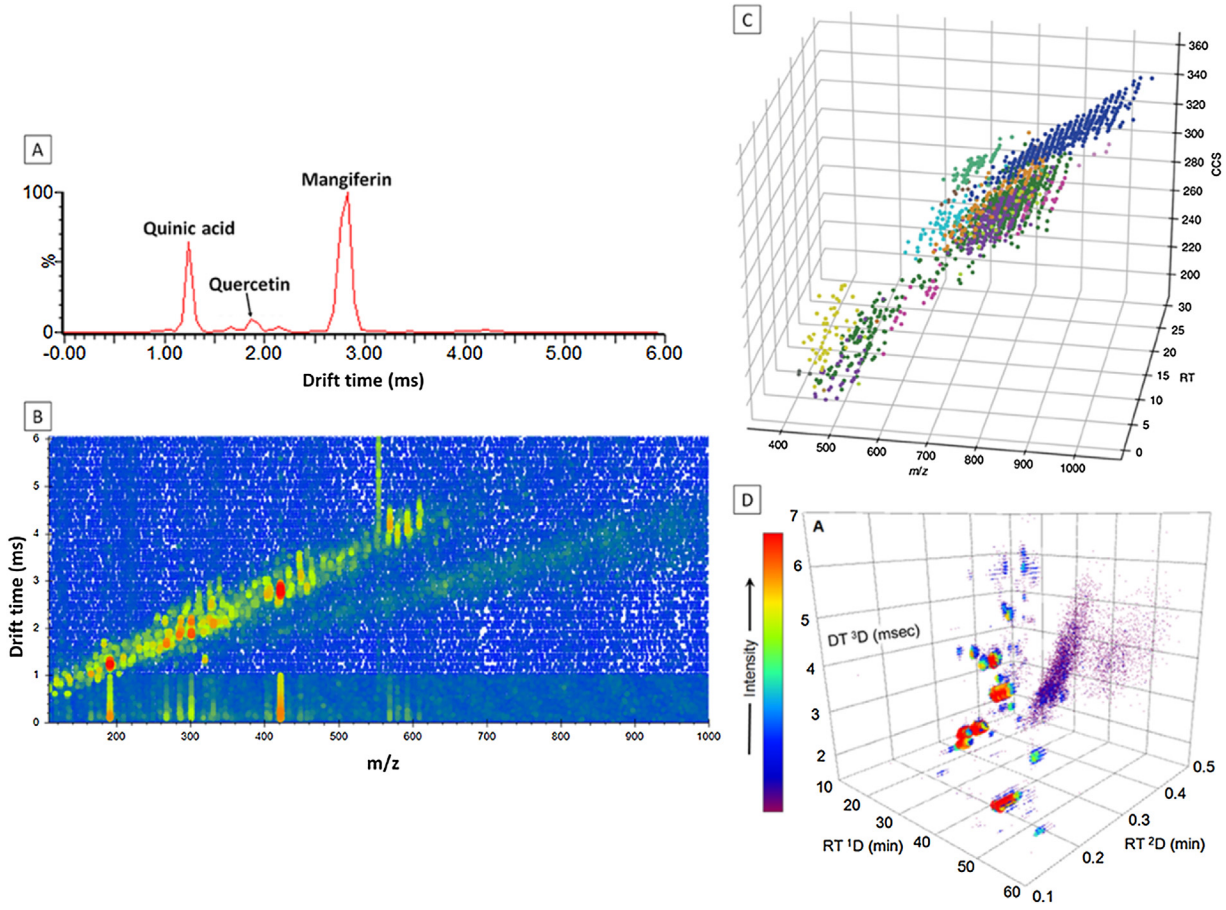

Fig. 4. Illustration of the data dimensionality in IMS hyphenation. (A) Ion mobility spectrum of *Cyclopia genistoides* (honeybush tea) phytochemicals (1-D data), (B) corresponding mass-mobility trendlines of *C. genistoides* phytochemicals (2-D data) (both unpublished data from our group), (C) LC-IMS-MS separation of lipids (3-D data) (reprinted with permission from [172]) and (D) three-dimensional representation of comprehensive two-dimensional LC (LC × LC)×IMS-MS separation of grape seed phenolics (MS dimension not represented) from [69].

in the analysis of flavonoids [69,120,151,166,177,203–207], phenolic acids [198,203,208–212], and tannins [69,212–217] in a variety of plants and their derived food products.

For the analysis of phenolic compounds, especially the hyphenation of reversed phase UHPLC (RP-UHPLC) with IMS-MS has found widespread application in the screening of complex plant extracts, where large numbers of metabolites can be putatively identified based on chromatographic, IMS and (ideally HR-) MS data. For example, Stander et al. identified 59 phenolic compounds in rooibos tea, including two unique dihydrochalcones and several new compounds, using a RP-UHPLC-TWIMS-MS method [207], while Yang et al. identified 95 metabolites in lettuce using the same methodology [203], and Schroeder et al. detected 151 metabolites in *Medicago truncatula* roots using RP-UHPLC-TIMS-HR-MS/MS [151].

Condensed tannins have been the subject of several IMS studies [69,212,215–217]. These compounds are exceedingly hard to analyse because of the large number of isomeric species found for higher oligomeric polymers, and as such multidimensional LC [69,218] and IMS [69,212,215–217] have been used to unravel the composition of complex condensed tannin fractions. A good example is the recent study of Li et al., who developed an advanced data analysis strategy based on mass defect filtering incorporating multidimensional IMS data (ML-MDF) for the detection of oligomeric procyanidins in a grape seed extract analysed by UHPLC-DTIMS-HRMS [215]. The data analysis protocol utilised drift time, accurate mass data, decimal masses, monoisotopic ion intervals and fragmentation pathways to assign 686 procyanidins in the analysed extract. Wang et al. used RP-UHPLC-TWIMS-HR-MS to assign up to 304 proanthocyanidins in cranberry [212,217]. Rue et al. showed that positive ESI-TWIMS-HR-MS can be used for a rapid screening method capable of differentiation between different classes of procyanidins, where IMS offered the benefit of resolving interference from multiply charged ions [216].

Although the ion filtering characteristics of FAIMS/DMS platforms are well recognised, time-dispersive platforms also provide cleaner mass spectra following filtering according to arrival time, which can translate into lower limits of detection (LODs) [89]. For example, Fenclova et al. studied silymarin flavonolignans in milk thistle extracts, and noted that compared to the traditional LC-qTOF quantitative data, the LC-DTIMS-qTOF quantitative approach demonstrated an extended linear range, lower detection limits and total separation of analytes of interest from interferences [205].

IMS has also found application in the analysis of plant pigments, including anthocyanins [210,211] and carotenoids [174,219]. Corinti et al. used IMS in combination with IR multiple photon dissociation (IRMPD) to investigate the differentiation of the anthocyanin epimers cyanidin 3-*O*-glucoside and –galactoside [210].

Although not strictly natural products, a relevant study by Chalet et al. utilised RP-UHPLC-TWIMS-HR-MS to study the phase II metabolites of flavonoids, where IMS was found to be beneficial in the separation of positional isomers of flavonol and flavone metabolites [220].

Somewhat surprisingly considering their importance as drug leads, since an early report in 2011 [126], IMS has found relatively limited application in the analysis of alkaloids [221–224]. Chung and Lam evaluated the use of FAIMS as a complementary method

to multiple reaction monitoring (MRM) transitions for the analysis of pyrrolizidine alkaloids and their N-oxides, although incorporation of IMS was found to decrease sensitivity [224]. Purves et al. used FAIMS-MS with methanol as gas modifier for the rapid separation and quantification of the pyrimidine glycosides vicine and convicine in faba beans [222]. The authors note that in the absence of FAIMS, the selective reaction monitoring (SRM) transitions of the ^{13}C isotopologue of vicine interferes with the shared transitions of convicine, which adversely affects quantification of the latter [222].

Ginsenosides, as important biological compounds in ginseng and key ingredient of traditional Chinese medicine (TCM), have been the focus of several studies. For example, using an untargeted UHPLC-IMS-HR-MS approach, Jia and co-workers were able to distinguish the flower buds of three *Panax* species (*P. ginseng*, *P. quinquefolius*, and *P. notoginseng*) associated with beneficial health effects [225]. The authors identified 32 ginsenoside (ginseng saponins) markers suitable for this purpose. $^{TW}CCS_{N2}$ values proved useful, using an in-house ginsenoside library, in the assignment of isomeric species involved in the differentiation of congeneric species. Chen and co-workers used FAIMS-MS/MS with 1-propanol as gas modifier as a rapid method to differentiate between Asian and American ginseng based on their profiles of ginsenoside isomers [226]. Zhang et al. developed a time-decoupled two-dimensional LC method hyphenated to TWIMS-HR-MS(/MS) which allowed them to report the detection of 201 ginsenosides in white and red ginseng samples [227]. In this study, IMS allowed the separation of ten pairs of isobaric ginsenosides which co-eluted following the two-dimensional separation. Subsequently, Zuo et al. used an off-line 2-D HILIC + RP-UHPLC method hyphenated to TWIMS-HR-MS and an in-house library to identify 323 ginsenosides in red and white ginseng [228]. Decroo et al. evaluated the utility of

Table 1
Summary of applications of ion mobility spectrometry for the analysis of secondary metabolites in natural product research (2015–2020) [271–274].

	Sample	IM Platform	Secondary metabolite(s)	Comment	References
Plant Secondary Metabolites	Olive oil from *Arbequina* olives	DTIMS	Volatile organic compounds (VOCs)	Assessed the shelf life of extra virgin olive oil according to container type and storage conditions by HS-GC-IMS.	[234]
	Chlorogenic acid standards	TWIMS	Mono- and di-caffeoylquinic acids	IMS-MS and –MS/MS used to assign regioisomeric mono- and dicaffeoylquinic acids. Prototropic isomers of 5-caffeoylquinic acid reported.	[256]
	Pelargonium peltatum leaves	TWIMS	Flavonoid glycoside	IMS enhanced the metabolite coverage of LAESI in biological tissues.	[261]
	Various fruits	HT-DTIMS	Anthocyanins	Implementation of Hadamard transform (HT) IMS-MS to profile anthocyanins in fruit, including distinguishing between isobaric anthocyanins.	[211]
	(+)-Catechin and (-)-epicatechin standards	TWIMS	Flavonoids	Separation of catechin epimers by TWIMS-MS through introduction of chiral selectors to form complexes.	[255]
	Whole dry hot chilli pepper	HT-DTIMS	Capsaicinoids	Implementation of HPLC-HT-IMS-TOF-MS to provide an additional separation dimension for the analysis of chilli pepper extracts.	[271]
	Citrus tree leaves	FAIMS (DMS)	Volatile organic compounds (VOCs)	GC-FAIMS used to distinguish VOC profiles of healthy vs. infected citrus to detect citrus greening disease.	[193]
	Papaver bracteatum	DTIMS	Alkaloids	Used IMS to detect thebaine, papaverine, and noscapine at various developmental stages in *P. bracteatum*.	[221]
	Ginkgo biloba leaves	DTIMS	Gallocatechin, flavonol derivatives	First hyphenation of 2D-LC and IMS. 2D-LC (LC+LC)-IMS-MS separation of analytes, identification using in-house CCS database.	[259]
	Fruits of *Gardenia jasminoides*	TWIMS	Carotenoids	IMS separation of crocin-3 and crocin-4 isomers (or tautomers).	[219]
	Apple/pear juice samples	FAIMS	Mono-caffeoylquinic acids	Separation three mono-caffeoylquinic acid positional isomers by FAIMS; rapid ESI-FAIMS-MS/MS method developed for their determination.	[209]
	Garcinia oblongifolia leaves	TWIMS	Polycyclic polyprenylated acylphloroglucinols (PPAPs)	Discrimination of 7 pairs of co-eluting isobaric PPAPs when IMS was added to UHPLC-MS. In total 140 PPAPs detected in *G. oblongifolia*.	[127]
	Olive oil	DTIMS	Volatile organic compounds (VOCs)	Discrimination of olive oils from different geographical regions (Italy vs Spain) using a prototype temperature-ramped HS-GC-IMS instrument.	[196]
	Olive oil and *Camellia* oil	DTIMS	Volatile organic compounds (VOCs)	Direct IMS using a portable instrument to analyse oil VOCs for adulteration detection.	[233]
	Faba bean (*Vicia faba* L.)	FAIMS	Alkaloids	Used FAIMS-MS with methanol gas modifier to separate vicine and convicine and to quantify these alkaloids in 40 faba bean genotypes.	[222]
	Essential oils	DTIMS	Terpenes	HS-GC-IMS analysis of 50 common terpenes in essential oils.	[232]
	Rooibos Tea (*Aspalathus linearis*) and Golden Tea (*A. pendula*)	TWIMS	Phenolic and flavonoid derivatives	Characterization of 59 phenolic metabolites, including several compounds detected in rooibos for the first time. Tautomers detected.	[272]
	Soybean root nodules	TWIMS	Flavonones and triterpenes	Employed LAESI-IMS-MS to explore the symbiosis between soybean (*Glycine* max L. Merr.) and *Bradyrhizobium japonicum*, revealing metabolic processes.	[262]
	Cannabis sativa L. plant	TWIMS	Cannabinoids	Isomeric separation of cannabinoids by TWIMS, $^{TW}CCS_{N2}$ values reported.	[42]
	Lettuce (*Lactuca sativa* L.)	TWIMS	Phenolic and flavonoid derivatives	Characterization of 12 metabolites using UHPLC-IMS-HR-MS.	[199]
	Dicaffeoylquinic acid standards	DTIMS	Geometrical isomers of 3,5-dicaffeoylquinic acid	Experimental collision cross sections were compared with theoretical structures to differentiate and identify *cis/cis, cis/trans, trans/cis, and trans/trans* 3,5-dicaffeoylquinic acid isomers.	[249]
Plant Secondary Metabolites	Primary and secondary metabolites, xenobiotic standards	DTIMS	Terpenes and flavonoids	Measured $^{DT}CCS_{N2}$ values for 500 small molecules to construct a freely available library.	[166]
	Flavonols, flavones, and catechin standards	TWIMS	Phase-II metabolites of flavonols, flavones, and catechins	RP-UHPLC-TIWMS-HR-MS used for metabolite analysis. IMS separation of positional isomers of the flavonol and flavone metabolites; position of the glucuronide moiety had a strong influence on CCS.	[220]
	Food samples	DMS	Pyrrolizidine alkaloids and their N-oxides	Combination of DMS and MRM provided a better selectivity for the target analytes but suffered from loss of sensitivity.	[224]
	Red chilli pepper	TWIMS	Carotenoids	Carotenoid fingerprinting of red chilli pepper using SFC×RP-UHPLC-PDA-IMS-MS.	[174]
	Poria cocos	TWIMS	Lanostane-type triterpene acids	121 lanostane-type triterpene acids detected in *Poria cocos* by UHPLC-IMS-MS^E using an in-house library.	[240]
	Brazilian *Coffea arabica*	DTIMS	Pyrazines, fatty acids, phenolic acids	On-line DTIMS-TOF-MS used to study the evolution of VOCs during coffee roasting.	[231]
	Cannabis sativa leave and flower tissue	DTIMS	Cannabinoids	IMS-MS used for the rapid quantification of isomeric cannabinoids THC and CBD.	[236]
	Uvaria chamae roots	TWIMS	Chalcones and dihydrochalcones	Structural characterization of chalcones and dihydrochalcones responsible for the antimicrobial activity of *Uvaria chamae* by UHPLC-IMS-MS.	[273]
	Cannabis sativa	DTIMS	Cannabinoids	IMS proposed for the rapid determination of cannabinoids (CBD+THC) in seized marijuana samples.	[237]
	Calendula officinales leaves	DTIMS	Unspecified organic compounds	First application of multiple heart-cutting 2D-GC-APCI-DTIMS-HR-MS system, applied to the analysis of medicinal herb.	[175]
	Moringa oleifera Lam	TWIMS	Moringin	Used IMS-MS and NMR to study the formation of a strong inclusion complex between moringin and α-cyclodextrins (CDs).	[274]
	Chocolate spread extract and 55 other food commodities	TWIMS	Steviol glycosides	Identification of steviol glycosides and their isomeric pairs. A steviol glycosides CCS value library was generated.	[124]
	Chestnut, red wine, grape seeds, rooibos tea (*Aspalathus linearis*)	TWIMS	Hydrolysable and condensed tannins, flavonoids, and phenolic acids	Demonstrated a HILIC×RP-LC×IMS-HR-MS separation system for the analysis of phenolics. Incorporation of IMS into LC×LC-MS enhanced sensitivity and increased peak capacity by a factor 13.	[69]
	American cranberry (*Vaccinium macrocarpon*) cultivars	TWIMS	Phenolics	Hyphenation of IMS to fuzzy chromatography mass spectrometric (FCMS) provided improved differentiation of cranberry cultivars by multivariate data analysis.	[198]
	American cranberry (*Vaccinium macrocarpon*) fruits and cultivars	TWIMS	Phenolics	More than 80 phenolics characterised by UHPLC-IMS-HR-MS. Co-eluting isomers (or adducts) discriminated by IMS.	[212]
	Peganum harmala L. seeds	DTIMS	Alkaloids	HILIC-ESI-IMS used to determine 13 alkaloids in *Peganum harmala*, where HILIC and IMS provide complementary selectivity.	[223]
	Leaf and head lettuce (*Lactuca sativa* L.) cultivars	TWIMS	Phenolic acid derivatives, glycosylated flavonoids, an iridoid	Putative identification of 95 metabolites by UHPLC-TWIMS-MS; IMS proved important in distinguishing isomers and removing false identifications.	[203]
	Honey	DTIMS	Volatile organic compounds (VOCs)	HS-GC-MS used for authenticity testing of honey based on VOC profiles.	[200]
	Red wine and grapes from *Vitis vinifera*	DTIMS	Phenolics, flavonoids and anthocyanins	UHPLC-TWIMS-HR-MS analysis of red wine phenolics, use of $^{DT}CCS_{N2}$ values as an identification point for wine metabolomics.	[120]

Table 1 (*Continued*)

Plant Secondary Metabolites	*Aesculus hippocastanum* (Horse chestnut)	TWIMS, cTWIMS	Triterpenoid saponins	Structural analysis of regioisomeric and stereoisomeric escin 1 by UHPLC-TWIMS-MS and cTWIMS-MS.	[253]
	Italian pomegranate (*Punica granatum*, L.)	TWIMS	Anthocyanins	Differentiation of epimeric anthocyanin glycosides (cyanidin-3-*O*-glucoside and -galactoside) using IR ion spectroscopy in a combined approach with IMS-HR-MS.	[210]
	Sea cucumber (*Holothuria forskali*), common soy (*Glycine max*), and quinoa (*Chenepodium quinoa*)	TWIMS	Mono- and bidesmosidic saponins	The potential of LC-TWIMS-HR-MS is demonstrated for the assignment of mono- and bidesmosidic saponins in plant and animal sources.	[123]
	Olive oil	DTIMS	Volatile organic compounds (VOCs)	Olive oil classification according to quality using HS-GC-IMS.	[201]
	Cannabis products (marijuana and hashish) leaves and flower tissues	TWIMS	Cannabinoids	Analysis of isomeric cannabinoid standards and *Cannabis* products. UHPLC-ESI-TWIMS-MS outperforms GC-MS and GC×GC-MS for isomeric characterisation.	[238]
	Olive oil	DTIMS	Volatile organic compounds (VOCs)	Temperature-ramped HS-GC-IMS to classify virgin olive oils (extra virgin olive oils (EVOO), virgin olive oil (VOO) and lampante olive oil (LOO)).	[202]
	Kumquat fruit (*Citrus japonica*)	DTIMS	Volatile organic compounds (VOCs)	Effects of processing methods on the volatile components of candied kumquats studied by HS-GC-IMS.	[183]
	Panax species (*P. ginseng*, *P. quinquefolius*, and *P. notoginseng*)	TWIMS	Ginsenosides (ginseng saponins)	Differentiated *Panax* species using 32 ginsenosides as markers. Isomers distinguished based on differences in CCS values utilizing an in-house ginsenoside library.	[225]
	Fresh and dried *Tricholoma matsutake* Singer	DTIMS	Volatile organic compounds (VOCs)	Differences in volatile compounds in pileus and stipe of fresh and dried *T. matsutake* mushrooms from different areas studied using HS-GC–IMS.	[184]
	Plant roots	DTIMS	Phenolic acids	IMS employed to assist in the determination of the co-eluted compounds not separated by HPLC.	[208]
	Passiflora species leaf tissue	TWIMS	C-glycosylflavone isomer pairs orientin/isoorientin and vitexin/isovitexin	Unequivocal identification of isomers based on UHPLC-TWIMS-HRMS data. Generation of a reference CCS library of "knowns" and "known–unknowns".	[251]
	Red wine, Grape seeds, Rooibos tea (*Aspalathus linearis*)	TWIMS	Phenolics	HILIC×RP-UHPLC×IMS-HR-MS analysis of phenolics in a range of samples. IMS data not discussed.	[218]
	Olive oil and Honey	DTIMS	Volatile organic compounds (VOCs)	Discrimination of olive oils and honey from different geographical regions using HS-GC-IMS and ATR/FT-IR spectroscopy. Explored data fusion as an effective strategy for improving authentication.	[185]
	Garcinia buchananii leaves, stem, and root bark tissue	TWIMS	Flavonoids and Xanthones	Characterization of 34 metabolites based on $^{TW}CCS_{N2}$ values to build a database in UNIFI informatics platform.	[177]
	Chestnut (*Castanea sativa*)	TWIMS and DTIMS	Hydrolysable tannins	HILIC- and RP-LC-IMS-HR-MS analysis chestnut hydrolysable tannins. 38 Ellagitannin and gallotannin species comprising 136 isomeric species putatively identified. Comparison of $^{TW}CCS_{N2}$ and $^{DT}CCS_{N2}$ values.	[213]
	Peruvian tara (*Caesalpinia spinosa*) pods	TWIMS	Hydrolysable tannins	Combination of IMS with HILIC- and RP-LC-HR-MS for the detailed analysis of gallotannins; 45 isomeric gallotannins tentatively assigned.	[214]
	Honey	DTIMS	Volatile organic compounds (VOCs)	Differentiation of adulterated honey, winter-harvested honey and summer-harvested honey using HS-GC-IMS.	[187]
	Honey	DTIMS	Volatile organic compounds (VOCs)	Discrimination of honey from *Apis mellifera* and *Apis cerana* bees using HS-GC-IMS.	[188]
Plant Secondary Metabolites	Asian and American ginseng	FAIMS (DMS)	Ginsenosides (ginseng saponins)	FAIMS-MS/MS used as a rapid method to differentiate between Asian and American ginseng based on their ginsenoside/pseudo-ginsenoside profiles.	[226]
	Jujube (*Zizyphus jujuba* Mill)	DTIMS	Volatile organic compounds (VOCs)	HS-GC-IMS used to monitor jujube fruit VOCs during cold storage to follow their evolution.	[186]
	White and red ginseng roots	TWIMS	Ginsenosides (ginseng saponins)	Time-decoupled 2-D UHPLC-TWIMS-HR-MS(/MS) used to detect 201 ginsenosides. Co-eluting isobaric ginsenosides resolved by IMS.	[227]
	Vangueria agrestis	TWIMS	Phenolic acids, flavonoids, terpene glycosides	Dried aerial parts and roots of *V. agrestis* analysed by UHPLC-IMS-HR-MS; 73 compounds identified.	[204]
	Silene genus (*S. otitis, S. nutans, S. maritime, S. viridiflora and S. fimbriata)*	TWIMS	Plant ecdysteroids	Incorporation of TWIMS into HPTLC-DESI-MS method enabled the separation of co-migrating/ isobaric ecdysteroids	[263]
	Silybum marianum (L.)	DTIMS	Flavonoids and flavonolignans	Characterisation of flavonolignans and taxifolin by UHPLC-DTIMS-MS, improved resolution of critical pairs and detection of unknown isomers by IMS.	[205]
	Fresh peppers (*Capsicum annuum* L.)	DTIMS	Volatile organic compounds (VOCs)	HS-GC-IMS used to follow changes in volatile flavour compounds of chilli peppers during hot air-drying.	[191]
	Cannabinoids	TWIMS	Cannabinoids	RP-UHPLC-TWIMS-HRMS method used to identify synthetic impurities in illicitly produced THC.	[239]
	Grape seed extracts	DTIMS	Procyanidins	Multidimensional limiting mass defect filter used in combination with RP-UHPLC-DTIMS-HR-MS for the characterization of 686 procyanidins of degrees of polymerisation of 1-15.	[215]
	Dried pericarps of *Citrus reticulata*	DTIMS	Volatile organic compounds (VOCs)	HS-GC-IMS used for detection of adulteration of dried pericarps based on VOC profiles.	[192]
	Protea leave and bract tissue	TWIMS and DTIMS	Phenolic and flavonoid derivatives	Characterization of 67 metabolites using UHPLC-TWIMS-HR-MS. Comparison of $^{TW}CCS_{N2}$ and $^{DT}CCS_{N2}$ values. Caffeoyl-*O*-polygalatol characterised for the first time, showed tautomeric ions.	[258]
	Olive oil	DMA	Volatile organic compounds (VOCs) and phenolic compounds	Chemical fingerprinting of olive oils by ESI-DMA-MS for classification purposes.	[194]
	Cocoa, cinnamon, peanut skins, cranberries, and crab apples	TWIMS	Procyanidins	Infusion IMS-MS used for the detection and class differentiation of higher order procyanidins with degrees of polymerisation (DPs) up to 24.	[216]
	Medicago truncatula root tissue	TIMS	Flavonoids and triterpenes	A $^{TIMS}CCS_{N2}$ library generated to aid in compound identification. 151 metabolites identified in *M. truncatula*, 40 of which were confirmed based on CCS values.	[151]
	Polygonatum verticillatum	DTIMS	Flavonoids and homoisoflavonoids	Quantitative analysis of flavonoids and homoisoflavonoids by UHPLC-DTIMS-HR-MS.	[206]
	Olive oil	DTIMS	Volatile organic compounds (VOCs)	Use of deep learning approaches and GC-IMS to classify virgin olive oils (extra virgin olive oils (EVOO), virgin olive oil (VOO) and lampante olive oil (LOO)).	[235]
	Cranberry juice concentrate	TWIMS	A-type and B-type proanthocyanins	304 proanthocyanins assigned using RP-UHPLC-TWIMS-HR-MS. Co-eluting isomeric (or tautomeric) ions of trimeric and tetrameric proanthocyanins detected by their unique drift times.	[217]
	Rice	DTIMS	Volatile organic compounds (VOCs)	Discrimination between white and yellowed rice based on VOCs profiles using HS-GC-IMS and HS-SPME-GC-MS.	[195]
	White and red ginseng	TWIMS	Ginsenoside (ginseng saponins)	Off-line 2D HILIC+RP-UHPLC-TWIMS-HR-MS analysis of ginsenosides. 323 ginsenosides detected in red and white ginseng using an in-house library.	[228]
Microbial Secondary Metabolites	Cheese	DTIMS	Volatile organic compounds (VOCs)	HS-MCC-GC-IMS used to study marker compounds linked to the ripening time in goat cheese samples.	[184]
	Microalgae (*Chlorella vulgaris, Dunaliella salina,* and *Phaeodactylum tricornutum*)	TWIMS	Carotenes, chlorophylls, and xanthophylls	UHPLC-UV-TWIMS-HR-MS^E used to analyse pigments in microalgae. 26 pigments (carotenes, chlorophylls, and xanthophylls) identified, IMS resolved 5 co-eluting isobaric pigments.	[119]
	Escherichia coli, Bacillus subtilis and *Staphylococcus aureus* strains	FAIMS	Volatile organic compounds (VOCs)	Distinct bacterial VOC profiles differentiated using a-IMS; fingerprints generated using ion currents in the FAIMS cell.	[197]
	Mycotoxin standards	TWIMS	Mycotoxins: aflatoxin, enniatin, fumonisin derivatives, ochratoxin A	TWIMS-derived $^{TW}CCS_{N2}$ database for mycotoxins generated, and its application demonstrated for the detection of mycotoxins in cereal-based samples.	[164]
	Escherichia coli, Bacillus subtilis and *Staphylococcus aureus* strains	FAIMS	Volatile organic compounds (VOCs)	Discrimination between selected bacteria based on their VOC profiles using a sensor array incorporating a-IMS.	[189]
	Fungi species	DTIMS	Volatile organic compounds (VOCs)	Use of GC-IMS to detect fungi contamination (and potential mycotoxin contamination) of barley grain based on VOCs profiles.	[190]
	Streptomyces coelicolor	TWIMS	Prodiginines	TWIMS used for the rapid separation of the prodiginines streptorubin B, butylcycloheptylprodigiosin and metacycloprodigiosin.	[264]
	Chanterelle (*Cantharellus cibarius Fr.*) mushrooms	FAIMS	Octadecadien-12-ynoic acids	Developed a sensitive quantitative UHPLC-FAIMS-MS/MS method to enable identification of key kokumi compounds	[269]

LC-TWIMS-HR-MS for the assignment of mono- and bidesmosidic saponins in plant and animal sources [123].

IMS has also found application in the analysis of volatile natural products of plant origin. One interesting application of IMS is in the analysis of volatile organic compounds (VOCs) for the detection/monitoring of bacterial infection in plant tissue [193,229,230]. For example, citrus greening disease (called Huanglongbing, HLB) caused by the bacterium *Candidatus Liberibacter* is hard to detect, since infected plants remain asymptomatic, whereas GC–MS and GC-DMS may be used to detect infected trees based on their VOC profiles. The GC-DMS methodology has been adapted for VOC analysis in enclosed branches such as in greenhouses [193].

Analysis of VOCs is also important in natural product-derived foods, and here IMS has also been applied. For example, Gloess et al. used DTIMS-TOF-MS connected via a corona discharge ionisation source to the exhaust gas outlet of a coffee roaster to follow the evolution of VOCs during coffee roasting [231]. In this system, the corona ionisation source provides both positive and negative ionisation, while IMS offered the resolution of several isobaric VOCs. Headspace (HS)-GC-IMS, typically performed on a commercial DTIMS instrument equipped with a tritium source, has found extensive application in food analysis, including pine mushrooms [184], jujube fruits during cold storage [186], chilli peppers during hot air drying [191], *Citri reticulatae* pericarpium [192], rice [195], essential oils [232], honey adulteration [185,187,188,200] and kumquats [183]. Many studies utilising IMS have focused on the analysis of olive oils, either using direct IMS analysis [233], or more commonly HS-GC-IMS [185,201,234,235], or recently ESI-DMA-MS to determine polar non-volatile constituents for classification purposes [194]. Applications reported include detection of adulteration [185,233], for classification purposes [201,202,235] and to study the shelf life [234]. Most of these studies use isothermal GC separations, although Gerhardt et al. reported a prototype temperature programming system to benefit from the superior resolving power for fingerprinting [196] and classification [202] purposes. A derivative of this approach is to use multi-capillary column (MCC) GC. HS-MCC-GC-IMS has similarly found application in the analysis of VOCs in goat cheese [182].

A number of recent papers dealt with cannabis analysis by IMS [42,236–239], where a particular focus has been on the use of IMS as a fast screening method for tetrahydrocannabinol (THC) and cannabidiol (CBD) [236,237].

Terpenoids are another important class of plant natural products which have benefited from the application of IMS, for example the analysis of lanostane-type triterpene acids by UHPLC-IMS-MS^E using an in-house constructed MS and IMS database [240], and the analysis of terpenes in essential oils using HS-GC-IMS [232].

Many plant secondary metabolites occur as isomeric pairs in nature. For instance, hydroxycinnamic acids commonly found in many plants are synthesized in the *trans*- configuration via the phenylpropanoid pathway [241], but readily convert to their *cis*-forms when exposed to UV-light, complicating their chromatographic analysis [43,242–244]. The latter geometrical isomers occur in low quantities and were thus considered to be biologically insignificant [241]. Some studies have noted, however, the presence of *cis*-isomers in plant tissues that have been exposed to solar UV radiation [245], and the natural occurrence of these geometrical isomers has also been highlighted [246]. This has prompted inquiry into the biological importance of *cis*-isomers, with significant bioactivity being attributed to the *cis*-forms [243,247,248]. The identification of these geometrical compounds using MS has proven to be challenging as they produce identical tandem MS spectra. Zheng et al. showed how a direct SLIM IMS-MS platform could be used to distinguish between the four geometrical isomers of 3,5-dicaffeolyquinic acid [249], a phytochemical which exhibits potent anti-HIV-1 activity. Using molecular docking studies, these four isomers were previously shown to interact differently with the HIV-1 integrase enzyme [247]. The authors compared experimental $^{DT}CCS_{N2}$ values with the theoretical CCS_{N2} for each *cis/trans* isomer, which allowed the photo-isomerisation process of 3,5-dicaffeolyquinic acid to be monitored, providing insight into the isomeric conversion pathway [249]. Accurate CCS prediction for individual molecules however requires significant computational resources. Gonzales et al. used a machine-learning approach using various molecular descriptors to develop models for the prediction of CCS values of 56 deprotonated phenolics, including positional isomers [250]. Compared to conventional trajectory method (TM) calculations, the proposed methods were rapid and computationally less expensive, enabling their facile integration into metabolite identification steps without compromising predictive strength [250].

The rapid discrimination of isomers is clearly of significant interest in natural product analysis. IMS-MS is increasingly being used for this purpose in a range of fields [47], also in natural products, both for screening and quality control and authentication of phytomedicines and medicinal plants. For instance, McCullagh et al. discuss the differentiation of the *C*-glycosylflavone isomer pairs orientin/isoorientin and vitexin/isovitexin using a UHPLC-TWIMS-HRMS method [251]. Interestingly, larger differences between $^{TW}CCS_{N2}$ values of the respective isomer pairs were observed in negative compared to positive ionisation mode. The method was used to quantify the target isomers in *Passiflora* species [251]. Tose and colleagues used UHPLC-TWIMS-HR-MS to distinguish between isomeric cannabinoids of *Cannabis sativa*, which exhibit different anxiety and psychotic-like symptoms [42]. $^{TW}CCS_{N2}$ values for the characterised cannabinoid isomers were calculated, and the authors note that more isomers could be distinguished for the hyphenated UHPLC method compared to direct infusion IMS-MS experiments. In a subsequent study the same group confirmed the superiority of the UHPLC-IMS-MS approach compared to GC—MS and GC × GC—MS for the analysis of cannabinoid isomers [238]. Another example can be found in *Stevia rebaudiana*, a well-known source of steviol glycosides, which are non-caloric sweeteners added to food commodities to influence the sweetness and bitterness of the product [252]. Multiple isomeric steviol glycosides often occur in the same product, which complicates their analysis for regulatory purposes. McCullagh and co-workers developed a UHPLC-IMS-MS method for the screening of these compounds [124], where the incorporation of IMS showed clear benefits in terms of resolving isomeric pairs and co-eluting compounds. A $^{TW}CCS_{N2}$ library of steviol glycosides was developed and applied for the screening of 55 food commodities.

Some plant secondary metabolite classes exist as both regio- and stereoisomers, such as the triterpenoid saponins. Colson et al. demonstrated how TWIMS could be used to differentiate regio- and stereoisomers of the escin family of saponins found in horse chestnut seeds [253]. UHPLC-TWIMS-MS on a commercial system provided separation of the four target escin/isoescin 1 isomers, whose subtle structural differences resulted in virtually identical arrival time distributions and CCS values [253]. Subsequent use of a high resolution cyclic TWIMS (cTWIMS) instrument providing R_p of ~250 ($CCS/\Delta CCS$) allowed partial separation of these isomers in infusion mode, while isolation of parent ions followed by judicious fragmentation in the trap and/or transfer IMS optics allowed confirmation of isomer identity [253]. Venter et al. showed in two reports how complementary hydrophilic interaction chromatography (HILIC) and reversed phase liquid chromatography (RP-LC) chromatographic separations hyphenated to TWIMS-HR-MS allows detailed analysis of mixtures of hydrolysable tannins (ellagitannins and gallotannins) [213,214]. These compounds comprise an inordinately large number of positional and stereoisomers, and the authors report that IMS proved especially useful in filtering

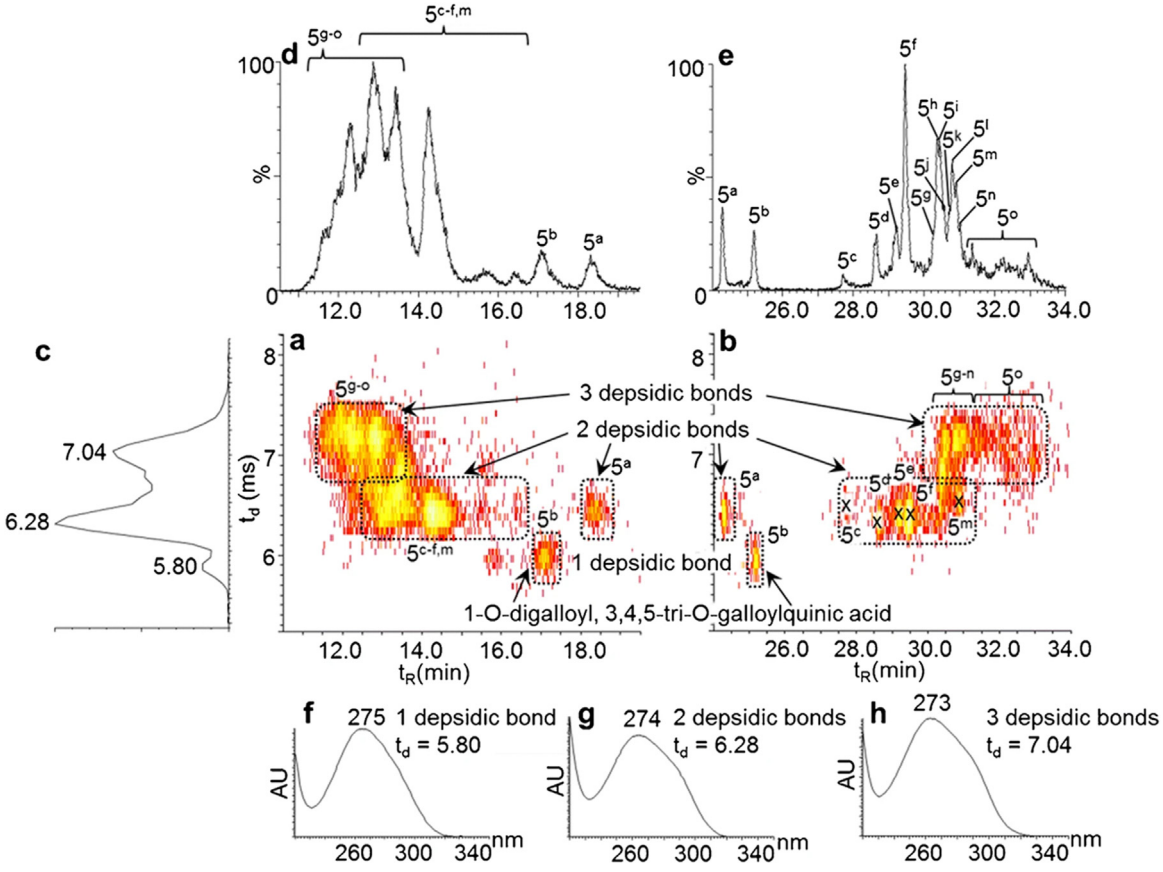

Fig. 5. a) HILIC × IMS and b) RP—LC × IMS contour plots obtained for the analysis of pentagalloylquinic acid derivatives in tara. IMS proved essential in the assignment of positional isomers, especially since arrival times increased with the number of depsidic bonds. The extracted ion arrival time plot is shown in c), extracted ion chromatograms for HILIC and RP—LC are shown in d) and e) and example UV spectra of isomers are shown in f-h). Reprinted with permission from [214].

mass spectral data according to arrival time to facilitate compound assignment. Furthermore, IMS allowed differentiation of several ellagitannin conformers/tautomers [213] and proved useful in distinguishing between positional gallotannin isomers (Fig. 5) [214].

In general, small molecule regioisomers are readily resolved by commercial IMS-MS instruments, while stereoisomers are more challenging and typically require an IMS resolving power > 300 to separate isomers exhibiting an ~0.4 % cross sectional difference (i.e. at the performance limit of current IMS instrumentation) [135]. The separation of enantiomers, with differences in CCS in the region of 0.1 %, requires the introduction of chiral selectors to form ion complexes [254,255]. This emphasises the importance of chromatographic separations in combination with IMS-MS for the resolution of complex isomeric mixtures [62,135,253].

In the context of isomer separation, the formation of prototropic ions (or tautomeric anions in negative ionisation mode), which differ in the position of the charged functional group [156,157,205,256,257] may hamper IMS data analysis and lead to incorrect assignments [92]. Indeed, several studies have reported the occurrence of prototropic/tautomeric ions in the analysis of phenolic natural products by IMS [205,207,213,214,256,258]. An example is presented in Fig. 6, where deprotonated tautomers of 3- and 5-*p*-coumaroyl-*O*-quinic acid are detected by UHPLC-TWIMS-MS. These likely correspond to the carboxylate and phenoxide ions, respectively, but could be mistaken for co-eluting isomers. The phenoxide ion has been shown to have a higher mobility than the carboxylate ion for *p*-hydroxybenzoic acid [157], pointing to the ion detected at the shorter arrival time in Fig. 6 likely corresponding to the phenoxide tautomer. The detection of these 'isomers' is influenced by the experimental conditions such as ion source conditions, IMS temperature, etc.) [92]. In a detailed study of this phenomenon, Xia and Attygalle note that ESI source conditions such as the probe spatial position, capillary voltage, desolvation gas temperature, and cone voltage all have an effect on the relative abundance of the phenoxide/carboxylate ions of *p*-hydroxybenzoic acid [157]. An increase in the capillary voltage, desolvation gas temperature, and cone voltage favoured the abundance of the phenoxide species, whereas proximity of the ESI capillary to the entrance-cone increases the abundance of the carboxylate species.

For highly complex plant extracts, multidimensional chromatographic methods are increasingly being used because of their exceptional resolving power. The hyphenation of multidimensional chromatographic methods to IMS-MS therefore provides an even more powerful separation method. The first work in this area, by Schmitz and co-workers [259], involved a continuous heartcutting 2D-LC method hyphenated to DTIMS-MS for the analysis of a *Ginkgo biloba* extract. Zhang et al. subsequently used a similar approach with TWIMS for the analysis of ginsenosides [227]. In our group a comprehensive three-dimensional HILIC × RP-UHPLC × IMS-HR-MS system was evaluated for the detailed characterisation of complex phenolic fractions [69]. The benefits of incorporating IMS in such a configuration include increased MS sensitivity for a certain mass range, improved mass-spectral data quality, and an increase in effective peak capacity by a factor 13 [69]. In a related study, Donato et al. coupled comprehensive two-dimensional supercritical fluid chromatography (SFC)×RP-UHPLC with IMS-HR-MS and demonstrated the utility of the approach for the analysis of carotenoids in chilli pepper, where IMS offered resolution of *cis*/*trans* geometric isomers [174]. A novel approach based on the first hyphenation of 2-D GC (in multiple heartcutting mode

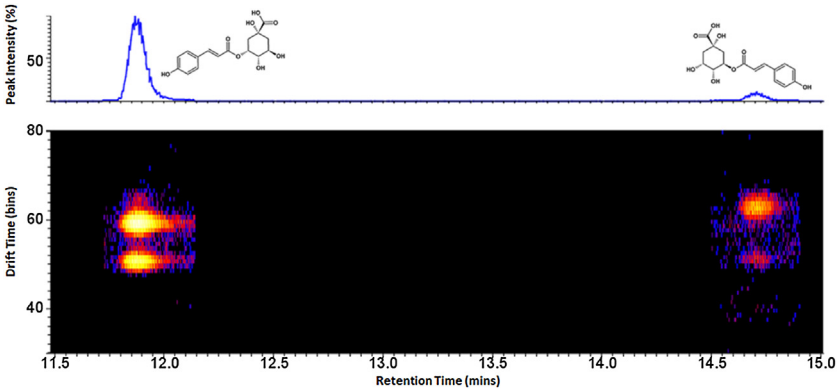

Fig. 6. Top: Extracted ion chromatogram at *m/z* 337 of the plant phenolic acids, 3-*p*-coumaroyl-*O*-quinic acid (earlier eluting peak) and 5-*p*-coumaroyl-*O*-quinic acid (later eluting peak) detected in *Protea* leaf tissue by UHPLC-TWIMS-HR-MS. Bottom: Arrival time vs. retention time plot showing the detection of tautomeric ions for both compounds, with the carboxylate ions (later arrival time ~ 60 bins) for both compounds being favoured under the experimental conditions. Source: supplementary data from [258].

using a modulation time of 20 s) through atmospheric pressure chemical ionisation (APCI) to DTIMS-QTOF-MS was reported by Lipok et al. for the analysis of medicinal herbs [175]. In another study, isobaric ginsenosides which were observed to co-elute by time-decoupled 2D-UHPLC-HR-MS were resolved when IMS was added [227].

An interesting application of IMS is in its incorporation into mass spectrometry imaging (MSI) by laser ablation electrospray ionisation (LAESI) [260]. Li et al. showed how the additional separation offered by IMS reduced chemical interference and improves the detection of isobaric compounds, including flavonoids, in *Pelargonium peltatum* leaves [261]. A similar conclusion was reached by Stopka et al. in their use of LAESI-IMS-MS to study the metabolites involved in the symbiotic interactions between soybean roots and rhizobia [262]. A unique application of IMS in natural product analysis is found in the work of Claude et al., who reported a high performance thin layer chromatography (HPTLC) method combined with desorption electrospray ionisation (DESI) and TWIMS-MS for the detection of plant ecdysteroids in members of the *Silene* plant family [263]. Akin to column chromatographic-MS methods, IMS was found to be beneficial in resolving isobaric species not separated by HPTLC in this case.

As alluded to in Section 2, the use of CCS libraries is gaining traction to facilitate compound identification; this applies in natural product analysis too. A good example of the use of DTIMS in combination with positive and negative ionisation for compound annotation can be found in a study by Causon et al., who derived $^{DT}CCS_{N2}$ values for putative identification of red wine phenolics for fingerprinting purposes [120]. Stark and co-workers established a database for the identification of natural products in *Garcinia* species by the UHPLC-TWIMS-HR-MS analysis of 34 reference compounds [177]. This allowed them to identify compounds based on retention time, accurate mass data for precursor and fragment ions, and CCS values – the latter showed excellent reproducibility. These authors also noted multiple arrival time distributions for several species, which were assigned to rotational isomers, and proposed the intensity ratio of these conformers as an additional identification criterion to reduce false positive identifications. TIMS has also been used for this purpose by Schroeder et al., who constructed a $^{TIMS}CCS_{N2}$ library containing 146 plant metabolites using UHPLC-TIMS-HR-MS/MS [151]. These authors demonstrated that $^{TIMS}CCS_{N2}$ values were characterised by an exceptional reproducibility. Zheng et al. directly measured $^{DT}CCS_{N2}$ values for 500 small molecules, including primary and secondary metabolites and xenobiotics [166], to construct a $^{DT}CCS_{N2}$ value library to match unknowns to a reduced number of possible candidate molecules when used in combination with retention time and exact mass data.

3.2. Microbial secondary metabolites

Bacteria, plants, and (to a lesser extent) marine organisms are important sources of pharmaceutical products. An early example of the application of IMS in marine natural product analysis may be found in the work of Esquenazi et al., who used TWIMS-MS for the characterisation of halogenated metabolites from three species of *Lyngbya*, cyanobacteria identified as prolific producers of bioactive metabolites [121]. ESI-TWIMS-MS was used for the analysis of crude extracts, where mass-mobility trendlines proved useful in distinguishing natural products of varying degrees of halogenation. Furthermore, MALDI imaging in combination with TWIMS-MS was used to visualise the location of selected metabolites in filaments of *L. majuscule* [121]. The high throughput benefit of IMS for natural product analysis was recently highlighted by Carlson and co-workers, who used TWIMS to separate the prodiginines streptorubin B, butylcycloheptylprodigiosin and metacycloprodigiosin, and highlighted the potential of the technique in this field [264].

As noted previously, IMS-MS is increasingly being used in food science [89], also in food safety applications [88]. One important food safety analysis is the determination of mycotoxins - globally, mycotoxin residue analysis is important for food safety and trade. Mycotoxins are toxic secondary fungal metabolites often found in important human crops. Several groups have explored the utility of IMS in mycotoxin detection [164,265,266]. Upon infection of the host organism, mycotoxins undergo chemical modifications leading to a range of possible derived products. These modification pose a challenge in routine LC-MS analyses due to the lack of standards, which may lead to the underestimation of the total mycotoxin content [265]. IMS has been shown to offer several benefits for the analysis of such modified mycotoxins [265]. Righetti and co-workers reported an ion mobility-derived mycotoxin database [164] containing more than 100 $^{TW}CCS_{N2}$ values measured for different adducts in both positive and negative ionisation modes. The reproducibility of the $^{TW}CCS_{N2}$ values was good for both LC-TWIMS-MS and direct infusion-TWIMS-MS, although values were noticeably smaller than literature $^{DT}CCS_{N2}$ values, likely due to the limitations of the TWIMS calibration using poly-alanine discussed in Section 2. The same group subsequently used UHPLC-DTIMS-HR-MS to study mycotoxin metabolites [266]. In a study by Erler et al., the analysis of volatile metabolites of 10 fungus species using HS-GC-APCI-IMS and HS-GC-APCI-MS was proposed to detect potential fungus contamination (i.e. an indirect method to

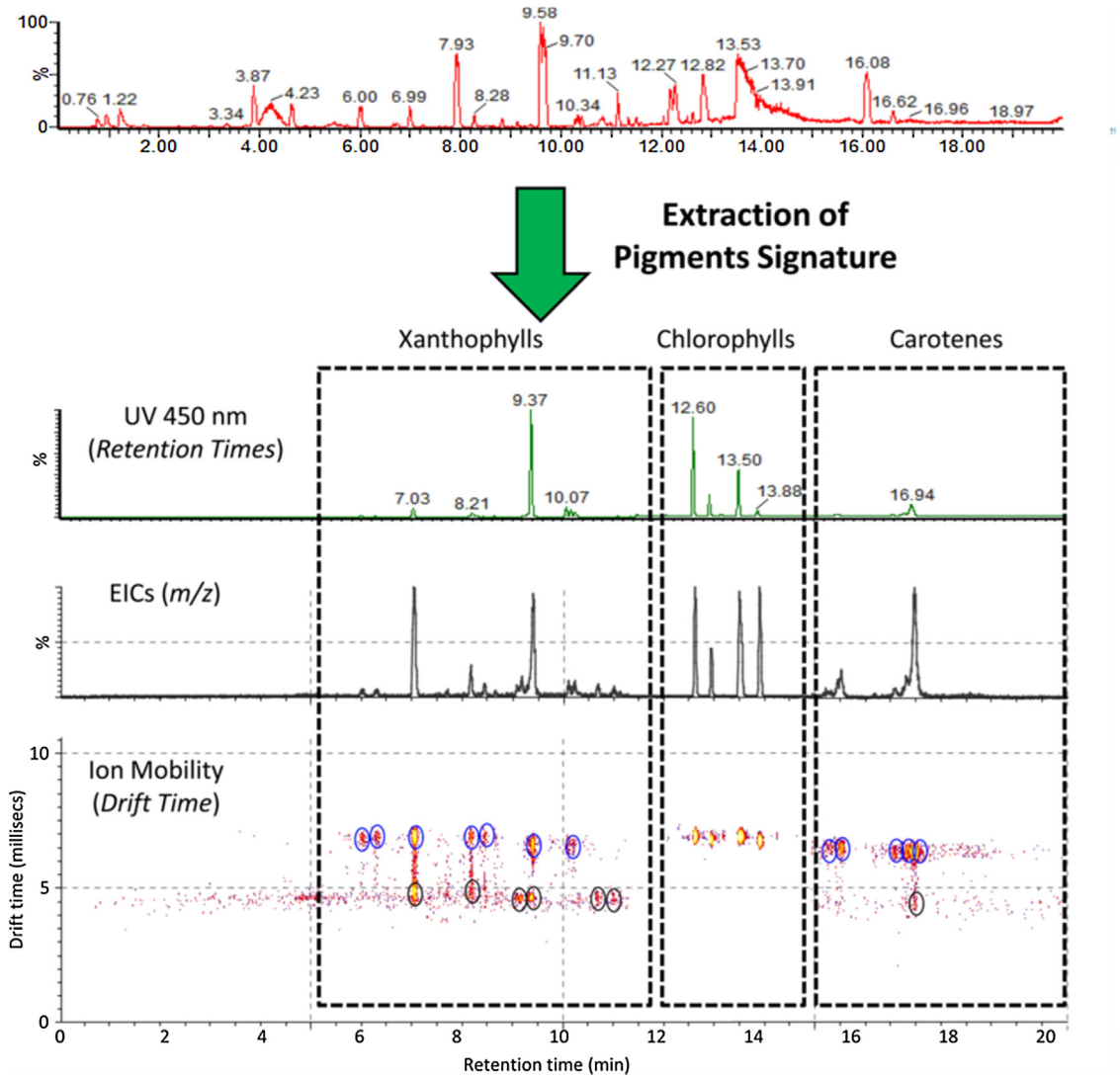

Fig. 7. UHPLC-UV-TWIMS-HR-MS analysis of microalgae pigments, demonstrating the complementary information obtained by UV, TWIMS and HR-MS detection. Reprinted with permission from [119].

identify potential mycotoxin contamination) [190]. APCI-IMS analysis showed differences in VOC distributions across fungus species belonging to different genera. The authors note that 92 % of the peaks detected using APCI-MS were also detected using a hand-held APCI-IMS instrument, which holds promise for potential onsite detection of fungus contamination. In the context of toxin analysis by IMS, Poyer et al. reported a HILIC-TWIMS-HR-MS method for the determination of the potent neurotoxin saxitoxin analogues produced by dinoflagellates and cyanobacteria, where HILIC provided separation of isomers, while non-sulphated analogous were differentiated by IMS-MS [267]. In a related study, Beach and co-workers used HILIC-FAIMS-MS/MS for the detection of the neurotoxin β-N-methylamino-L-alanine (BMAA) [268]. The method was applied to the detection of BMAA in cycad plant tissue, a cyanobacterial reference material, and mussel tissues, and the quantitative capabilities of the HILIC-FAIMS-MS/MS for the quantification of BMAA were demonstrated. Mittermeier and co-workers also reported a quantitative UHPLC-FAIMS-MS/MS method for the accurate quantitative determination of kokumi-enhancing octadecadien-12-ynoic acids in mushrooms [269].

Pacini et al. used a UHPLC-UV-TWIMS-MS method for the analysis of microalgae pigments, including carotenoids, chlorophylls and xanthophylls [119]. The authors characterised 26 pigments based on the UHPLC-UV-TWIM-MS profiles (Fig. 7), while TWIMS allowed resolution of five co-eluting 5 isobaric pigments.

The application of IMS for rapid microbial detection can be beneficial for the early diagnosis of infection [189,197,270]. At the point of infection suspicion, a broad-spectrum antibiotic therapy is often prescribed due to the lack of knowledge of the particular pathogen [270]; only after 2–4 days following microbiological diagnosis can a narrow-spectrum therapy be prescribed. Early pathogen detection is clearly essential for the early initiation of appropriate therapy. Bocos-Bintintan et al., extending previous work in this area [197], used a miniaturised sensor array incorporating aspiration IMS (a-FAIMS), metal oxide, semiconductor and a field effect transistor (FET) sensors (Fig. 8A) to discriminate between three bacterial strains, namely *Escherichia coli*, *Bacillus subtilis* and *Staphylococcus aureus*, by detecting their emitted volatile metabolites at three incubation time stages (24, 48 and 72 h after the start of the incubation cycle) [189]. To discriminate between the bacterial strains using only the a-IMS data, a supervised data analysis model (partial least squares–discriminant analysis (PLS-DA)) was used. The authors note differences between the control (growth media) and the bacterial strains (growth media containing inoculated bacteria) (Fig. 8B), as well as differences between the three bacterial strains sampled on the same day (Fig. 8C).

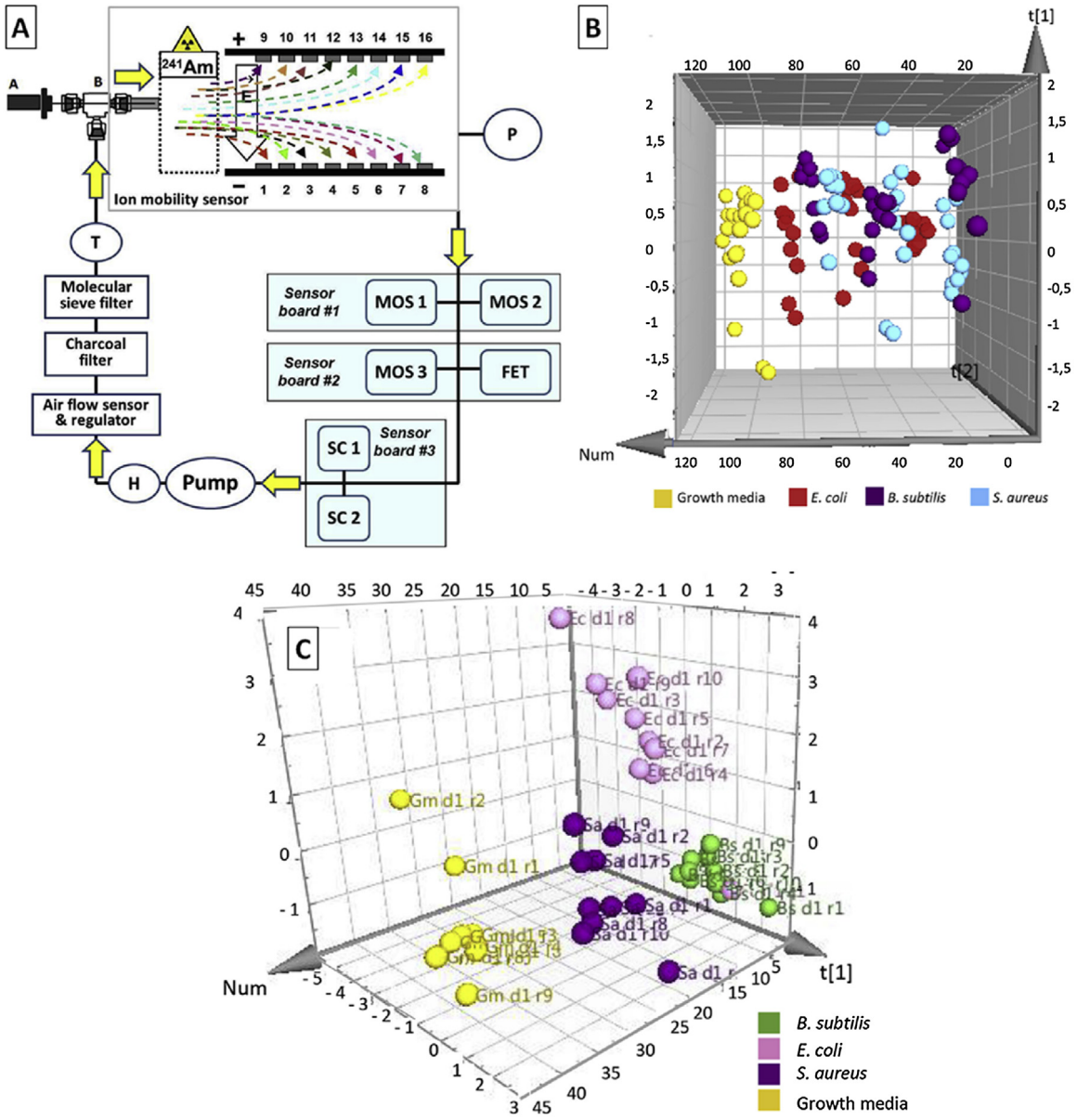

Fig. 8. (A) Schematic diagram of the a-IMS instrument utilised for the analyses of volatile metabolites emitted by bacterial strains *Escherichia coli*, *Bacillus subtilis* and *Staphylococcus aureus*. Differences (B) between the bacterial strains and the control, as well as (C) between the bacterial strains, were observed. Reprinted with permission from [189].

4. IMS in natural product analysis: advantages, limitations, and future directions

The field of IMS has experienced extraordinary growth in the last decade, resulting in a rapid increase in the number of applications of the technique for complex sample analysis. That this situation is, albeit to a lesser extent, also mirrored in the analysis of natural products is evident from the reports listed in this review. This is perhaps not surprising considering the well-publicised benefits of IMS: its speed, compatibility with chromatography and MS, complementary separation mechanism, and ability to measure CCS values. Applied in the field of natural product analysis, the potential for enhanced separation of bioactive isomers and isobars, the option to filter MS data according to arrival time to provide improved MS data, flexibility of operational modes and increased confidence in metabolite identification are particularly useful. The use of CCS values as an additional identification point promises to be an important development with the emergence of reliable CCS databases for different compound classes.

Inconsistencies in how IMS data is acquired and interpreted, especially in early literature, as well as data and instrumental complexity, cost and differing capabilities represent some hurdles to researchers looking to enter the field. Although much emphasis is placed on the separation performance of IMS, and examples of multiple arrival times for co-eluting isobars abound in literature, it is relevant to note that these occurrences are relatively rare: for complex samples, by far the majority of analytes are separated chromatographically and/or distinguished by MS. IMS should therefore rather be seen as a complementary technique in hyphenation with chromatography-MS for such applications, albeit a very promising one with few drawbacks. Further work on the incorporation of IMS data into widely used data analysis platforms is required for the technique to gain more widespread acceptance in natural product analysis, although ongoing developments in this area are

promising. The quantitative capabilities of IMS have received little attention in natural product analysis, and is therefore another area requiring further exploration.

Reviewing the papers listed in Table 1 shows that by far the majority of IMS applications to natural product analysis during the last six years used commercial DTIMS and TWIMS instruments (~42 and 45 %, respectively), and the major application areas are in the analysis of phenolics and food-related volatiles. Nevertheless, the range of instrumentation, analytical methods and target analytes covered in these works point to the versatility of the technique for natural product analysis.

It can reasonably be concluded that IMS represents an important development in the establishment of more powerful analytical tools for the improved characterisation of natural products, and as such its application in this field is expected to grow rapidly in the near future. Advanced analytical methods incorporating IMS provides the tools required to support a revival in natural product drug discovery.

CRediT authorship contribution statement

Keabetswe Masike: Investigation, Data curation, Writing - original draft. **Maria A. Stander:** Supervision, Writing - review & editing. **André de Villiers:** Conceptualization, Writing - review & editing.

Declaration of Competing Interest

The authors declare that they have no known competing financial interests or personal relationships that could have appeared to influence the work reported in this paper.

Acknowledgements

The authors would like to acknowledge financial support from Sasol (Collaborative grant to AdV), the Central Analytical Facility of Stellenbosch University and the National Research Foundation of South Africa (grant 118530 to AdV and post-graduate bursary 121613 to KM).

References

[1] D.J. Newman, G.M. Cragg, Natural products as sources of new drugs over the nearly four decades from 01/1981 to 09/2019, J. Nat. Prod. 83 (2020) 770–803, http://dx.doi.org/10.1021/acs.jnatprod.9b01285.
[2] G.M. Cragg, D.J. Newman, K.M. Snader, Natural products in drug discovery and development, J. Nat. Prod. 60 (1997) 52–60, http://dx.doi.org/10.1021/np9604893.
[3] D.J. Newman, G.M. Cragg, K.M. Snader, Natural products as sources of new drugs over the period 1981-2002, J. Nat. Prod. 66 (2003) 1022–1037, http://dx.doi.org/10.1021/np030096l.
[4] D.J. Newman, G.M. Cragg, Natural products as sources of new drugs over the last 25 years, J. Nat. Prod. 70 (2007) 461–477, http://dx.doi.org/10.1021/np068054v.
[5] D.J. Newman, G.M. Cragg, Natural products as sources of new drugs over the 30 years from 1981 to 2010, J. Nat. Prod. 75 (2012) 311–335, http://dx.doi.org/10.1021/np200906s.
[6] D.J. Newman, G.M. Cragg, Natural products as sources of new drugs from 1981 to 2014, J. Nat. Prod. 79 (2016) 629–661, http://dx.doi.org/10.1021/acs.jnatprod.5b01055.
[7] J.W.H. Li, J.C. Vederas, Drug discovery and natural products: end of an era or an endless frontier? Science (80-.) 325 (2009) 161–165, http://dx.doi.org/10.1126/science.1168243.
[8] D.A. Dias, S. Urban, U. Roessner, A historical overview of natural products in drug discovery, Metabolites 2 (2012) 303–336, http://dx.doi.org/10.3390/metabo2020303.
[9] G. Walsh, Biopharmaceutical benchmarks 2018, Nat. Biotechnol. 36 (2018) 1136–1145, http://dx.doi.org/10.1038/nbt.4305.
[10] G.M. Cragg, D.J. Newman, Natural products: a continuing source of novel drug leads, Biochim. Biophys. Acta - Gen. Subj. 1830 (2013) 3670–3695, http://dx.doi.org/10.1016/j.bbagen.2013.02.008.
[11] A.L. Harvey, R. Edrada-Ebel, R.J. Quinn, The re-emergence of natural products for drug discovery in the genomics era, Nat. Rev. Drug Discov. 14 (2015) 111–129, http://dx.doi.org/10.1038/nrd4510.
[12] R. Croteau, M.T. Kutchan, G.N. Lewis, Natural products (secondary metabolites), in: B. Buchannan, W. Gruissem, R.L. Jones (Eds.), Biochem. Mol. Biol. Plants, American Society of Plant Physiologists, Rockvile, 2000, pp. 1250–1318, http://dx.doi.org/10.1201/b11003-3.
[13] F. Bourgaud, A. Gravot, S. Milesi, E. Gontier, Production of plant secondary metabolites: a historical perspective, Plant Sci. 161 (2001) 839–851, http://dx.doi.org/10.1016/S0168-9452(01)00490-3.
[14] A. Crozier, B.I. Jaganath, N.M. Clifford, Phenols, polyphenols and tannins: an overview, in: A. Crozier, N.M. Clifford, H. Ashihara (Eds.), Plant Second. Metab. Occur. Struct. Role Hum. Diet, Blackwell Publishing Ltd, 2006, pp. 1–25, https://doi.org/1-4051-2509-8 Library.
[15] A. Rodriguez-Mateos, D. Vauzour, C.G. Krueger, D. Shanmuganayagam, J. Reed, L. Calani, P. Mena, D. Del Rio, A. Crozier, Bioavailability, bioactivity and impact on health of dietary flavonoids and related compounds: an update, Arch. Toxicol. 88 (2014) 1803–1853, http://dx.doi.org/10.1007/s00204-014-1330-7.
[16] E. Dittmann, M. Gugger, K. Sivonen, D.P. Fewer, Natural product biosynthetic diversity and comparative genomics of the Cyanobacteria, Trends Microbiol. 23 (2015) 642–652, http://dx.doi.org/10.1016/j.tim.2015.07.008.
[17] S. Hasan, M. Ansari, A. Ahmad, M. Mishra, Major bioactive metabolites from marine fungi: a review, Bioinformation 11 (2015) 176–181, http://dx.doi.org/10.6026/97320630011176.
[18] N.P. Keller, G. Turner, J.W. Bennett, Fungal secondary metabolism - from biochemistry to genomics, Nat. Rev. Microbiol. 3 (2005) 937–947, http://dx.doi.org/10.1038/nrmicro1286.
[19] J. Kennedy, K. Auclair, S.G. Kendrew, C. Park, J.C. Vederas, C.R. Hutchinson, Modulation of polyketide synthase activity by accessory proteins during lovastatin biosynthesis, Science (80-.) 284 (1999) 1368–1372, http://dx.doi.org/10.1126/science.284.5418.1368.
[20] M.H. Walter, D. Strack, Carotenoids and their cleavage products: biosynthesis and functions, Nat. Prod. Rep. 28 (2011) 663–692, http://dx.doi.org/10.1039/c0np00036a.
[21] S.G. Sparg, M.E. Light, J. Van Staden, Biological activities and distribution of plant saponins, J. Ethnopharmacol. 94 (2004) 219–243, http://dx.doi.org/10.1016/j.jep.2004.05.016.
[22] Y. Bahrami, W. Zhang, C.M.M. Franco, Distribution of saponins in the sea cucumber holothuria lessoni; the body wall versus the viscera, and their biological activities, Mar. Drugs 16 (2018), http://dx.doi.org/10.3390/md16110423.
[23] D. Singh, P.K. Chaudhuri, Structural characteristics, bioavailability and cardioprotective potential of saponins, Integr. Med. Res. 7 (2018) 33–43, http://dx.doi.org/10.1016/j.imr.2018.01.003.
[24] M.S. Butler, A.A.B. Robertson, M.A. Cooper, Natural product and natural product derived drugs in clinical trials, Nat. Prod. Rep. 31 (2014) 1612–1661, http://dx.doi.org/10.1039/c4np00064a.
[25] B. Haefner, Drugs from the deep: marine natural products as drug candidates, Drug Discov. Today 8 (2003) 536–544, http://dx.doi.org/10.1016/S1359-6446(03)02713-2.
[26] J.L. Wolfender, G. Marti, A. Thomas, S. Bertrand, Current approaches and challenges for the metabolite profiling of complex natural extracts, J. Chromatogr. A 1382 (2015) 136–164, http://dx.doi.org/10.1016/j.chroma.2014.10.091.
[27] M.S.S. Amaral, Y. Nolvachai, P.J. Marriott, Comprehensive two-dimensional gas chromatography advances in technology and applications: biennial update, Anal. Chem. 92 (2020) 85–104, http://dx.doi.org/10.1021/acs.analchem.9b05412.
[28] A.C. Peterson, G.C. Mcalister, S.T. Quarmby, J. Griep-raming, J.J. Coon, Development and Characterization of a GC-Enabled QLT-Orbitrap for High-Resolution and High-Mass Accuracy GC / MS, 82, 2010, pp. 8618–8628.
[29] K.A. Schug, I. Sawicki, D.D. Carlton, H. Fan, H.M. McNair, J.P. Nimmo, P. Kroll, J. Smuts, P. Walsh, D. Harrison, Vacuum ultraviolet detector for gas chromatography, Anal. Chem. 86 (2014) 8329–8335, http://dx.doi.org/10.1021/ac5018343.
[30] K. Broeckhoven, G. Desmet, Advances and challenges in extremely high-pressure liquid chromatography in current and future analytical scale column formats, Anal. Chem. 92 (2020) 554–560, http://dx.doi.org/10.1021/acs.analchem.9b04278.
[31] R. Hayes, A. Ahmed, T. Edge, H. Zhang, Core-shell particles: preparation, fundamentals and applications in high performance liquid chromatography, J. Chromatogr. A 1357 (2014) 36–52, http://dx.doi.org/10.1016/j.chroma.2014.05.010.
[32] B.W.J. Pirok, D.R. Stoll, P.J. Schoenmakers, Recent developments in two-dimensional liquid chromatography: fundamental improvements for practical applications, Anal. Chem. 91 (2019) 240–263, http://dx.doi.org/10.1021/acs.analchem.8b04841.
[33] M. Ganzera, S. Sturm, Recent advances on HPLC/MS in medicinal plant analysis—an update covering 2011–2016, J. Pharm. Biomed. Anal. 147 (2018) 211–233, http://dx.doi.org/10.1016/j.jpba.2017.07.038.
[34] A. De Villiers, P. Venter, H. Pasch, Recent advances and trends in the liquid-chromatography-mass spectrometry analysis of flavonoids, J. Chromatogr. A 1430 (2015) 16–78, http://dx.doi.org/10.1016/j.chroma.2015.11.077.

[35] M. Holčapek, R. Jirásko, M. Lísa, Recent developments in liquid chromatography-mass spectrometry and related techniques, J. Chromatogr. A 1259 (2012) 3–15, http://dx.doi.org/10.1016/j.chroma.2012.08.072.

[36] H. Wu, J. Guo, S. Chen, X. Liu, Y. Zhou, X. Zhang, X. Xu, Recent developments in qualitative and quantitative analysis of phytochemical constituents and their metabolites using liquid chromatography-mass spectrometry, J. Pharm. Biomed. Anal. 72 (2013) 267–291, http://dx.doi.org/10.1016/j.jpba.2012.09.004.

[37] J. Xing, C. Xie, H. Lou, Recent applications of liquid chromatography-mass spectrometry in natural products bioanalysis, J. Pharm. Biomed. Anal. 44 (2007) 368–378, http://dx.doi.org/10.1016/j.jpba.2007.01.010.

[38] W. Xu, G. Luo, F. Yu, Q. Jia, Y. Zheng, X. Bi, J. Lei, Characterization of anthocyanins in the hybrid progenies derived from Iris dichotoma and I. domestica by HPLC-DAD-ESI/MS analysis, Phytochemistry 150 (2018) 60–74, http://dx.doi.org/10.1016/j.phytochem.2018.03.003.

[39] A. Doerr, DIA mass spectrometry, Nat. Methods 12 (2015) 35, http://dx.doi.org/10.1038/nmeth.3234.

[40] R.S. Plumb, K.A. Johnson, P. Rainville, B.W. Smith, I.D. Wilson, J.M. Castro-Perez, J.K. Nicholson, UPLC/MSE; a new approach for generating molecular fragment information for biomarker structure elucidation, Rapid Commun. Mass Spectrom. 20 (2006) 1989–1994, http://dx.doi.org/10.1002/rcm.2550.

[41] A.W. Zuardi, J.A.S. Crippa, J.E.C. Hallak, F.A. Moreira, F.S. Guimarães, Cannabidiol, a Cannabis sativa constituent, as an antipsychotic drug, Braz. J. Med. Biol. Res. 39 (2006) 421–429, http://dx.doi.org/10.1590/S0100-879X2006000400001.

[42] L.V. Tose, N.A. Santos, R.R.T. Rodrigues, M. Murgu, A.F. Gomes, G.A. Vasconcelos, P.C.T. Souza, B.G. Vaz, W. Romão, Isomeric separation of cannabinoids by UPLC combined with ionic mobility mass spectrometry (TWIM-MS)—part I, Int. J. Mass Spectrom. 418 (2017) 112–121, http://dx.doi.org/10.1016/j.ijms.2016.10.018.

[43] M.M. Makola, P.A. Steenkamp, I.A. Dubery, M.M. Kabanda, N.E. Madala, Preferential alkali metal adduct formation by cis geometrical isomers of dicaffeoylquinic acids allows for efficient discrimination from their trans isomers during ultra-high-performance liquid chromatography/quadrupole time-of-flight mass spectrometry, Rapid Commun. Mass Spectrom. 30 (2016) 1011–1018, http://dx.doi.org/10.1002/rcm.7526.

[44] K. Masike, N. Madala, Synchronized survey scan approach allows for efficient discrimination of isomeric and isobaric compounds during LC-MS/MS analyses, J. Anal. Methods Chem. 2018 (2018) 1–9, http://dx.doi.org/10.1155/2018/2046709.

[45] K.E. Burnum-Johnson, X. Zheng, J.N. Dodds, J. Ash, D. Fourches, C.D. Nicora, J.P. Wendler, T.O. Metz, K.M. Waters, J.K. Jansson, R.D. Smith, E.S. Baker, Ion mobility spectrometry and the omics: distinguishing isomers, molecular classes and contaminant ions in complex samples, TrAC - Trends Anal. Chem. 116 (2019) 292–299, http://dx.doi.org/10.1016/j.trac.2019.04.022.

[46] A.J. Levy, N.R. Oranzi, A. Ahmadireskety, R.H.J. Kemperman, M.S. Wei, R.A. Yost, Recent progress in metabolomics using ion mobility-mass spectrometry, TrAC - Trends Anal. Chem. 116 (2019) 274–281, http://dx.doi.org/10.1016/j.trac.2019.05.001.

[47] Q. Wu, J.-Y. Wang, D.-Q. Han, Z.-P. Yao, Recent advances in differentiation of isomers by ion mobility mass spectrometry, TrAC Trends Anal. Chem. 124 (2020), 115801, http://dx.doi.org/10.1016/j.trac.2019.115801.

[48] R. Cumeras, E. Figueras, C.E. Davis, J.I. Baumbach, I. Gràcia, Review on Ion Mobility Spectrometry. Part 2: hyphenated methods and effects of experimental parameters, Analyst 140 (2015) 1391–1410, http://dx.doi.org/10.1039/c4an01101e.

[49] J.C. May, J.A. McLean, Ion mobility-mass spectrometry: time-dispersive instrumentation, Anal. Chem. 87 (2015) 1422–1436, http://dx.doi.org/10.1021/ac504720m.

[50] J.N. Dodds, E.S. Baker, Ion mobility spectrometry: fundamental concepts, instrumentation, applications, and the road ahead, J. Am. Soc. Mass Spectrom. 30 (2019) 2185–2195, http://dx.doi.org/10.1007/s13361-019-02288-2.

[51] A.T. Kirk, A. Bohnhorst, C.-R. Raddatz, M. Allers, S. Zimmermann, Ultra-high-resolution ion mobility spectrometry—current instrumentation, limitations, and future developments, Anal. Bioanal. Chem. 411 (2019) 6229–6246, http://dx.doi.org/10.1007/s00216-019-01807-0.

[52] D.C. Collins, M.L. Lee, Developments in ion mobility spectrometry-mass spectrometry, Anal. Bioanal. Chem. 372 (2002) 66–73, http://dx.doi.org/10.1007/s00216-001-1195-5.

[53] A.B. Kanu, P. Dwivedi, M. Tam, L. Matz, H.H. Hill, Ion mobility-mass spectrometry, J. Mass Spectrom. 43 (2008) 1–22, http://dx.doi.org/10.1002/jms.1383.

[54] W. Jiang, R.A.S. Robinson, Ion mobility-mass spectrometry, in: Encycl. Anal. Chem., John Wiley & Sons, Ltd, Chichester, UK, 2013, http://dx.doi.org/10.1002/9780470027318.a9292.

[55] M.A. Balm, H.H. Hill, Tunable selective detection for capillary gas chromatography by ion mobility monitoring, Anal. Chem. 54 (1982) 38–43, http://dx.doi.org/10.1021/ac00238a013.

[56] A.B. Kanu, H.H. Hill, Ion mobility spectrometry detection for gas chromatography, J. Chromatogr. A 1177 (2008) 12–27, http://dx.doi.org/10.1016/j.chroma.2007.10.110.

[57] J. Li, R.W. Purves, J.C. Richards, Coupling capillary electrophoresis and high-field asymmetric waveform ion mobility spectrometry mass spectrometry for the analysis of complex lipopolysaccharides, Anal. Chem. 76 (2004) 4676–4683, http://dx.doi.org/10.1021/ac049850d.

[58] M.A. Ewing, M.S. Glover, D.E. Clemmer, Hybrid ion mobility and mass spectrometry as a separation tool, J. Chromatogr. A 1439 (2016) 3–25, http://dx.doi.org/10.1016/j.chroma.2015.10.080.

[59] X. Zheng, R. Wojcik, X. Zhang, Y.M. Ibrahim, K.E. Burnum-Johnson, D.J. Orton, M.E. Monroe, R.J. Moore, R.D. Smith, E.S. Baker, Coupling front-end separations, ion mobility spectrometry, and mass spectrometry for enhanced multidimensional biological and environmental analyses, Annu. Rev. Anal. Chem. 10 (2017) 71–92, http://dx.doi.org/10.1146/annurev-anchem-061516-045212.

[60] V. D'Atri, T. Causon, O. Hernandez-Alba, A. Mutabazi, J.L. Veuthey, S. Cianferani, D. Guillarme, Adding a new separation dimension to MS and LC–MS: What is the utility of ion mobility spectrometry? J. Sep. Sci. 41 (2018) 20–67, http://dx.doi.org/10.1002/jssc.201700919.

[61] K.A. Morrison, B.H. Clowers, Fundamentals and applications of incorporating chromatographic separations with ion mobility-mass spectrometry, TrAC Trends Anal. Chem. 119 (2019), 115625, http://dx.doi.org/10.1016/j.trac.2019.115625.

[62] T. Werres, J. Leonhardt, M. Jäger, T. Teutenberg, Critical comparison of liquid chromatography coupled to mass spectrometry and three different ion mobility spectrometry systems on their separation capability for small isomeric compounds, Chromatographia 82 (2019) 251–260, http://dx.doi.org/10.1007/s10337-018-3640-z.

[63] R.M. Räsänen, P. Dwivedi, F.M. Fernández, T.J. Kauppila, Desorption atmospheric pressure photoionization and direct analysis in real time coupled with travelling wave ion mobility mass spectrometry, Rapid Commun. Mass Spectrom. 28 (2014) 2325–2336, http://dx.doi.org/10.1002/rcm.7028.

[64] A. Kaufmann, P. Butcher, K. Maden, S. Walker, M. Widmer, Does the ion mobility resolving power as provided by commercially available ion mobility quadrupole time-of-flight mass spectrometry instruments permit the unambiguous identification of small molecules in complex matrices? Anal. Chim. Acta 1107 (2020) 113–126, http://dx.doi.org/10.1016/j.aca.2020.02.032.

[65] P. Dwivedi, A.J. Schultz, H.H. Hill, Metabolic profiling of human blood by high-resolution ion mobility mass spectrometry (IM-MS), Int. J. Mass Spectrom. 298 (2010) 78–90, http://dx.doi.org/10.1016/j.ijms.2010.02.007.

[66] B. Shrestha, A. Vertes, High-throughput cell and tissue analysis with enhanced molecular coverage by laser ablation electrospray ionization mass spectrometry using ion mobility separation, Anal. Chem. 86 (2014) 4308–4315, http://dx.doi.org/10.1021/ac500007t.

[67] A. Basit, S. Pontis, D. Piomelli, A. Armirotti, Ion mobility mass spectrometry enhances low-abundance species detection in untargeted lipidomics, Metabolomics 12 (2016) 1–10, http://dx.doi.org/10.1007/s11306-016-0971-3.

[68] J.C. May, R.L. Gant-Branum, J.A. McLean, Targeting the untargeted in molecular phenomics with structurally-selective ion mobility-mass spectrometry, Curr. Opin. Biotechnol. 39 (2016) 192–197, http://dx.doi.org/10.1016/j.copbio.2016.04.013.

[69] P. Venter, M. Muller, J. Vestner, M.A. Stander, A.G.J. Tredoux, H. Pasch, A. De Villiers, Comprehensive three-dimensional LC × LC × ion mobility spectrometry separation combined with high-resolution MS for the analysis of complex samples, Anal. Chem. 90 (2018) 11643–11650, http://dx.doi.org/10.1021/acs.analchem.8b03234.

[70] S.M. Stow, T.J. Causon, X. Zheng, R.T. Kurulugama, T. Mairinger, J.C. May, E.E. Rennie, E.S. Baker, R.D. Smith, J.A. McLean, S. Hann, J.C. Fjeldsted, An interlaboratory evaluation of drift tube ion mobility-mass spectrometry collision cross section measurements, Anal. Chem. 89 (2017) 9048–9055, http://dx.doi.org/10.1021/acs.analchem.7b01729.

[71] G. Paglia, J.P. Williams, L. Menikarachchi, J.W. Thompson, R. Tyldesley-Worster, S. Halldórsson, O. Rolfsson, A. Moseley, D. Grant, J. Langridge, B.O. Palsson, G. Astarita, Ion mobility derived collision cross sections to support metabolomics applications, Anal. Chem. 86 (2014) 3985–3993, http://dx.doi.org/10.1021/ac500405x.

[72] J.C. May, C.R. Goodwin, J.A. McLean, Ion mobility-mass spectrometry strategies for untargeted systems, synthetic, and chemical biology, Curr. Opin. Biotechnol. 31 (2015) 117–121, http://dx.doi.org/10.1016/j.copbio.2014.10.012.

[73] T. Mairinger, T.J. Causon, S. Hann, The potential of ion mobility–mass spectrometry for non-targeted metabolomics, Curr. Opin. Chem. Biol. 42 (2018) 9–15, http://dx.doi.org/10.1016/j.cbpa.2017.10.015.

[74] M.-D. Luo, Z.-W. Zhou, Z.-J. Zhu, The application of ion mobility-mass spectrometry in untargeted metabolomics: from separation to identification, J. Anal. Test. 4 (2020) 163–174, http://dx.doi.org/10.1007/s41664-020-00133-0.

[75] S.J. Valentine, X. Liu, M.D. Plasencia, A.E. Hilderbrand, R.T. Kurulugama, S.L. Koeniger, D.E. Clemmer, Developing liquid chromatography ion mobility mass spectometry techniques, Expert Rev. Proteomics 2 (2005) 553–565, http://dx.doi.org/10.1586/14789450.2.4.553.

[76] Y. Zhong, S.-J. Hyung, B.T. Ruotolo, Ion mobility–mass spectrometry for structural proteomics, Expert Rev. Proteomics 9 (2012) 47–58, http://dx.doi.org/10.1586/epr.11.75.

[77] C.D. Chouinard, G. Nagy, R.D. Smith, E.S. Baker, Ion mobility-mass spectrometry in Metabolomic, lipidomic, and proteomic analyses, Compr.

Anal. Chem. 83 (2019) 123–159, http://dx.doi.org/10.1016/bs.coac.2018.11.001.
[78] M. Kliman, J.C. May, J.A. McLean, Lipid analysis and lipidomics by structurally selective ion mobility-mass spectrometry, Biochim. Biophys. Acta - Mol. Cell Biol. Lipids 1811 (2011) 935–945, http://dx.doi.org/10.1016/j.bbalip.2011.05.016.
[79] G. Astarita, G. Paglia, K. Yu, Ion-mobility mass spectrometry in metabolomics and lipidomics, LC-GC North Am. 33 (2015) 702–709.
[80] G. Paglia, M. Kliman, E. Claude, S. Geromanos, G. Astarita, Applications of ion-mobility mass spectrometry for lipid analysis, Anal. Bioanal. Chem. 407 (2015) 4995–5007, http://dx.doi.org/10.1007/s00216-015-8664-8.
[81] J. Tu, Z. Zhou, T. Li, Z.J. Zhu, The emerging role of ion mobility-mass spectrometry in lipidomics to facilitate lipid separation and identification, TrAC - Trends Anal. Chem. 116 (2019) 332–339, http://dx.doi.org/10.1016/j.trac.2019.03.017.
[82] A.L. Rister, E.D. Dodds, Steroid analysis by ion mobility spectrometry, Steroids 153 (2020), 108531, http://dx.doi.org/10.1016/j.steroids.2019.108531.
[83] Y. Mu, B.L. Schulz, V. Ferro, Applications of ion mobility-mass spectrometry in carbohydrate chemistry and glycobiology, Molecules 23 (2018) 1–17, http://dx.doi.org/10.3390/molecules23102557.
[84] K. Ortmayr, T.J. Causon, S. Hann, G. Koellensperger, Increasing selectivity and coverage in LC-MS based metabolome analysis, TrAC - Trends Anal. Chem. 82 (2016) 358–366, http://dx.doi.org/10.1016/j.trac.2016.06.011.
[85] J.L. Ren, A.H. Zhang, L. Kong, X.J. Wang, Advances in mass spectrometry-based metabolomics for investigation of metabolites, RSC Adv. 8 (2018) 22335–22350, http://dx.doi.org/10.1039/c8ra01574k.
[86] X. Zhang, K. Quinn, C. Cruickshank-Quinn, R. Reisdorph, N. Reisdorph, The application of ion mobility mass spectrometry to metabolomics, Curr. Opin. Chem. Biol. 42 (2018) 60–66, http://dx.doi.org/10.1016/j.cbpa.2017.11.001.
[87] Z. Karpas, Applications of ion mobility spectrometry (IMS) in the field of foodomics, Food Res. Int. 54 (2013) 1146–1151, http://dx.doi.org/10.1016/j.foodres.2012.11.029.
[88] M. Hernández-Mesa, A. Escourrou, F. Monteau, B. Le Bizec, G. Dervilly-Pinel, Current applications and perspectives of ion mobility spectrometry to answer chemical food safety issues, TrAC - Trends Anal. Chem. 94 (2017) 39–53, http://dx.doi.org/10.1016/j.trac.2017.07.006.
[89] M. Hernández-Mesa, D. Ropartz, A.M. García-Campaña, H. Rogniaux, G. Dervilly-Pinel, B. Le Bizec, Ion mobility spectrometry in food analysis: principles, current applications and future trends, Molecules 24 (2019) 1–28, http://dx.doi.org/10.3390/molecules24152706.
[90] S.M. Stow, N.M. Lareau, K.M. Hines, C.R. Mcnees, C.R. Goodwin, B.O. Bachmann, J.A. Mclean, Structural separations for natural product characterization by Ion Mobility-Mass spectrometry: fundamental theory to emerging applications, Nat. Prod. Anal. Instrum.Methods, Appl. (2014) 397–431, http://dx.doi.org/10.1002/9781118876015.ch11, 9781118466.
[91] A.C. Schrimpe-Rutledge, S.D. Sherrod, J.A. McLean, Improving the discovery of secondary metabolite natural products using ion mobility–mass spectrometry, Curr. Opin. Chem. Biol. 42 (2018) 160–166, http://dx.doi.org/10.1016/j.cbpa.2017.12.004.
[92] V. Gabelica, A.A. Shvartsburg, C. Afonso, P. Barran, J.L.P. Benesch, C. Bleiholder, M.T. Bowers, A. Bilbao, M.F. Bush, J.L. Campbell, I.D.G. Campuzano, T. Causon, B.H. Clowers, C.S. Creaser, E. De Pauw, J. Far, F. Fernandez-Lima, J.C. Fjeldsted, K. Giles, M. Groessl, C.J. Hogan, S. Hann, H.I. Kim, R.T. Kurulugama, J.C. May, J.A. McLean, K. Pagel, K. Richardson, M.E. Ridgeway, F. Rosu, F. Sobott, K. Thalassinos, S.J. Valentine, T. Wyttenbach, Recommendations for reporting ion mobility Mass Spectrometry measurements, Mass Spectrom. Rev. 38 (2019) 291–320, http://dx.doi.org/10.1002/mas.21585.
[93] K. Michelmann, J.A. Silveira, M.E. Ridgeway, M.A. Park, Fundamentals of trapped ion mobility spectrometry, J. Am. Soc. Mass Spectrom. 26 (2015) 14–24, http://dx.doi.org/10.1007/s13361-014-0999-4.
[94] M.E. Ridgeway, M. Lubeck, J. Jordens, M. Mann, M.A. Park, Trapped ion mobility spectrometry: a short review, Int. J. Mass Spectrom. 425 (2018) 22–35, http://dx.doi.org/10.1016/j.ijms.2018.01.006.
[95] M.J. Cohen, F.W. Karasek, Plasma chromatographytm -a new dimension for gas chromatography and mass spectrometry, J. Chromatogr. Sci. 8 (1970) 330–337, http://dx.doi.org/10.1093/chromsci/8.6.330.
[96] H.E. Revercomb, E.A. Mason, Theory of plasma chromatography/gaseous electrophoresis, A Review, Anal. Chem. 47 (1975) 970–983, http://dx.doi.org/10.1021/ac60357a043.
[97] G. Von Helden, M.T. Hsu, N. Gotts, M.T. Bowers, Carbon cluster cations with up to 84 atoms: structures, formation mechanism, and reactivity, J. Phys. Chem. 97 (1993) 8182–8192, http://dx.doi.org/10.1021/j100133a011.
[98] W.S. Barnes, D.W. Martin, E.W. McDaniel, Mass spectrographic identification of the ion observed in hydrogen mobility experiments, Phys. Rev. Lett. 6 (1961) 110–111, http://dx.doi.org/10.1103/PhysRevLett.6.110.
[99] J. Gieniec, L.L. Mack, K. Nakamae, C. Gupta, V. Kumar, M. Dole, Electrospray mass spectroscopy of macromolecules: application of an ion-drift spectrometer, Biol. Mass Spectrom. 11 (1984) 259–268, http://dx.doi.org/10.1002/bms.1200110602.
[100] D.E. Clemmer, R.R. Hudgins, M.F. Jarrold, Naked protein conformations: cytochrome c in the gas phase, J. Am. Chem. Soc. 117 (1995) 10141–10142, http://dx.doi.org/10.1021/ja00145a037.
[101] G. von Helden, T. Wyttenbach, M.T. Bowers, Conformation of macromolecules in the gas phase: use of matrix-assisted laser desorption methods in ion chromatography, Science (80-.) 267 (1995) 1483–1485, http://dx.doi.org/10.1126/science.267.5203.1483.
[102] T. Wyttenbach, G. von Helden, M.T. Bowers, Gas-phase conformation of biological molecules: bradykinin, J. Am. Chem. Soc. 118 (1996) 8355–8364, http://dx.doi.org/10.1021/ja9535928.
[103] K.B. Shelimov, D.E. Clemmer, R.R. Hudgins, M.F. Jarrold, Protein structure in Vacuo: gas-phase conformations of BPTI and cytochrome c, J. Am. Chem. Soc. 119 (1997) 2240–2248, http://dx.doi.org/10.1021/ja9619059.
[104] C. Wu, W.F. Siems, G.R. Asbury, H.H. Hill, Electrospray ionization high-resolution ion mobility spectrometry-mass spectrometry, Anal. Chem. 70 (1998) 4929–4938, http://dx.doi.org/10.1021/ac980414z.
[105] T. Wyttenbach, P.R. Kemper, M.T. Bowers, Design of a new electrospray ion mobility mass spectrometer, Int. J. Mass Spectrom. 212 (2001) 13–23, http://dx.doi.org/10.1016/S1387-3806(01)00517-6.
[106] K. Giles, S.D. Pringle, K.R. Worthington, D. Little, J.L. Wildgoose, R.H. Bateman, Applications of a travelling wave-based radio-frequency-only stacked ring ion guide, Rapid Commun. Mass Spectrom. 18 (2004) 2401–2414, http://dx.doi.org/10.1002/rcm.1641.
[107] S.I. Merenbloom, R.S. Glaskin, Z.B. Henson, D.E. Clemmer, High-resolution ion cyclotron mobility spectrometry, Anal. Chem. 81 (2009) 1482–1487, http://dx.doi.org/10.1021/ac801880a.
[108] M.F. Bush, Z. Hall, K. Giles, J. Hoyes, C.V. Robinson, B.T. Ruotolo, Collision cross sections of proteins and their complexes: a calibration framework and database for gas-phase structural biology, Anal. Chem. 82 (2010) 9557–9565, http://dx.doi.org/10.1021/ac1022953.
[109] S.M. Zucker, S. Lee, N. Webber, S.J. Valentine, J.P. Reilly, D.E. Clemmer, An ion Mobility/Ion Trap/Photodissociation instrument for characterization of ion structure, J. Am. Soc. Mass Spectrom. 22 (2011) 1477–1485, http://dx.doi.org/10.1007/s13361-011-0179-8.
[110] X. Zhang, R. Knochenmuss, W.F. Siems, W. Liu, S. Graf, H.H. Hill, Evaluation of Hadamard transform atmospheric pressure ion mobility time-of-flight mass spectrometry for complex mixture analysis, Anal. Chem. 86 (2014) 1661–1670, http://dx.doi.org/10.1021/ac403435p.
[111] M. Groessl, S. Graf, R. Knochenmuss, High resolution ion mobility-mass spectrometry for separation and identification of isomeric lipids, Analyst 140 (2015) 6904–6911, http://dx.doi.org/10.1039/c5an00838g.
[112] Y.M. Ibrahim, E.S. Baker, W.F. Danielson, R.V. Norheim, D.C. Prior, G.A. Anderson, M.E. Belov, R.D. Smith, Development of a new ion mobility (quadrupole) time-of-flight mass spectrometer, Int. J. Mass Spectrom. 377 (2015) 655–662, http://dx.doi.org/10.1016/j.ijms.2014.07.034.
[113] L. Deng, Y.M. Ibrahim, A.M. Hamid, S.V.B. Garimella, I.K. Webb, X. Zheng, S.A. Prost, J.A. Sandoval, R.V. Norheim, G.A. Anderson, A.V. Tolmachev, E.S. Baker, R.D. Smith, Ultra-high resolution ion mobility separations utilizing traveling waves in a 13 m serpentine path length structures for lossless ion manipulations module, Anal. Chem. 88 (2016) 8957–8964, http://dx.doi.org/10.1021/acs.analchem.6b01915.
[114] A.M. Hamid, S.V.B. Garimella, Y.M. Ibrahim, L. Deng, X. Zheng, I.K. Webb, G.A. Anderson, S.A. Prost, R.V. Norheim, A.V. Tolmachev, E.S. Baker, R.D. Smith, Achieving high resolution ion mobility separations using traveling waves in compact multiturn structures for lossless ion manipulations, Anal. Chem. 88 (2016) 8949–8956, http://dx.doi.org/10.1021/acs.analchem.6b01914.
[115] J. Ujma, K. Giles, M. Morris, P.E. Barran, New high resolution ion mobility mass spectrometer capable of measurements of collision cross sections from 150 to 520 K, Anal. Chem. 88 (2016) 9469–9478, http://dx.doi.org/10.1021/acs.analchem.6b01812.
[116] S.D. Pringle, K. Giles, J.L. Wildgoose, J.P. Williams, S.E. Slade, K. Thalassinos, R.H. Bateman, M.T. Bowers, J.H. Scrivens, An investigation of the mobility separation of some peptide and protein ions using a new hybrid quadrupole/travelling wave IMS/oa-ToF instrument, Int. J. Mass Spectrom. 261 (2007) 1–12, http://dx.doi.org/10.1016/j.ijms.2006.07.021.
[117] F.A. Fernandez-Lima, D.A. Kaplan, M.A. Park, Note: Integration of trapped ion mobility spectrometry with mass spectrometry, Rev. Sci. Instrum. 82 (2011) 1–5, http://dx.doi.org/10.1063/1.3665933.
[118] K. Giles, J. Ujma, J. Wildgoose, S. Pringle, K. Richardson, D. Langridge, M. Green, A cyclic ion mobility-mass spectrometry system, Anal. Chem. 91 (2019) 8564–8573, http://dx.doi.org/10.1021/acs.analchem.9b01838.
[119] T. Pacini, W. Fu, S. Gudmundsson, A.E. Chiaravalle, S. Brynjolfson, B.O. Palsson, G. Astarita, G. Paglia, Multidimensional analytical approach based on UHPLC-UV-ion mobility-MS for the screening of natural pigments, Anal. Chem. 87 (2015) 2593–2599, http://dx.doi.org/10.1021/ac504707n.
[120] T.J. Causon, V. Ivanova-Petropulos, D. Petrusheva, E. Bogeva, S. Hann, Fingerprinting of traditionally produced red wines using liquid chromatography combined with drift tube ion mobility-mass spectrometry, Anal. Chim. Acta 1052 (2019) 179–189, http://dx.doi.org/10.1016/j.aca.2018.11.040.
[121] E. Esquenazi, M. Daly, T. Bahrainwala, W.H. Gerwick, P.C. Dorrestein, Ion mobility mass spectrometry enables the efficient detection and identification of halogenated natural products from cyanobacteria with minimal sample preparation, Bioorg. Med. Chem. 19 (2011) 6639–6644, http://dx.doi.org/10.1016/j.bmc.2011.06.081.
[122] A. Bauer, J. Luetjohann, F.S. Hanschen, M. Schreiner, J. Kuballa, E. Jantzen, S. Rohn, Identification and characterization of pesticide metabolites in Brassica species by liquid chromatography travelling wave ion mobility quadrupole time-of-flight mass spectrometry (UPLC-TWIMS-QTOF-MS), Food Chem. 244 (2018) 292–303, http://dx.doi.org/10.1016/j.foodchem.2017.09.131.

[123] C. Decroo, E. Colson, V. Lemaur, G. Caulier, J. De Winter, G. Cabrera-Barjas, J. Cornil, P. Flammang, P. Gerbaux, Ion mobility mass spectrometry of saponin ions, Rapid Commun. Mass Spectrom. 33 (2019) 22–33, http://dx.doi.org/10.1002/rcm.8193.

[124] M. McCullagh, D. Douce, E. Van Hoeck, S. Goscinny, Exploring the complexity of steviol glycosides analysis using ion mobility mass spectrometry, Anal. Chem. 90 (2018) 4585–4595, http://dx.doi.org/10.1021/acs.analchem.7b05002.

[125] K.M. Hines, J.R. Enders, J.A. McLean, Multidimensional separations by ion mobility-mass spectrometry, in: Encycl. Anal. Chem., John Wiley & Sons, Ltd, Chichester, UK, 2012, http://dx.doi.org/10.1002/9780470027318.a9313.

[126] J. Sun, A. Baker, P. Chen, Profiling the indole alkaloids in yohimbe bark with ultraperformance liquid chromatography coupled with ion mobility quadrupole time-of-flight mass spectrometry, Rapid Commun. Mass Spectrom. 25 (2011) 2591–2602, http://dx.doi.org/10.1002/rcm.5158.

[127] H. Zhang, D. Zheng, H.H. Li, H. Wang, H.S. Tan, H.X. Xu, Diagnostic filtering to screen polycyclic polyprenylated acylphloroglucinols from Garcinia oblongifolia by ultrahigh performance liquid chromatography coupled with ion mobility quadrupole time-of-flight mass spectrometry, Anal. Chim. Acta 912 (2016) 85–96, http://dx.doi.org/10.1016/j.aca.2016.01.039.

[128] F. Meier, S. Beck, N. Grassl, M. Lubeck, M.A. Park, O. Raether, M. Mann, Parallel accumulation-serial fragmentation (PASEF): multiplying sequencing speed and sensitivity by synchronized scans in a trapped ion mobility device, J. Proteome Res. 14 (2015) 5378–5387, http://dx.doi.org/10.1021/acs.jproteome.5b00932.

[129] J.N. Dodds, J.C. May, J.A. McLean, Correlating resolving power, resolution, and collision cross section: unifying cross-platform assessment of separation efficiency in ion mobility spectrometry, Anal. Chem. 89 (2017) 12176–12184, http://dx.doi.org/10.1021/acs.analchem.7b02827.

[130] J.C. May, C.R. Goodwin, N.M. Lareau, K.L. Leaptrot, C.B. Morris, R.T. Kurulugama, A. Mordehai, C. Klein, W. Barry, E. Darland, G. Overney, K. Imatani, G.C. Stafford, J.C. Fjeldsted, J.A. McLean, Conformational ordering of biomolecules in the gas phase: nitrogen collision cross sections measured on a prototype high resolution drift tube ion mobility-mass spectrometer, Anal. Chem. 86 (2014) 2107–2116, http://dx.doi.org/10.1021/ac4038448.

[131] K. Giles, J.P. Williams, I. Campuzano, Enhancements in travelling wave ion mobility resolution, Rapid Commun. Mass Spectrom. 25 (2011) 1559–1566, http://dx.doi.org/10.1002/rcm.5013.

[132] J.A. Silveira, M.E. Ridgeway, M.A. Park, High resolution trapped ion mobility spectrometery of peptides, Anal. Chem. 86 (2014) 5624–5627, http://dx.doi.org/10.1021/ac501261h.

[133] A.A. Shvartsburg, D.C. Prior, K. Tang, R.D. Smith, High-resolution differential ion mobility separations using planar analyzers at elevated dispersion fields, Anal. Chem. 82 (2010) 7649–7655, http://dx.doi.org/10.1021/ac101413k.

[134] A.A. Shvartsburg, T.A. Seim, W.F. Danielson, R. Norheim, R.J. Moore, G.A. Anderson, R.D. Smith, High-definition differential ion mobility spectrometry with resolving power up to 500, J. Am. Soc. Mass Spectrom. 24 (2013) 109–114, http://dx.doi.org/10.1007/s13361-012-0517-5.

[135] J.N. Dodds, J.C. May, J.A. McLean, Investigation of the complete suite of the leucine and isoleucine isomers: toward prediction of ion mobility separation capabilities, Anal. Chem. 89 (2017) 952–959, http://dx.doi.org/10.1021/acs.analchem.6b04171.

[136] K.J. Adams, D. Montero, D. Aga, F. Fernandez-Lima, Isomer separation of polybrominated diphenyl ether metabolites using nanoESI-TIMS-MS, Int. J. Ion Mobil. Spectrom. 19 (2016) 69–76, http://dx.doi.org/10.1007/s12127-016-0198-z.

[137] L. Deng, I.K. Webb, S.V.B. Garimella, A.M. Hamid, X. Zheng, R.V. Norheim, S.A. Prost, G.A. Anderson, J.A. Sandoval, E.S. Baker, Y.M. Ibrahim, R.D. Smith, Serpentine ultralong path with extended routing (SUPER) high resolution traveling wave ion Mobility-MS using structures for lossless ion manipulations, Anal. Chem. 89 (2017) 4628–4634, http://dx.doi.org/10.1021/acs.analchem.7b00185.

[138] A.V. Tolmachev, I.K. Webb, Y.M. Ibrahim, S.V.B. Garimella, X. Zhang, G.A. Anderson, R.D. Smith, Characterization of ion dynamics in structures for lossless ion manipulations, Anal. Chem. 86 (2014) 9162–9168, http://dx.doi.org/10.1021/ac502054p.

[139] A.T. Kirk, C.R. Raddatz, S. Zimmermann, Separation of isotopologues in ultra-high-resolution ion mobility spectrometry, Anal. Chem. 89 (2017) 1509–1515, http://dx.doi.org/10.1021/acs.analchem.6b03300.

[140] R.S. Glaskin, M.A. Ewing, D.E. Clemmer, Ion trapping for ion mobility spectrometry measurements in a cyclical drift tube, Anal. Chem. 85 (2013) 7003–7008, http://dx.doi.org/10.1021/ac4015066.

[141] E.A. Mason, H.W. Schamp, Mobility of gaseous lons in weak electric fields, Ann. Phys. (N.Y) 4 (1958) 233–270, http://dx.doi.org/10.1016/0003-4916(58)90049-6.

[142] R.T. Kurulugama, E. Darland, F. Kuhlmann, G. Stafford, J. Fjeldsted, Evaluation of drift gas selection in complex sample analyses using a high performance drift tube ion mobility-QTOF mass spectrometer, Analyst 140 (2015) 6834–6844, http://dx.doi.org/10.1039/c5an00991j.

[143] K.M. Hines, J.C. May, J.A. McLean, L. Xu, Evaluation of collision cross section calibrants for structural analysis of lipids by traveling wave ion mobility-mass spectrometry, Anal. Chem. 88 (2016) 7329–7336, http://dx.doi.org/10.1021/acs.analchem.6b01728.

[144] J. Hofmann, W.B. Struwe, C.A. Scarff, J.H. Scrivens, D.J. Harvey, K. Pagel, Estimating collision cross sections of negatively charged N- glycans using traveling wave ion mobility-mass spectrometry, Anal. Chem. 86 (2014) 10789–10795, http://dx.doi.org/10.1021/ac5028353.

[145] B.T. Ruotolo, J.L.P. Benesch, A.M. Sandercock, S.J. Hyung, C.V. Robinson, Ion mobility-mass spectrometry analysis of large protein complexes, Nat. Protoc. 3 (2008) 1139–1152, http://dx.doi.org/10.1038/nprot.2008.78.

[146] K.M. Hines, D.H. Ross, K.L. Davidson, M.F. Bush, L. Xu, Large-scale structural characterization of drug and drug-like compounds by high-throughput ion mobility-mass spectrometry, Anal. Chem. 89 (2017) 9023–9030, http://dx.doi.org/10.1021/acs.analchem.7b01709.

[147] M.F. Bush, I.D.G. Campuzano, C.V. Robinson, Ion mobility mass spectrometry of peptide ions: effects of drift gas and calibration strategies, Anal. Chem. 84 (2012) 7124–7130, http://dx.doi.org/10.1021/ac3014498.

[148] G. Paglia, P. Angel, J.P. Williams, K. Richardson, H.J. Olivos, J.W. Thompson, L. Menikarachchi, S. Lai, C. Walsh, A. Moseley, R.S. Plumb, D.F. Grant, B.O. Palsson, J. Langridge, S. Geromanos, G. Astarita, Ion mobility-derived collision cross section as an additional measure for lipid fingerprinting and identification, Anal. Chem. 87 (2015) 1137–1144, http://dx.doi.org/10.1021/ac503715v.

[149] J.G. Forsythe, A.S. Petrov, C.A. Walker, S.J. Allen, J.S. Pellissier, M.F. Bush, N.V. Hud, F.M. Fernández, Collision cross section calibrants for negative ion mode traveling wave ion mobility-mass spectrometry, Analyst 140 (2015) 6853–6861, http://dx.doi.org/10.1039/c5an00946d.

[150] D.R. Hernandez, J.D. DeBord, M.E. Ridgeway, D.A. Kaplan, M.A. Park, F. Fernandez-Lima, Ion dynamics in a trapped ion mobility spectrometer, Analyst 139 (2014) 1913–1921, http://dx.doi.org/10.1039/c3an02174b.

[151] M. Schroeder, S.W. Meyer, H.M. Heyman, A. Barsch, L.W. Sumner, Generation of a collision cross section library for multi-dimensional plant metabolomics using UHPLC-trapped ion mobility-MS/MS, Metabolites 10 (2020), http://dx.doi.org/10.3390/metabo10010013.

[152] H. Ouyang, C. Larriba-Andaluz, D.R. Oberreit, C.J. Hogan, The collision cross sections of iodide salt cluster ions in air via differential mobility analysis-mass spectrometry, J. Am. Soc. Mass Spectrom. 24 (2013) 1833–1847, http://dx.doi.org/10.1007/s13361-013-0724-8.

[153] C.B. Morris, J.C. May, K.L. Leaptrot, J.A. McLean, Evaluating separation selectivity and collision cross section measurement reproducibility in helium, nitrogen, argon, and carbon dioxide drift gases for drift tube ion mobility–Mass spectrometry, J. Am. Soc. Mass Spectrom. 30 (2019) 1059–1068, http://dx.doi.org/10.1021/jasms.8b06014.

[154] K.J. Pacholarz, P.E. Barran, Distinguishing loss of structure from subunit dissociation for protein complexes with variable temperature ion mobility mass spectrometry, Anal. Chem. 87 (2015) 6271–6279, http://dx.doi.org/10.1021/acs.analchem.5b01063.

[155] J.C. May, C.B. Morris, J.A. McLean, Ion mobility collision cross section compendium, Anal. Chem. 89 (2017) 1032–1044, http://dx.doi.org/10.1021/acs.analchem.6b04905.

[156] S. Warnke, J. Seo, J. Boschmans, F. Sobott, J.H. Scrivens, C. Bleiholder, M.T. Bowers, S. Gewinner, W. Schöllkopf, K. Pagel, G. Von Helden, Protomers of benzocaine: solvent and permittivity dependence, J. Am. Chem. Soc. 137 (2015) 4236–4242, http://dx.doi.org/10.1021/jacs.5b01338.

[157] H. Xia, A.B. Attygalle, Effect of electrospray ionization source conditions on the tautomer distribution of deprotonated p-Hydroxybenzoic acid in the gas phase, Anal. Chem. 88 (2016) 6035–6043, http://dx.doi.org/10.1021/acs.analchem.6b01230.

[158] F. Lanucara, S.W. Holman, C.J. Gray, C.E. Eyers, The power of ion mobility-mass spectrometry for structural characterization and the study of conformational dynamics, Nat. Chem. 6 (2014) 281–294, http://dx.doi.org/10.1038/nchem.1889.

[159] D.S. Wishart, D. Tzur, C. Knox, R. Eisner, A.C. Guo, N. Young, D. Cheng, K. Jewell, D. Arndt, S. Sawhney, C. Fung, L. Nikolai, M. Lewis, M.A. Coutouly, I. Forsythe, P. Tang, S. Shrivastava, K. Jeroncic, P. Stothard, G. Amegbey, D. Block, D.D. Hau, J. Wagner, J. Miniaci, M. Clements, M. Gebremedhin, N. Guo, Y. Zhang, G.E. Duggan, G.D. MacInnis, A.M. Weljie, R. Dowlatabadi, F. Bamforth, D. Clive, R. Greiner, L. Li, T. Marrie, B.D. Sykes, H.J. Vogel, L. Querengesser, HMDB: The human metabolome database, Nucleic Acids Res. 35 (2007) 521–526, http://dx.doi.org/10.1093/nar/gkl923.

[160] C.A. Smith, G. O'Maille, E.J. Want, C. Qin, S.A. Trauger, T.R. Brandon, D.E. Custodio, R. Abagyan, G. Siuzdak, METLIN: A metabolite mass spectral database, Ther. Drug Monit. 27 (2005) 747–751, http://dx.doi.org/10.1097/01.ftd.0000179845.53213.39.

[161] J.E. Kyle, N. Aly, X. Zheng, K.E. Burnum-Johnson, R.D. Smith, E.S. Baker, Evaluating lipid mediator structural complexity using ion mobility spectrometry combined with mass spectrometry, Bioanalysis 10 (2018) 279–289, http://dx.doi.org/10.4155/bio-2017-0245.

[162] K.L. Leaptrot, J.C. May, J.N. Dodds, J.A. McLean, Ion mobility conformational lipid atlas for high confidence lipidomics, Nat. Commun. 10 (2019), http://dx.doi.org/10.1038/s41467-019-08897-5.

[163] S.J. Valentine, M.D. Plasencia, X. Liu, M. Krishnan, S. Naylor, H.R. Udseth, R.D. Smith, D.E. Clemmer, Toward plasma proteome profiling with ion mobility-mass spectrometry, J. Proteome Res. 5 (2006) 2977–2984, http://dx.doi.org/10.1021/pr060232i.

[164] L. Righetti, A. Bergmann, G. Galaverna, O. Rolfsson, G. Paglia, C. Dall'Asta, Ion mobility-derived collision cross section database: application to mycotoxin analysis, Anal. Chim. Acta 1014 (2018) 50–57, http://dx.doi.org/10.1016/j.aca.2018.01.047.

[165] S. Stephan, J. Hippler, T. Köhler, A.A. Deeb, T.C. Schmidt, O.J. Schmitz, Contaminant screening of wastewater with HPLC-IM-qTOF-MS and

LC+LC-IM-qTOF-MS using a CCS database, Anal. Bioanal. Chem. 408 (2016) 6545–6555, http://dx.doi.org/10.1007/s00216-016-9820-5.
[166] X. Zheng, N.A. Aly, Y. Zhou, K.T. Dupuis, A. Bilbao, V.L. Paurus, D.J. Orton, R. Wilson, S.H. Payne, R.D. Smith, E.S. Baker, A structural examination and collision cross section database for over 500 metabolites and xenobiotics using drift tube ion mobility spectrometry, Chem. Sci. 8 (2017) 7724–7736, http://dx.doi.org/10.1039/c7sc03464d.
[167] J.A. Picache, B.S. Rose, A. Balinski, K.L. Leaptrot, S.D. Sherrod, J.C. May, J.A. McLean, Collision cross section compendium to annotate and predict multi-omic compound identities, Chem. Sci. 10 (2019) 983–993, http://dx.doi.org/10.1039/c8sc04396e.
[168] Z. Zhou, X. Shen, J. Tu, Z.J. Zhu, Large-scale prediction of collision cross-section values for metabolites in ion mobility-mass spectrometry, Anal. Chem. 88 (2016) 11084–11091, http://dx.doi.org/10.1021/acs.analchem.6b03091.
[169] Z. Zhou, J. Tu, X. Xiong, X. Shen, Z.J. Zhu, LipidCCS: prediction of collision cross-section values for lipids with high precision to support ion mobility-mass spectrometry-based lipidomics, Anal. Chem. 89 (2017) 9559–9566, http://dx.doi.org/10.1021/acs.analchem.7b02625.
[170] P.L. Plante, É. Francovic-Fontaine, J.C. May, J.A. McLean, E.S. Baker, F. Laviolette, M. Marchand, J. Corbeil, Predicting ion mobility collision cross-sections using a deep neural network: DeepCCS, Anal. Chem. 91 (2019) 5191–5199, http://dx.doi.org/10.1021/acs.analchem.8b05821.
[171] L. Bijlsma, R. Bade, A. Celma, L. Mullin, G. Cleland, S. Stead, F. Hernandez, J.V. Sancho, Prediction of collision cross-section values for small molecules: application to pesticide residue analysis, Anal. Chem. 89 (2017) 6583–6589, http://dx.doi.org/10.1021/acs.analchem.7b00741.
[172] S.M. Colby, D.G. Thomas, J.R. Nunez, D.J. Baxter, K.R. Glaesemann, J.M. Brown, M.A. Pirrung, N. Govind, J.G. Teeguarden, T.O. Metz, R.S. Renslow, ISiCLE: a quantum chemistry pipeline for establishing in silico collision cross section libraries, Anal. Chem. 91 (2019) 4346–4356, http://dx.doi.org/10.1021/acs.analchem.8b04567.
[173] S.M. Colby, J.R. Nuñez, N.O. Hodas, C.D. Corley, R.R. Renslow, Deep learning to generate in silico chemical property libraries and candidate molecules for small molecule identification in complex samples, Anal. Chem. 92 (2020) 1720–1729, http://dx.doi.org/10.1021/acs.analchem.9b02348.
[174] P. Donato, D. Giuffrida, M. Oteri, V. Inferrera, P. Dugo, L. Mondello, Supercritical fluid chromatography × ultra-high pressure liquid chromatography for red chilli pepper fingerprinting by photodiode array, quadrupole-time-of-Flight and ion mobility mass spectrometry (SFC × RP-UHPLC-PDA-Q-ToF MS-IMS), Food Anal. Methods 11 (2018) 3331–3341, http://dx.doi.org/10.1007/s12161-018-1307-x.
[175] C. Lipok, J. Hippler, O.J. Schmitz, A four dimensional separation method based on continuous heart-cutting gas chromatography with ion mobility and high resolution mass spectrometry, J. Chromatogr. A 1536 (2018) 50–57, http://dx.doi.org/10.1016/j.chroma.2017.07.013.
[176] E. Szymańska, A.N. Davies, L.M.C. Buydens, Chemometrics for ion mobility spectrometry data: recent advances and future prospects, Analyst 141 (2016) 5689–5708, http://dx.doi.org/10.1039/c6an01008c.
[177] T.D. Stark, J. Ranner, B. Stiglbauer, P. Weiss, S. Stark, O.B. Balemba, T. Hofmann, Construction and application of a database for a five-dimensional identification of natural compounds in Garcinia species by means of UPLC-ESI-TWIMS-TOF-MS: introducing gas phase polyphenol conformer drift time distribution intensity ratios, J. Agric. Food Chem. 67 (2019) 975–985, http://dx.doi.org/10.1021/acs.jafc.8b06157.
[178] C.A. Smith, E.J. Want, G. O'Maille, R. Abagyan, G. Siuzdak, XCMS: Processing mass spectrometry data for metabolite profiling using nonlinear peak alignment, matching, and identification, Anal. Chem. 78 (2006) 779–787, http://dx.doi.org/10.1021/ac051437y.
[179] P. Martínez-Lozano, E. Criado, G. Vidal, S. Cristoni, F. Franzoso, M. Piatti, P. Brambilla, Differential mobility analysis-mass spectrometry coupled to XCMS algorithm as a novel analytical platform for metabolic profiling, Metabolomics 9 (2013) 30–43, http://dx.doi.org/10.1007/s11306-011-0319-y.
[180] B.X. MacLean, B.S. Pratt, J.D. Egertson, M.J. MacCoss, R.D. Smith, E.S. Baker, Using skyline to analyze data-containing liquid chromatography, ion mobility spectrometry, and mass spectrometry dimensions, J. Am. Soc. Mass Spectrom. 29 (2018) 2182–2188, http://dx.doi.org/10.1007/s13361-018-2028-5.
[181] L.G. Migas, A.P. France, B. Bellina, P.E. Barran, ORIGAMI: a software suite for activated ion mobility mass spectrometry (aIM-MS) applied to multimeric protein assemblies, Int. J. Mass Spectrom. 427 (2018) 20–28, http://dx.doi.org/10.1016/j.ijms.2017.08.014.
[182] J. Gallegos, R. Garrido-Delgado, L. Arce, L.M. Medina, Volatile metabolites of goat cheeses determined by ion mobility spectrometry. Potential applications in quality control, Food Anal. Methods 8 (2015) 1699–1709, http://dx.doi.org/10.1007/s12161-014-0050-1.
[183] X. Hu, R. Wang, J. Guo, K. Ge, G. Li, F. Fu, S. Ding, Y. Shan, Changes in the volatile components of candied kumquats in different processing methodologies with headspace-gas chromatography-ion mobility spectrometry, Molecules 24 (2019), http://dx.doi.org/10.3390/molecules24173053.
[184] M. Li, R. Yang, H. Zhang, S. Wang, D. Chen, S. Lin, Development of a fl avor fi ngerprint by HS-GC – IMS with PCA for volatile compounds of tricholoma matsutake singer, Food Chem. 290 (2019) 32–39, http://dx.doi.org/10.1016/j.foodchem.2019.03.124.
[185] S. Schwolow, N. Gerhardt, S. Rohn, P. Weller, Data fusion of GC-IMS data and FT-MIR spectra for the authentication of olive oils and honeys—is it worth to go the extra mile? Anal. Bioanal. Chem. 411 (2019) 6005–6019, http://dx.doi.org/10.1007/s00216-019-01978-w.
[186] L. Yang, J. Liu, X. Wang, R. Wang, F. Ren, Q. Zhang, Y. Shan, S. Ding, Characterization of volatile component changes in jujube fruits during cold storage by using headspace-gas chromatography-ion mobility spectrometry, Molecules 24 (2019) 1–21, http://dx.doi.org/10.3390/molecules24213904.
[187] X. Wang, S. Yang, J. He, L. Chen, J. Zhang, Y. Jin, J. Zhou, Y. Zhang, A green triple-locked strategy based on volatile-compound imaging, chemometrics, and markers to discriminate winter honey and sapium honey using headspace gas chromatography-ion mobility spectrometry, Food Res. Int. 119 (2019) 960–967, http://dx.doi.org/10.1016/j.foodres.2019.01.004.
[188] X. Wang, K.M. Rogers, Y. Li, S. Yang, L. Chen, J. Zhou, Untargeted and targeted discrimination of honey collected by Apis cerana and Apis mellifera based on volatiles using HS-GC-IMS and HS-SPME-GC–MS, J. Agric. Food Chem. 67 (2019) 12144–12152, http://dx.doi.org/10.1021/acs.jafc.9b04438.
[189] V. Bocos-Bintintan, C.L.P. Thomas, I.A. Ratiu, Sensors' array of aspiration ion mobility spectrometer as a tool for bacteria discrimination, Talanta 206 (2020) 1–14, http://dx.doi.org/10.1016/j.talanta.2019.120233.
[190] A. Erler, D. Riebe, T. Beitz, H.-G. Löhmannsröben, D. Grothusheitkamp, T. Kunz, F.-J. Methner, Characterization of volatile metabolites formed by molds on barley by mass and ion mobility spectrometry, J. Mass Spectrom. 55 (2020) 1–10, http://dx.doi.org/10.1002/jms.4501.
[191] S. Ge, Y. Chen, S. Ding, H. Zhou, L. Jiang, Y. Yi, F. Deng, R. Wang, Changes in volatile flavor compounds of peppers during hot air drying process based on headspace-gas chromatography-ion mobility spectrometry (HS-GC-IMS), J. Sci. Food Agric. 100 (2020) 3087–3098, http://dx.doi.org/10.1002/jsfa.10341.
[192] W. Lv, T. Lin, Z. Ren, Y. Jiang, J. Zhang, F. Bi, L. Gu, H. Hou, J. He, Rapid discrimination of Citrus reticulata 'Chachi' by headspace-gas chromatography-ion mobility spectrometry fingerprints combined with principal component analysis, Food Res. Int. 131 (2020), 108985, http://dx.doi.org/10.1016/j.foodres.2020.108985.
[193] M.M. McCartney, S.L. Spitulski, A. Pasamontes, D.J. Peirano, M.J. Schirle, R. Cumeras, J.D. Simmons, J.L. Ware, J.F. Brown, A.J.Y. Poh, S.C. Dike, E.K. Foster, K.E. Godfrey, C.E. Davis, Coupling a branch enclosure with differential mobility spectrometry to isolate and measure plant volatiles in contained greenhouse settings, Talanta 146 (2016) 148–154, http://dx.doi.org/10.1016/j.talanta.2015.08.039.
[194] M.Y. Piñero, M. Amo-González, R.D. Ballesteros, L.R. Pérez, G.F. de la Mora, L. Arce, Chemical fingerprinting of olive oils by electrospray ionization-differential mobility analysis-mass spectrometry: a new alternative to food authenticity testing, J. Am. Soc. Mass Spectrom. 31 (2020) 527–537, http://dx.doi.org/10.1021/jasms.9b00006.
[195] X. Zhang, Z. Dai, X. Fan, M. Liu, J. Ma, W. Shang, J. Liu, P. Strappe, C. Blanchard, Z. Zhou, A study on volatile metabolites screening by HS-SPME-GC-MS and HS-GC-IMS for discrimination and characterization of white and yellowed rice, Cereal Chem. 97 (2020) 496–504, http://dx.doi.org/10.1002/cche.10264.
[196] N. Gerhardt, M. Birkenmeier, D. Sanders, S. Rohn, P. Weller, Resolution-optimized headspace gas chromatography-ion mobility spectrometry (HS-GC-IMS) for non-targeted olive oil profiling, Anal. Bioanal. Chem. 409 (2017) 3933–3942, http://dx.doi.org/10.1007/s00216-017-0338-2.
[197] I.A. Ratiu, V. Bocos-Bintintan, A. Patrut, V.H. Moll, M. Turner, C.L.P. Thomas, Discrimination of bacteria by rapid sensing their metabolic volatiles using an aspiration-type ion mobility spectrometer (a-IMS) and gas chromatography-mass spectrometry GC-MS, Anal. Chim. Acta 982 (2017) 209–217, http://dx.doi.org/10.1016/j.aca.2017.06.031.
[198] Y. Wang, P. Chen, Comparison of ion mobility fuzzy chromatography mass spectrometric (imFCMS) fingerprinting and FCMS fingerprinting for differentiation of american cranberry cultivars, J. Anal. Test. 2 (2018) 223–234, http://dx.doi.org/10.1007/s41664-018-0059-3.
[199] X. Yang, L. Feng, L. Zhao, X. Liu, D. Hassani, D. Huang, Effect of glycine nitrogen on lettuce growth under soilless culture: a metabolomics approach to identify the main changes occurred in plant primary and secondary metabolism, J. Sci. Food Agric. 98 (2018) 467–477, http://dx.doi.org/10.1002/jsfa.8482.
[200] N. Arroyo-Manzanares, M. García-Nicolás, A. Castell, N. Campillo, P. Viñas, I. López-García, M. Hernández-Córdoba, Untargeted headspace gas chromatography – ion mobility spectrometry analysis for detection of adulterated honey, Talanta 205 (2019), 120123, http://dx.doi.org/10.1016/j.talanta.2019.120123.
[201] Mdel M. Contreras, N. Jurado-Campos, L. Arce, N. Arroyo-Manzanares, A robustness study of calibration models for olive oil classification: targeted and non-targeted fingerprint approaches based on GC-IMS, Food Chem. 288 (2019) 315–324, http://dx.doi.org/10.1016/j.foodchem.2019.02.104.
[202] N. Gerhardt, S. Schwolow, S. Rohn, P.R. Pérez-cacho, Quality assessment of olive oils based on temperature-ramped HS-GC-IMS and sensory evaluation : comparison of di ff erent processing approaches by, Food Chem. 278 (2019) 720–728, http://dx.doi.org/10.1016/j.foodchem.2018.11.095.
[203] X. Yang, S. Wei, B. Liu, D. Guo, B. Zheng, L. Feng, Y. Liu, F.A. Tomás-Barberán, L. Luo, D. Huang, A novel integrated non-targeted metabolomic analysis reveals significant metabolite variations between different lettuce (Lactuca sativa. L) varieties, Hortic. Res. 5 (2018) 1–14, http://dx.doi.org/10.1038/s41438-018-0050-1.

[204] B. Avula, J.Y. Bae, Y.H. Wang, M. Wang, A.G. Osman, K. Smith, J. Yuk, Z. Ali, R. Plumb, G. Isaac, I.A. Khan, Chemical profiling and characterization of phenolic acids, flavonoids, terpene glycosides from Vangueria agrestis using ultra-high-performance liquid chromatography/ion mobility quadrupole time-of-flight mass spectrometry and metabolomics approach, Biomed. Chromatogr. (2020), http://dx.doi.org/10.1002/bmc.4840.

[205] M. Fenclova, M. Stranska-Zachariasova, F. Benes, A. Novakova, P. Jonatova, V. Kren, L. Vitek, J. Hajslova, Liquid chromatography–drift tube ion mobility–mass spectrometry as a new challenging tool for the separation and characterization of silymarin flavonolignans, Anal. Bioanal. Chem. 412 (2020) 819–832, http://dx.doi.org/10.1007/s00216-019-02274-3.

[206] S. Sharma, R. Joshi, D. Kumar, Quantitative analysis of flavonols, flavonol glycoside and homoisoflavonoids in Polygonatum verticillatum using UHPLC-DAD-QTOF-IMS and evaluation of their antioxidant potential, Phytochem. Anal. 31 (2020) 333–339, http://dx.doi.org/10.1002/pca.2899.

[207] M.A. Stander, B.E. Van Wyk, M.J.C. Taylor, H.S. Long, Analysis of phenolic compounds in rooibos tea (Aspalathus linearis) with a comparison of flavonoid-based compounds in natural populations of plants from different regions, J. Agric. Food Chem. 65 (2017) 10270–10281, http://dx.doi.org/10.1021/acs.jafc.7b03942.

[208] Y. Lu, J. Guo, J. Yu, J. Guo, X. Jia, W. Liu, P. Tian, Two-dimensional analysis of phenolic acids in seedling roots by high performance liquid chromatography-electrospray ionization-ion mobility spectrometry, Anal. Methods 11 (2019) 610–617, http://dx.doi.org/10.1039/c8ay02288g.

[209] J.L. Willems, M.M. Khamis, W. Mohammed Saeid, R.W. Purves, G. Katselis, N.H. Low, A. El-Aneed, Analysis of a series of chlorogenic acid isomers using differential ion mobility and tandem mass spectrometry, Anal. Chim. Acta 933 (2016) 164–174, http://dx.doi.org/10.1016/j.aca.2016.05.041.

[210] D. Corinti, A. Maccelli, M.E. Crestoni, S. Cesa, D. Quaglio, B. Botta, C. Ingallina, L. Mannina, A. Tintaru, B. Chiavarino, S. Fornarini, IR ion spectroscopy in a combined approach with MS/MS and IM-MS to discriminate epimeric anthocyanin glycosides (cyanidin 3-O-glucoside and -galactoside), Int. J. Mass Spectrom. 444 (2019), 116179, http://dx.doi.org/10.1016/j.ijms.2019.116179.

[211] W. Liu, X. Zhang, W.F. Siems, H.H. Hill, D. Yin, Rapid profiling and identification of anthocyanins in fruits with Hadamard transform ion mobility mass spectrometry, Food Chem. 177 (2015) 225–232, http://dx.doi.org/10.1016/j.foodchem.2015.01.034.

[212] Y. Wang, N. Vorsa, P.D.B. Harrington, P. Chen, Nontargeted metabolomic study on variation of phenolics in different cranberry cultivars using UPLC-IM - HRMS, J. Agric. Food Chem. 66 (2018) 12206–12216, http://dx.doi.org/10.1021/acs.jafc.8b05029.

[213] P. Venter, T. Causon, H. Pasch, A. de Villiers, Comprehensive analysis of chestnut tannins by reversed phase and hydrophilic interaction chromatography coupled to ion mobility and high resolution mass spectrometry, Anal. Chim. Acta 1088 (2019) 150–167, http://dx.doi.org/10.1016/j.aca.2019.08.037.

[214] P. Venter, H. Pasch, A. de Villiers, Comprehensive analysis of tara tannins by reversed-phase and hydrophilic interaction chromatography coupled to ion mobility and high-resolution mass spectrometry, Anal. Bioanal. Chem. 411 (2019) 6329–6341, http://dx.doi.org/10.1016/j.aca.2019.08.037.

[215] M.N. Li, H.Y. Wang, R. Wang, C.R. Li, B.Q. Shen, W. Gao, P. Li, H. Yang, A modified data filtering strategy for targeted characterization of polymers in complex matrixes using drift tube ion mobility-mass spectrometry: application to analysis of procyanidins in the grape seed extracts, Food Chem. 321 (2020), 126693, http://dx.doi.org/10.1016/j.foodchem.2020.126693.

[216] E.A. Rue, J.A. Glinski, R.B. Van Breemen, Ion Mobility - Mass Spectrometry for the Separation and Analysis of Procyanidins, 2020, http://dx.doi.org/10.1002/jms.4377.

[217] Y. Wang, Pde B. Harrington, T. Chang, X. Wu, P. Chen, Analysis of cranberry proanthocyanidins using UPLC–ion mobility–high-resolution mass spectrometry, Anal. Bioanal. Chem. 412 (2020) 3653–3662, http://dx.doi.org/10.1007/s00216-020-02601-z.

[218] M. Muller, A.G.J. Tredoux, A. De Villiers, Application of kinetically optimised online HILIC × RP-LC methods hyphenated to high resolution MS for the analysis of natural phenolics, Chromatographia 82 (2019) 181–196, http://dx.doi.org/10.1007/s10337-018-3662-6.

[219] L. Wang, S. Liu, X. Zhang, J. Xing, Z. Liu, F. Song, A strategy for identification and structural characterization of compounds from Gardenia jasminoides by integrating macroporous resin column chromatography and liquid chromatography-tandem mass spectrometry combined with ion-mobility spectrometry, J. Chromatogr. A 1452 (2016) 47–57, http://dx.doi.org/10.1016/j.chroma.2016.05.026.

[220] C. Chalet, B. Hollebrands, H.G. Janssen, P. Augustijns, G. Duchateau, Identification of phase-II metabolites of flavonoids by liquid chromatography–ion-mobility spectrometry–mass spectrometry, Anal. Bioanal. Chem. 410 (2018) 471–482, http://dx.doi.org/10.1007/s00216-017-0737-4.

[221] M. Rezaei, M.R. Naghavi, A.H. Hosseinzadeh, A. Abbasi, Measurement of some benzylisoquinoline alkaloids in different organs of persian poppy during ontogenetical stages, Chem. Biodivers. 13 (2016) 539–543, http://dx.doi.org/10.1002/cbdv.201500172.

[222] R.W. Purves, H. Zhang, H. Khazaei, A. Vandenberg, Rapid analysis of medically relevant compounds in faba bean seeds using FAIMS and mass spectrometry, Int. J. Ion Mobil. Spectrom. 20 (2017) 125–135, http://dx.doi.org/10.1007/s12127-017-0226-7.

[223] Z. Wang, D. Kang, X. Jia, H. Zhang, J. Guo, C. Liu, Analysis of alkaloids from Peganum harmala L. sequential extracts by liquid chromatography coupled to ion mobility spectrometry, J. Chromatogr. B 1096 (2018) 73–79, http://dx.doi.org/10.1016/j.jchromb.2018.08.021.

[224] S.W.C. Chung, C.H. Lam, Development of an analytical method for analyzing pyrrolizidine alkaloids in different groups of food by UPLC-MS/MS, J. Agric. Food Chem. 66 (2018) 3009–3018, http://dx.doi.org/10.1021/acs.jafc.7b06118.

[225] L. Jia, T. Zuo, C. Zhang, W. Li, H. Wang, Y. Hu, X. Wang, Y. Qian, W. Yang, H. Yu, Simultaneous profiling and holistic comparison of the metabolomes among the flower buds of Panax ginseng, Panax quinquefolius, and Panax notoginseng by UHPLC/IM-QTOF-HDMSE-Based metabolomics analysis, Molecules 24 (2019) 2188, http://dx.doi.org/10.3390/molecules24112188.

[226] R. Wu, X. Chen, W.J. Wu, Z. Wang, Y.L.E. Wong, Y.L.W. Hung, H.T. Wong, M. Yang, F. Zhang, T.W.D. Chan, Rapid differentiation of asian and american ginseng by differential ion mobility spectrometry-tandem mass spectrometry using stepwise modulation of gas modifier concentration, J. Am. Soc. Mass Spectrom. 30 (2019) 2212–2221, http://dx.doi.org/10.1007/s13361-019-02317-0.

[227] H. Zhang, J.M. Jiang, D. Zheng, M. Yuan, Z.Y. Wang, H.M. Zhang, C.W. Zheng, L.B. Xiao, H.X. Xu, A multidimensional analytical approach based on time-decoupled online comprehensive two-dimensional liquid chromatography coupled with ion mobility quadrupole time-of-flight mass spectrometry for the analysis of ginsenosides from white and red ginsengs, J. Pharm. Biomed. Anal. 163 (2019) 24–33, http://dx.doi.org/10.1016/j.jpba.2018.09.036.

[228] T. Zuo, C. Zhang, W. Li, H. Wang, Y. Hu, W. Yang, L. Jia, X. Wang, X. Gao, D. Guo, Offline two-dimensional liquid chromatography coupled with ion mobility-quadrupole time-of-flight mass spectrometry enabling four-dimensional separation and characterization of the multicomponents from white ginseng and red ginseng, J. Pharm. Anal. (2020), http://dx.doi.org/10.1016/j.jpha.2019.11.001.

[229] A.A. Aksenov, A. Pasamontes, D.J. Peirano, W. Zhao, A.M. Dandekar, O. Fiehn, R. Ehsani, C.E. Davis, Detection of huanglongbing disease using differential mobility spectrometry, Anal. Chem. 86 (2014) 2481–2488, http://dx.doi.org/10.1021/ac403469y.

[230] M. Rutolo, J.A. Covington, J. Clarkson, D. Iliescu, Detection of potato storage disease via gas analysis: a pilot study using field asymmetric ion mobility spectrometry, Sensors (Switzerland) 14 (2014) 15939–15952, http://dx.doi.org/10.3390/s140915939.

[231] A.N. Gloess, C. Yeretzian, R. Knochenmuss, M. Groessl, International Journal of Mass Spectrometry On-line analysis of coffee roasting with ion mobility spectrometry – mass spectrometry (IMS – MS), Int. J. Mass Spectrom. 424 (2018) 49–57, http://dx.doi.org/10.1016/j.ijms.2017.11.017.

[232] R. Rodríguez-Maecker, E. Vyhmeister, S. Meisen, A. Rosales Martinez, A. Kuklya, U. Telgheder, Identification of terpenes and essential oils by means of static headspace gas chromatography-ion mobility spectrometry, Anal. Bioanal. Chem. 409 (2017) 6595–6603, http://dx.doi.org/10.1007/s00216-017-0613-2.

[233] L. Liu, C. Hu, L. Liu, S. Zhang, K. Chen, D. He, Rapid detection and separation of olive oil and Camellia oil based on ion mobility spectrometry fingerprints and chemometric models, Eur. J. Lipid Sci. Technol. 119 (2017) 1–9, http://dx.doi.org/10.1002/ejlt.201500463.

[234] R. Garrido-Delgado, M.M. Dobao-Prieto, L. Arce, J. Aguilar, J.L. Cumplido, M. Valcárcel, Ion mobility spectrometry versus classical physico-chemical analysis for assessing the shelf life of extra virgin olive oil according to container type and storage conditions, J. Agric. Food Chem. 63 (2015) 2179–2188, http://dx.doi.org/10.1021/jf505415f.

[235] B. Vega-márquez, I. Nepomuceno-chamorro, N. Jurado-campos, Deep Learning Techniques to Improve the Performance of Olive Oil Classification, 7, 2020, pp. 1–10, http://dx.doi.org/10.3389/fchem.2019.00929.

[236] M. Hädener, M.Z. Kamrath, W. Weinmann, M. Groessl, High-resolution ion mobility spectrometry for rapid Cannabis potency testing, Anal. Chem. 90 (2018) 8764–8768, http://dx.doi.org/10.1021/acs.analchem.8b02180.

[237] K. Leiman, L. Colomo, S. Armenta, M. De Guardia, F.A. Esteve-turrillas, Talanta Fast extraction of cannabinoids in marijuana samples by using hard-cap espresso machines, Talanta 190 (2018) 321–326, http://dx.doi.org/10.1016/j.talanta.2018.08.009.

[238] N.A. dos Santos, L.V. Tose, M. Murgu, R.M. Kuster, R.S. Ortiz, F.A.O. Camargo, B.G. Vaz, Analysis of Isomeric Cannabinoid Standards and, J. Braz. Chem. Soc., 30, 2019, pp. 60–70.

[239] T.D. Kiselak, R. Koerber, G.F. Verbeck, Synthetic route sourcing of illicit at home cannabidiol (CBD) isomerization to psychoactive cannabinoids using ion mobility-coupled-LC–MS/MS, Forensic Sci. Int. 308 (2020), 110173, http://dx.doi.org/10.1016/j.forsciint.2020.110173.

[240] G.F. Feng, Y. Zheng, Y. Sun, S. Liu, Z.F. Pi, F.R. Song, Z.Q. Liu, A targeted strategy for analyzing untargeted mass spectral data to identify lanostane–type triterpene acids in Poria cocos by integrating a scientific information system and liquid chromatography–tandem mass spectrometry combined with ion mobility spectro, Anal. Chim. Acta 1033 (2018) 87–99, http://dx.doi.org/10.1016/j.aca.2018.06.048.

[241] M.L. Salum, R. Erra-Balsells, High purity cis-cinnamic acid preparation for studying physiological role of trans-cinnamic and cis-cinnamic acids in

higher plants, Environ. Control Biol. 51 (2013) 1–10, http://dx.doi.org/10.2525/ecb.51.1.
[242] M.N. Clifford, J. Kirkpatrick, N. Kuhnert, H. Roozendaal, P.R. Salgado, LC-MSn analysis of the cis isomers of chlorogenic acids, Food Chem. 106 (2008) 379–385, http://dx.doi.org/10.1016/j.foodchem.2007.05.081.
[243] K. Masike, F. Tugizimana, N. Ndlovu, E. Smit, L. du Preez, I. Dubery, E. Madala, Deciphering the influence of column chemistry and mass spectrometry settings for the analyses of geometrical isomers of L-chicoric acid, J. Chromatogr. B Anal. Technol. Biomed. Life Sci. 1052 (2017) 73–81, http://dx.doi.org/10.1016/j.jchromb.2017.03.023.
[244] K. Masike, I. Dubery, P. Steenkamp, E. Smit, E. Madala, Revising reverse-phase chromatographic behavior for efficient differentiation of both positional and geometrical isomers of dicaffeoylquinic acids, J. Anal. Methods Chem. 2018 (2018), http://dx.doi.org/10.1155/2018/8694579.
[245] H. Karaköse, R. Jaiswal, S. Deshpande, N. Kuhnert, Investigation of the photochemical changes of chlorogenic acids induced by ultraviolet light in model systems and in agricultural practice with Stevia rebaudiana cultivation as an example, J. Agric. Food Chem. 63 (2015) 3338–3347, http://dx.doi.org/10.1021/acs.jafc.5b00838.
[246] M.I. Mhlongo, L.A. Piater, P.A. Steenkamp, N.E. Madala, I.A. Dubery, Metabolomic fingerprinting of primed tobacco cells provide the first evidence for the biological origin of cis-chlorogenic acid, Biotechnol. Lett. 37 (2015) 205–209, http://dx.doi.org/10.1007/s10529-014-1645-8.
[247] M.M. Makola, I.A. Dubery, G. Koorsen, P.A. Steenkamp, M.M. Kabanda, L.L. Du Preez, N.E. Madala, The effect of geometrical isomerism of 3,5-Dicaffeoylquinic acid on its binding affinity to HIV-Integrase enzyme: a molecular docking study, evidence-based complement, Altern. Med. 2016 (2016) 1–10, http://dx.doi.org/10.1155/2016/4138263.
[248] Y.L. Chen, S.T. Huang, F.M. Sun, Y.L. Chiang, C.J. Chiang, C.M. Tsai, C.J. Weng, Transformation of cinnamic acid from trans- to cis-form raises a notable bactericidal and synergistic activity against multiple-drug resistant Mycobacterium tuberculosis, Eur. J. Pharm. Sci. 43 (2011) 188–194, http://dx.doi.org/10.1016/j.ejps.2011.04.012.
[249] X. Zheng, R.S. Renslow, M.M. Makola, I.K. Webb, L. Deng, D.G. Thomas, N. Govind, Y.M. Ibrahim, M.M. Kabanda, I.A. Dubery, H.M. Heyman, R.D. Smith, N.E. Madala, E.S. Baker, Structural elucidation of cis/trans dicaffeoylquinic acid photoisomerization using ion mobility spectrometry-mass spectrometry, J. Phys. Chem. Lett. 8 (2017) 1381–1388, http://dx.doi.org/10.1021/acs.jpclett.6b03015.
[250] G.B. Gonzales, G. Smagghe, S. Coelus, D. Adriaenssens, K. De Winter, T. Desmet, K. Raes, J. Van Camp, Collision cross section prediction of deprotonated phenolics in a travelling-wave ion mobility spectrometer using molecular descriptors and chemometrics, Anal. Chim. Acta 924 (2016) 68–76, http://dx.doi.org/10.1016/j.aca.2016.04.020.
[251] M. McCullagh, C.A.M. Pereira, J.H. Yariwake, Use of ion mobility mass spectrometry to enhance cumulative analytical specificity and separation to profile 6-C/8-C-glycosylflavone critical isomer pairs and known–unknowns in medicinal plants, Phytochem. Anal. 30 (2019) 424–436, http://dx.doi.org/10.1002/pca.2825.
[252] B.H. de Oliveira, J.F. Packer, M. Chimelli, D.A. de Jesus, Enzymatic modification of stevioside by cell-free extract of Gibberella fujikuroi, J. Biotechnol. 131 (2007) 92–96, http://dx.doi.org/10.1016/j.jbiotec.2007.05.035.
[253] E. Colson, C. Decroo, D. Cooper-Shepherd, G. Caulier, C. Henoumont, S. Laurent, J. De Winter, P. Flammang, M. Palmer, J. Claereboudt, P. Gerbaux, Discrimination of regioisomeric and stereoisomeric saponins from Aesculus hippocastanum seeds by ion mobility mass spectrometry, J. Am. Soc. Mass Spectrom. 30 (2019) 2228–2237, http://dx.doi.org/10.1007/s13361-019-02310-7.
[254] V. Domalain, M. Hubert-Roux, V. Tognetti, L. Joubert, C.M. Lange, J. Rouden, C. Afonso, Enantiomeric differentiation of aromatic amino acids using traveling wave ion mobility-mass spectrometry, Chem. Sci. 5 (2014) 3234–3239, http://dx.doi.org/10.1039/c4sc00443d.
[255] A. Troc, M. Zimnicka, W. Danikiewicz, Separation of catechin epimers by complexation using ion mobility mass spectrometry, J. Mass Spectrom. 50 (2015) 542–548, http://dx.doi.org/10.1002/jms.3560.
[256] N. Kuhnert, G.H. Yassin, R. Jaiswal, M.F. Matei, C.H. Grün, Differentiation of prototropic ions in regioisomeric caffeoyl quinic acids by electrospray ion mobility mass spectrometry, Rapid Commun. Mass Spectrom. 29 (2015) 675–680, http://dx.doi.org/10.1002/rcm.7151.
[257] H. Xia, A.B. Attygalle, Untrapping kinetically trapped ions: the role of water vapor and ion-source activation conditions on the gas-phase protomer ratio of benzocaine revealed by ion-mobility mass spectrometry, J. Am. Soc. Mass Spectrom. 28 (2017) 2580–2587, http://dx.doi.org/10.1007/s13361-017-1806-9.
[258] K. Masike, A. De Villiers, E.W. Hoffman, D.J. Brand, T. Causon, M.A. Stander, Detailed phenolic characterization of protea pure and hybrid cultivars by liquid chromatography-ion mobility-high resolution mass spectrometry (LC-IM-HR-MS), J. Agric. Food Chem. 68 (2020) 485–502, http://dx.doi.org/10.1021/acs.jafc.9b06361.
[259] S. Stephan, C. Jakob, J. Hippler, O.J. Schmitz, A novel four-dimensional analytical approach for analysis of complex samples, Anal. Bioanal. Chem. 408 (2016) 3751–3759, http://dx.doi.org/10.1007/s00216-016-9460-9.
[260] M. Sans, C.L. Feider, L.S. Eberlin, Advances in mass spectrometry imaging coupled to ion mobility spectrometry for enhanced imaging of biological tissues, Curr. Opin. Chem. Biol. 42 (2018) 138–146, http://dx.doi.org/10.1016/j.cbpa.2017.12.005.
[261] H. Li, B.K. Smith, L. Márk, P. Nemes, J. Nazarian, A. Vertes, Ambient molecular imaging by laser ablation electrospray ionization mass spectrometry with ion mobility separation, Int. J. Mass Spectrom. 377 (2015) 681–689, http://dx.doi.org/10.1016/j.ijms.2014.06.025.
[262] S.A. Stopka, B.J. Agtuca, D.W. Koppenaal, L. Paša-Tolić, G. Stacey, A. Vertes, C.R. Anderton, Laser-ablation electrospray ionization mass spectrometry with ion mobility separation reveals metabolites in the symbiotic interactions of soybean roots and rhizobia, Plant J. 91 (2017) 340–354, http://dx.doi.org/10.1111/tpj.13569.
[263] E. Claude, M. Tower, R. Lafont, I.D. Wilson, R.S. Plumb, High performance thin-layer chromatography of plant ecdysteroids coupled with desorption electrospray ionisation–Ion mobility–Time of flight high resolution mass spectrometry (HPTLC/DESI/IM/ToFMS), Chromatographia 83 (2020) 1029–1035, http://dx.doi.org/10.1007/s10337-020-03917-9.
[264] A.P. Marshall, A.R. Johnson, M.M. Vega, R.J. Thomson, E.E. Carlson, Ion mobility mass spectrometry as an efficient tool for identification of streptorubin B in Streptomyces coelicolor M145, J. Nat. Prod. 83 (2020) 159–163, http://dx.doi.org/10.1021/acs.jnatprod.9b00828.
[265] L. Righetti, G. Paglia, G. Galaverna, C. Dall'Asta, Recent advances and future challenges in modified mycotoxin analysis: why HRMS has become a key instrument in food contaminant research, Toxins (Basel) 8 (2016), http://dx.doi.org/10.3390/toxins8120361.
[266] L. Righetti, M. Fenclova, L. Dellafiora, J. Hajslova, M. Stranska-Zachariasova, C. Dall'Asta, High resolution-ion mobility mass spectrometry as an additional powerful tool for structural characterization of mycotoxin metabolites, Food Chem. 245 (2018) 768–774, http://dx.doi.org/10.1016/j.foodchem.2017.11.113.
[267] S. Poyer, C. Loutelier-Bourhis, G. Coadou, F. Mondeguer, J. Enche, A. Bossée, P. Hess, C. Afonso, Identification and separation of saxitoxins using hydrophilic interaction liquid chromatography coupled to traveling wave ion mobility-mass spectrometry, J. Mass Spectrom. 50 (2015) 175–181, http://dx.doi.org/10.1002/jms.3515.
[268] D.G. Beach, E.S. Kerrin, M.A. Quilliam, Selective quantitation of the neurotoxin BMAA by use of hydrophilic-interaction liquid chromatography–differential mobility spectrometry–tandem mass spectrometry (HILIC–DMS–MS/MS), Anal. Bioanal. Chem. 407 (2015) 8397–8409, http://dx.doi.org/10.1007/s00216-015-9012-8.
[269] V.K. Mittermeier, K. Pauly, A. Dunkel, T. Hofmann, Ion-mobility-Based liquid chromatography–Mass spectrometry quantitation of taste-enhancing Octadecadien-12-ynoic acids in mushrooms, J. Agric. Food Chem. 68 (2020) 5741–5751, http://dx.doi.org/10.1021/acs.jafc.0c02034.
[270] M. Jünger, W. Vautz, M. Kuhns, L. Hofmann, S. Ulbricht, J.I. Baumbach, M. Quintel, T. Perl, Ion mobility spectrometry for microbial volatile organic compounds: a new identification tool for human pathogenic bacteria, Appl. Microbiol. Biotechnol. 93 (2012) 2603–2614, http://dx.doi.org/10.1007/s00253-012-3924-4.
[271] W. Liu, X. Zhang, R. Knochenmuss, W.F. Siems, H.H. Hill, Multidimensional separation of natural products using liquid chromatography coupled to hadamard transform ion mobility mass spectrometry, J. Am. Soc. Mass Spectrom. 27 (2016) 810–821, http://dx.doi.org/10.1007/s13361-016-1346-8.
[272] M.A. Stander, B.-E. Van Wyk, M.J.C. Taylor, H.S. Long, Analysis of phenolic compounds in rooibos tea (Aspalathus linearis) with a comparison of flavonoid-based compounds in natural populations of plants from different regions, J. Agric. Food Chem. 65 (2017) 10270–10281, http://dx.doi.org/10.1021/acs.jafc.7b03942.
[273] H. Koudokpon, N. Armstrong, T.V. Dougnon, F. Loko, E. Chabrière, J.M. Rolain, Antibacterial Activity of Chalcone and Dihydrochalcone Compounds from Uvaria chamae Roots Against Multidrug-Resistant Bacteria, 2018, 2018.
[274] D. Mathiron, R. Iori, S. Pilard, T.S. Rajan, D. Landy, E. Mazzon, P. Rollin, F. Djedaïni-Pilard, A combined approach of NMR and mass spectrometry techniques applied to the α-cyclodextrin/moringin complex for a novel bioactive formulation, Molecules 23 (2018), http://dx.doi.org/10.3390/molecules23071714.